Multiscale modelling of plasma cell differentiation in the germinal center

Elena Merino Tejero

Multiscale modelling of plasma cell differentiation in the germinal center

Elena Merino Tejero

Multiscale modelling of plasma cell differentiation in the germinal center
Elena Merino Tejero, Amsterdam, The Netherlands, 2022

The research described in this thesis was performed at the Bioinformatics Laboratory, Department of Epidemiology and Data Science at the Amsterdam University Medical Centers, Amsterdam, the Netherlands.

Printing of this thesis was financially sponsored by the Academic Medical Center, Amsterdam UMC, Amsterdam, the Netherlands.

Multiscale modelling of plasma cell differentiation in the germinal center

ACADEMISCH PROEFSCHRIFT

ter verkrijging van de graad van doctor
aan de Universiteit van Amsterdam
op gezag van de Rector Magnificus
prof. dr. M.H.W. Frings-Dresen and prof. dr. J.A. Reekers
ten overstaan van een door het College voor Promoties ingestelde commissie,
in het openbaar te verdedigen in de Agnietenkapel
op maandag 7 november 2022, te 14.00 uur
door Elena Merino Tejero
geboren te Madrid

Promotiecommissie

Promotor:	prof. dr. ing A.H.C. van Kampen	AMC-UvA
Copromotores:	dr. J.E.J. Guikema	Universiteit van Amsterdam
	dr. ir. H.C.J. Hoefsloot	Universiteit van Amsterdam
Overige leden:	prof. dr. A.H. Maitland-van der Zee	AMC-UvA
	prof. dr. C.A. Russel	AMC-UvA
	prof. dr. A.K. Smilde	Universiteit van Amsterdam
	prof. dr. P.M.A. Sloot	Universiteit van Amsterdam
	dr. H.B. Jacobs	NKI-AvL
	prof. dr. R.E.M. Toes	Universiteit Leiden

Faculteit der Geneeskunde

Contents

1. Introduction 8
1.1. Adaptive Immunity 8
1.2. Germinal center reaction..... 10
1.3. Mechanisms of memory B-cell and plasma cell differentiation in the germinal center..... 12
1.4. The role of the GC in disease..... 19
1.5. Repertoire sequencing experiments..... 19
1.6. Computational modeling to study biological systems 20
1.7. Outline of thesis..... 26

2. Multiscale modelling of germinal center recapitulates the temporal transition from memory B cell to plasma cell differentiation as regulated by antigen affinity-based Tfh cell help 27
2.1. Abstract..... 27
2.2. Introduction..... 28
2.3. Methods..... 31
2.4. Results 37
2.6. Acknowledgements 49
2.7. Conflict of Interest..... 50
2.8. Supplementary Information..... 50

3. Coupled antigen and BLIMP1 asymmetric division with a large segregation between daughter cells recapitulates the temporal transition from memory B cells to plasma cells and a DZ-to-LZ ratio in the germinal center..... 69
3.1. Abstract..... 69
3.2. Introduction..... 70
3.3. Methods..... 71
3.4. Results 78
3.5. Discussion..... 88
3.6. Acknowledgements 90
3.7. Supplementary Information..... 90

4. Multiscale modeling recapitulates the effect of genetic alterations associated with diffuse large B-cell lymphoma in the germinal center dynamics..... 94
4.1. Abstract..... 94
4.2. Introduction..... 95
4.3. Methods..... 97
4.4. Results 104
4.5. Discussion..... 114

4.6. Acknowledgements 117
4.7. Supplementary Information 117

5. Generation of repertoire sequencing data from a computational model of the germinal center 122
5.1. Abstract 122
5.2. Introduction 123
5.3. Methods 126
5.4. Results 133
5.5. Discussion 139
5.6. Acknowledgements 142
5.7. Supplementary Information 143

6. Discussion 152
6.1. Output cell differentiation based on Ag status versus BLIMP1 level 153
6.2. Memory B-cell differentiation 154
6.3. Asymmetric division of Ag and TFs 154
6.4. Genetic alterations that lead to DLBCL 155
6.5. Generation of repertoire sequencing data 157

Summary 158

Samenvatting 159

List of Publications 160

PhD training 161

Curriculum Vitae 162

Acknowledgements 163

References 164

Chapter 1

Introduction

1.1. Adaptive Immunity

The adaptive immune system enables the selective elimination of specific foreign substances and microorganisms by means of specific antigen receptors (AgRs) expressed by T- and B-cells. The adaptive immune system has a humoral component that is characterized by antibody (Ab) responses, and cell-mediated components that specifically destroys invading pathogens. Next to antigens (Ags) derived from microorganisms, toxins, pollens and self-altered molecules can act as Ags, triggering an immune response. The adaptive immune system displays three main characteristics:

(1) Ab specificity
(2) Ab diversity
(3) Immunological memory

B and T cells are key components of the adaptive immune system since they are able to specifically recognize a large variety of Ags through their AgRs. Each individual AgR is capable of binding with one or more Ags with a particular specificity. Cross-reactive AgRs bind to several related Ags while promiscuous AgRs bind to unrelated Ags (James and Tawfik, 2009). AgRs with high specificity for the Ag can precisely detect the target Ag. B-cells produce Abs, also known as immunoglobulin (Ig), that can either be membrane bound (B-cell receptor, BcR) or be secreted as soluble molecules, whereas T cells exclusively express membrane bound AgRs (T-cell receptor, TcR). The BcR interacts with Ag in its native form, whereas the TcR can only recognize processed Ag in the context of a major histocompatibility complex (MHC) molecule.

AgR are formed by heavy and light chains, each of which has constant and variable regions. Heavy chain genes contain multiple copies of three different segments of the variable region. These are known as the variable (V), diversity (D) and joining (J) segments. Light chain genes contain V and J but not D segments. During the cell development, imprecise gene rearrangement results in the combination of one copy of each segment to produce a unique AgR. All members of a B-/T-cell progeny that have the same AgR are known as clonotypes (Oltz, 2001). Current theoretical, combinatorial calculations of the human

immune repertoire size suggest there are about 10^{15} possible AgRs, due to recombinatorial processes (Rees, 2020). While the number of heavy-chain V(D)J clonotypes in circulation has been estimated to be much lower, around 9 and 17 million (Soto *et al.*, 2019). Factually, the immune repertoire is diverse enough to ensure that there will be an Ab to fit almost any potential Ag, albeit with low affinity. After repeated stimulation by Ag, B cells can make Abs that bind their Ag with much higher affinity in a process called affinity maturation (Rees, 2020). Additional processes such as somatic recombination of V(D)J genes that encode the BcR and induce junctional diversity, and pairing of different BcR heavy and light chains induce part of the BcR diversity (Schroeder and Cavacini, 2010). Somatic hypermutation (SHM), taking place in the germinal center (GC; see below), and class-switch recombination (CSR) induce further diversity during B-cell division. SHMs mainly affect the V(D)J genes encoding the Ag-binding variable regions of the Ig heavy and light chains (Jacob *et al.*, 1991). Contrarily, CSR is a DNA recombination process that replaces the Ig constant region of IgM expressing B cells for the isotype that can best protect against the Ag (Wang *et al.*, 2018). The BcR harbors three complementary determining regions (CDR1, CDR2, CDR3) that encompass the most variable parts of the Ab and are responsible for Ag binding. The four BcR framework regions (FWRs) mostly provide structural support for the CDRs (Lefranc *et al.*, 2005; Hood, 2008; Sela-Culang *et al.*, 2013).

Upon contact with Ag, B cells are activated and migrate towards secondary lymphoid organs, such as the spleen and lymph nodes, and into the boundary between T and B-cell rich areas where they interact with a specialized subset of Ag-specific CD4+ T cells, termed T follicular helper (Tfh) cells (Okada *et al.*, 2005). B cells are then directed either into follicular areas, where the GC reaction takes place, or to extra follicular areas, where they proliferate and differentiate into long or short-lived plasma cells (PCs) respectively provided they receive appropriate costimulatory signals from Tfh cells (Pereira *et al.*, 2010). As a result of the GC reaction, B cells may also differentiate into memory B cells (MBCs) producing an immunological memory such that it can respond faster when the pathogen is encountered again in the future (Ripperger and Bhattacharya, 2021).

After primary immunization, MBCs and PCs appear in blood quickly due to the initiation of the adaptive immune response (Blink *et al.*, 2005). Many of the short-lived PCs that appear early before the initiation of the GC reaction, die through apoptosis in a few days (Smith *et al.*, 1997). Long-lived PCs ultimately home to the bone marrow (Chan and Brink, 2012) and secrete protective high affinity soluble Igs or antibodies (Abs) over extended periods of time (Slifka *et al.*, 1995). In contrast, MBCs preferably locate at the site of their formation, although they also recirculate and generate a fast and intense response upon re-exposure (Thorbecke and Baine, 2021). Notably, GCs have been found to be IgM dominated (Roco *et al.*, 2019). Memory T cells are also preserved after an infection, ready to mediate an enhanced and accelerated response to reinfection. Thus, B and T cells are responsible for a durable adaptive immunological response (Jarjour *et al.*, 2021).

1.2. Germinal center reaction

Germinal centers (GCs) are dynamic anatomical structures that appear in B-cell follicles of secondary lymphoid organs where the B-cell affinity maturation process takes place during which the B-cell receptor affinity increases over time (N. S. De Silva and Klein, 2015). Interactions with Tfh cells at the T and B-cell rich boundary drive initial B-cell proliferation. Proliferating B-cells may either migrate to extrafollicular areas, where they expand and differentiate into PCs providing an immediate source of Ag-specific Abs, or remain localized in B-cell follicles, where they seed GCs (Gatto and Brink, 2010).

GCs comprise two functional zones: a dark zone (DZ) and a light zone (LZ) (Victora *et al.*, 2010). GC B cells constantly migrate between zones (Schwickert *et al.*, 2007). The motility of B cells is partially dependent on the chemokine – receptor pairs CXCL12-CXCR4 and CXCL13-CXCR5 (Wu *et al.*, 2019). B-cells, at a centroblast (CB) state, mainly express CXCR4 and are attracted by CXCL12-expressing reticular cells (CRC) towards the DZ (Allen *et al.*, 2007b). CBs undergo rapid proliferation during which SHMs take place, which increase or decrease the binding affinity of the BcR for the Ag. This generates a broad range of BcR affinities for the Ag (Jacob *et al.*, 1991; N. S. De Silva and Klein, 2015). Although it has long been thought that CSR also occurs during DZ B-cell division, it now appears that this process precedes the GC reaction (Roco *et al.*, 2019). After proliferation, CBs that fail to express a functional BcR due to crippling mutations undergo cell death (Stewart *et al.*, 2018). CBs that express functional BcRs may differentiate to centrocytes (CCs), express CXCR5 and are attracted by CXCL13-expressing follicular dendritic cells (FDC) towards the LZ (Allen *et al.*, 2007b). In the LZ the CCs undergo a process known as positive selection (Nakagawa and Calado, 2021). During this process, LZ B cells interact through their BcR with opsonized Ag presented by FDCs (Heesters *et al.*, 2014). This interaction leads to BcR derived survival signals, which partially rescue B cells from programed apoptosis (Mayer *et al.*, 2017).

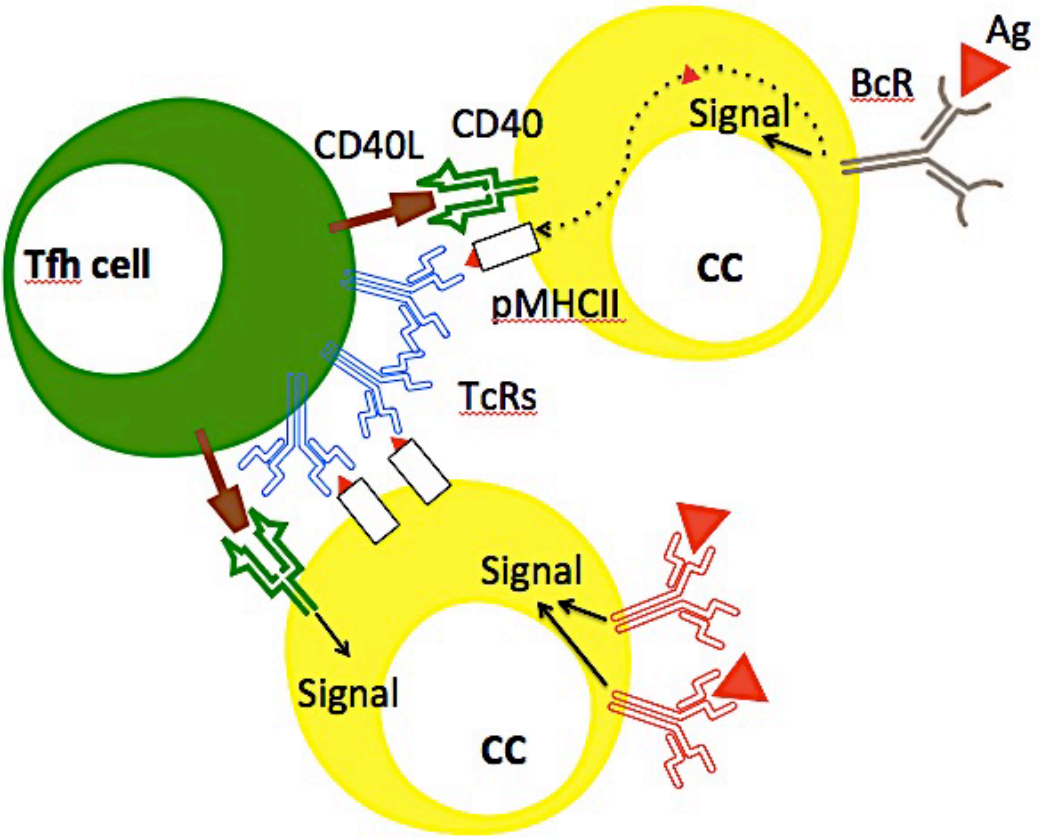

Figure 1: Schematic overview of CC competition during the Tfh cell selection. CCs are represented in yellow with different BcRs (indicated with different colors). The grey BcR has a lower affinity for the Ag, leading to a decreased Ag internalization, BcR signal and pMHCII presentation. The red BcR has a higher affinity for the Ag, leading to an increased Ag internalization, BcR signal and pMHCII presentation. The Tfh cell (green) interacts with two CCs simultaneously but the signal polarizes towards the CC with highest pMHCII concentration. The Ag is represented as a red triangle. pMHCII is represented with a white square bound to a peptide derived from the Ag. CD40(L) are represented in green and brown. The T-cell receptor (TcR) is shown in blue. The dotted line represents the Ag internalization process and the arrows represent signaling process**.**

B cells internalize and process and present the resulting peptides as a peptide-MHCII (pMHCII) complex on their surface enabling the interaction with TcRs of Tfh cells. Higher BcR affinity is directly associated with the ability to capture an increased amount of Ag leading to a higher pMHCII concentration (Allen *et al.*, 2007b). Tfh cells may interact with different B cells simultaneously but their signal polarizes towards the B-cell with highest pMHCII concentration (Figure 1) (Duchez *et al.*, 2011). Nevertheless, this mechanism was found to be significantly more stringent during the GC initiation phase (Yeh *et al.*, 2018). Sufficient Tfh cell-derived signals fully rescue B cells from undergoing apoptosis (Mayer *et al.*, 2017), promotes LZ to DZ migration (Davidzohn *et al.*, 2019), induces rescued B cells into a proliferative state (Gitlin *et al.*, 2015) and initiates MBC and PC differentiation (Muto *et al.*, 2010; Shinnakasu *et al.*, 2016). Division can be initiated in both zones although it takes place in the DZ (Allen *et al.*, 2007b; Victora *et al.*, 2010). Once in the DZ, B cells divide twice on average (Gitlin *et al.*, 2014). The number of divisions individual B cells will undergo in the DZ is

dependent on the Tfh cell signal intensity (Mesin *et al.*, 2016). During division, Ag distributes asymmetrically in 72% of the cases among the progeny leading to higher amounts of pMHCII in Ag inheriting B-cells (Dustin and Meyer-Hermann, 2012; Thaunat *et al.*, 2012). Rescued B cells may either differentiate to MBCs and PCs and exit or stay in the GC for further rounds of proliferation, SHM and (positive) selection (Mesin *et al.*, 2016). It has been predicted through computational modeling and indirectly validated through the use of multiphoton microscopy data that Ag-inheriting B-cells differentiate to PCs and leave the GC through the DZ (Victora *et al.*, 2010; Meyer-Hermann *et al.*, 2012). Yet, direct experimental evidence is still lacking. It is also unknown how and when MBCs leave the GC. Nevertheless, studies have shown the GC output undergoes a temporal switch by which most MBCs are produced before the peak of the GC response and most PCs are produced afterwards (Florian J Weisel *et al.*, 2016; Zhang *et al.*, 2018). Many of the GC processes including GC initiation and termination, B-cell positive and negative selection, and differentiation are not fully understood. Furthermore, the GC dynamics has been shown to be highly variable (Wittenbrink *et al.*, 2011b). Finally, GC processes contribute to a variety of disease states including autoimmunity, allergy, and cancer (Cyster and Allen, 2019) and are relevant for vaccine design, which underscores the importance of understanding them.

1.3. Mechanisms of memory B-cell and plasma cell differentiation in the germinal center

1.3.1. Cellular mechanisms

B-cell activation mechanisms that lead to the formation of PCs and MBCs have been intensely studied, however, they are numerous and not all aspects are completely understood. In particular, the signals that control the differentiation of positively selected B cells towards PC versus MBC fate remain largely unknown. Two main cellular processes have been proposed to be involved in the differentiation of B cells, namely positive selection and signaling (Nakagawa and Calado, 2021) and asymmetric division of Ag (Dustin and Meyer-Hermann, 2012; Meyer-Hermann *et al.*, 2012). Finally, other relevant cellular processes, such as cell division, differentiation or death, and CSR have shown to have highly variable durations, suggesting a role of stochastic internal B-cell processes in driving B-cell differentiation and other B-cell outcomes (Hasbold *et al.*, 2004; Duffy *et al.*, 2012; Zhou *et al.*, 2018).

1.3.1.1. Positive selection and signaling

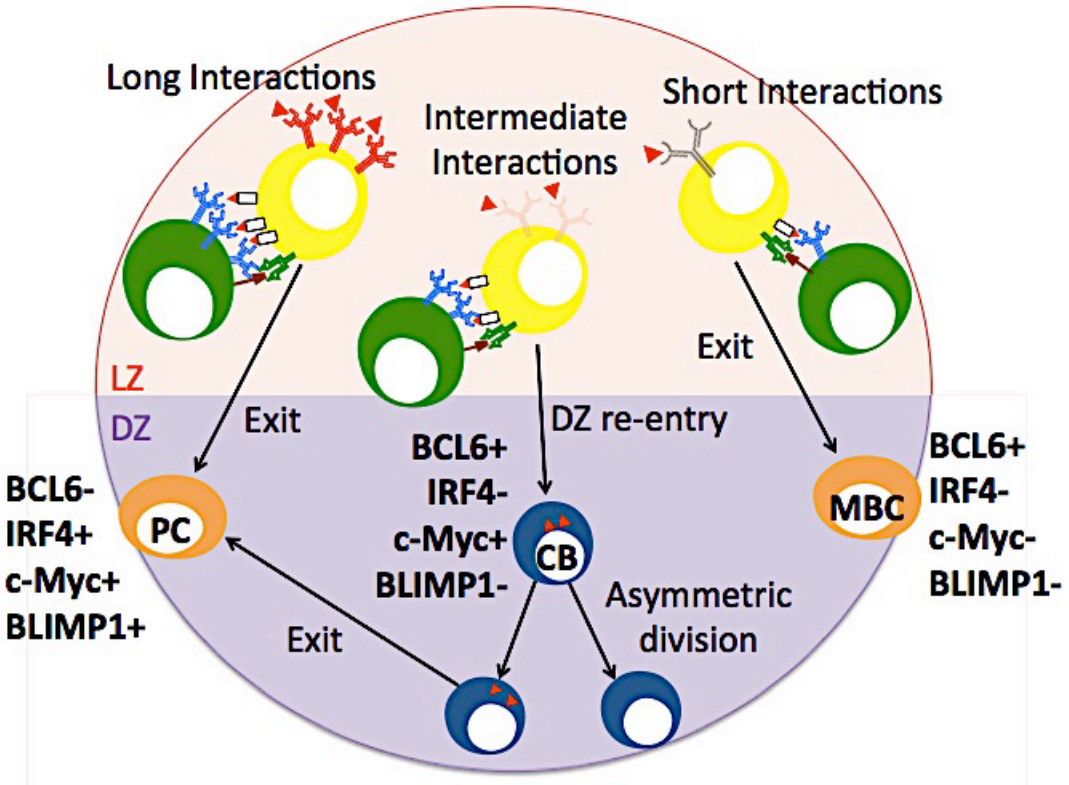

Figure 2: Schematic overview of the main B-cell mechanisms proposed to be involved in MBC and PC differentiation. Three CCs bound to 1,2 or 3 Ags represent CCs with low, intermediate and high affinities for the Ag, leading to short, intermediate and long CC -Tfh interactions (MHCII and CD40 mediated) in the LZ (for further information see Figure 1). Higher affinity CCs may establish longer and more interactions promoting PC differentiation (BCL6-, IRF4+, c-Myc+ and BLIMP1+) and exit from the GC. Intermediate affinity CCs may establish intermediate lasting interactions promoting re-entry of CCs to the DZ as CBs (BCL6+, IRF4-, c-Myc+ and BLIMP1-). Low affinity CCs may establish weaker and shorter interactions promoting MBC differentiation (BCL6+, IRF4-, c-Myc- and BLIMP1-) and exit from the GC. During CB division, Ag is distributed asymmetrically. While the effect of this mechanism on the fate of the cell it is unknown. Some theories suggest Ag-inheriting daughter CBs may differentiate to PCs and exit the GC. CBs are represented in blue. MBC and PCs are represented in orange.

During the GC reaction high-affinity B-cells are positively selected at the expense of lower affinity cells that, consequently, go into apoptosis. The precise cellular and molecular mechanisms remain to be established but BcR and CD40 signaling play an important role. Several studies have shown the role of the selection process in the initiation and progression towards PC differentiation. BcR signals delivered by high affinity BcR-Ag interaction during the selection process in the LZ initiates PC differentiation (Chan and Brink, 2012; Kräutler *et al.*, 2017; Turner *et al.*, 2017, 2018). BLIMP1 (see molecular mechanisms) is expressed in high but not in low affinity LZ B cells. Nevertheless, also high affinity DZ B cells showed a higher expression of canonical PC genes (e.g., BLIMP1, Sdc1, Cd93, Igj, Xbp1) compared to low affinity DZ and LZ B cells (Kräutler *et al.*, 2017). BcR

signaling, however, was not sufficient to promote differentiation into PCs but potentiated B-cell expansion and PC formation when limited by the amount of Tfh cell help (Turner *et al.*, 2018). Signals delivered by Tfh cell have also shown to be required in the progression to PC fate (Kräutler *et al.*, 2017; Turner *et al.*, 2018). Acquisition of Tfh cell help was sufficient to induce B-cell division and PC formation, even in the absence of BcR engagement with Ag (Hasbold *et al.*, 2004; Turner *et al.*, 2018). Affinity and duration of B-cell - Tfh cell CD40-mediated interactions have been proposed to regulate positively selected B-cell fate. High affinity B cells may establish long-lasting interactions with Tfh cells that promote PC fate while low affinity B cells may only establish short-lasting interactions that lead to the MBC fate (Figure 2) (Kurosaki *et al.*, 2015; Ise and Kurosaki, 2019). Interestingly, some studies showed that the CD40 signal did not affect PC production (Kräutler *et al.*, 2017) while others have shown that CD40 signaling is a requirement for PC differentiation (Florian J Weisel *et al.*, 2016; Ise *et al.*, 2018). Apart from CD40L induced signaling, chemokine signals, such as IL-21, and other protein molecules, such as type I IFNs and sFASL, promote PC differentiation in vitro (van Asten *et al.*, 2021).

1.3.1.2. Asymmetric Division

Internalized Ag was analyzed in *in vivo* and *in vitro* mouse B cells showing that it is distributed asymmetrically prior to division in approximately 72% of the B cells studied (Thaunat *et al.*, 2012). This polarization is also maintained during cell division resulting in an asymmetric division of Ag in both daughter cells. The same study showed that after asymmetric division, Ag-inheriting (pMHC-high) daughter B-cell are more efficient in receiving T cell help, which may affect the fate of the B-cell. It was also argued through computational modeling that asymmetric division may largely affect the production of PCs (Dustin and Meyer-Hermann, 2012). Later, a more comprehensive computational model of the GC reaction proposed asymmetric division of Ag as an additional mechanism for PC differentiation together with the selection process (Figure 2) (Meyer-Hermann *et al.*, 2012). This was based on indirect experimental evidence since the inclusion of this mechanism resulted in GC transzone migration rates and DZ-to-LZ ratio in agreement with experimental data (Victora *et al.*, 2010). Furthermore, asymmetric inheritance of transcription factors (TFs), such as B-cell lymphoma 6 (BCL6) (Barnett *et al.*, 2012), Myelocytomatosis viral oncogene (c-Myc) and interferon regulatory factor 4 (IRF4) (Lin *et al.*, 2015) , and signaling molecules, such as IL-21 (Barnett *et al.*, 2012), during B-cell division has also been observed. Nevertheless, there is no direct evidence that relate asymmetric inheritance of the above-mentioned molecules and B-cell fate.

1.3.1.3. Temporal switch

A recent study suggested that the production of MBCs and PCs is, to some extent, temporally divided resulting in a first wave of MBCs followed by an increased production of PCs at later time points during a GC reaction. This phenomenon has

been coined 'temporal switch' (Florian J Weisel *et al.*, 2016). In this study it was observed that long-lived MBCs harboring few Ig mutations, are mostly produced during the early phase of the GC reaction in the spleen, while highly mutated long-lived bone marrow PCs were mostly produced during the later phase. Furthermore, long-lived bone marrow PCs were found to be almost exclusively derived from high-affinity GC B-cells (Chan and Brink, 2012). Contrarily, long-lived splenic MBCs were found to have less mutations and lower affinity although there are also MBCs with high affinity (Shinnakasu *et al.*, 2016). A temporal evolution of Tfh cell population in the GC was proposed to cause the temporal switch (Florian J Weisel *et al.*, 2016). To that end, a study showed that Tfh cell density declines significantly at the time when the GC reaction is switching its output (Wollenberg *et al.*, 2011). A temporal switch is in line with the notion that MBCs comprise a broader range of affinities and specificities to respond to pathogen (Ag) variants (Akkaya *et al.*, 2020).

1.3.1.4. Stochasticity

In response to activation mechanisms, such as Ag and T-dependent signals, B-cells can be directed towards different fates, such as differentiation, CSR, proliferation or death. An in vitro study analyzed the duration of these independent, internal and stochastic B-cell processes in many pairs of siblings. The study showed that correlation between the duration of some of these processes could determine fate outcomes. Stochastic competition of the different timings can explain the observed number of B cells that undertake each B-cell fate. As an example, for asymmetric sibling B-cell fates where one of the siblings divides and the other one dies, a high correlation between the time to divide and time to die across siblings was found. This indicated that asymmetric fates could be expected when the time to divide and die are similar (Duffy *et al.*, 2012). Consequently, the study points towards stochastic epigenetic processes as responsible for influencing the expression levels of molecular regulators involved in the different B-cell processes. Along these lines, another in vitro study measured the times to differentiate, divide, and die of many pairs of sibling B cells. CD40 signal strength was also varied to determine its influence on B-cell fate outcomes. They found that CD40 signal strength did not directly affect B-cell fate. Instead, it significantly affected the time to divide and not to die or differentiate (Zhou *et al.*, 2018). Finally, the role of the B-cell division process in determining PC fate during the GC reaction has also been studied. A direct relation between the number of divisions and the number of PCs produced was observed (Hasbold *et al.*, 2004). This increase in PC production could also be explained through an unknown division-associated mechanism. While these findings do not exclude the role of the above-mentioned Ag and T-dependent signals in determining B-cell fate but rather offers an indirect mechanism and explains why B cells are capable of differentiating in the complete absence of specific signals based on their internal state.

1.3.2. Molecular mechanisms regulating the GC reaction

Numerous TFs are involved in the regulation of the GC processes that lead to B-cell differentiation. The expression of these TFs is regulated by the magnitude of external signals received during the interaction with Ag and Tfh cells.

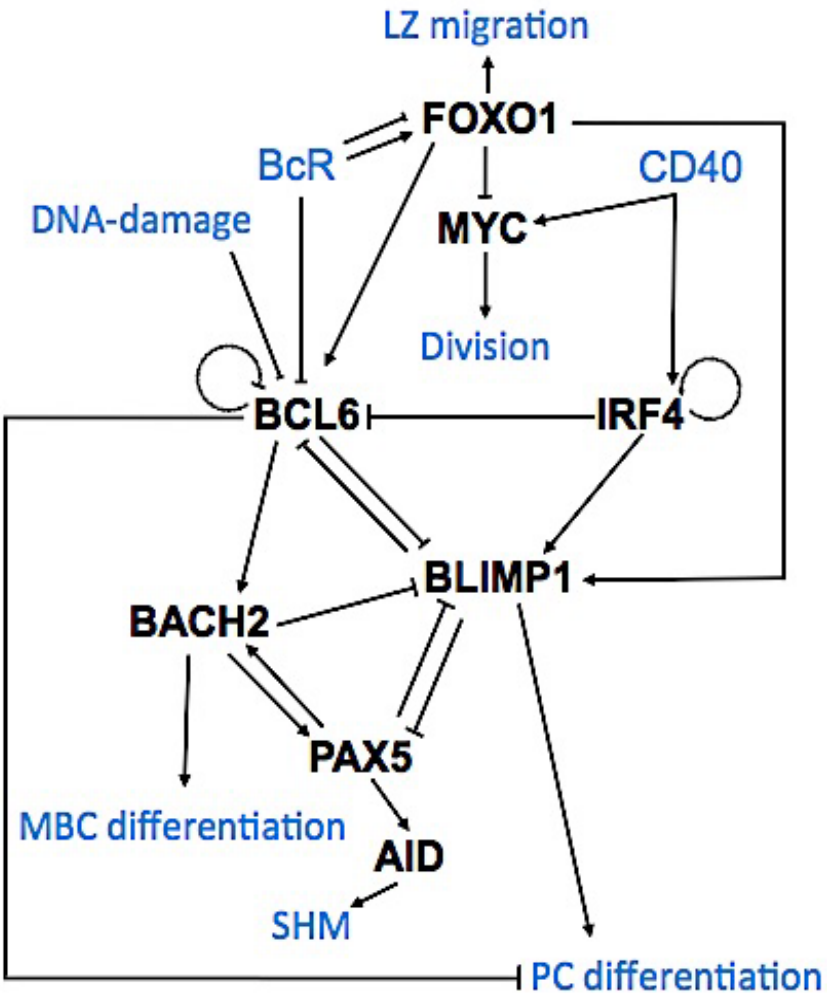

Figure 3: Part of the B-cell gene regulatory network involved in MBC and PC differentiation. TFs are marked in bold. Arrows and bar-headed lines between nodes indicate activation or inhibition. Receptors and cellular processes are indicated in blue.

BCL6 is a major player of the GC reaction since it is key in the GC initiation and maintenance, required for the affinity maturation to take place which results in the production of high-affinity B cells (Ye *et al.*, 1997). It has been shown to modulate the expression of genes involved in B-cell activation, differentiation, cell cycle arrest, and apoptosis (Ye *et al.*, 1997; Shaffer *et al.*, 2000; Niu *et al.*, 2003; Tunyaplin *et al.*, 2004). BCL6 expression induces GC formation and is expressed in pre-GC B cells (Duy *et al.*, 2010) and DZ GC B cells. Finally, BCL6 is regulated by several signals resulting from DNA-damage, and BcR and CD40 stimulation,

which result in the degradation or downregulation of BCL6 (Basso and R. Dalla-favera, 2010) (Figure 3).

Among other targets, BCL6 inhibits B-lymphocyte-induced maturation protein 1 (BLIMP1) and the IRF4 TFs, which are crucial for PC development in the GC (Figure 3). BLIMP1 is expressed in PCs and is involved in their Ab secretory phenotype (Tunyaplin *et al.*, 2004). IRF4 acts upstream (Sciammas *et al.*, 2011) and downstream (Klein *et al.*, 2006) of BLIMP1. Furthermore, both TFs are expressed in a subset of LZ B cells and are required for PC phenotype development in response to CD40 stimulation (Klein *et al.*, 2006). Consistent with their patterns of expression that is restricted to BCL6-negative B cells, BLIMP1 and IRF4 transcriptionally repress BCL6 (Shaffer *et al.*, 2002). Furthermore, IRF4 binds to its own promoter, resulting in a positive feedback mechanism by which PCs maintain a high IRF4 expression (Shaffer *et al.*, 2009).

Paired box protein Pax-5 (PAX5) is a TF required for the establishment of the B-cell lineage identity and the induction of CSR and SHM (Figure 3) (Schebesta *et al.*, 2007). PAX5 and BLIMP1 mutually repress each other. PAX5 and BTB domain and CNC homolog 2 (BACH2) mutually activate each other (Muto *et al.*, 2010). Thus, BACH2 orchestrates the dynamics of PAX5 and BLIMP1 by inducing a delay in BLIMP1 up-regulation, which is crucial for the CSR and SHM processes to take place prior to PC differentiation (Muto *et al.*, 2010). BACH2 is also crucial for MBC development in the GC (Shinnakasu *et al.*, 2016) but not for PC development since BACH2 represses BLIMP1 (Muto *et al.*, 2010). While BACH2 is induced by BCL6 (Laidlaw and Cyster, 2020), down-regulation of BCL6 and up-regulation of BACH2 are both required for MBC fate induction (Ise *et al.*, 2018). GC B cells that receive low levels of Tfh cell help also maintain elevated BACH2 expression (Laidlaw and Cyster, 2020). Nevertheless, it is worthwhile mentioning that BACH2 and BCL6 expression have been found to be strongly correlated (Thomas *et al.*, 2019).

c-Myc and forkhead box protein O 1 (FOXO1) are critical for GC B-cell selection, survival and division (Figure 3) (Dominguez-Sola *et al.*, 2012). FOXO1 is a TF that is repressed by BcR signal while c-Myc is repressed by FOXO1 and induced by CD40. Both BcR signaling, which inactivates FOXO1, and CD40 signals are required for a high c-Myc induction (Luo *et al.*, 2018). c-Myc is expressed exclusively in LZ B cells undergoing positive selection and induces DZ B-cell state. In response to graded doses of Ag, c-Myc expression is directly proportional to the amount of pMHCII. Furthermore, the level of c-Myc expression dictates the number of B-cell divisions in the DZ (Finkin *et al.*, 2019). FOXO1 can then be induced by BcR, through AKT/p-S6 pathway, which is required to induce the Tfh cell-mediated transition from LZ to the DZ B-cell phenotype (Luo *et al.*, 2018). Finally, FOXO1 may induce BCL6 (Tang *et al.*, 2002) while also inducing PC BLIMP1 (Vogel *et al.*, 2014).

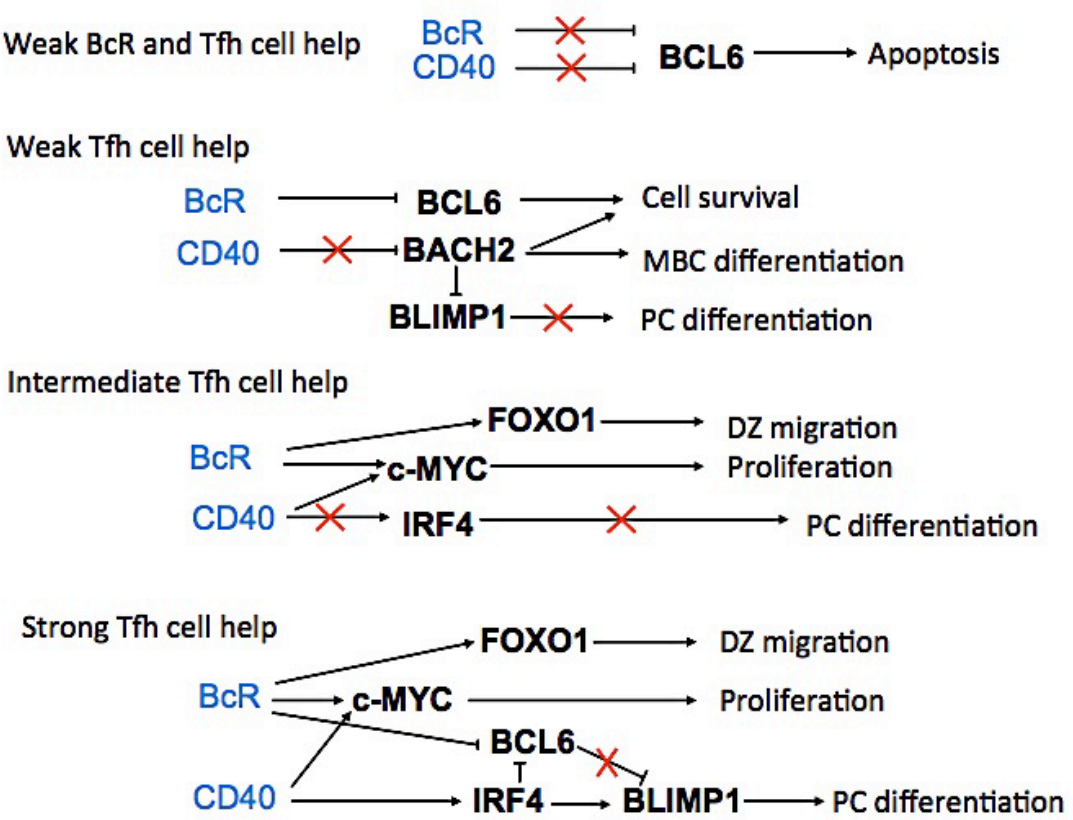

Figure 4: Diagram representing B-cell pathways involved in different B-cell processes in response to different levels of BcR and Tfh cell help. TFs are marked in bold. Arrows and bar-headed lines between nodes indicate activation or inhibition. Red crosses indicate absence of activation or inhibition. Receptors are shown in blue. Figure adapted from (Laidlaw and Cyster, 2020).

Low affinity LZ GC B cells generally undergo apoptosis due to failure to receive sufficient BcR and CD40 signals to inhibit BCL6, which promotes GC B cell apoptosis (Laidlaw and Cyster, 2020). GC B cells that receive sufficient BcR signal repress BCL6 and induce B-cell survival. If in combination with low levels of CD40 signal, B-cells do not repress BACH2, which further inhibits apoptosis and predispose them to differentiate into MBCs. These cells also fail to express c-Myc, which is necessary to promote B-cell division, and BLIMP1, which induces PC development (Figure 4). Intermediate levels of CD40 signal, in combination with sufficient BcR signal, result in the induction of c-Myc and subsequent induction FOXO1, which lead to a highly proliferative DZ B-cell state. Intermediate levels of CD40 signal do not drive sufficient IRF4 expression preventing PC differentiation. High levels of CD40 signal, in combination with sufficient BcR signal, allows for IRF4 induction, BCL6 inhibition and BLIMP1 induction leading to PC differentiation (Laidlaw and Cyster, 2020).

While these are the most studied mechanisms involved in the regulation of GC B-cell processes, this is a complex process with many other TFs and signaling pathways involved which might be relevant.

1.4. The role of the GC in disease

Without doubt, the GC reaction is indispensable to respond to pathogens or other substances but the high rate of B-cell proliferation and SHM that enables this reaction is not without risk for disease. Understanding the mechanisms of affinity maturation, and PC and MBC differentiation during the GC reaction are necessary for prevention or treatment of diseases. Understanding the GC reaction may help in the development of (improved) vaccines resulting in antibodies of higher affinity and specificity to increase their ability to stop chronic viral infection (Mesin *et al.*, 2016). The GC is involved in the development of most mature B-cell lymphomas, and drives autoAb-driven autoimmune diseases. In addition, SHM may lead to the production of auto-Abs. If negative selection fails then this may result in auto-immune disease (Bönelt *et al.*, 2019). The combination of SHM and high B-cell proliferation may lead to GC-derived malignancies (Bönelt *et al.*, 2019) but this comes at the expense of a non-negligible probability that, for example, during affinity maturation within GCs, off-target SHM can take place initiating B-cell malignancies such as B-cell lymphomas, which mostly derive from GC B cells (Attaf *et al.*, 2021). Importantly, most mature B-cell lymphoma originates from GC B cells. For instance, diffuse large B-cell lymphoma (DLBCL), the most common subtype of non-Hodgkin's lymphoma, is a GC derived, aggressive and heterogeneous disease (Alizadeh *et al.*, 2000). Abnormal expression of certain TFs, such as constitutive BCL6 expression, and consequent inactivation of IRF4 and BLIMP1, is key in promoting DLBCL by enforcing the proliferative phenotype of GC B cells, while suppressing DNA damage responses and by blocking PC differentiation (Basso and Dalla-Favera, 2012). Ectopic GCs can be generated in inflamed local tissue (e.g., lungs, skin, nasal mucosa) during an allergic reaction (Gatto and Brink, 2010). Allergic reactions occur due to the presence of Ag-boung-IgE Abs produced locally by PCs (Coker *et al.*, 2003). The latter study suggested that SHMs and CSR of high affinity B-cells exiting the ectopic GC reaction could lead to the generation of IgE producing PCs.

1.5. Repertoire sequencing experiments

Naïve and GC generated AgR repertoires in blood or tissue can be profiled using next generation sequencing technologies (Robinson, 2015; Liu *et al.*, 2021). These BcR and TcR repertoire sequencing experiments have been applied for a broad range of applications including vaccinology, infection, and (auto)immune disorders (van Schaik *et al.*, 2014; Galson *et al.*, 2015; Wang *et al.*, 2015, 2019; Bashford-Rogers *et al.*, 2019; Nakagawa *et al.*, 2021). Typically, the pre-processing of repertoire sequencing results in a set of clones and their abundances in the measured samples. Additional bioinformatics analyses are then performed to address the specific research question (Greiff *et al.*, 2015). A specific (auto)immune response will skew the BcR repertoire towards Abs binding the Ag. Although repertoire sequencing does not provide information about

binding affinities, it is generally assumed that higher abundant clones (dominant clones) have higher affinities due to their Ag-driven expansion and selection in GCs. Therefore, in principle, dominant clones that have expanded in the GC provide good candidates to further characterize, for example, binding specificity and affinity, neutralization capacity, and functional properties (Marks and Deane, 2020). Nevertheless, it would be interesting to know: (1) the relation between clonal abundance and affinity, (2) the variation of binding affinities within a clone and (3) the effect of inflated PC and/or MBC mRNA on the abundance measurement. Unfortunately, measuring the binding affinity for hundreds or thousands of clones resulting from repertoire sequencing is virtually infeasible.

1.6. Computational modeling to study biological systems

1.6.1. Complexity of biological systems

The degree to which gene regulatory networks (GRNs) affect cell behaviors is crucial to understand the processes of life. The elucidation of these networks and their regulation of cellular processes is a complex task due to (1) their spatiotemporal dynamics; (2) the large-scale nature of GRNs; (3) the (unknown) interactions between the individual components to generate a collective behavior; (4) the non-linearity of this collective behavior due to, among other factors, the presence of regulatory mechanisms such as feedback or feedforward (Janson, 2012). To fully understand biological processes a synergistic approach between experimenting and computational modeling is necessary. As part of this integrative approach, computational models have been used to study the dynamics of biological systems at different scales starting from the molecular level to cellular, tissue, organs, and even the whole organism level. Multiscale approaches have been developed and applied to combine different scales (Cappuccio *et al.*, 2016).

Systems biology is an integrative discipline that combines a wide range of experimental and modeling methods to understand complex biological systems (Ma'ayan, 2017). Systems medicine stems from systems biology, implementing and translating the more basic approaches to applied clinical research and practice to the direct benefit of patients (Kolch and Fitzmaurice, 2017). Systems medicine involves the implementation of such computational approaches in medical concepts, research and practice (Stéphanou *et al.*, 2018).

A model is an abstract representation of a system that can be turned into a mathematical or computational description, which can be used to understand the functioning of the system, as well as for suggesting new hypotheses, making predictions, studying emergent properties and developing new experimental designs. Models can be mathematical and/or computational. Multiscale models **(**MSMs) can be used to integrate mathematical and computational descriptions of

processes operating at different spatial, temporal and organizational levels (Eftimie *et al.*, 2016).

1.6.2. Model developing steps

The process of building models is similar across all modeling methods. While the details may slightly vary from one to another, a general understanding of the common steps, and the underlying assumptions needed for the analysis, provides a useful framework in which the results can be interpreted. The basic steps are: (1) data preparation and understanding, (2) model assembly, (3) model validation and (4) model delivery (Biecek, 2019). Once the experiment is designed, the data is collected, carefully selected and there is a general understanding of the dataset, a model is constructed that is in agreement with the measurements. New models can emerge from the combination of old models. Further, parameter estimation methods are used to estimate unknown parameters. Then, a careful assessment of the model is done, if there is a good fit between experimental data and the data generated by the model some of the model assumptions might be validated. Otherwise, the process is repeated until the model appropriately fits the data. Finally, decisions that lead to the final model need to be documented in an understandable way using reports, graphs, tables, and other communication strategies (Biecek, 2019).

1.6.3. Ordinary differential equation modeling

Ordinary differential equation (ODE) models are mathematical models that can be defined, in the simplest scenario, involving a function f(x), of a dependent variable, such as a TF concentration (x), and its derivative with respect to an independent variable, such as time (t) (Eq 1) (Rodriguez-fernandez and Iii, 2013).

Eq 1: $$\frac{dx}{dt} = f(x)$$

The function f(x) generally contains one or more (unknown) parameters, such as kinetic parameters in the case of molecular reactions. A solution to the equation, a function of the independent variable, can be obtained when specifying an initial value for the dependent variable. This can be done numerically or in special cases, analytically. ODEs can then be used to simulate the dynamics of the dependent variable. This can be applied to the study of mechanisms of biological processes (Rodriguez-fernandez and Iii, 2013).

ODE models can be used to represent the structure of GRNs by specifying the regulatory relations between genes and the signalling pathways involved. They have been typically used to quantitatively study the dynamics of GRNs, which cannot be obtained from only the topology of a network (Bruggeman *et al.*, 2013). Parameters, representing production, binding, decay and other molecular processes, can be estimated using, for example, time-resolved microarray gene

or protein expression data (Rodriguez-fernandez and Iii, 2013). The system can be formulated in terms of reaction-rate equations and kinetics, such as the law mass action and Michaelis-Menten kinetics. Dynamics of a GRN includes changes in the concentration of a TF with respect to time. When the rates of production of all the molecules equal the rates of decay the system is considered to be in steady states. Transition between steady states can only be driven by perturbation of the system (Bruggeman *et al.*, 2013).

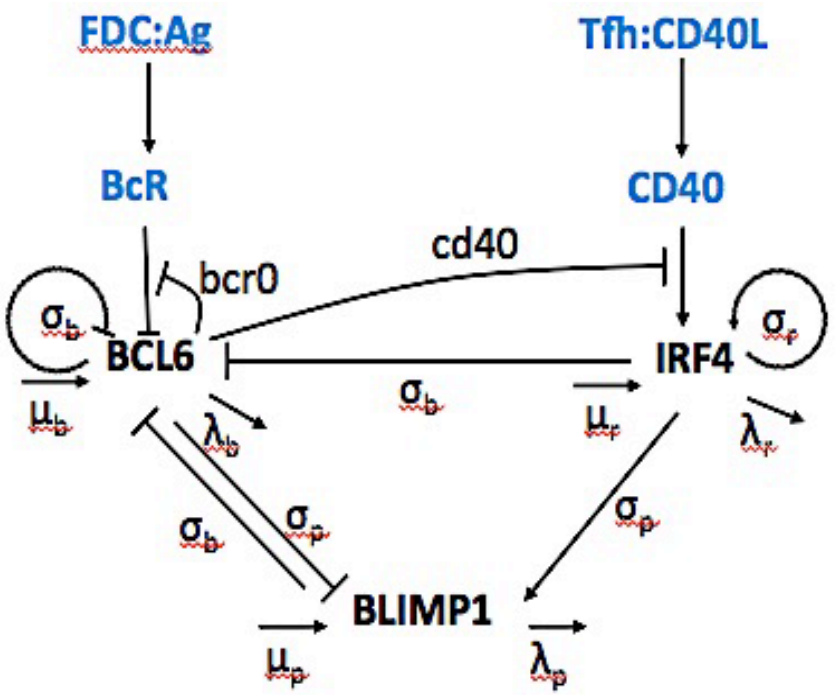

$$\frac{dp}{dt} = \mu_p + \sigma_p \frac{k_b^2}{k_b^2 + b^2} + \sigma_p \frac{r^2}{k_r^2 + r^2} - \lambda_p p$$

$$\frac{db}{dt} = \mu_b + \sigma_b \frac{k_p^2}{k_p^2 + p^2} \frac{k_b^2}{k_b^2 + b^2} \frac{k_r^2}{k_r^2 + r^2} - (\lambda_b + bcr0 \frac{k_b^2}{k_b^2 + b^2})b$$

$$\frac{dr}{dt} = \mu_r + \sigma_r \frac{r^2}{k_r^2 + r^2} + cd40 \frac{k_b^2}{k_b^2 + b^2} - \lambda_r r$$

Figure 5: Diagram and mathematical equations of a model representing a GRN involved in PC differentiation. This model can be translated to a system of ODEs that incorporate the parameters shown in this network. TFs are represented as follows, BCL6 (b) IRF4 (r) and BLIMP1 (p); and rates of the different B-cell reactions are defined as follows, basal transcription (μ), degradation (λ), maximal induced transcription (σ), range of BCR-induced degradation of BCL6 (bcr0) and range of CD40-induced transcription of IRF4 (cd40). Nodes represent molecules or molecular complexes. Arrows and bar-headed lines between nodes indicate activation or inhibition. Signaling inputs and receptors are indicated in blue.

ODEs are complex and often unresolved. Nevertheless, a previous study of an ODE model describing a GRN comprising three TFs was assumed to provide sufficient explanation to describe terminal B-cell differentiation into PCs in the GC (Martínez *et al.*, 2012). The three key TFs were BCL6, BLIMP1 and IRF4, which regulated each other and were affected by BcR and CD40 signaling with a total of six interactions (Figure 5). Steady-state analysis of the BCL6 and BLIMP1 expression levels for different values of BcR stimulation shows a bistable regime characterized by the existence of three steady-states, two stable and one unstable. One of the stable steady-states is characterized by high BCL6 and low BLIMP1 levels, representing GC B-cell state, while the other one is characterized by low BCL6 and high BLIMP1 levels, representing PC state. Increasing BcR stimulation moves the system form the GC B-cell closer to the PC state. In the absence of CD40 signal, this is a reversible process when decreasing the total BcR signal strength. Thus, BcR stimulation does not explain the irreversible nature of PC differentiation. Further analysis of the system shows a bistable behavior dependent on the ratio of all IRF4 synthesis to degradation kinetic parameters. Upon CD40 stimulation, low ratios result in a system with only one steady state resulting in the return of the IRF4 level when CD40 signalling is aborted. For intermediate ratios, a bistable behavior is observed corresponding to GC B-cell and PC steady states. Finally, high ratios lead to irreversible transition towards the single PC state caused by the IRF4 positive feedback loop. Such finding indicated the critical role of CD40 signal in increasing the IRF4 concentration, which then drives PC development.

1.6.4. Agent based modeling

Agent based models (ABMs (Chaudhry, 2016)) are computational models that evolved from cellular automata (CA (Malleta and Pillis, 2006)) models and are used to study complex behaviors that emerge from the interactions of individual entities or agents. ABM allows a biological system to be modelled with a collection of agents that interact and make decisions on the basis of a set of pre-defined rules. Agents have different states and may also interact with their environment for a defined period of time. Interactions can be modeled using rates or probabilities introducing stochasticity in the system. In contrast to deterministic ODE models, ABMs remain valid in small size (discrete) populations where stochastic effects have an important role (Meyer-Hermann *et al.*, 2009). Time and space representation are discrete although lattice-free approaches have been used (Glen *et al.*, 2019). ABMs are useful when the individual behavior is nonlinear, discrete, heterogeneous, has memory, path-dependence and/or include learning and adaptation. Furthermore, they are an efficient tool to study spatial dynamics of a system. Nevertheless, they require a complex internal state and space representation, which can be a limitation for empirical validation and rules can be heuristic. Since ABM are stochastic multiple simulations must be performed to assess the model's behavior, which can become computation intensive and time consuming. (Bonabeau, 2002).

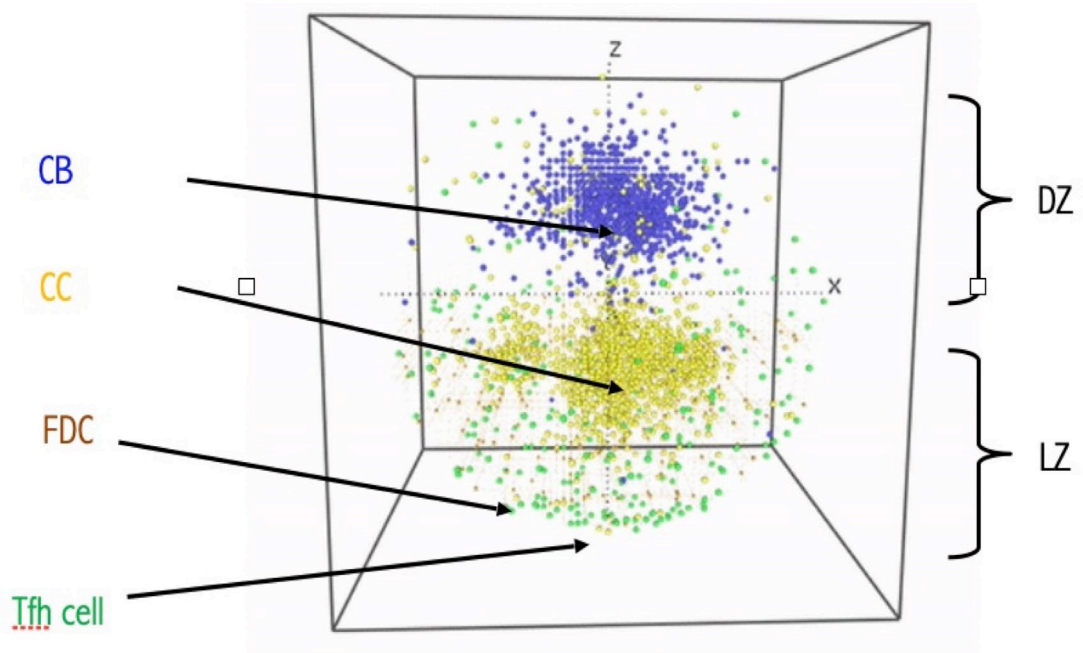

Figure 6: ABM in which the GC is represented as a 3D spherical grid. The DZ and LZ are separated by an x-y plane. Cells are represented as spheres that occupy a single grid point. In the DZ, B-cells have a CB phenotype (blue). In the LZ, the B-cells have a CC phenotype (yellow). FDCs (brown) and Tfh cells (green) are restricted to the LZ.

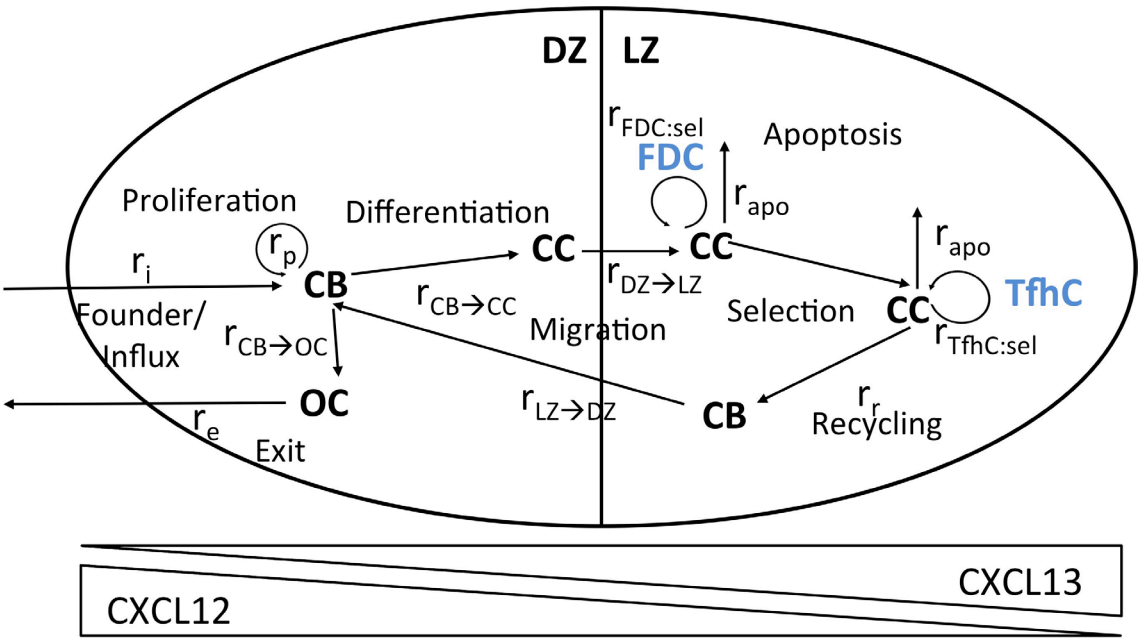

Figure 7: Diagram of the ABM B-cell processes in the GC, which take place in the DZ or LZ. Nodes represent B-cells with three different B-cell states: CCs, CBs and output cells (OCs).. OCs represent the collection of PCs and MBCs. Arrows between nodes indicate processes that take place. Rates of the different processes are defined as follows: influx (r_i), proliferation (r_p), differentiation ($r_{CB\to CC}$, $r_{CB\to OC}$), apoptosis (r_{apo}), zone migration ($r_{DZ\to Lz}$and $r_{LZ\to DZ}$), selection ($r_{FDC:sel}$ and $r_{TfhC:sel}$), recycling (r_r) and exit (r_e). The GC reaction is initiated with one or more founder CBs in the GC or with a pre-defined rate of inflow. Proliferation of recycled CBs can be asymmetric. CBs may undergo SHMs. The GC has two zones, namely the DZ and LZ. Spatial chemokine gradients of CXCL12 and CXCL13 are represented below the GC. CXCL12 is mainly present in the DZ and CXCL13 in the LZ, and are responsible for the directed movement of the cells.

As an example, an ABM model of the GC reaction, named hyphasma, has been developed based on experimental data and current knowledge of the GC. (Meyer-Hermann *et al.*, 2012). The GC is represented by a 3D-sphere of grid points (Figure 6). Two predefined chemokine gradients are imposed on the sphere representing the zonal GC structure. Agents are the cells that are present during the GC reaction and comprise B cells, FDCs, Tfh cells and output cells (OCs), which comprise MBCs and PCs but for which no distinction is made in the model. Different cell types are governed by different sets of rules reflecting the main biological processes that take place during the GC reaction. From a mechanistic perspective, the rules determine the cellular dynamics by defining B-cell motility, DZ B-cell division and SHM, transition between DZ and LZ, LZ B-cell apoptosis, LZ B-cell Ag acquisition through their interaction with FDCs and positive selection by Tfh cells during the selection process, DZ B-cell differentiation towards OCs (Figure 7). Rates are formulated into probabilities or internal time clocks. As aforementioned, the computational study showed that B cells selected by Tfh cells after successful Ag processing always return to the DZ for asymmetric division (Meyer-Hermann *et al.*, 2012). Acquired Ag is inherited by one daughter cell only. Ag-retaining B cells differentiate to OCs and leave the GC through the DZ. Such findings resulted in an early emergence of high-affinity Abs and increased amount of derived PCs.

1.6.5. Multiscale modeling

MSMs aim to connect two or more models constructed for different time and/or space scales (Versypt, 2021). MSMs provide a useful framework to investigate immune processes because it allows integrating the molecular (e.g., GRN, metabolism) and cellular (e.g., proliferation, differentiation) mechanisms. This enables, for example, the possibility to investigate the effect of molecular perturbations (e.g., dysregulation of TFs) on the cellular level (Eftimie *et al.*, 2016). Combining an ABMs with ODEs can be a useful way to substitute heuristic ABM rules with GRN that determine cell behavior, and which can be based on experimental (omics) data. Nevertheless, the connection of different levels in these models has their own challenges. Firstly, we may lack knowledge how a molecular network affects a cellular process. For example, how do transcription factors like c-Myc control the number of B-cell divisions in the GC DZ or, vice versa, how do signals like CD40 and BcR signaling affect the levels of the TFs In most cases this requires further experimental studies but, alternatively, we can attempt to simplify the model without sacrificing its utility too much. Secondly, processes modeled in a MSM will generally take place at (largely) different temporal and spatial scales. For example, the transcription of a gene and translation to a protein takes place in the order of minutes to hours. The subsequent interaction of the proteins as part of a molecular network evolves over hours to days. These networks will then determine the progression of the GC reaction with a duration in the order of weeks to months. The basic question is how we can understand and predict this long-term GC reaction in terms of molecular events that are of much shorter duration. Finally, MSMs can become very computationally intensive when aiming to model long-term (GC) processes

at a time scale of the fastest (molecular) processes. (Noble, 2012). Stochastic simulation algorithms, such as the Gillespie algorithm, can be used to model systems of stochastic equations efficiently and accurately while decreasing computational power and time. This can be done through the discretization of the time of the simulation. The time resolution can be made reaction-dependent such that at each time step, reactions that will be solved can be selected based on their rate constants (Thomas *et al.*, 2019). While this selection procedure also has a computing cost, it allows for faster reactions to have a smaller time scale than slower ones. Nevertheless, it is still an open question what is the best way to combine different time scales.

1.7. Outline of thesis

We have developed a MSM of the GC reaction to investigate PC differentiation, asymmetric B-cell division, and the development of diffuse large B-cell lymphoma (DLBCL). In **Chapter 2** we introduce the model in which we have integrated two pre-existing models. One model is the so-called LEDA ABM developed by Meyer-Hermann and collaborators (Meyer-Hermann *et al.*, 2012). This model comprises the most comprehensive model of the GC available today, and basically represents the cellular processes of the GC reaction. The second model is a GRN comprising three TFs ((BCL6, IRF4, and BLIMP1), which are assumed to represent the core network in PC differentiation. This model includes BcR signalling to account for the interaction of the BcR with the Ag, and CD40 signalling to account for the interaction of the B-cell with the Tfh cells. This network is represented by a system of ODEs and was developed by Martínez and co-workers (Martínez *et al.*, 2012). We used the ODE model to replace some of the heuristic ABM rules that control PC differentiation. We used the resulting MSM to investigate the role of asymmetric Ag division, opposed to BLIMP1 expression, in PC differentiation. In particular we considered the role of Tfh cell help and CD40 signaling. This work raised new questions with respect to the role of asymmetric division of Ag and TFs in PC differentiation. In **Chapter 3** we investigated the extent to which asymmetric segregation of Ag and/or TFs (BCL6, IRF4, and BLIMP1) recapitulates known dynamics of the GC reaction and PC differentiation. In **Chapter 4** we apply the MSM to investigate the effect of common genetic alterations in DLBCL on the cellular level. We investigated eight different scenarios comprising different (combinations of) alterations to demonstrate how a GC MSM can be used to predict how genetic defects affect cellular behavior and may result in B-cell lymphoma. Finally, in **Chapter 5** we use our model to enhance the interpretation of B-cell repertoire sequencing data. In particular we show how affinity is potentially related to clonal abundances measured in typical repertoire sequencing experiments, and how MBCs and/or PCs can disturb the identification of dominant clones.

Chapter 2

Multiscale modelling of germinal center recapitulates the temporal transition from memory B cell to plasma cell differentiation as regulated by antigen affinity-based Tfh cell help

Elena Merino Tejero[#], Danial Lashgari[#], Rodrigo Garcia Valiente, Xuefeng Gao, Fabien Crauste, Philip A Robert, Michael Meyer-Hermann, María Rodríguez Martínez, Marieke van Ham, Jeroen E.J. Guikema, Huub Hoefsloot, Antoine H.C. van Kampen

[#]Equally contributed

2.1. Abstract

Germinal Centers (GCs) play a key role in the adaptive immune system since they are able to produce Memory B cells (MBCs) and plasma cells (PCs) that produce high affinity antibodies (Abs) for an effective immune protection. The mechanisms underlying B-cell-fate decisions are not well understood but asymmetric division of antigen (Ag), B-cell receptor (BcR) affinity, interactions between B-cells and T follicular helper (Tfh) cells (triggering CD40 signaling), and regulatory interactions of transcription factors (TFs) have all been proposed to play a role. In addition, a temporal switch from MBC to PC differentiation during the GC reaction has been shown. To investigate if Ag affinity-based Tfh cell help recapitulates the temporal switch we implemented a multiscale model (MSM) that integrates cellular interactions with a core gene regulatory network (GRN) comprising B-cell lymphoma 6 (BCL6), interferon regulatory factor 4 (IRF4), and B-lymphocyte-induced maturation protein 1 (BLIMP1). Using this model, we show that affinity-based CD40 signaling in combination with asymmetric division of B-cells result in switch from MBC to PC generation during the course of the GC reaction. We also show that cell fate division is unlikely to be (solely) based on asymmetric division of Ag but that BLIMP1 is a more important factor.

Altogether, our model enables to test the influence of molecular modulations of the CD40 signaling pathway on the production of GC output cells (OCs). [1]

2.2. Introduction

GCs are anatomical structures located inside B-cell follicles within secondary lymphoid organs that play an important role in the adaptive immune system (Meyer-Hermann *et al.*, 2012; N. S. De Silva and Klein, 2015). Through subsequent rounds of cell proliferation, SHM and positive selection the BcR is optimized for Ag binding in a process called affinity maturation. This eventually results in the development of MBCs and PCs that produce high affinity Abs, which provide an effective immune protection. GCs comprise two functional zones. In the dark zone (DZ), centroblasts (CBs) rapidly proliferate and accumulate somatic hyper mutations (SHMs) in the genes that encode their BcR. The light zone (LZ) is mainly characterized by the presence of centrocytes (CCs), follicular dendritic cells (FDCs) that present Ag in the form of immune complexes to GC B cells (Allen and Cyster, 2008), and Tfh cells. CCs capture and internalize Ag through their BcR in an affinity-dependent manner triggering survival signals. Subsequently, the Ag is processed by the CCs resulting in histocompatibility molecules II (pMHCII) presented to the Tfh cells. Hence, B cells compete in an affinity-dependent way for interaction with Tfh cells, facilitating CD40 and cytokine signaling to become positively selected. Positively selected CCs may return to the CB state and recycle to the DZ to undergo further rounds of proliferation and SHM. Alternatively, positively selected CCs may differentiate to MBCs or PCs (Kräutler *et al.*, 2017; Higgins *et al.*, 2019; Ionescu and Urschel, 2019; Ise and Kurosaki, 2019; Shlomchik *et al.*, 2019). Recently, it was also shown that GC B-cell migration influences PC development (Reimer *et al.*, 2020) The cellular and molecular mechanisms that regulate PC and MBC differentiation remain largely unknown, while such knowledge would crucially advance our understanding of GC-associated diseases such as B-cell lymphomas and autoimmune disorders. In this research we present a MSM integrating molecular and cellular mechanisms to investigate PC differentiation.

In vivo studies in which Tfh-dependent positive selection of CCs was triggered in a BcR-independent fashion using the DEC205 surface lectin indicated that the interaction of CCs with Tfh cells critically determines positive selection and subsequent generation of PCs (Victora *et al.*, 2010; Shulman *et al.*, 2014).

[1] This chapter is based on Merino Tejero E, Lashgari D, García-Valiente R, Gao X, Crauste F, Robert PA, Meyer-Hermann M, Martínez MR, van Ham SM, Guikema JEJ, Hoefsloot H, van Kampen AHC. Multiscale Modeling of Germinal Center Recapitulates the Temporal Transition From Memory B Cells to Plasma Cells Differentiation as Regulated by Antigen Affinity-Based Tfh Cell Help. Frontiers in immunology (2021) 11:620716.

Other studies suggested that BcR signaling, but not Tfh interaction, initiates PC differentiation (Arpin *et al.*, 1995; Kräutler *et al.*, 2017; Luo *et al.*, 2019; Shlomchik *et al.*, 2019). The role of BcR signaling in PC differentiation is supported by the observation that long-lived PCs in bone marrow produce high-affinity Abs that contain many SHMs (Smith *et al.*, 1997; Phan, 2006; Chan and Brink, 2012; Kräutler *et al.*, 2017). Smith and co-workers showed that the extend of affinity maturation of MBCs and PCs differs for NP hapten-specific B-cell responses typically resulting in high-affinity PCs and low-affinity MBCs (Smith *et al.*, 1997). Other work suggested a temporal switch during the GC reaction resulting in the production of MBCs primarily during the early GC phase while long-lived bone-marrow (BM) PCs are generated at later stages (Florian J Weisel *et al.*, 2016). In support, Shinnakasu and co-workers showed that lower affinity cells at earlier stages of the GC reaction are favored to enter the MBC compartment and also suggested that high-affinity GC B cells are preferentially selected to enter the cell-cycle and undergo PC differentiation (Shinnakasu *et al.*, 2016).

Previously, an agent-based model (ABM) was developed that assumes that all CCs positively selected by Tfh cells subsequently recycle to the DZ for further proliferation, mutation and differentiation (Meyer-Hermann *et al.*, 2012). Experimental evidence for this model was in part provided by demonstrating PC precursors in the DZ (Kräutler *et al.*, 2017; Ise *et al.*, 2018; Steiniger *et al.*, 2020). This computational model was dubbed LEDA (LEave the GC through the DArk zone) and distributes the captured Ag asymmetrically during cell division to the daughter cells. The Ag-retaining cells differentiate into PCs and leave the GC (Meyer-Hermann *et al.*, 2012). Other models were investigated in this paper, such as LEDAX, in which the decision about differentiation is already taken during the interaction with Tfh cells in the LZ irrespective of asymmetric division. A probabilistic decision is made after symmetric division in the DZ to decide if the B-cell differentiates to an output cell or heads for another round of selection. Nevertheless, we wanted to test the effect of asymmetric division on PC differentiation and, therefore, we used the LEDA model as a starting point. However, direct experimental evidence that asymmetric division determines cell fate is lacking.

A large body of research focuses on the molecular mechanisms underlying PC and MBC differentiation including epigenetics (Herviou *et al.*, 2019; Azagra *et al.*, 2020; Fujii *et al.*, 2020), the role of various TFs, and GRN (e.g., (Nutt *et al.*, 2011; Davidzohn *et al.*, 2019; Roy *et al.*, 2019; Liu *et al.*, 2020)). Our MSM is built on a core GRN comprising three TFs (BCL6, IRF4, and BLIMP1) that are directly involved in PC differentiation. The TF BLIMP1 is essential for PC differentiation and regulates a large number of target genes required for the function of these cells (Minnich *et al.*, 2016). For example, BLIMP1 represses class II transactivator (CIITA) and activation-induced cytidine deaminase (AID), thereby inhibiting Ag presentation and GC associated AID-dependent Ig gene diversifications, respectively (Piskurich *et al.*, 2000; Minnich *et al.*, 2016). BLIMP1, however, may not initiate PC differentiation which has been suggested to start by down-regulation of the Paired Box 5 (PAX5) and BCL6 proteins, which

supports the theory that BcR signaling, resulting from BcR – Ag interaction, initiates this process (Kräutler *et al.*, 2017). BcR signaling results in the repression of BCL6 (Basso and R. Dalla-favera, 2010), which is an important factor for BcR diversification and sustained cell proliferation. However, other studies have shown that IRF4 initiates plasmablast (PB) differentiation by inducing expression of BLIMP1 (Kwon *et al.*, 2009; Muto *et al.*, 2010). This does not exclude the possibility that BcR signals are involved in increasing IRF4 levels. CD40 signaling, resulting from CC – Tfh interaction, upregulates IRF4, which subsequently activates BLIMP1 and leads to PC differentiation. In PCs, IRF4 can also bind to its own promoter to create a positive feedback mechanism that maintains high IRF4 expression and, consequently, BLIMP1 expression (Shaffer *et al.*, 2009). BLIMP1 is generally considered to repress gene expression but it may also induce gene expression of IRF4 and other genes (Minnich *et al.*, 2016). BCL6 is highly expressed in GC B cells and inhibits both the expression of BLIMP1 and IRF4. BCL6 binds to its own promoter to inhibit its own transcription thereby resulting in an autoregulatory negative feedback loop (Basso and Dalla-Favera, 2015). In turn, BLIMP1 and IRF4 repress BCL6, which is down-regulated in PC differentiation.

It is challenging to integrate the cellular and molecular mechanisms involved in PC differentiation since details about the effect of cellular interactions through signaling on the underlying molecular networks are not known in full detail. Conversely, the effect of GRN states on cell behavior or phenotype also remains to be elucidated in more detail. Moreover, these mechanisms operate at different time scales. One way of proceeding is to model (affinity dependent) signals resulting from cellular interactions that affect the underlying GRN, which in turn determines cell fate. We present a MSM integrating molecular and cellular mechanisms to investigate PC differentiation. In particular, we integrate two pre-existing and published computational models: the cell-based LEDA model (Meyer-Hermann *et al.*, 2012) and a differential equation-based GRN including BCL6, IRF4, and BLIMP1 (Martínez *et al.*, 2012). This GRN model considers BcR and CD40 signals delivered to the B cells but it assumes that only the CD40 signal initiates and progresses differentiation. Other (cytokine-driven) signals during B/T-cell interactions are neglected in our model. Our MSM integrates and investigates asymmetric division and (affinity-based) CD40 signaling in PC differentiation.

Using this model, we show that affinity-based CD40 signaling in combination with asymmetric division result in MBC and PC generation in accordance with the temporal switch. In contrast, a constant strong CD40 signal does only result in PCs, while a constant weak signal results in MBC output throughout the GC reaction. We also conclude that cell fate division is unlikely to be (solely) based on asymmetric division of Ag since this does not result in the differentiation of all high-level BLIMP1 B-cells. Vice versa, PCs differentiated on the basis of high BLIMP1 levels are a mixture of cells with and without internalized Ag indicating that not only Ag retaining cells engage in differentiation. We propose experiments to validate our computational findings. Altogether, our model enables to test the

influence of molecular modulations of CD40 signaling pathway onto the production of MBC and PCs.

2.3. Methods

2.3.1. Computational model at the cellular level

The MSM that we developed is an extension of the pre-existing 'hyphasma' model, which is a detailed ABM of the GC that simulates the behavior of individual GC cells and their interactions (Figure 8A) (Meyer-Hermann *et al.*, 2012; Robert *et al.*, 2017). Under the so-called LEDA hypothesis, it assumes that output cells exit the GC from the DZ after asymmetric division. Here, we summarize the relevant aspects of this model. The model simulates a GC reaction for 21 days (504 hours) at a time resolution of 0.002 hours (7.2 seconds). Parameters for the ABM in our simulations are provided as Supplementary Files (Simulation_Parameters.pdf). The GC is represented as a three-dimensional sphere of grid points with N=64 grid points in each direction (lattice constant = 5μm). This grid hosts agents that represent CCs, CBs, Tfh cells, and FDCs. In addition, pre-calculated gradients of CXCL12 and CXCL13 chemokines are imposed on this grid. Originally, the ABM was initiated with a fixed number of three founder B cells (Meyer-Hermann *et al.*, 2012). However, in our simulations we assumed a continuous influx of, on average, 2 cells per hour in the first 96 hours resulting in approximately 100 founder cells accounting for the observation that early GCs are highly polyclonal (Tas *et al.*, 2016; Meyer-Hermann *et al.*, 2018). The behavior in terms of division, differentiation, interaction, and cell death between these cells is defined by a set of rules. CBs, CCs and Tfh cells move according to persistent random-walk based on chemokine gradients, while FDCs have a fixed position on the grid. The affinity of the BcR is defined as the Manhattan distance (L1 norm) between the BcR and the Ag within a four dimensional 'shape space' (Perelson and Oster, 1979; Meyer-Hermann *et al.*, 2001). This distance represents the minimum number of SHMs required for the BcR to acquire maximum affinity for the Ag. Hence, the BcR sequence is not explicitly encoded but rather the shape space position of a B-cell determines its BcR affinity. SHM moves the BcR one step in the shape space thereby increasing or decreasing the distance to the Ag, which is converted to an affinity value between 0 and 1 using a Gaussian weight function. The discrete nature of the shape space translates to 25 discrete affinity values (Supplementary Figures 1 and 2).

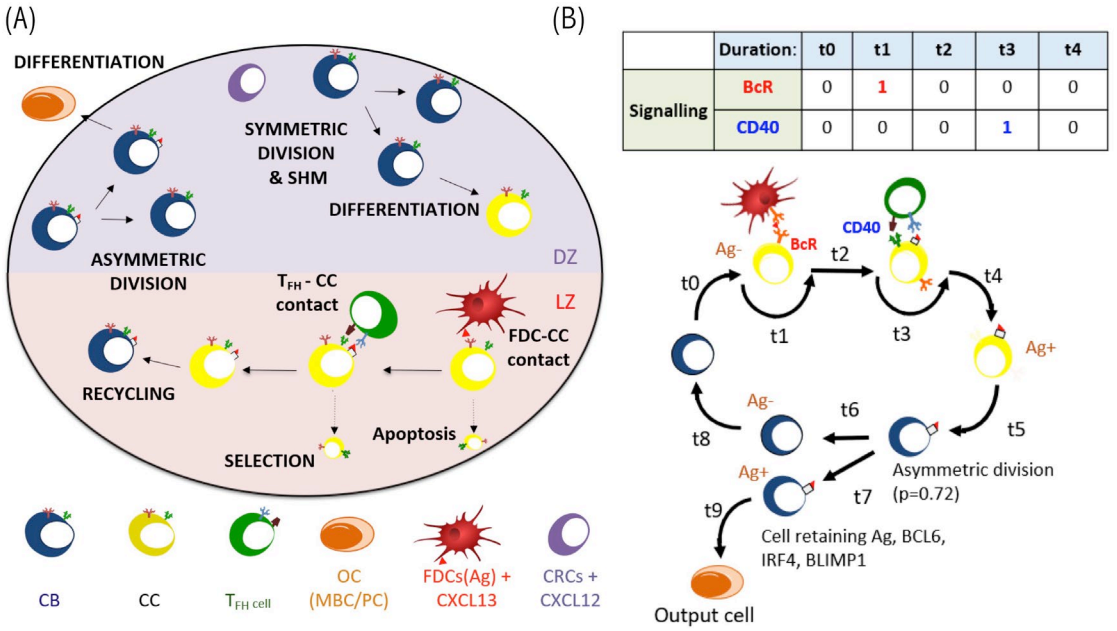

Figure 8: (A) Overview of cellular processes in the ABM. In an established GC a DZ and a LZ are distinguished. CBs and CCs prefer to move in the direction of the CXCL12 and CXCL13 chemokines produced by the CRCs and FDCs respectively. Tfh cells prefer to move towards the LZ. FDCs carry Ag that can be captured by CCs. CCs may be positively selected through interaction with Tfh cells after which they can recycle to the dark. In the DZ the CB will (a)symmetrically divide. After cell division, an output cell is produced, or the cell differentiates to a CC. Cells die through apoptosis if they do not interact with the FDC and Tfh cells. (B) Schematic overview of the BcR and CD40 signaling events during the GC reaction. Durations *t* indicate non-fixed time intervals (cell states). At the end of each interval the concentrations of BCL6, IRF4, and BLIMP1 are updated using the differential equations. A CB (Ag-; blue cell) differentiates to a CC (Ag-; yellow cell) within a time duration *t0*. The CC interacts with the FDC for a time duration *t1* during which BcR signaling occurs. Subsequently, CD40 signaling is active for duration *t3* during B-cell – Tfh interaction. Successful interaction will result in an Ag+ cell. Asymmetric division occurs with a probability p=0.72. Differentiation of CB to a CC always initializes the CC to Ag-.

In the model, B cells (CBs) proliferate in the DZ while accumulating BcR mutations, and migrate as CCs to the LZ where they can interact with FDCs to capture Ag with a rate depending on the BcR affinity. This provides survival signals to the CCs and rescues them from apoptosis. Higher affinity CCs will capture more Ag and, subsequently, will outcompete lower affinity CCs for Tfh interaction to become positively selected. If the Tfh interacts with many B cells at a time it will signal to the one with highest amount of internalized Ag. The positively selected CCs are recycled into CBs and migrate to the DZ for further rounds of division and SHM. The number of divisions of recycled CBs depends on the amount of captured Ag during the selection process. During cell division the Ag is asymmetrically distributed in 72% of the cell divisions (Thaunat *et al.*, 2012). Daughter cells that receive the captured Ag differentiate to output cells after one or more divisions and exit the GC. Daughter cells that did not receive Ag cycle back to the LZ as CCs. Daughter cells of CBs that divide symmetrically receive half of the Ag and both become CCs.

2.3.2. Computational model at the molecular level

Martínez and co-workers developed a computational model representing a core GRN involved in PC differentiation (Figure 9A) (Martínez *et al.*, 2012). This model includes three TFs, i.e., BCL6, BLIMP1 and IRF4 that are modeled by ordinary differential equations (ODEs). The level of these genes is controlled by the BcR and CD40 signals (Supplementary Information, Equations 1 to 5; Supplementary Table 1 lists the parameter values for the model). This GRN represents a bistable system with one state (BCL6 high, BLIMP1 and IRF4 low) denoting the CBs/CCs and a second state (BLIMP1 and IRF4 high, BCL6 low) representing PCs (Figure 9B).

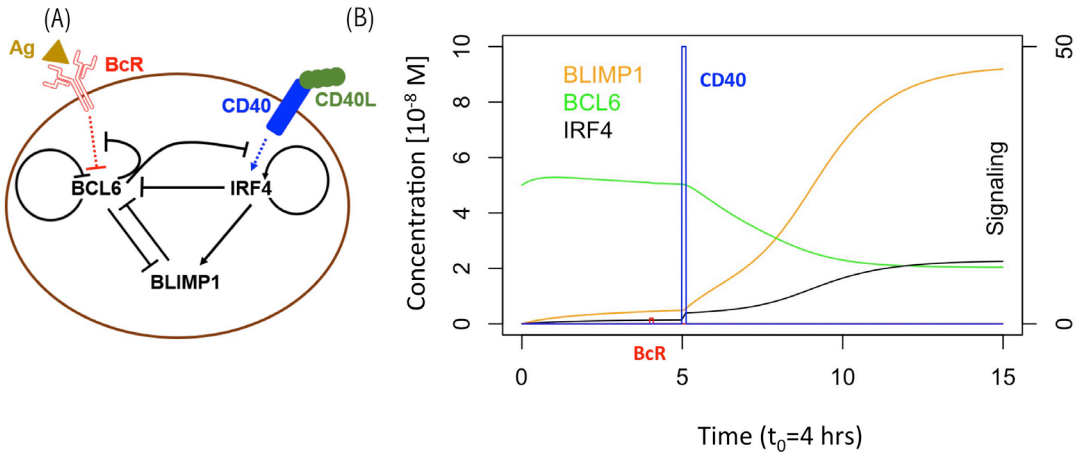

Figure 9: (A) B-cell with GRN and signaling events. Arrows indicate activation. Bar-headed lines denote inhibition. BCL6 is inhibited upon binding of the Ag to the BcR. IRF4 is activated upon binding of CD40L to CD40 during Tfh – B-cell interaction. (B) GRN temporal dynamics upon binding of Ag and CD40L. Each time unit represents 4 hours. The protein levels of BCL6 (blue), IRF4 (black) and BLIMP1 (orange) have units of 10^{-8}M and are shown over an interval of 60 hours. The BcR signal (red) and CD40 signal (green) are present for a short duration (*t1* and *t3* in Figure 8B). BcR signaling results in a slight temporary change in TF concentrations. In contrast, CD40 signaling results in a switch of all TF levels going from a B-cell to a PC (BLIMP1+) phenotype (in approximately 40 hours in this example). CD40 signal intensity in the multiscale model varies between 0 and 50. BcR signal is fixed to 1.

GC B cells integrate upstream signals from BcR and CD40 signaling pathways. When a BcR signal is induced through binding with the Ag, then BCL6 is degraded. However, its level is rapidly restored to the initial steady state (BCL6 high) when the signal is removed (unbinding of Ag). The CD40 signal induced during interaction with a Tfh cell increases transcription of IRF4, which in turn increases, the level of BLIMP1 resulting in the PC phenotype (BLIMP1+). This state is irreversible due to the positive autoregulatory feedback of IRF4 and the cooperative binding of the TFs to the DNA.

2.3.3. Multiscale model

To enable the investigation of cellular and molecular mechanisms involved in PC differentiation we integrated the ABM and the GRN through the embedding of the GRN (set of ODEs) in each individual B-cell and output cell of the ABM (Figure 10). This was achieved by adding additional properties (ODEs, (initial) TF levels, and BcR/CD40 signal) to each agent (cell) of the ABM.

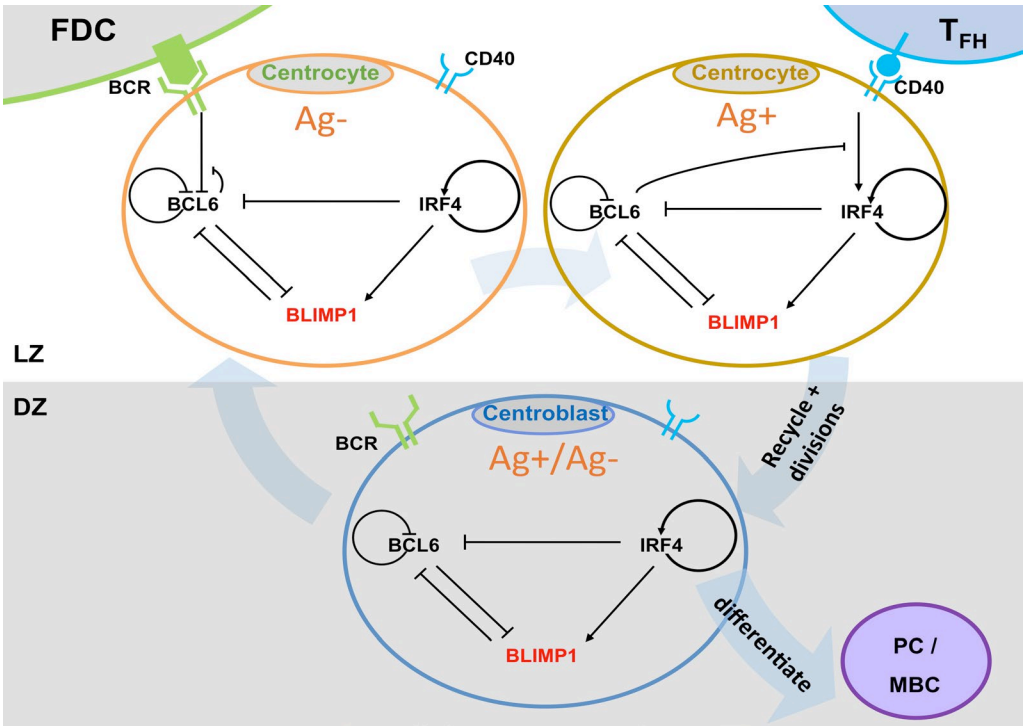

Figure 10: MSM for PC differentiation. The cellular ABM and molecular GRN ODE models are integrated by embedding the GRN in each B-cell and output cell of the ABM. Signals through the BcR (FDC interaction) and CD40 (Tfh interaction) change the state (TF concentrations) of the GRN, which is updated at every time step of the ABM. A positively selected CC becomes Ag+ by definition. In scenario 1 simulations an Ag+ cell differentiates to an output cell after asymmetric cell division. In scenario 2, sufficient CD40 signaling may increase BLIMP1 levels to obtain a PC phenotype (BLIMP1+). For precise cell type definitions see Table 2 and Supplementary Figures 6-8 and 20.

Founder cells and daughter cells resulting cell division are initialized with the same initial concentrations for BCL6, IRF4, and BLIMP1. The cell-based ABM and the GRN model operate at different time scales, e.g., weeks and hours respectively. Consequently, the relatively fast changes in the GRN affect the longer-term outcome on the cell level. This is accomplished by updating the TF concentrations at every time step (7.2 s) of the ABM while taking into account transcription and degradation rates, and using the levels of the TFs of the previous time point as initial values for the ODEs. If a CC binds to the FDC (Figure 8B) it receives a constant BcR signal (bcr0=1 in the ODE) for the duration *t1* of binding. If the CC binds to a Tfh cell it will receive a CD40 signal (see below) for the duration *t3* of binding. BcR and CD40 signals never occur simultaneously because binding to the Tfh cell only occurs after detaching from the FDC.

It has been shown that TFs may distribute unequally in daughter CBs after division (Lin *et al.*, 2015). Consequently, it has been hypothesized that asymmetric division may affect cell fate. Therefore, the MSM allows for asymmetric division of both Ag and the TFs with a probability of 0.72 (Meyer-Hermann *et al.*, 2012; Thaunat *et al.*, 2012). Following asymmetric division, the TF concentrations become zero in one daughter cell while the other daughter cell assumes the concentration from the parent cell. In a symmetric division the TF and Ag concentrations in both daughter cells are set to half the concentrations of the parent cell.

2.3.3.1. Tfh facilitated CD40 signaling

The MSM considers a constant or an affinity-based CD40 signal by defining cd40 (see Supplementary information Equations 1 – 5; Supplementary Table 1). The magnitude of the constant signal was set to 50 to ensure that after Tfh contact the BLIMP1 level of the B-cell sufficiently increases to eventually differentiate to a PC while also maintaining typical GC dynamics (e.g., CB and CC cell count profiles). For the affinity-based signal we assume that higher affinity B cells capture more Ag and present more pMHCII to Tfh cells resulting in an increased Tfh – B-cell interaction and, therefore, an increased CD40 signaling. The affinity-based CD40 signal was defined by setting cd40=affinity*50. Since affinity assumes values between 0 and 1, the CD40 signal has a strength between 0 and 50. This ensures that at maximum affinity the B-cell will always differentiate into a PC while at lower affinities MBCs will be produced (see below). Note that in simulations 3 and 4 (see below) higher values of the CD40 signal results in PC differentiation even after symmetric division (which reduces the BLIMP1 level by 50%) because the BLIMP1 level will rapidly return to its high-level equilibrium value due to the positive autoregulatory feedback of IRF4 that also remains at a relatively high level (Supplementary Figures 3 - 5).

2.3.3.2. Simulations

Table 1 shows the five simulations that were performed. The parameters for each simulation are provided as Supplementary Files. Scenario 1 simulations 1 and 2 represent a model in which asymmetric division of Ag determines cell fate. The Ag-retaining daughter cell (Ag+) differentiates to an output cell. In these simulations we tracked the CD40 signaling and the levels of the TFs but the GRN does not affect the fate of the B-cell and, therefore, does not affect the outcome of the simulation. However, after completion of Scenario 1 simulations we inspect the BLIMP1 level of the output cells to define a PC and MBC subset (see cell definitions below and Supplementary Figure 20). Scenario 2 simulations 3, 4 and 5 represent the model in which we use the BLIMP1 level to decide on cell fate. In these simulations cells with a high BLIMP1 concentration will differentiate to PCs regardless of the Ag state (Ag+ or Ag-) of the cell. For both cell-fate decision rules we compare results obtained with a constant and affinity-based CD40 signal. In simulation 5 we use a constant CD40 signaling with cd40=10. All simulations

are terminated after 21 days. In the result section we present the outcome of these 5 individual simulations. However, we also repeated Simulation 3 and 4 30 times with different random seeds, which shows that the amount of variability observed in the temporal dynamics (Supplementary Figures 16 – 19) is limited. Also, the resulting variability in the reported percentages is very low (standard error <0.01, most standard deviations <1%; Supplementary Tables 3 and 4). Scenario 1 simulations were not repeated but a similar amount of variability is expected.

Table 1: Definition of simulations.

		CD40 signal	
		Constant	**Affinity-based**
Decision rule for differentiation	**Ag inheritance** (Scenario 1)	Simulation 1 (CD40=50)	Simulation 2
	BLIMP1 level (Scenario 2)	Simulation 3 (CD40=50) Simulation 5 (CD40=10)	Simulation 4

2.3.3.3. Definition of (output) cells

Table 2 shows the definition of cell types in Scenario 1 (Ag+ decision rule) and Scenario 2 (BLIMP1+ decision rule) simulations. Supplementary Figures 6-8 and 20 provide further explanation. In Scenario 2 we do not explicitly discriminate between MBCs and PCs but define 'output' cells solely on the basis of its Ag status, i.e., the daughter cells that retains the Ag after asymmetric division (Ag+ cell) differentiates to an output cell (Meyer-Hermann *et al.*, 2012). In a post-simulation step we use the BLIMP1 level to classify the output cells to PCs (Ag+ and BLIMP1+; $\geq 8.10^{-8}$M) and MBCs (Ag+ and BLIMP1-; $<8.10^{-8}$M). We have defined MBCs in this way because a BLIMP1- cell does not represent a PC while in this model an Ag+ cell was defined as an output cell. Although this is not an ideal MBC definition it correctly recapitulates the MBC dynamics as observed in Weisel and co-workers (Florian J Weisel *et al.*, 2016). In the MSM a recycled CB is, by definition, Ag+ and goes through one or multiple rounds of divisions prior to differentiation to an output cell. Consequently, Ag+ cells represent a mixture of recycled CBs, dividing cells, and output cells. In Scenario 1, dividing Ag+ cells that have the potential to become a PC (i.e., Ag+/BLIMP1+) are annoted as PBs to allow a further discrimination between cell states in the model. In Scenario 1, Ag- output cells are non-existent by definition and, hence, all Ag- cells are CBs or CCs. In Scenario 2, cells may become a PC if they are BLIMP1+ irrespective of its Ag status and, consequently, PCs may either be Ag+ or Ag-. BLIMP1+ cells that are not (yet) output cells are annotated as PB (Ag+ or Ag-). In Scenario 2, Ag+/BLIMP1- output cells are considered to be MBCs.

Table 2: Definition of cell types based on Ag status and BLIMP1. NA = Not applicable.

		Scenario 1		Scenario 2	
		BLIMP1+	**BLIMP1-**	**BLIMP1+**	**BLIMP1-**
OUTPUT CELL	**Ag+**	PC	MBC	PC	MBC
NOT OUTPUT CELL	**Ag+**	PB	CB	PB	CB
OUTPUT CELL	**Ag -**	NA	NA	PC	NA
NOT OUTPUT CELL	**Ag-**	CB/CC	CB/CC	PB	CB/CC

2.3.3.4. Software

The MSM was implemented in C++ and simulations were done on a MacOS Mojave 10.14.5 operation system. Run times of a single simulation take approximately 8 hours on a single core of an Intel Core i7 processor. Model repetitions were carried out on the Dutch national e-infrastructure with the support of SURF Cooperative (www.surfsara.nl). Output files of the simulation were analysed in R (Core Team, 2019) version 3.5.3 using various libraries: forcats (0.5.0), purr (0.3.4), tidyr (1.0.3), tibble (3.0.1), ggplot(2_3.3.0), tidyverse (1.3.0), viridis (0.5.1), viridisLite (0.3.0), ggnewscale (0.4.1), readr (1.3.1), dplyr (0.8.5). The MSM is available from GitHub (https://github.com/EDS-Bioinformatics-Laboratory/MSM_PCdifferentiation).

2.4. Results

2.4.1. Ag inheritance-based GC output with constant and strong CD40 signal exclusively produces PCs (Scenario 1)

We wondered how the levels of BLIMP1 compared to internalised-Ag status (Ag+ or Ag-) in GC B-cell population when CD40 signal was constant and strong. This served as a reference for Scenario 2 simulations (Table 1). The Scenario 1 model is based on the hypothesis that Ag-retaining (Ag+) cells differentiate to a mixture of PC and MBC output cells. This theory in which asymmetric division drives PC differentiation resulting in PCs from the earliest stages of the GC reaction seems incompatible with the experimentally observed temporal switch (Florian J Weisel *et al.*, 2016). Figure 11A shows the overall dynamics of Simulation 1. The CB and CC counts show a typical GC response with the total cell count approximating about 3800 cells at 142 hours (6 days). Figure 11B shows the DZ-to-LZ ratio, which fluctuates around 2 in agreement with *in vivo* experiments (Victora *et al.*, 2010). Figure 12A shows the number of PCs during the GC reaction, which by definition emerge from the very initial stages of the GC reaction. Figure 12C

shows that the affinity of these PCs increases during the course of the GC reaction.

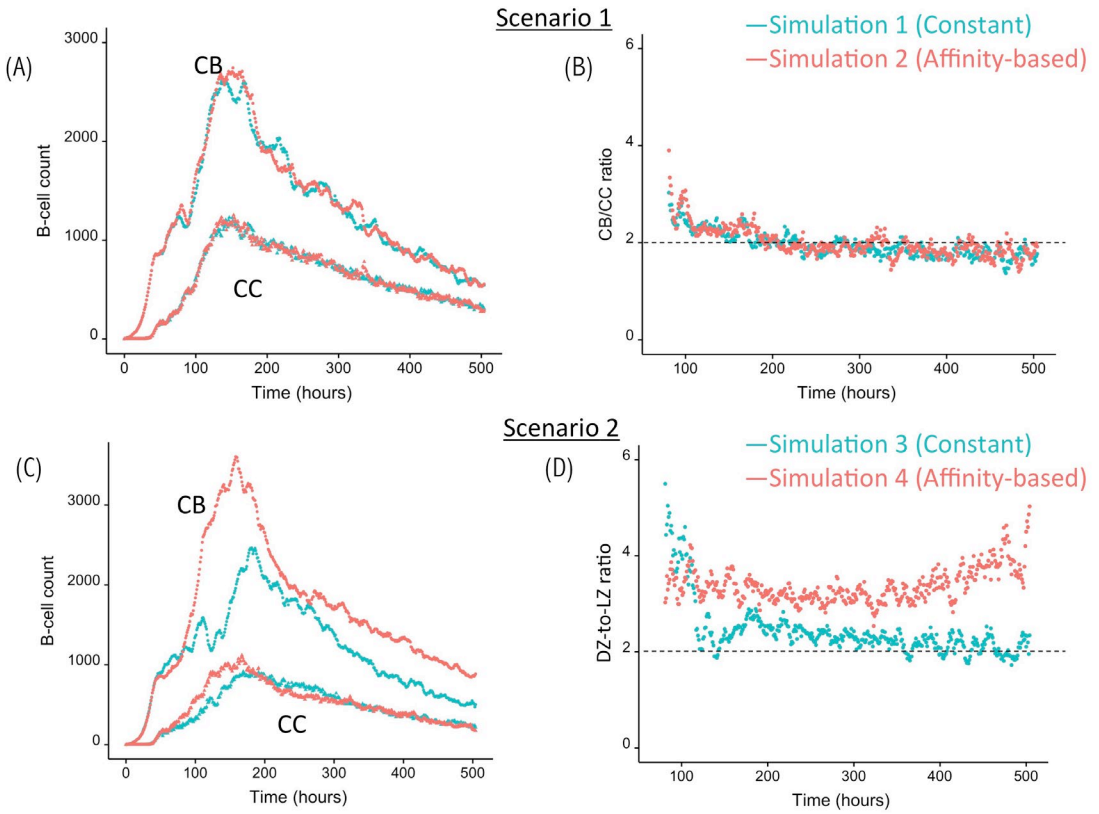

Figure 11: Overall GC dynamics with constant CD40 signal (CD40=50; blue) and affinity-based CD40 signal (red). (A) Scenario 1. Number of CBs (top curves) and CCs (bottom curves). (B) Scenario 1. DZ-to-LZ ratio calculated from CB and CC counts. (C) Scenario 2. Number of CBs (top curves) and CCs (bottom curves). (D) Scenario 2. DZ-to-LZ ratio calculated from CB and CC counts.

Table 3: Percentages of cell types at day 21.

	Scenario 1		**Scenario 2**		
	Constant CD40=50	Affinity-based	Constant CD40=50	Affinity-based	Constant CD40=10
PC	5	5	14	13	3
PB	20	19	28	26	18
MBC	0	0.3	0	0.3	2
CB/CC	75	76	58	61	77
	100.0	100.0	100.0	100.0	100.0

Table 3 shows the percentages of (output) cells at day 21 of the simulation. The full tables and cell counts are listed in the Supplementary File Table_Counts.xlsx. Inspection of the BLIMP1 level of the output cells facilitates post-simulation differentiation between PCs (Ag+/BLIMP1+) and MBCs (Ag+/BLIMP1-). During the GC reaction, about 5% (15,136 cells) of all CCs (290,291) differentiate to a PC (Ag+/BLIMP1+) while no MBCs (Ag+/BLIMP1-) are generated because the constant but strong CD40 signaling enforces high BLIMP1 levels for Ag+ cells. A fraction of PB (Ag+/BLIMP1+) cells do not develop into output cells due to symmetric cell division, which generates two Ag- daughter cells (Supplementary Figure 7). The subset of Ag- cells (CBs and CCs), which are not output cells nor PBs comprise a mixture of BLIMP1+ and BLIMP1- representing 12 and 62% of all cells respectively. Consequently, an additional maximum of 12% (36,124 cells) could potentially have developed into a PC if BLIMP1 level was considered as a criterion for differentiation. Figure 13A shows the distribution of PCs (Ag+/BLIMP1+), PBs (Ag+), and CCs/CBs (Ag-/BLIMP1- , Ag-/BLIMP1+). No MBCs are produced. CCs and CBs are distributed over all affinity classes and have BLIMP1 levels below the threshold ($<8.10^{-8}$M) that defines PCs. PCs (high BLIMP1 level) emerge from the early stages but their number and affinity increase with time. Finally, the figure shows an increasing number of Ag+ cells that increase in affinity over time but do are not output cells. About 79% of the subset of Ag+ cells did not develop into output cells despite their high BLIMP1 levels. In addition, about 17% of the Ag- cells are BLIMP1+.

In summary, the Scenario 1 model with constant CD40 signaling simulation produces PCs of low to high affinities but no MBCs due to the strong CD40 signal. Approximately 75% of the PCs are generated after the peak response of the output cells (Figure 12A; Supplementary Figure 9) and are of relatively high affinity due to ongoing affinity maturation (Figure 12C). A large fraction of the Ag+ cells are BLIMP1+ while most Ag- cells are BLIMP1-. Considering BLIMP1 levels of the Ag- cells, a larger number of PCs should potentially have been generated.

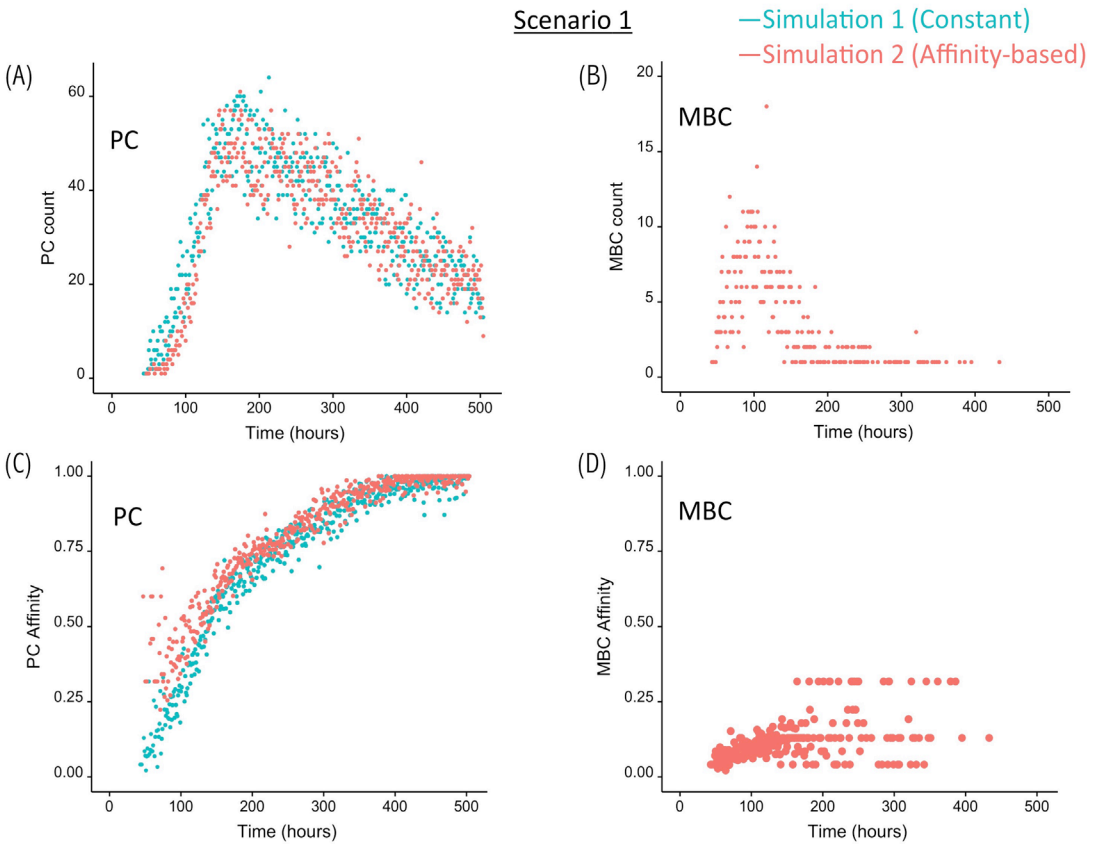

Figure 12: OCs for Scenario 1 simulations with a constant CD40 signal (CD40=50; blue) or affinity-based CD40 signal (red). (A) Number of PCs, (B) number of MBCs, (C) PC affinity, and (D) MBC affinity during GC reaction. Post-simulation inspection of BLIMP1 levels of the output cells (Ag+) allows to discriminate between PCs (Ag+/BLIMP1+) and MBCs (Ag+/BLIMP1-). No MBCs are produced with a constant CD40 signal.

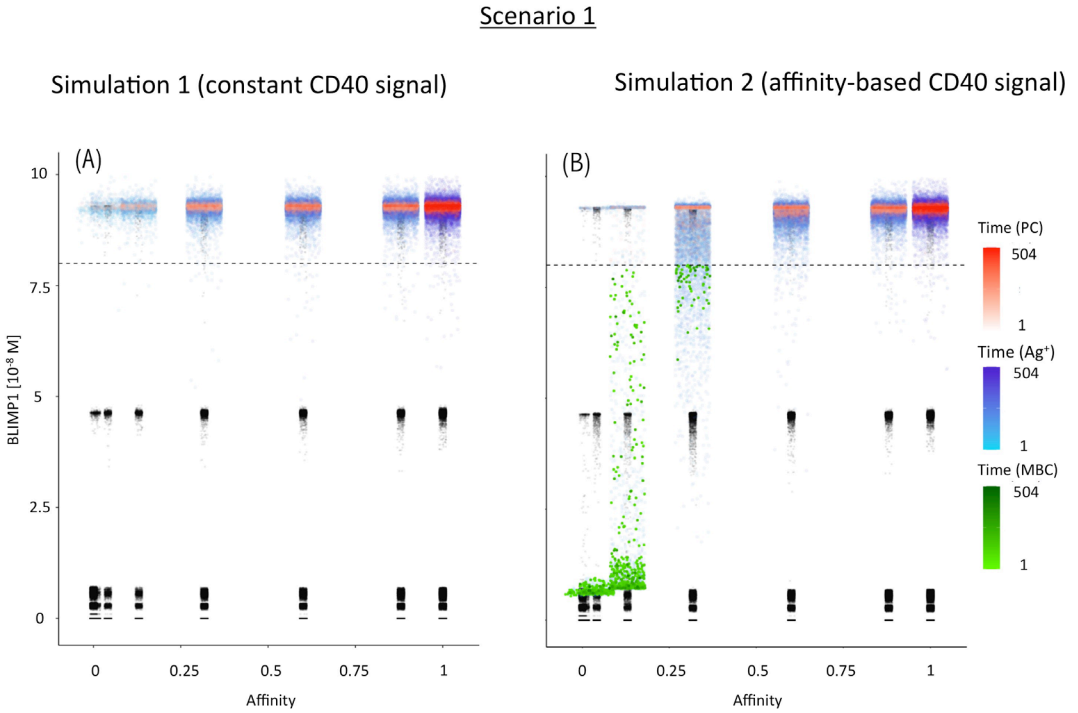

Figure 13: Distribution of PCs, MBCs, and Ag+ (but not PC/MBC) cells with respect to their affinity, BLIMP1 level, and time of generation for Scenario 1 simulations. (A) Constant CD40 signaling (no MBCs). (B) Affinity-based CD40 signaling (early MBCs). Each dot represents a cell. Black dots represent cells other than PCs, MBCs, Ag+. Color gradient represents time from 1 to 504 hours. Affinity assumes discrete values. Dotted line represents the BLIMP1 threshold ($8*10^{-8}$M) for PC differentiation. Intermediate BLIMP1 levels arise mainly due to symmetric division of cells with high BLIMP1 level. Since values are recorded only in case of an event (e.g., cell division, Tfh interaction, differentiation) and because of steep curve of the BLIMP1 profile after Tfh-cell contact, BLIMP1 levels seem restricted to particular values but are not. Low and high BLIMP1 levels represent steady-states. Jittering of affinity values has been applied to prevent too many overlapping data points but causes some overlap of the lower affinity classes.

2.4.2. Ag inheritance-based GC output with a strong affinity-based CD40 signal enables the production of both PCs and MBCs (Scenario 1)

Since no MBCs (Ag+/BLIMP1-) were generated in Simulation 1, we wanted to investigate the effect on output cell subsets (post-simulation) when applying an affinity-based CD40 signal to control the levels of BLIMP1. In this simulation (Simulation 2), the generation of output cells is still fully determined by Ag inheritance after asymmetric division and, consequently, CD40 signaling nor BLIMP1 level affects the cell fate or GC reaction. Consequently, the overall dynamics of this simulation is approximately the same as for the first simulation (Figure 11). Difference in overall dynamics result from stochasticity in the model. Figure 12A and 12C shows the number of PCs and corresponding affinity during the GC reaction. Figure 12B and 12D show the number of MBCs (Ag+/BLIMP1-) and affinity respectively. In contrast to Simulation 1, low affinity MBCs are

generated during the earlier phase of the GC response and generation of PCs seems slightly delayed although stochasticity in the model prevents a firm conclusion. The number of PCs at the end of the GC reaction is similar to Simulation 1 (5% of all cells corresponding to 14,303 cells; Table 3). In addition, 833 (0.3%) MBCs were generated. The number of PBs, CCs, and CBs is similar to Simulation 1. Also, in this simulation an additional 35,159 Ag- cells (12% of all cells) could potentially have developed into a PC if the BLIMP1 level was used as a decision rule for PC differentiation during the simulation. Figure 13B shows that MBCs are of low affinity, have BLIMP1 levels below the PC threshold ($<8.10^{-8}$M) and are generated during the early phase of the GC response. Increased affinity abolished MBCs as a result of increasing BLIMP1 level resulting in a transition to PCs with BLIMP1 levels above the threshold. We also observe that at affinity=0.25 a larger number of Ag+ cells with intermediate BLIMP1 levels occur, which is a consequence of affinity-based signaling in which cells that have weaker CD40 signaling more slowly increase their BLIMP1 levels. About 75% of the subset of Ag+ cells did not develop into output cells despite high BLIMP1 levels. In addition, about 16% of the Ag- cells are BLIMP1+.

In summary, affinity-based CD40 signaling simulation produces a mixture of early lower affinity MBCs followed by later higher affinity PCs. Approximately 76% of the PCs are generated after the peak response of the output cells (Figure 11A) while 85% of the MBCs are produced prior to the peak response (Figure 11B; Supplementary Figure 11). This temporal shift is in agreement with recent findings (Florian J Weisel *et al.*, 2016). Overall, we see that a large fraction of Ag+ non-output cells are BLIMP1+ and, therefore, a larger number of PCs should potentially have been generated.

2.4.3. BLIMP1 and Ag-defined fate decisions do not lead to MBC generation under strong constant CD40 signal (Scenario 2)

We then wondered whether we could determine cell fate based on the coupling of BLIMP1 level and Ag status under a strong constant CD40 signal. In this simulation (Simulation 3), the generation of PCs is fully based on BLIMP1 levels and does not take Ag status into account, i.e., subsequent to a series of cell divisions the CBs with high BLIMP1 levels (≥8M) differentiate to PCs (Ag+BLIMP1+ or Ag-BLIMP1+). In addition, Ag-retaining cells with low BLIMP1 levels (<8M) differentiate to MBCs (Ag+BLIMP1-). Figure 11C shows the overall GC dynamics, which is similar to Scenario 1 simulations but the DZ-to-LZ ratio slightly increased (Figure 11D). The effect of stochasticity on the overall GC dynamics and the DZ-to-LZ ratio is limited as shown from repeated simulations in Supplementary Figures 16 and 17. Figure 14A and C shows the number of PCs and corresponding affinity. No MBCs are produced in this simulation due to strong CD40 signaling that enforces high BLIMP1 levels and, consequently, only PCs are generated. This was not surprising considering Simulation 1. However, the number of PCs at the end of the GC reaction is about a factor 3 larger compared to Simulation 1 (14% of all cells corresponding to 38,684 cells; Table 3). The

number of PBs is slightly larger compared to the Simulation 1 while the number of CBs and CCs are slightly reduced. Approximately 33% of all BLIMP1+ cells (115,310) differentiate to PCs and about two-third of these cells are Ag-. The distribution of PCs, and Ag+ cells (Figure 15A) is similar compared to Simulation 1 (Figure 12A) but PCs now assume BLIMP1 levels ranging from 8 to about 9 while in Simulation 1 all Ag+ output cells assumed the highest possible BLIMP1 level (i.e., ~9). The bimodal distribution is observed since some CBs will differentiate immediately when the BLIMP1 level passes the threshold while other cells may engage in one or more cell divisions giving BLIMP1 additional time to reach its maximum value.

In summary, the MSM allows to couple the decision for differentiation based on both BLIMP1 level and Ag status. With a constant strong CD40 signaling the Scenario 2 simulation produces only PCs of low to high affinities but no MBCs. Substantially more PCs are generated in comparison to Simulation 1 and 72% of these PCs are generated after the peak response of the output cells (Figure 14A; Supplementary Figure 10), which are of relatively high affinity (Figure 14C). The slight increase in DZ-to-LZ ratio implies that the transzone migration rates in Scenario 2 are no longer in full agreement with the patterns observed in (Victora *et al.*, 2010).

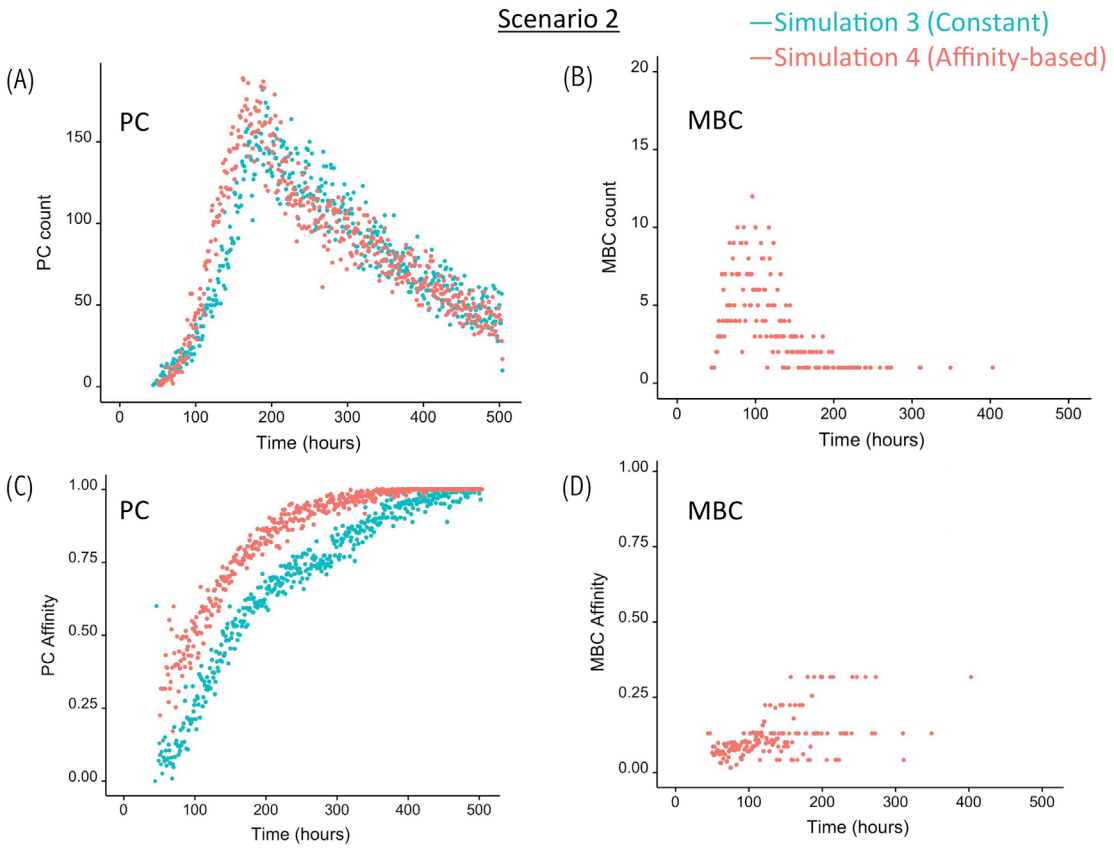

Figure 14: OCs for Scenario 2 simulations with a constant CD40 signal (CD40=50; blue) or affinity-based CD40 signal (red). (A) Number of PCs (Ag+BLIMP1+, Ag-BLIMP1+), (B) number of MBCs (Ag+BLIMP1-), (C) PC affinity, and (D) MBC affinity during GC reaction. No MBCs are produced with a constant CD40 signal.

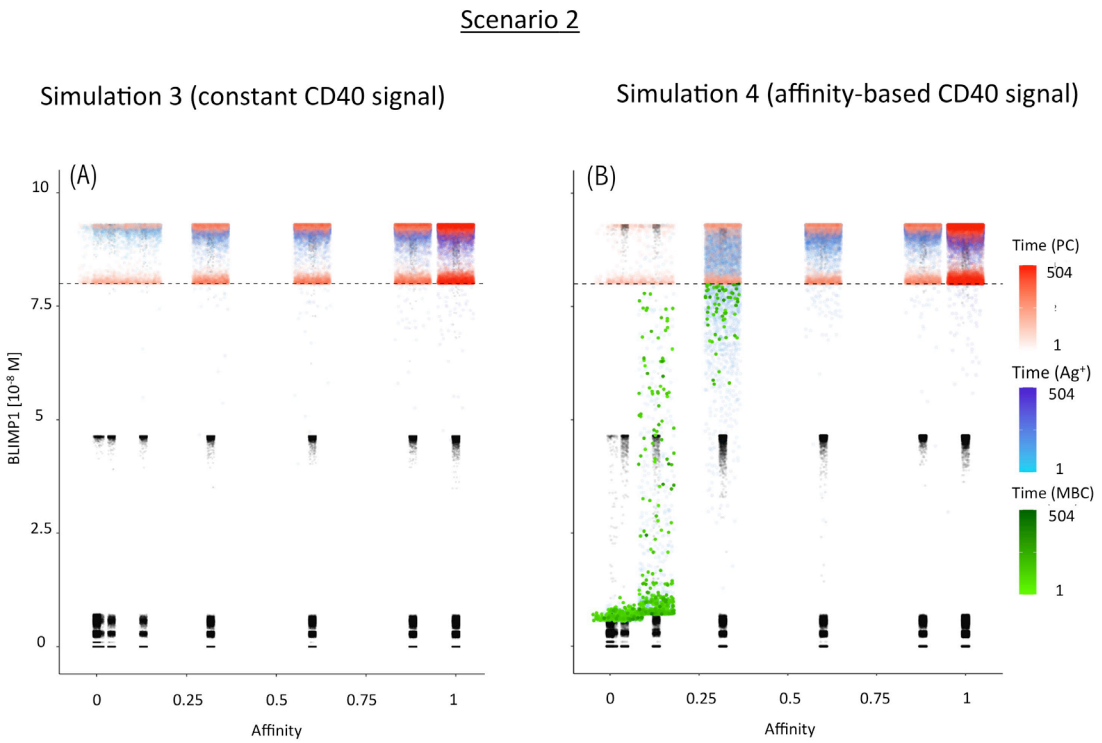

Figure 15: Distribution of PCs, MBCs, and Ag+ (but not PC nor MBC) cells with respect to their affinity, BLIMP1 level, and time of generation for Scenario 2 simulations. (A) Constant CD40 signaling (CD40=50; no MBCs). (B) Affinity-based CD40 signaling (early MBCs). For a further description see Figure 13.

2.4.4. BLIMP1- and Ag-defined fate decisions under a strong affinity-based CD40 signal produce MBCs and show a temporal switch (Scenario 2)

Considering no MBCs were generated under strong constant CD40 signal we wondered whether the decision for differentiation based on BLIMP1 level and Ag status under an affinity-based CD40 signal produces both PCs and MBCs. The overall GC dynamics of this simulation (Simulation 4) is shown in Figure 11C which are clearly different from Simulation 3 in which a constant CD40 signal was used. The number of CCs is similar, but the number of CBs largely increased resulting in an increased DZ-to-LZ ratio to approximately 3 to 4 (Figure 11D). The effect of stochasticity in the model on GC dynamics and DZ-to-LZ ratio is shown in Supplementary Figures 18 and 19 for 30 repetitions. Figure 14A shows that the number of PCs in Simulation 3 (38,684 cells) and Simulation 4 (35,670) is similar but, overall, the PCs have a higher affinity (Figure 14C). Affinity-based signaling results in the generation of MBCs of low affinity mostly during the early phase of the GC response (Figure 14B, C). The number of PCs at the end of the GC reaction is approximately a factor 2.5 larger compared to Simulation 2 that also involved affinity-based signaling (13% of all cells; Table 3). The percentage

of MBCs (0.3%; 781 cells) is comparable to Simulation 2. This corresponds to 0.5% of all BLIMP1- cells. Similar to simulation 3, approximately 33% of all BLIMP1+ cells (107,943) differentiate to a PC and about two-third of these cells are Ag-. The distribution of PCs, MBCs, and Ag+ cells is shown in Figure 15B.

In summary, in Scenario 2 the affinity-based CD40 signaling simulation produces PCs and a small fraction of MBCs. However, substantially more PCs are generated in comparison to Scenario 1. 75% of these PCs are generated after the peak response of the output cells while 89% of the MBCs are produced prior to this peak and are of lower affinity. (Figure 14; Supplementary Figure 12). Although we now observed a temporal shift there is a significant increase in the DZ-to-LZ ratio indicating transzone migration rates that are not in agreement with (Victora *et al.*, 2010). We also observed that a substantial fraction of the PCs are Ag- indicating that the decision for PC differentiation should not (fully) be based on Ag status.

2.4.5. BLIMP- and Ag-defined fate decisions under weak constant CD40 signal produce MBCs but fail to show a temporal switch (Scenario 2)

In Simulation 3 we used a strong and constant CD40 signal (cd40=50) that prevented the generation of MBCs because Tfh cell help will always sufficiently increase the BLIMP1 level to exclusively result in PC differentiation. In contrast in Simulation4 we allowed the CD40 signal to vary with affinity resulting in a temporal switch from MBCs to PCs. Since a constant high-level is not realistic (i.e., no MBCs are produced) we questioned if we could generate both MBCs and PCs by using a constant but lower CD40 signal (cd40=10; Simulation 5). In this simulation the overall GC dynamics is similar to the other simulations (Supplementary Figure 14A). The DZ-to-LZ ratio fluctuates around a value of 2 (Supplementary Figure 14B). The total number of cells during the course of the GC reaction is comparable to the other simulations. Compared with Simulation 3, a constant and weak CD40 signaling indeed results in the generation of MBCs and even increased five-fold (2%; 5,048 cells) at the expense of a lower number of PCs (3%; 10,204 cells; Supplementary file Table_Counts.xlsx). However, since the CD40 signal strength does not change over time this simulation does not result in a temporal switch but a steady but low production of MBCs throughout the GC reaction (Supplementary Figure 13). We also observe that only Ag+BLIMP1+ and no Ag-BLIMP1+ PCs are generated reflecting that cells that divided symmetrically result in daughter cells with BLIMP1 and IRF4 concentrations that are never high enough to return to the BLIMP1+ state. Figure 16 shows the distribution of the PCs, MBCs and Ag+ cells. About 73% of the PCs are produced after the peak of the output cell production and also the majority of the MBCs (74%) are produced after the peak (Supplementary Figure 15). In Figure 17 we show an example of the temporal dynamics of B-cell lineage during the GC reaction starting with a founder cell that eventually results in PC differentiation. It shows how BLIMP1 level, Ag status, and affinity evolves as a

result of the synergistic interaction between the molecular and cellular level at different events in the MSM.

In summary, a constant and weak CD40 signaling strengths is able to produce MBCs throughout the GC reaction at the expense of PCs and, consequently, no temporal switch is observed.

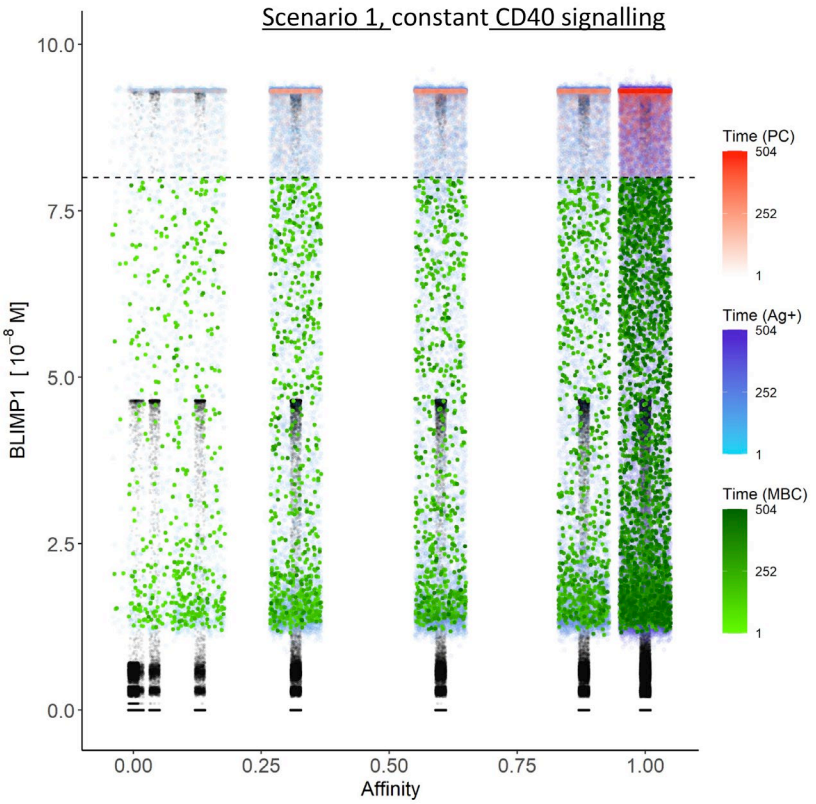

Figure 16: Distribution of PCs, MBCs, and Ag+ (but not PC nor MBC) cells with respect to their affinity, BLIMP1 level, and time of generation for Scenario 2 simulations. Constant CD40 signaling (CD40=10). For a further description see Figure 13.

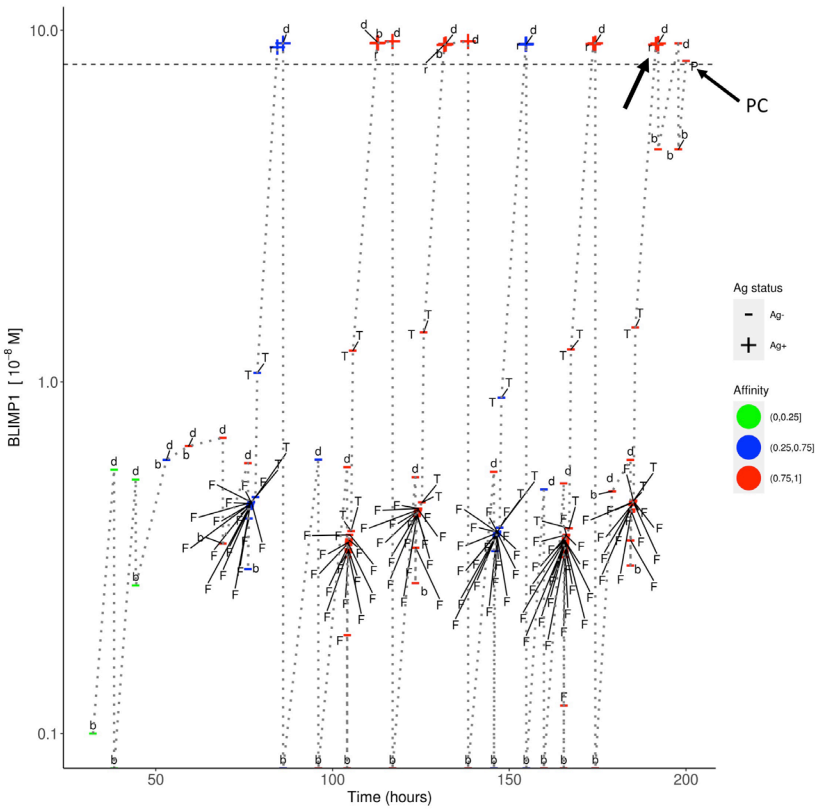

Figure 17: Temporal dynamics of B-cell lineage for Scenario 2, affinity-based CD40 signalling (Simulation 4). The dotted lines traces the lineage of a single founder B-cell entering at the initial phase of the GC reaction up to a PC differentiation event at about 200 hours. At each event (d=division, b=born, F=FDC contact, T=Tfh interaction, r=recycle to DZ, P=PC differentiation) the BLIMP1 level, Ag status (Ag+/Ag-), and affinity (low, medium high) is shown. The horizontal dotted line represents the BLIMP1 threshold for PC differentiation. CBs go through one or more cell divisions (d, b) before differentiating to CCs to have interaction with the FDC and Tfh cells. The affinity of the B-cells in this lineage shows an overall increase although SHM may also decrease affinity (red to blue color). Ag- cells are created from asymmetric division. BLIMP1 level varies in time as a result of transcriptional activity and (a)symmetric division. After interaction with a Tfh cell, the BLIMP1 level increases due to CD40 signaling. Asymmetric division may leave the BLIMP1 level unchanged or reduce it to 0. Symmetric division reduces the concentration with 50% . In this particular lineage we observe that a Ag+BLIMP1+ cell (indicated by the arrow) asymmetrically divides resulting in a Ag-BLIMP1- cell, which subsequently increases its BLIMP1 level again in subsequent divisions, and final differentiates to a PC (Ag-BLIMP1+).

2.5. Discussion

We presented a MSM integrating cellular and molecular mechanisms, operating at different time scales, to investigate output cell differentiation based on Ag status and/or BLIMP1 level. In this paper we compared these mechanisms for cell-fate determination under various instances of CD40 signaling.

An important insight from our model (Simulations 2 and 4) is the observation that regulation of the BLIMP1 level through affinity-dependent but not constant CD40 signaling, results in the occurrence of a temporal transition from MBC to PC

output during the GC reaction (Florian J Weisel *et al.*, 2016),(Pélissier *et al.*, 2020). In addition, Simulation 2 showed that the LEDA theory (i.e., a mechanism in which the decision for output cell differentiation is solely based on asymmetric division but not on BLIMP1 level) does not exclude a temporal transition. However, scenario 1 simulations produce BLIMP1+ cells of which approximately 33% are Ag- showing that a decision for differentiation solely based on Ag status is not adequate since this will exclude a large number of BLIMP1+ cells from PC differentiation. Inspection of the PCs (BLIMP1+ cells) of the Scenario 2 simulations shows that these are a mixture of Ag+ (~11%) and Ag- (~22%) cells. This also argues against asymmetric inheritance as sole mechanism for PC differentiation. It is known that high affinity GC B cells present more pMHCII molecules to Tfh cells resulting in increased expression of CD40L and hence stronger CD40 signaling which determines cell phenotype (Jaiswaf and Crof, 1997; Schwickert *et al.*, 2007, 2011; Ise *et al.*, 2018; Koike *et al.*, 2019) and results in faster and more cell divisions in the DZ (Phan, 2006; Gitlin *et al.*, 2014, 2015; Ise *et al.*, 2018).

The lack of experimental data to support our findings is clearly a weakness of our work and complementary experiments are required to validate the results from our simulations. In particular, we propose experiments to generate data about the (1) average number of PCs and MBCs that leave a single GC during its life time; (2) extend and/or role of (a)symmetric division of Ag and TFs in relation to cell fate; (3) quantitative relationship between BcR affinity, CD40 signaling strength and BLIMP1 level.

One other apparent weakness of the MSM concerns the definition of MBCs as Ag+BLIMP1- cells. Although mechanisms of MBC differentiation are even less understood than for PC differentiation, we needed a route to generate both MBCs and PCs to make the model more realistic. Noticeably, lack of MBCs would have had a (small) effect on the overall GC dynamics. In favour of our approach is the observation that MBCs have indeed low BLIMP1 levels (Kräutler *et al.*, 2017) and the observation of a temporal switch with low affinity MBCs and higher affinity PCs. The current definition, however, implies that Ag status (Ag+) is one of the determinants in MBC differentiation and that also MBCs leave the GC through the DZ. However, there is no experimental evidence to support this assumption at this stage. The generation of MBCs could be improved by modeling of BACH2 (Muto *et al.*, 2010; Shinnakasu *et al.*, 2016) and the contribution of the CD40 pathway to MBC differentiation. Inclusion of the BACH2 in the GRN is, however, not sufficient as was recently shown in another model (Thomas *et al.*, 2019). One way forward is to model different cell fate (apoptosis, MBC or PC differentiation, and DZ recycling) for different levels of Tfh cell help, and to include MYC, FOXO1, IL-4, and IL-21 (Luo *et al.*, 2018; Laidlaw and Cyster, 2020). However, the work of Krautler and co-workers seems to support the conclusion that Tfh-cell acts via signals other than CD40. Moreover, the stochastic selection of low-affinity B cells has been proposed as yet another mechanism to produced MBCs (Smith *et al.*, 1997; Zhou *et al.*, 2018; Pélissier *et al.*, 2020) or PCs (Hasbold *et al.*, 2004; Dustin and Meyer-Hermann, 2012; Zhou *et al.*, 2018).

One assumption in the MSM concerns the asymmetric division of TFs. It has been shown that BCL6 and IRF4 may distribute unequally in daughter CBs after division (Barnett *et al.*, 2012; Lin *et al.*, 2015), and it has been hypothesized that this may affect cell fate. To the best of our knowledge, neither symmetric nor asymmetric distribution of BLIMP1 during division has been reported.

Results from our simulations show that approximately 15,000 – 35,000 PCs and 800 MBCs are produced in a single GC reaction corresponding to about 5 – 14% and 0.3% respectively of all GC cells. Although data is available regarding numbers of PCs and MBCs generated spleen and bone marrow during an immune response (e.g., Sugimoto-Ishige and co. (Sugimoto-Ishige *et al.*, 2020) , Yusuke and co. (Kishi *et al.*, 2010), J. Imm., 185, 211, Weisel and co. (Florian J Weisel *et al.*, 2016)), these numbers always represent percentages of observed PCs/MBCs from total number of splenic or bone marrow cells, which are impossible to translate to number of output cells from a single GC and, therefore, not directly comparable with our results.

In a recent study it was shown that both BcR signaling and help from Tfh cells are required for positive selection of CCs, as signaling pathways that emanate from the BcR and CD40 ligation are rewired in GC B cells. In contrast to naïve B cells, GC B cells require both signals to induce the c-Myc TF, which is a critical mediator of GC B-cell survival, cell-cycle reentry, and a marker of positive selection (Luo *et al.*, 2018). These results indicate that CCs compete for Tfh-cell help in a BcR affinity-dependent fashion. It also has been proposed that c-Myc^{+}Bcl6^{lo}IRF4^{+} cells are most likely PC precursors while Myc^{+}Bcl6^{hi}IRF4^{-} will recycle to the DZ (Ise and Kurosaki, 2019). However, cells with low BCL6 and higher IRF4 or BLIMP1 expression have also been found in the DZ, which supports the recycling model our MSM (Kräutler *et al.*, 2017; Ise *et al.*, 2018). In support for our model, it has been shown that DZ B cells displayed a more prominent PC gene signature than LZ B cells (Arpin *et al.*, 1995; Kräutler *et al.*, 2017). Similarly, high-affinity LZ B cells showed a strong PC signature including a high expression of IRF4 in high-affinity CCs. Their experiments indicated that PC differentiation is initiated by signals delivered to high-affinity B cells in the LZ with subsequent transition to a late PC phenotype occurring after migration to the DZ.

These and other, sometimes contradicting studies, on MBC and PC differentiation clearly show the need for additional research to unravel mechanisms underlying cell-fate decisions in the GC. Further extensions of our MSM are expected to contribute to this.

2.6. Acknowledgements

We thank Olivier Gandrillon (Ens, Lyon) for his contribution to the MSM. We thank Barbera van Schaik to setup a Virtual Machine provided by the Dutch national e-infrastructure with the support of SURF Cooperative, to process large output files. This work is supported by a CASyM Exchange Research Grant, COSMIC

(www.cosmic-h2020.eu) which has received funding from the European Union's Horizon 2020 research and innovation programme under the Marie Skłodowska-Curie grant agreement No 765158, and by the Human Frontier Science Program 570 (RGP0033/2015).

2.7. Conflict of Interest

Author María Rodríguez Martínez was employed by the company IBM. The remaining authors declare that the research was conducted in the absence of any commercial or financial relationships that could be construed as a potential conflict of interest.'

2.8. Supplementary Information

2.8.1. Computational model of gene regulatory network

The GRN involved in PC differentiation and which we used in the MSM comprises a pre-existing model (Martínez *et al.*, 2012). This model, comprising ordinary differential equations (ODE; Eq 2 - 4), describe the dynamics of three TFs, i.e., BCL6 (b), BLIMP1 (p) and IRF4 (r) in terms of their dissociation constant (k), transcription (μ) and degradation rates (λ). 'Squares' in the equations represent Hill coefficients that enter due to the assumption of cooperative binding. The effect of the upstream BcR and CD40 signals is integrated through two separate equations (Eq 5 - 6). We embedded this model without any changes in our MSM. Parameter values, units and description are given in Supplementary Table 1 and were derived from literature or from fitting the model to gene expression data obtained from human GC B cells and PCs (see (Martínez *et al.*, 2012)). ODEs were solved using an adaptive Euler method. Several parameters are normalized by a unit of time (t_0=4 hrs) representing the mean lifetime of BCL6, IRF4, and BLIMP1. In this unit the degradation rates are 1. The unit of concentration was taken as $C_0 = 10^{-8}$M representing the average dissociation constants of IRF4 and BLIMP1 binding to its binding sites. In this unit all dissociation constants are 1. Parameter bcr_0 represent the maximum BcR signal strength and is set to 1 in all simulations. The value of cd40 represents the constant (cd40=50, cd40=10) or affinity-based (affinity*50) CD40 signal (see main text). For further information about this model we refer to Martínez and colleagues (Martínez *et al.*, 2012). The initial values for the concentrations of BCL6, IRF4 and BLIMP1 at the start of the simulation are 11.26, 0.1, and 0.1 $*10^{-8}$M respectively.

$$\textbf{Eq 2}: \frac{dp}{dt} = \mu_p + \sigma_p \frac{k_b^2}{k_b^2 + b^2} + \sigma_p \frac{r^2}{k_r^2 + r^2} - \lambda_p p$$

$$\textbf{Eq 3}: \frac{db}{dt} = \mu_b + \sigma_b \frac{k_p^2}{k_p^2 + p^2} \frac{k_b^2}{k_b^2 + b^2} \frac{k_r^2}{k_r^2 + r^2} - (\lambda_b + BCR)b$$

$$\textbf{Eq 4}: \frac{dr}{dt} = \mu_r + \sigma_r \frac{r^2}{k_r^2 + r^2} + CD40 - \lambda_r r$$

$$\textbf{Eq 5}: BCR = bcr0 \frac{k_b^2}{k_b^2 + b^2}$$

$$\textbf{Eq 6}: CD40 = cd40 \frac{k_b^2}{k_b^2 + b^2}$$

Supplementary Table 1: Parameters for the computational ODE model of the GRN. Parameters are normalized by a unit of time (t_0) and concentration (C_0).

Parameter	Value	Units	Description
μ_p	10^{-6}	C_0/t_0	Basal transcription rate
μ_b	2		
μ_r	0.1		
σ_p	9	C_0/t_0	Maximum induced transcription rate
σ_b	100		
σ_r	2.6		
κ_p	1	C_0	Dissociation constant: ligand concentration that produces half of the maximum induced transcription rate
κ_b	1		
κ_r	1		
λ_p	1	$1/t_0$	Degradation rate
λ_b	1		
λ_r	1		
bcr0	1	$1/t_0$	Range of BCR-induced degradation of BCL6
cd40	0-50	C_0/t_0	Range of CD40-induced transcription of IRF4. (Constant: cd40=50, cd40=10, Affinity-based: cd40=affinity*50)
C_0	10^{-8}	M	Concentration unit
t_0	4	h	Time unit

2.8.2. Agent-based model

2.8.2.1. Software and parameter values

The agent-based model (ABM) is described in more detail in Meyer-Hermann (2012) (Meyer-Hermann *et al.*, 2012) and Robert (2017) (Robert *et al.*, 2017) and references therein. The C++ software that we used for the simulations is available on request. Parameter values for the simulations listed in Supplementary files Parameters_1 to Parameters_5 for simulation 1 to 5 respectively. For a further explanation of the parameters see Robert (2017) (Robert *et al.*, 2017).

2.8.2.2. Affinity classes

The discrete 4-dimensional shape space that represents affinity translates to 25 affinity classes shown in Supplementary Figure 1 (Perelson and Oster, 1979; Meyer-Hermann *et al.*, 2001). Since affinity for founder cells is initialized at a Manhattan distance (1-norm) of 4-8 the B-cells mostly assume the upper ~10 affinity classes from 10^{-5} to 1 as is shown in Supplementary Figure 2 for PCs produced in the Scenario 1, affinity-based CD40 signaling simulation (simulation 2).

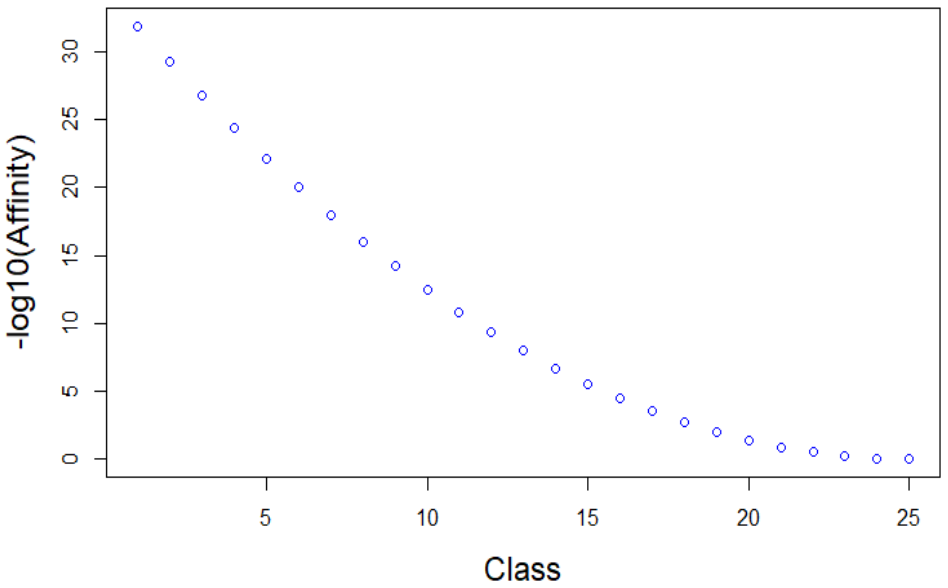

Supplementary Figure 1: 28 affinity classes. Affinity is represented on a logarithmic scale corresponding to affinity values of 1 to less than 10^{-40}.

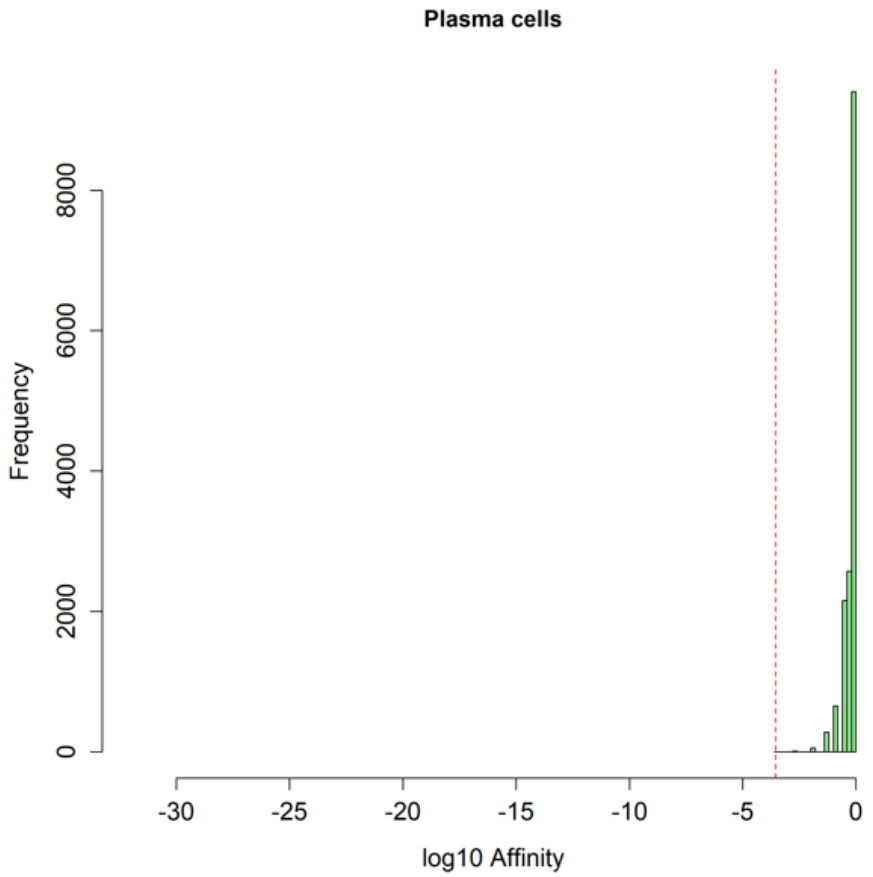

Supplementary Figure 2: Affinity distribution of PCs generated in Scenario 1, constant CD40=50 simulation. Only the upper affinity classes are utilized as a result of the initialization of founder cells.

2.8.3. Single cell lineages

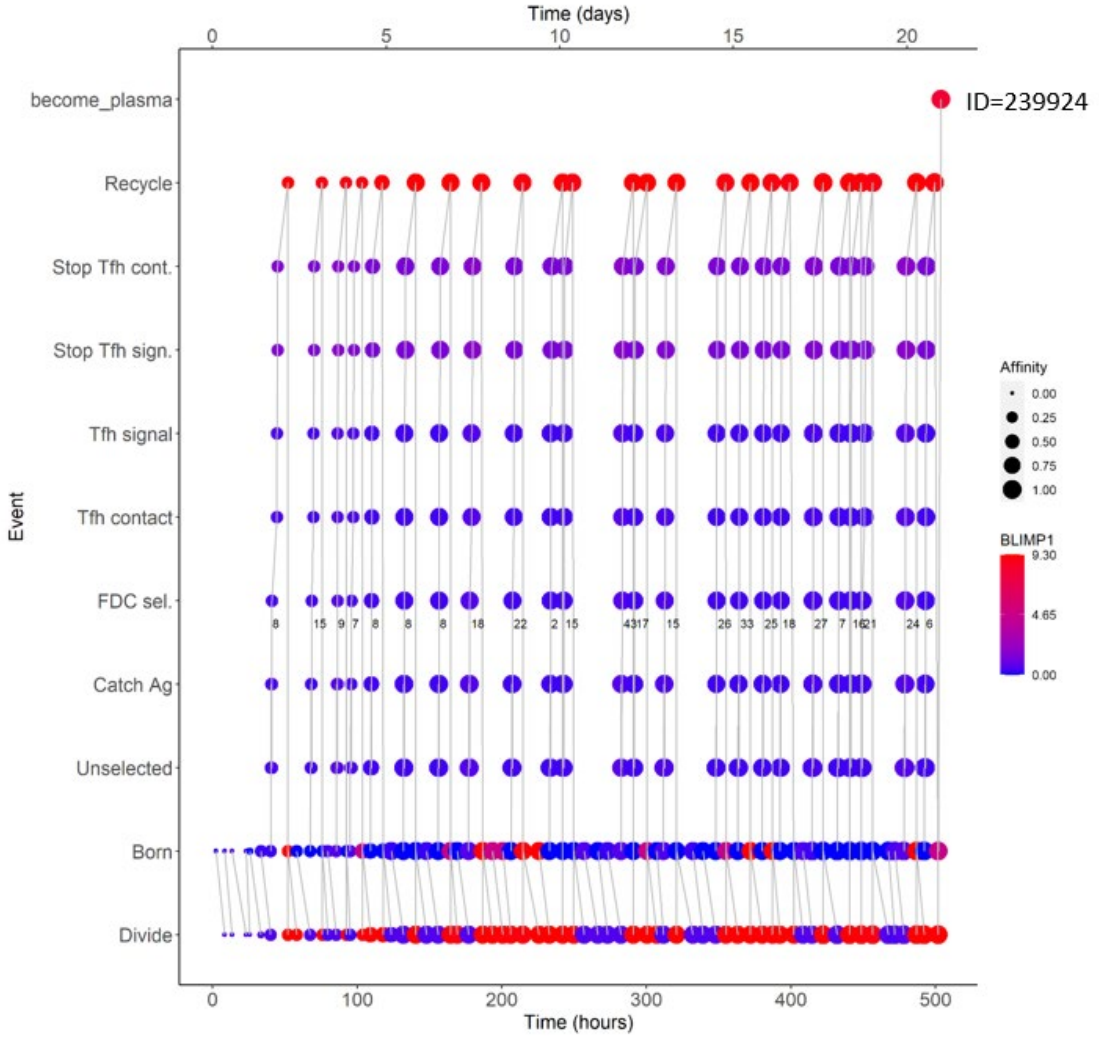

Supplementary Figure 3: Scenario 2, Constant CD40 signal. The PC (ID=239924) was selected and the full lineage was traced back to the initial founder cell. Note that at every cell division we obtain two daughter cells but since we trace back from the end to the beginning only one daughter cell after each division is shown. The bottom and top x-axis show the time in hours and days. The y-axis denotes the sequence of events each cell goes through unless it dies. The numbers inside the figure denote the number of attempts to bind the FDC. Size of the dots denote affinity. We observe that founder cells have a low affinity, while the final PC has a high affinity. Colors show the BLIMP1 level. In this particular lineage we observe that, as expected, the BLIMP1 level quickly goes up after Tfh interaction. At this stage the B-cell has been positively selected and will recycle to the DZ to engage in one or more cell divisions. In this particular lineage each sequence of cell divisions ends with an asymmetric division, which results in one of the daughter cells to have no BLIMP1 preventing it from differentiating to a PC. Only after the last division at around 21 days the cell differentiates to a PC. This is shown more clearly for a smaller time interval in Supplementary Figure 4.

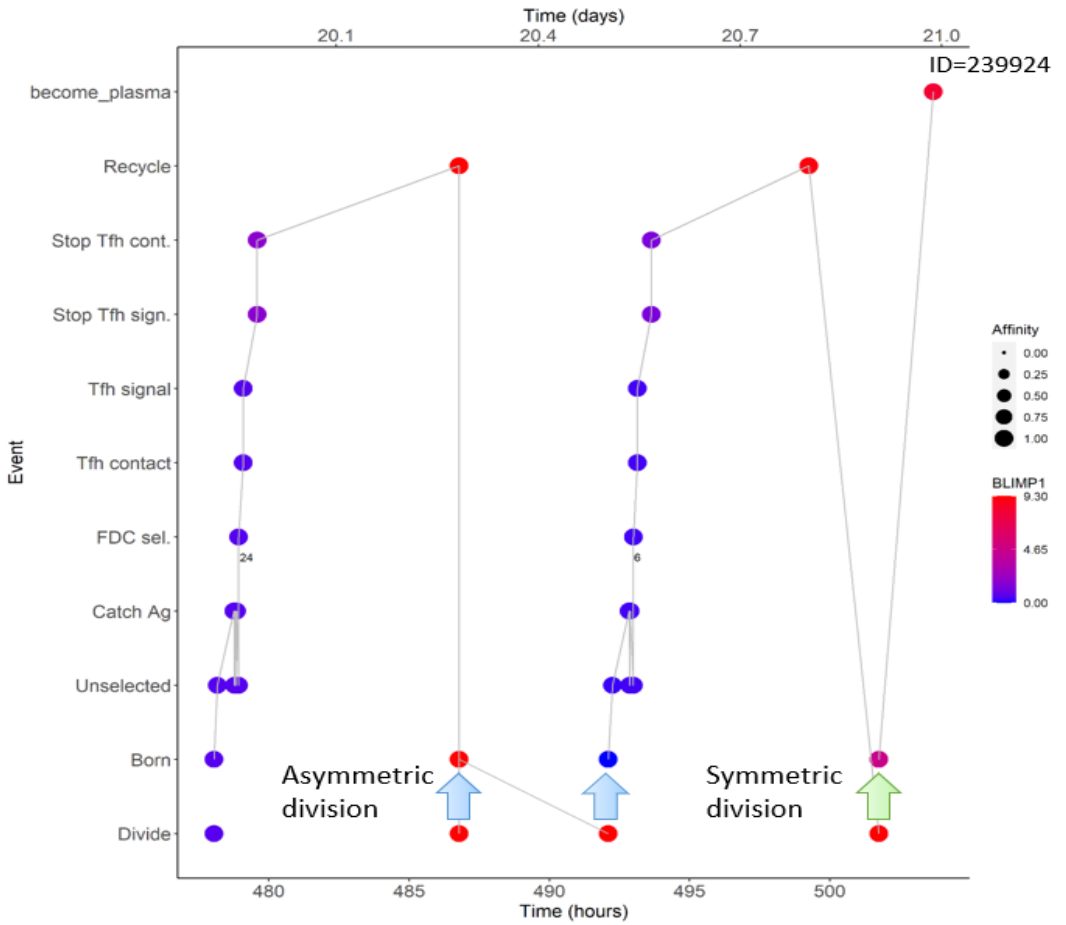

Supplementary Figure 4: Scenario 2, Constant CD40 signal. This shows the last part of the lineage from Supplementary Figure 3. We selected the cell (PC; ID=239924) and traced back the lineage until t=475 hours. Here, a cell with a high BLIMP1 level engages in a first asymmetric division (blue arrow; t=487) where the resulting daughter cells receives all BLIMP1. Subsequently, a second asymmetric division follows (blue arrow; t=493) where the daughter cell does not receive any BLIMP1 and prevents the cell from differentiating to a PC. Only in the final symmetric division (t=502) the BLIMP1 level of the daughter cells stays high enough to enable PC differentiation.

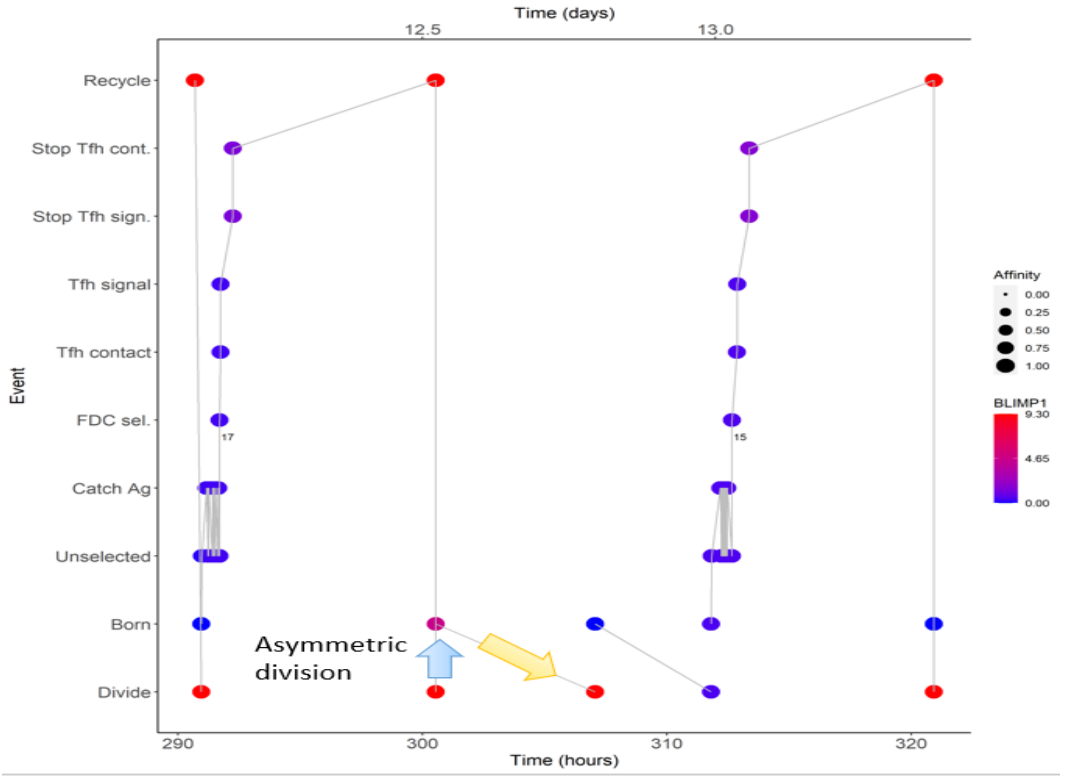

Supplementary Figure 5: Scenario 2, Constant CD40 signal. This shows part of the lineage Supplementary Figure 3. Here the lineage is shown from t=290 to t=325 hours. We observe that a cell with a high BLIMP1 level symmetrically divides (t=301) resulting in a daughter cell with an intermediate BLIMP1 level (blue arrow). However, within the time of the next division the BLIMP1 levels returns to its high equilibrium value (BLIMIP1+; yellow arrow), after which an asymmetric division at t=307) results in a daughter cells without any BLIMP.

2.8.4. Cell type definitions

Supplementary Table 2: Definition of cell types. NA=not applicble. In Scenario 1 simulations Ag+ cells (after asymmetric division) become and output cell, which are divided in PCs and MBCs based on post-simulation inspection of BLIMP1 level. In Scenario 2 simulations the BLIMP1 level is used to decide if a cell differentiates to an output cell. See main text (method section) for further details.

		Scenario 1		Scenario 2	
		BLIMP1+	BLIMP1-	BLIMP1+	BLIMP1-
OUTPUT CELL	Ag+	**PC**	**MBC**	**PC**	**MBC**
NOT OUTPUT CELL	Ag+	**PB**	**CB**	**PB**	**CB**
OUTPUT CELL	Ag -	**NA**	**NA**	**PC**	**NA**
NOT OUTPUT CELL	Ag-	**CB/CC**	**CB/CC**	**PB**	**CB/CC**

The following figures (Supplementary Figure 6,7 and 8) give three examples of how different cell types are annotated.

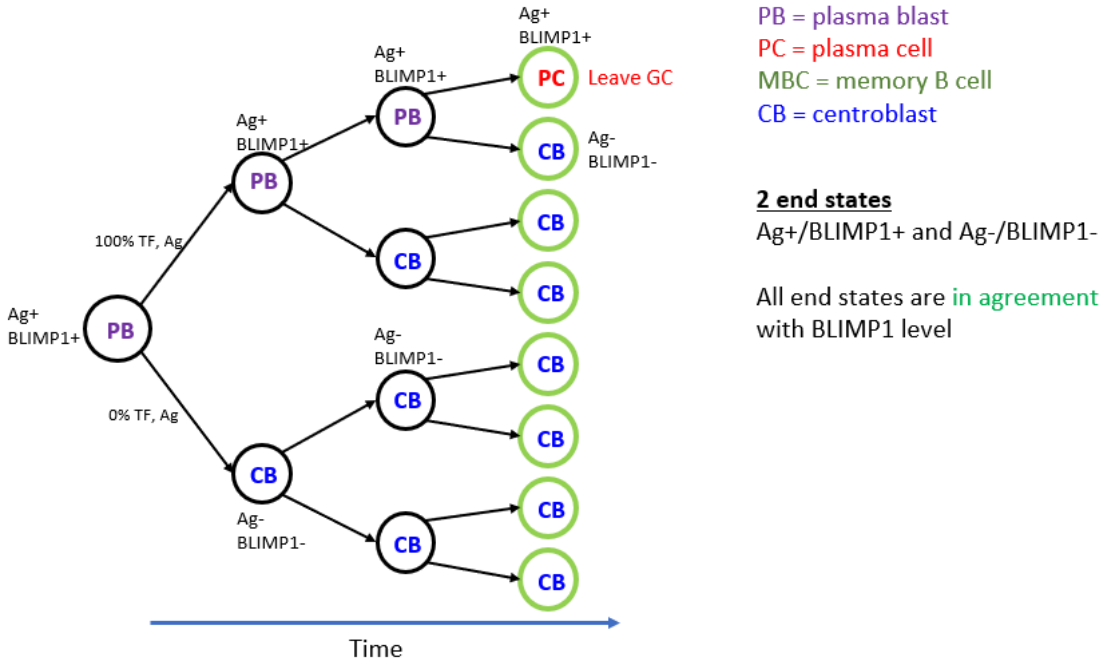

Supplementary Figure 6: Scenario 1, Ag decision rule. This figure shows 3 cell divisions that are all asymmetric. The parent cell is Ag+ (by definition) and BLIMP1+. As a result of asymmetric division, the Ag and BLIMP1 is inherited by only one of the daughter cells (Ag+/BLIMP1+) while the other daughter cell becomes Ag-/BLIMP1-. After 3 divisions we are left with 8 cells in only two different states. In this scenario only the Ag+ cells become output cells (a single cell in this example), which is annotated as a PC. This is in agreement (green circle) with the PC definition based on the BLIMP1 level, i.e., BLIMP1+. The 7 other cells are CBs. The three ancestors of the PC are annotated as a PB.

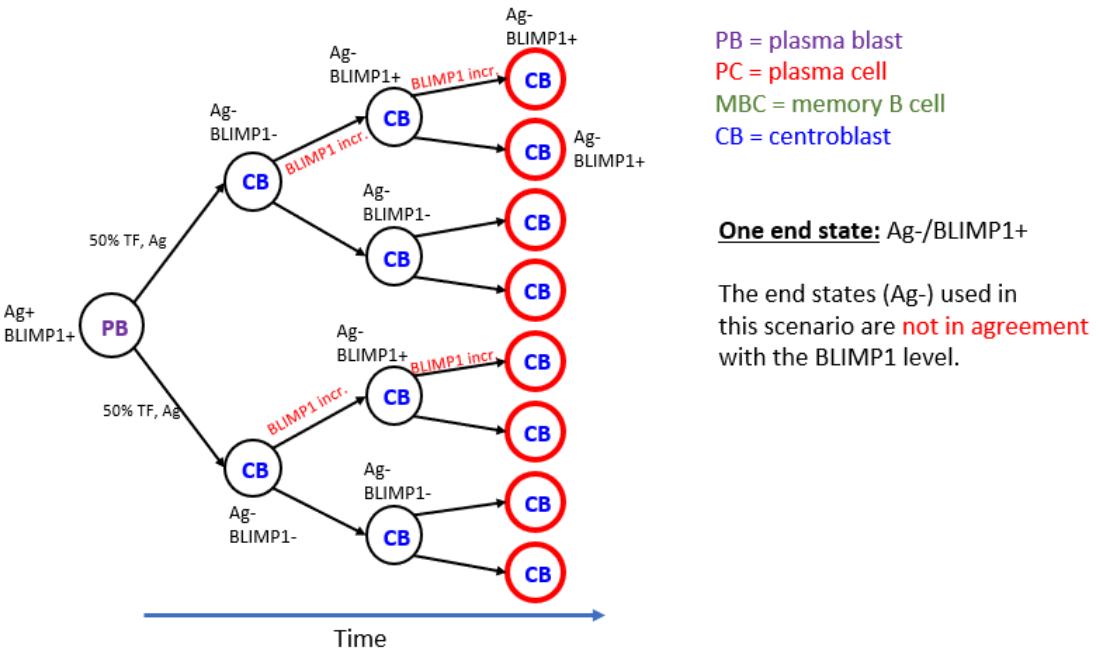

Supplementary Figure 7: Scenario 1, Ag decision rule. This figure shows 3 cell divisions that are all symmetric. The parent cell is Ag+ (by definition) and BLIMP1+ and annotated as a PB since it is Ag+/BLIMP1+ although it eventually does not become an output cell. Due to symmetric division both daughter cells receive 50% of the Ag and BLIMP1 and, therefore, become Ag-/BLIMP1- cells. However, since BLIMP1 (and IRF4) are still at a relatively high they will quickly return to a high BLIMP1 level (see Supplementary Figure 3 for an example) due to the bistable nature of the GRN. Consequently, in Scenario 1 no output cells result (all cells are Ag-) while considering the BLIMP1 level, all these cells

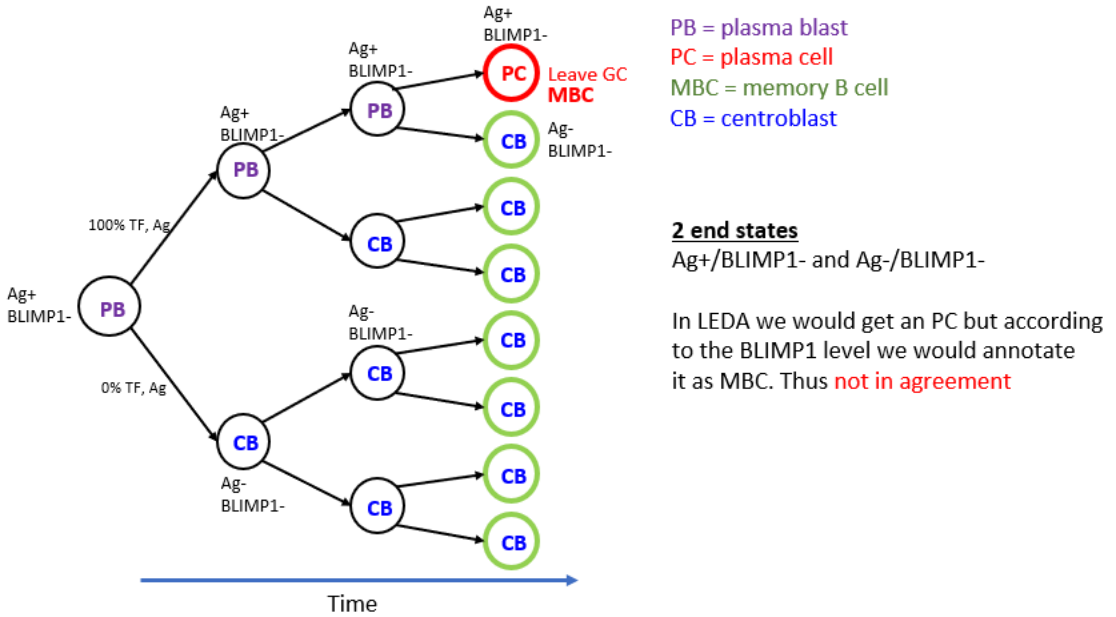

Supplementary Figure 8: Scenario 1, Ag decision rule. This figure shows 3 cell divisions that are all asymmetric. The parent cell is Ag+ (by definition) and BLIMP1- and annotated as a PB since it leads to an PC (Ag+ output cell). In Scenario 2 simulations we would have denoted the output cell (PC) as an MBC because it has a low BLIMP1 level and therefor it is not in agreement with the definition used in LEDA.

2.8.5. Cell counts

Supplementary File Counts_and_Percentages.xlsx comprises cell counts and calculated percentages from the simulations. https://www.frontiersin.org/articles/10.3389/fimmu.2020.620716/full#supplementary-material.

2.8.6. Results

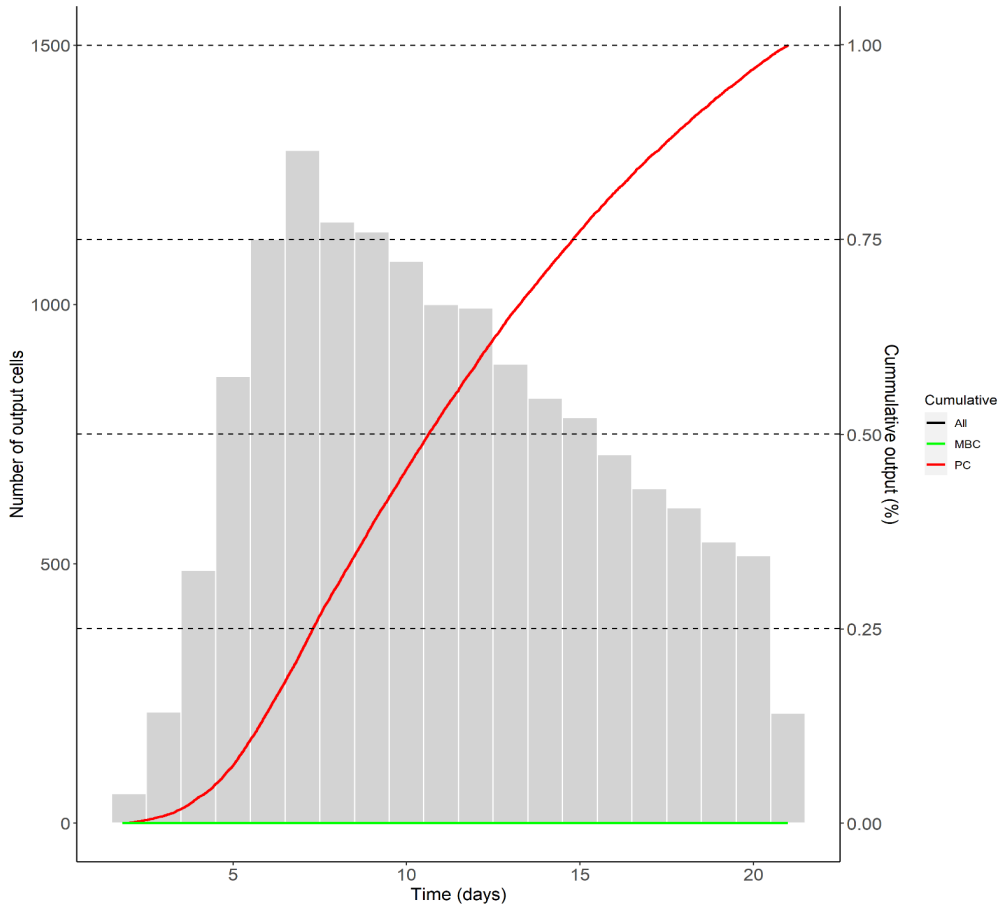

Supplementary Figure 9: Scenario 1, Constant cd40 (cd40=50). (Cumulative) number of output cells. Histogram represents the number of output cells per day. Red and green line represents the cumulative number of PCs and MBCs respectively. No MBCs are produced in this simulation and, therefore, the red and black lines coincide. About 76% of the PCs are produced after the peak of output cells at day 7. Note: percentages of PCs and MBCs are calculated relative to the total number of PCs and MBCs respectively (not relative to the total number of output cells).

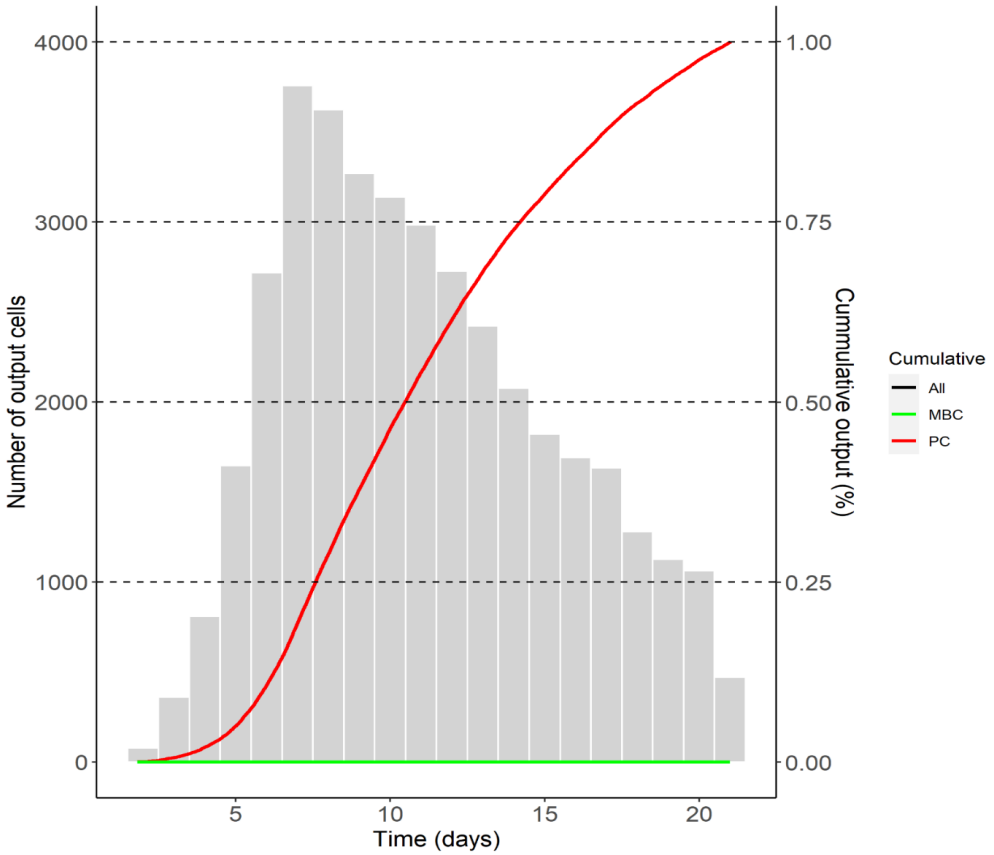

Supplementary Figure 10: Scenario 2, Constant cd40 (cd50=50). (Cumulative) number of output cells. Histogram represents the number of output cells per day. Red and green line represents the cumulative number of PCs and MBCs respectively. No MBCs are produced in this simulation and, therefore, the red and black line coincide. About 72% of the PCs are produced after the peak at day 7. Note: percentages of PCs and MBCs are calculated relative to the total number of PCs and MBCs respectively (not relative to the total number of output cells).

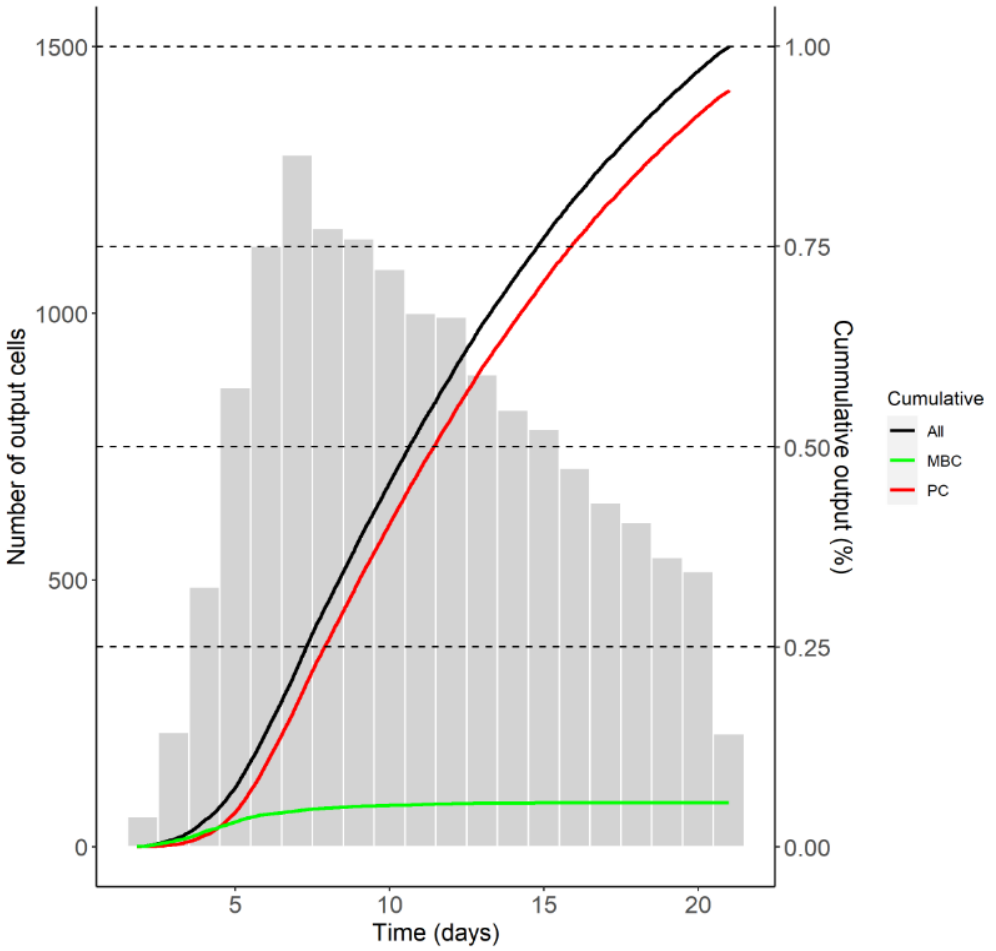

Supplementary Figure 11: Scenario 1, Affinity-based cd40. (Cumulative) number of output cells. Histogram represents the number of output cells per day. Red and green line represents the cumulative number of PCs and MBCs respectively. About 76% of the PCs are produced after the peak at day 7. 85% of the MBCs are produced prior to day 7. Note: percentages of PCs and MBCs are calculated relative to the total number of PCs and MBCs respectively (not relative to the total number of output cells).

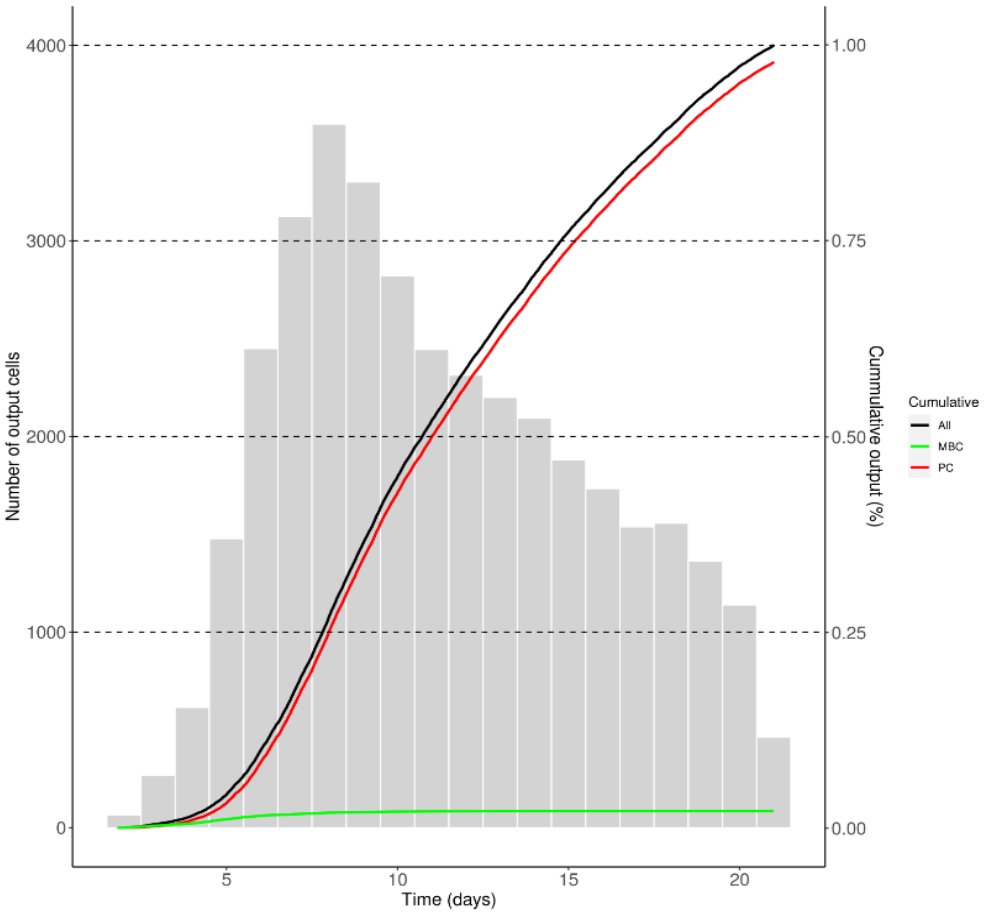

Supplementary Figure 12: Scenario 2, Affinity-based cd40. (Cumulative) number of output cells. Histogram represents the number of output cells per day. Red and green line represents the cumulative number of PCs and MBCs respectively. About 75% of the PCs are produced after the peak at day 8. 89% of the MBCs are produced prior to day 8. Note: percentages of PCs and MBCs are calculated relative to the total number of PCs and MBCs respectively (not relative to the total number of output cells).

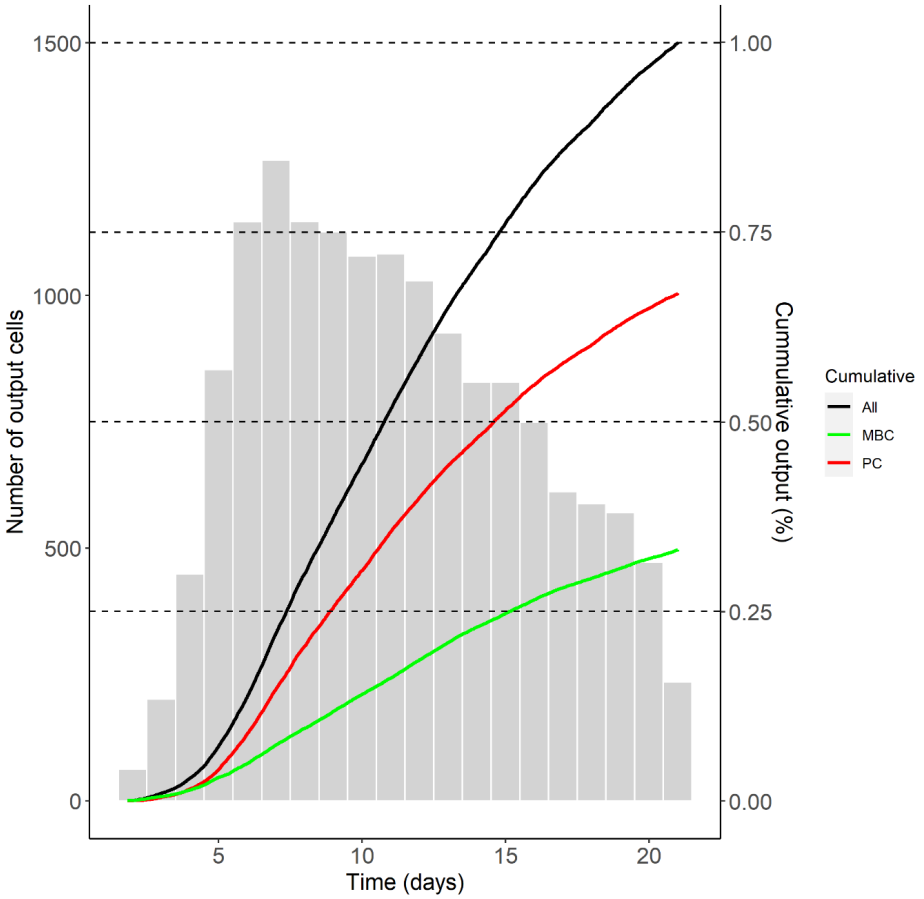

Supplementary Figure 13: Scenario 2, Constant cd40 (cd40=10). (Cumulative) number of output cells. Histogram represents the number of output cells per day. Red and green line represent the cumulative number of PCs and MBCs respectively. About 73% of the PCs are produced after the peak at day 8. Only 26% of MBCs are produced prior to the peak at day 8. Note: percentages of PCs and MBCs are calculated relative to the total number of PCs and MBCs respectively (not relative to the total number of output cells).

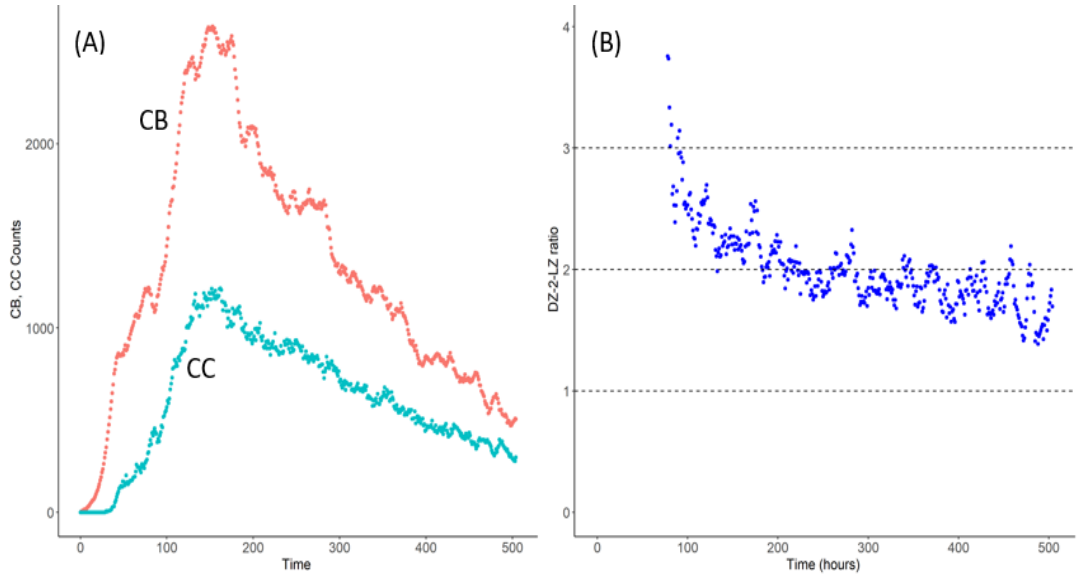

Supplementary Figure 14: Scenario 2, Constant cd40 (cd40=10). Overall GC dynamics. (A) CB and CC counts. (B) DZ-2-LZ ratio.

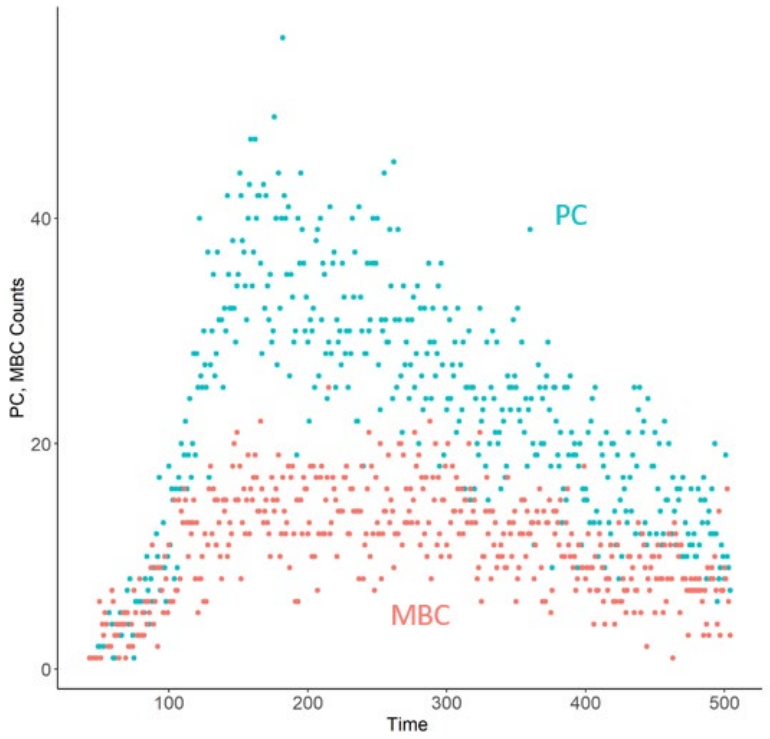

Supplementary Figure 15: Scenario 2, Constant cd40 (cd40=10). Number of PCs and MBCs generated during the GC reaction.

2.8.7. Variation in cell dynamics in repeated simulations

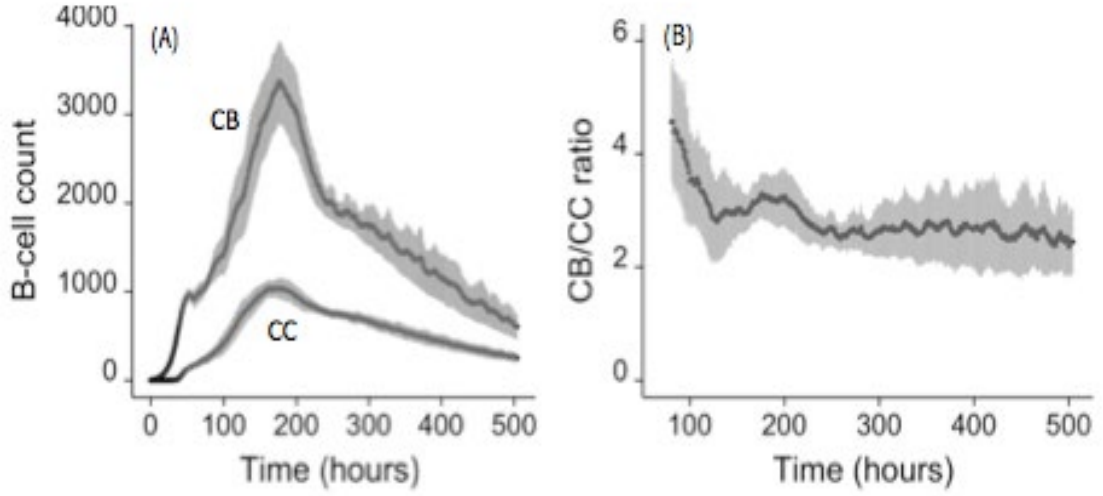

Supplementary Figure 16: Scenario 2, Constant (cd40=50). Overall GC dynamics. (A) CB and CC counts. (B) DZ-to-LZ ratio. Mean and standard deviation of 30 different random seeds are shown.

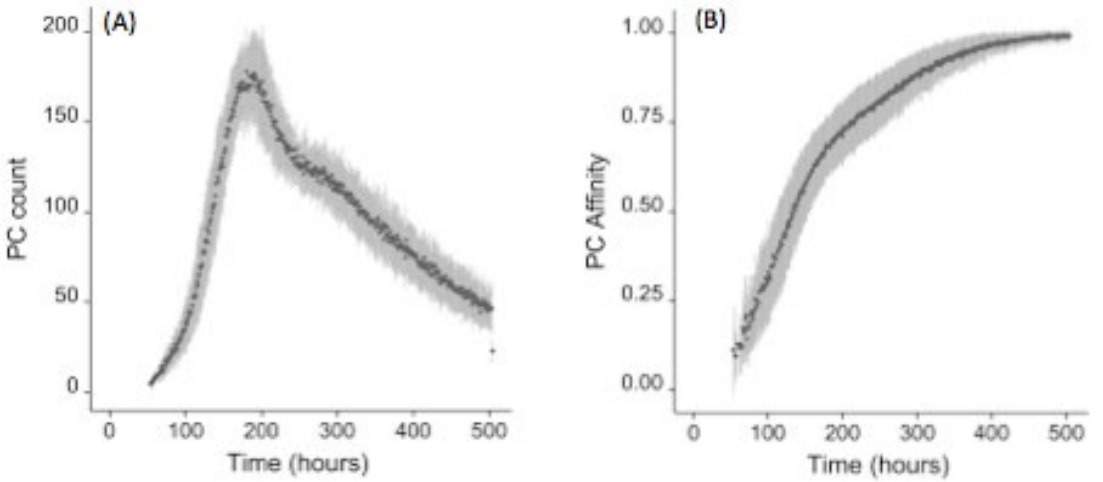

Supplementary Figure 17: Scenario 2, Constant (cd40=50). (A) Number of PCs and (B) Affinity of PCs generated during the GC reaction. No MBCs were generated. Mean and standard deviation of 30 different random seeds are shown.

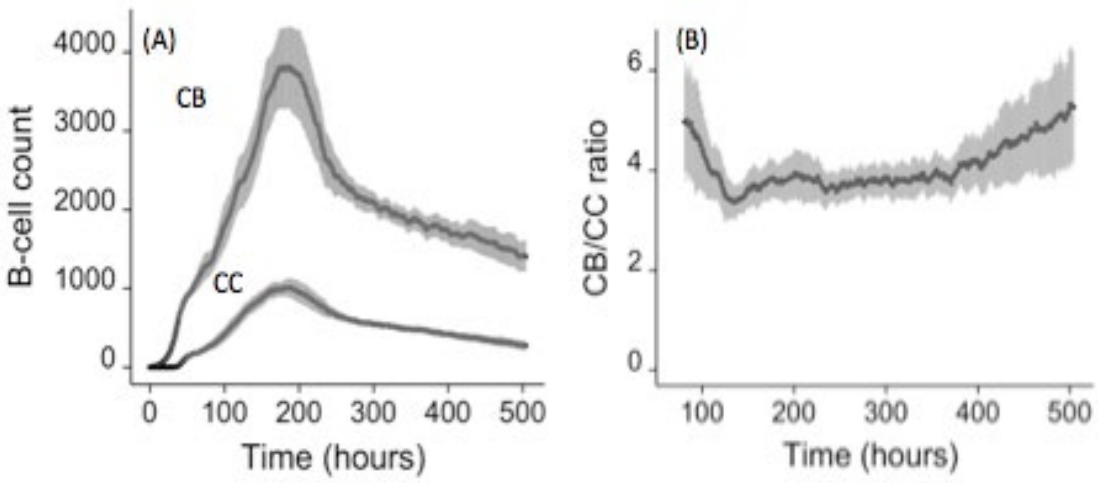

Supplementary Figure 18: Scenario 2, affinity-dependent (cd40=50*affinity). Overall GC dynamics. (A) CB and CC counts. (B) DZ-to-LZ ratio. Mean and standard deviation of 30 different random seeds are shown.

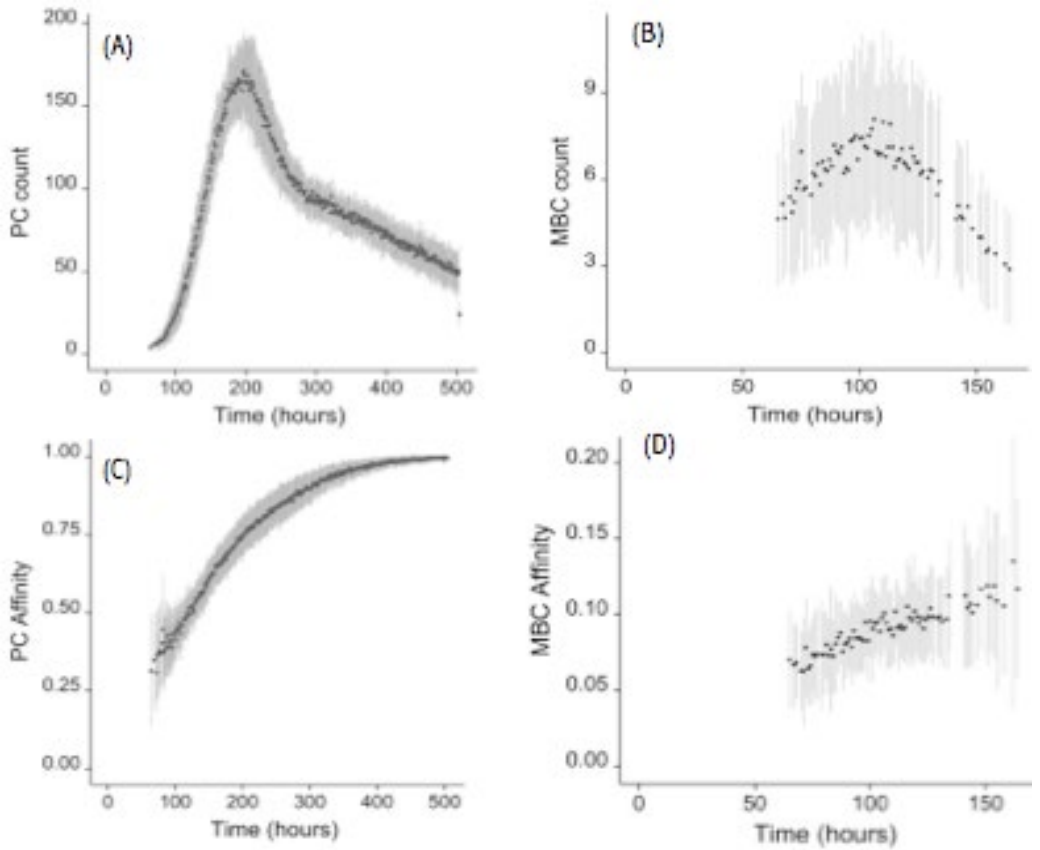

Supplementary Figure 19: Scenario 2, affinity-dependent (cd40=5*affinity). (A) Number of PCs, (B) Number of MBCs, (C) Affinity of PCs and (D) Affinity of MBCs generated during the GC reaction. Mean and standard deviation of 30 different seeds are shown.

Supplementary Table 3: Variability in calculated percentages based on 30 repetitions of Simulation 3 (Scenario 2, constant CD40 signal). Avg=average, sd=standard deviation, se=standard error, min=minimum, max=maximum, Paper=value refered to in the main text.

Scenario 2		Constant CD40 signal		CD40=50			
		BLIMP1+ avg (%)	**sd**	**se**	**min**	**max**	**Paper**
OUTPUT CELL	Ag+	4.3	0.2	0.0	4.0	4.7	4.7
NOT OUTPUT CELL	Ag+	17.6	0.4	0.0	16.5	18.3	18.3
OUTPUT CELL	Ag-	9.2	0.1	0.0	8.9	9.4	9.2
NOT OUTPUT CELL	Ag-	9.8	0.2	0.0	9.2	10.1	9.3
		BLIMP1- avg (%)	**sd**	**se**	**min**	**max**	**Paper**
OUTPUT CELL	Ag+	0.0	0.0	0.0	0.0	0.0	0.00
NOT OUTPUT CELL	Ag+	0.0	0.0	0.0	0.0	0.1	0.05
OUTPUT CELL	Ag-	0.0	0.0	0.0	0.0	0.0	0.00
NOT OUTPUT CELL	Ag-	59.1	0.5	0.0	58.1	60.7	58.31

Supplementary Table 4: Variability in calculated percentages based on 30 repetitions of Simulation 4 (Scenario 2, affinity-based CD40 signal). Avg=average, sd=standard deviation, se=standard error, min=minimum, max=maximum, Paper=value refered to in the main text. Note that variability is small for all percentages except for BLIMP1-/Ag+/No output cell. However, this Ag+/BLIIMP1- cell is not of particular interest in our analyses. Similarly, the Ag-/BLIMP1- has a somewhat larger standard deviation (1.7%) but also this cell type we do not explicitly consider.

Scenario 2		Affinity-based CD40 signal					
		BLIMP1+ avg (%)	**sd**	**se**	**min**	**max**	**Paper**
OUTPUT CELL	Ag+	3.8	0.3	0.0	3.2	4.4	4.1
NOT OUTPUT CELL	Ag+	15.6	0.9	0.0	14.0	17.3	16.6
OUTPUT CELL	Ag-	8.3	0.3	0.0	7.6	8.8	8.6
NOT OUTPUT CELL	Ag-	9.1	0.2	0.0	8.6	9.4	9.1
		BLIMP1- avg (%)	**sd**	**se**	**min**	**max**	**Paper**
OUTPUT CELL	Ag+	0.2	0.0	0.0	0.2	0.3	0.28
NOT OUTPUT CELL	Ag+	6.7	3.3	0.0	2.5	14.2	3.53
OUTPUT CELL	Ag-	0.0	0.0	0.0	0.0	0.0	0.00
NOT OUTPUT CELL	Ag-	56.2	1.7	0.0	52.0	58.6	57.78

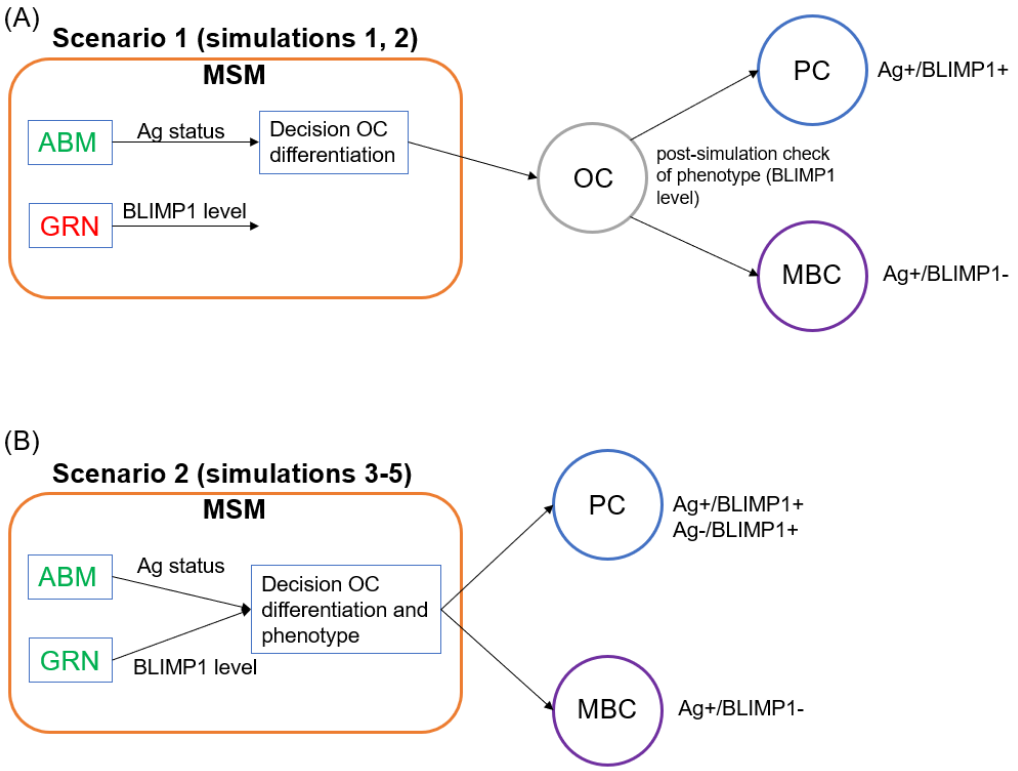

Supplementary Figure 20: Cell-fate decision and phenotype definition of output cells (OC) in Scenario 1 and Scenario 2 simulations. (A) In Scenario 1 the decision for OC differentiation is made at the ABM level (cell level) based on Ag status (Ag-retaining cells after asymmetric division will differentiate to an OC) but BLIMP1 level determines final phenotype (PC or MBC) after production of the OCs. (B) In Scenario 2 both the Ag status and BLIMP1 level are used to decide for OC differentiation and phenotype. Note, only in Simulations 1 and 3 no MBCs are produced.

Chapter 3

Coupled antigen and BLIMP1 asymmetric division with a large segregation between daughter cells recapitulates the temporal transition from memory B cells to plasma cells and a DZ-to-LZ ratio in the germinal center

Elena Merino Tejero[#], Danial Lashgari[#], Rodrigo García-Valiente, Jiaojiao He, Philippe A. Robert, Michael Meyer-Hermann, Jeroen E.J. Guikema, Huub Hoefsloot, Antoine H.C. van Kampen

[#]Equally contributed

3.1. Abstract

Memory B cells (MBCs) and antibody (Ab)-secreting plasma cells (PCs) are generated within germinal centers (GCs) during affinity maturation in which B-cell proliferation, selection, differentiation, and self-renewal play important roles. The mechanisms behind MBC and PC differentiation in GCs are not well understood. However, it has been suggested that cell fate is (partially) determined by asymmetric cell division, which involves the unequal distribution of cellular components to both daughter cells. To investigate what level and/or probability of asymmetric segregation of several fate determinant molecules, such as the Ag and transcription factors (TFs) (B-cell lymphoma 6 (BCL6), interferon regulatory factor 4 (IRF4), and B-lymphocyte-induced maturation protein 1 (BLIMP1) recapitulates the temporal switch and dark zone (DZ)-to-light zone (LZ) ratio in the GC, we implemented a multiscale model (MSM) that combines a core gene regulatory network (GRN) for PC differentiation with a model describing the cellular interactions and dynamics in the GC. Our simulations show that BLIMP1

driven PC differentiation together with coupled asymmetric division of antigen (Ag) and BLIMP1 with a large segregation between the daughter cells results in a GC DZ-to-LZ ratio and a temporal switch from MBCs to PCs that have been observed in experiments. [1]

3.2. Introduction

MBCs and antibody-secreting PCs are generated within GCs during affinity maturation in which B-cell proliferation, selection, differentiation, and self-renewal play important roles in the GC reaction (N. S. De Silva and Klein, 2015). Positive selection of B cells is facilitated by collecting Ag presented by follicular dendritic cells (FDCs) and subsequent engagement in T follicular helper (Tfh) cells contacts. B cells with higher-affinity B-cell receptors (BcRs) are thought to receive more help from Tfh cells due to increased presentation of histocompatibility molecule II (pMHCII) on their surface. Selected B cells recycle to the DZ to further divide and differentiate as output cells (OCs), or to enter a next cycle of selection (recycling).

The mechanisms behind MBC and PC differentiation into OCs from GCs are not well understood. However, in other systems, such as Drosophila, it has been suggested that cell fate is (partially) determined by asymmetric cell division, which involves the unequal distribution of cellular components to both daughter cells (Neumüller and Knoblich, 2009). Another study exclusively analyzed the distribution of Ag in *in vivo* and *in vitro* mouse B cells showing that accumulated Ag is maintained in a polarized distribution prior to the division in approximately 72% of the B cells, and that this polarization is maintained during cell division resulting in an asymmetric division of Ag over both daughter cells (Thaunat *et al.*, 2012). The daughter cell that receives more Ag as a result of asymmetric division was postulated to be more efficient in receiving T cell help, both at the B-T cell border and in the GC, which may affect cell fate (Thaunat *et al.*, 2012). In the same issue it was argued and shown by computational modeling that asymmetric division may largely affect the production of PCs (Dustin and Meyer-Hermann, 2012). Later, a more comprehensive computational model of the GC reaction predicted that asymmetric division of Ag might co-determine B-cell fate since inclusion of this mechanism resulted in GC transzone migration rates and DZ-to-LZ ratio in agreement with experimental data (Victora *et al.*, 2010; Meyer-Hermann *et al.*, 2012).

[1] This chapter is based on Merino Tejero E, Lashgari D, García-Valiente R, Jiaojiao H, Robert PA, Meyer-Hermann M, Guikema JEJ, Hoefsloot H, van Kampen AHC. Coupled Antigen and BLIMP1 Asymmetric Division With a Large Segregation Between Daughter Cells Recapitulates the Temporal Transition From Memory B Cells to Plasma Cells and a DZ-to-LZ Ratio in the Germinal Center. Frontiers in immunology (2021) 12:716240.

In addition to asymmetric Ag division, *in vitro* studies have shown that other B-cell fate-altering molecules, such as transcriptional regulator BCL6 and the receptor for interleukin-21 (IL-21R), segregate asymmetrically in approximately 44% of mitotic GC B cells (Barnett *et al.*, 2012). In contrast, IRF4 was mostly symmetrically distributed (11% asymmetry comparable to tubulin). The same study suggested that CD40 signaling facilitates TF asymmetry by providing polarity cues to B cells. However, other polarity cues (e.g., cell-cell contacts (Lin *et al.*, 2015)), TFs (e.g., BLIMP1 transcription (Radtke and Bannard, 2019)) and signaling pathways (e.g., nuclear factor kappa-light-chain-enhancer of activated B cells (Nf-kB)) may drive asymmetric division and/or B-cell fate.

Regardless of the mechanism, asymmetric division has been shown to result in daughter cells with unequal amounts of Ag and/or TF. The amount of segregation seems to vary for different TFs and this might be dependent on polarity cues, signaling pathways and strength, and/or stochastic events. We hypothesized that (the level of) Ag and TF (BCL6, IRF4, BLIMP1) segregation affects GC dynamics and B-cell fate in different ways or to different extents. To test this hypothesis we implemented a MSM that combines a core GRN for B-cell of PC differentiation with a model describing the cellular interactions and dynamics in the GC.

Our simulations show that BLIMP1 driven PC differentiation coupled to asymmetric division of Ag and BLIMP1 with a large segregation between the daughter cells results in a GC transzone migration and a temporal switch from MBCs to PCs that are both observed in experiments (Victora *et al.*, 2010; Florian J Weisel *et al.*, 2016). Consequently, these computational results prompt for more direct experiments aimed to verify of falsify this mechanism for PC differentiation.

3.3. Methods

3.3.1. Multiscale model

To enable the investigation of cellular and molecular mechanisms involved in PC differentiation we recently developed a MSM (Merino Tejero *et al.*, 2020) that integrates an agent based model (ABM) of the GC reaction (Meyer-Hermann *et al.*, 2012) with a GRN involved in PC differentiation (Martínez *et al.*, 2012). We slightly modified this model to investigate the effect of asymmetric Ag and TF division. In brief, the ABM contains the main processes that take place in the GC reaction, which lasts for 21 days (504 hours). B cells at the centroblast (CB) state divide in the DZ while accumulating SHMs in their BcR. They then differentiate to centrocytes (CCs) and migrate to the LZ where they may encounter FDCs and Tfh cells. FDCs carry Ag in their membrane, which is internalized by CCs when in contact with an affinity dependent rate. This provides CCs with survival signals that temporarily rescue them from apoptosis and allow them to undergo further

encounter(s) with Tfh cells. CCs with higher internalized Ag, thus higher affinity for the Ag will outcompete other CCs with less internalized Ag. CCs are then fully rescued from apoptosis and recycle back to the DZ as CBs. Recycled CBs further divide asymmetrically in 72% of the cases where all of the internalized Ag goes to one of the daughter cells. The GRN of PC differentiation comprises three TFs (BLIMP1, BCL6 and IRF4) that regulate each other and are affected by upstream BcR and CD40 signals. BCL6 is involved in maintaining GC B-cell phenotype while IRF4 and BLIMP1 promote PC differentiation and exit from the GC. Initial TF concentration in founder CBs were based on microarray data (Martínez *et al.*, 2012) and defined as follows (BLIMP1=0, BCL6=5, and IRF4=0) to achieve the high BCL6 and low BLIMP1 and IRF4 steady state. CCs receive signals through BcR and CD40 respectively when in contact with FDCs or Tfh cells. While BcR signal strength is constant, CD40 signal strength depends on affinity, which can ranges in the model between 0 and 1, and determines the cell fate. The GRN is a bistable system with one state (BCL6 high, BLIMP1 and IRF4 low) being the intracellular state of CBs, CCs and MBCs and a second state (BLIMP1 and IRF4 high, BCL6 low) representing the intracellular state of PCs. After dividing, recycled CBs that inherited all of the internalized Ag, and/or are in BLIMP1 high state, differentiate to OCs, either MBCs or PCs, while the remaining CBs differentiate to CCs and stay in the GC. Ag in the CCs is removed giving no advantage in further rounds of selection.

3.3.1.1. Definition of output cells and Memory versus PC differentiation fate

Table 4 shows the cell type definition based on Ag status and BLIMP1 level. Recycled CBs that finish dividing may differentiate to PCs at any time of the GC reaction (Figure 18) when BLIMP1 reaches the differentiation threshold ($\geq 8.10^{-8}$M) and become BLIMP1+ irrespective of its Ag status and, consequently, PCs may either be Ag+ or Ag-. BLIMP1+ cells that are not (yet) OCs are annotated as PB (Ag+ or Ag-). Ag+/BLIMP1- OCs are considered to be MBCs. This definition correctly recapitulates the MBC dynamics as described in Weisel and co-workers (Florian J Weisel *et al.*, 2016). Finally, Ag-/BLIMP1- CBs stay in the GC and recycle back to the LZ as CCs.

Table 4. Definition of OCs (PCs and MBCs) in terms of Ag status and BLIMP1 level.

PC	Ag+ / BLIMP1+	Ag- / BLIMP1+
MBC	Ag+ / BLIMP1-	

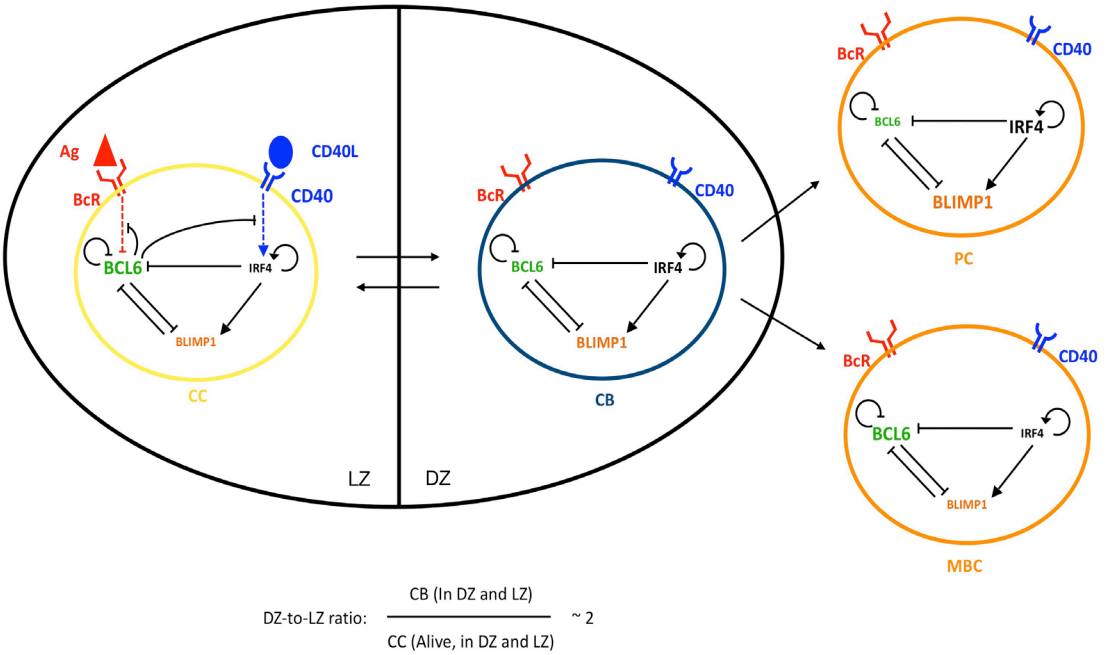

Figure 18: Four GC B-cells representing the PC differentiation process: CC (yellow), CB (blue) , PC (orange) and MBC (orange). CBs are mainly present in the DZ and CCs in the LZ while PCs and MBCs are mainly generated in the DZ and then exit the GC. Transition between CBs and CCs is reversible while transition between CBs and PCs or MBCs is irreversible. The DZ-toLZ ratio is the ratio of CBs to non-apoptotic CCs present in both zones and fluctuates around 2. An intracellular GRN comprising three TFs is embedded in each B-cell: BCL6 (green), IRF4 (black) and BLIMP1 (orange). The size of each TF represents the expression levels in the cell state. The CC BcR may bind to Ag (red) or the CD40L (blue) when receiving Tfh-cell help, resulting in BcR and CD40 signaling respectively, which changes the state of the network. . Arrows between cells represent transition. Arrows between TFs, BcR and/or CD40 indicate activation. Bar-headed lines denote inhibition.

3.3.1.2. Modelling of asymmetric division

In the current model we do not distinguish between different mechanisms that lead to asymmetry but only assume that Ag and TFs (BCL6, IRF4, BLIMP1) can be unequally distributed between the two daughter cells. Asymmetric division is parameterized by a probability (P) of asymmetric division and a polarity level (L) representing the extent of asymmetry. Following experimental observations from Thaunat and coworkers, we set the probability for asymmetric division of Ag to either P_{Ag}=0.0 or P_{Ag}=0.72 (Thaunat *et al.*, 2012). The same study showed that Ag division can happened both symmetrically and asymmetrically, which is why we did not further investigate asymmetric Ag probabilities of 100%. Consequently, in 0% or 72% of the cell divisions, the Ag is distributed asymmetrically over the daughter cells. The probability of asymmetric division for TFs is unknown and, therefore, we used three different probabilities: P_{TF}=0.0, P_{TF}=0.72 or P_{TF}=1.0. Consequently, in 0%, 72% or 100% of the cell divisions the TFs are distributed asymmetrically over the daughter cells. In the current model, when the Ag and TFs are asymmetrically distributed in the same division, high Ag and TF polarity levels are directed towards the same daughter cell. Nevertheless,

in this study we are interested in simulating the effect of simultaneous asymmetric division of Ag and TFs.

The polarity level (L_{Ag} and L_{TF}) of asymmetry represents the concentration of Ag and TFs in one daughter cell expressed as the fraction of Ag and TFs in the parent cell; the second daughter cell, by definition, assumes a concentration of 1-polarity. Consequently, a polarity level of L=0.5 represents symmetric division (the concentration of Ag and TFs in each daughter cell is 50% of the parent cell). An asymmetric division probability P=0.0, by definition, corresponds to a polarity level (L=0.5). A polarity level of L=1.0 results in one daughter cell that has taken all Ag and/or TFs from the parent cell, while the other daughter cell will receive none. In the simulations the TFs may segregate with a different polarity levels (L_{BLIMP1}, L_{BCL6}, L_{IRF4}).

3.3.1.3. Simulations of multiscale model

We performed two sets of GC simulations. In the first set of 9 simulations (Table 5) the TFs co-segregate with equal polarity levels while in the second set of 27 simulations (Table 6) the TFs may co-segregate with different polarity levels. Simulation 3 from the first set (Table 5) is considered the reference simulation in which there is asymmetric division of Ag (P_{Ag}) but always symmetric division of TFs. We consider this simulation as the reference since in the original LEDA model no TFs were modeled while asymmetric Ag division showed to result in a correct DZ-to-LZ ratio. The DZ-to-LZ ratio was calculated as the ratio of CBs to non-apoptotic CCs present in both zones (Figure 18). Since Simulations 1 – 3 from the second set of 27 simulations (Table 6) were the only cases to show differences in the MBC and PC dynamics, we repeated these simulations 15 times with different random seeds. Supplementary Figures 21 - 23 show the results from these repetitions and demonstrate there is a limited variability in the temporal dynamics. Therefore, we did not repeat the other simulations since these are expected to give a similar amount of variation.

Table 5. Simulated asymmetry of TF concentrations (polarity level L_{TF}) in daughter cells after division. When mode of Ag division is asymmetric the probability and polarity level are P_{Ag}=0.72; L_{Ag}=1.0 otherwise these are set to (P_{Ag}=0.0; L_{Ag}=0.5) for symmetric Ag division. In these 9 simulations BCL6, IRF4 and BLIMP1 are co-segregated.

		Mode Ag division	
		Asymmetric	Symmetric
Simulation	**Description**	**TF Polarity level (L_{TF})**	
1	(i) Symmetric Ag and TF division (P_{Ag}=P_{TF}=0)	N.A.	0.5
2	(ii) Symmetric Ag division and asymmetric TF division (P_{Ag}=0, P_{TF}=0.72)	N.A.	1.0
3	(iii) Symmetric TF division and asymmetric Ag division (**reference;** P_{Ag}=0.72, P_{TF}=0)	0.5	0.5
4	(iv) Asymmetric TF division only if mode of Ag division is asymmetric (**coupled asymmetric division**; P_{Ag}=P_{TF}=0.72)	1.0	0.5
5		0.9	0.5
6		0.75	0.5
7	(v) Always asymmetric TF division regardless of mode of Ag division (**uncoupled asymmetric division**; P_{Ag}=0.72, P_{TF}=1.0))	1.0	1.0
8		0.9	0.9
9		0.75	0.75

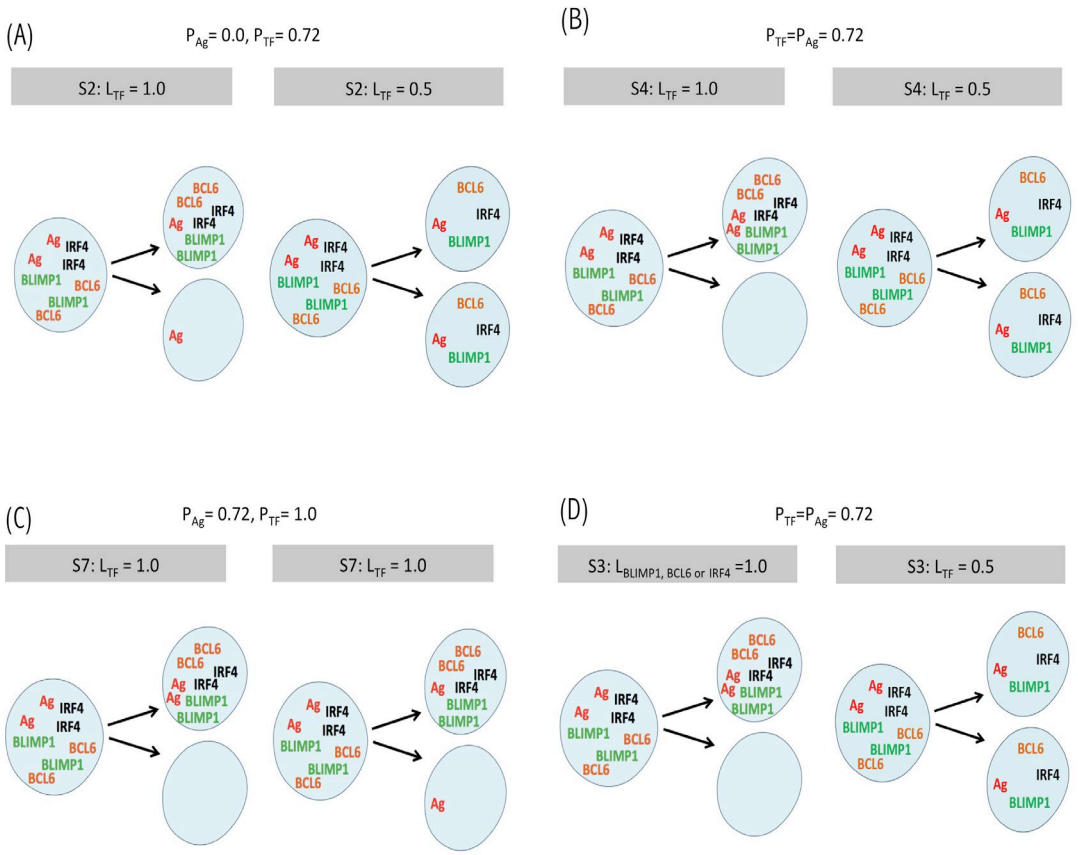

Figure 19: Scheme of internalized Ag and TF division patterns modeled in a selection of simulations (Table 2 and 3) (A) Simulation 2, symmetric Ag and asymmetric TF distribution (L_{TF}=1.0), (B) Simulation 4, coupled asymmetric division (L_{TF}=1.0), (C) Simulation 7, uncoupled asymmetric division (L_{TF}=1.0), and (D) Simulation 3, partial asymmetric co-segregation of TFs and Ag (P_{TF}=P_{Ag}=0.72; L_{Ag}=1.0) while varying the level of BLIMP1 (L_{BLIMP1}=1.0). Internalized Ag (red) and TF (orange, green, black) are shown in the parent and two daughter cells. The probability and polarity levels are shown in the grey box.

In the first set of simulations we studied different combinations of Ag and TF (a)symmetric division (Table 5). In these simulations the TF are co-segregated over the daughter cells according to the polarity levels (L_{TF}) shown in the Table 5. The polarity level for the asymmetric Ag division is always L_{Ag}=1.0. These nine simulations represent five scenarios: (i) TFs and Ag divide symmetrically (P_{TF}=P_{Ag}=0.0) (ii) TFs divide asymmetrically with probability P_{TF}= 0.72 while Ag always divides symmetrically (P_{Ag}= 0.0; Figure 19A). (iii) TFs divide symmetrically (P_{TF}=0.0) while Ag can divide asymmetrically (P_{Ag}=0.72; reference). (iv) TFs divide asymmetrically (P_{TF}= 0.72) only when Ag divides asymmetric (P_{Ag}=1.0; Figure 19B), (iv) TFs always divide asymmetrically (P_{TF}=1.0) while Ag divides asymmetrically with probability P_{Ag}=0.72 (Figure 19C).

Table 6. Simulated asymmetry of TFs concentrations (P_{TF}=0.72; polarity levels $L_{BLIMP1,}$ L_{IRF4} and L_{BCL6}) in daughter cells after asymmetric division. TFs divide asymmetrically if Ag divides asymmetrically (P_{Ag}= P_{TF} =0.72; L_{Ag}=1.0). In these 27 simulations BCL6, IRF4 and BLIMP1 do not always co-segregate with same polarity levels.

	Mode Ag division			
	Asymmetric			Symmetric
	Polarity level (L_{TF})			
Simulations	BLIMP1 (L_{BLIMP1})	IRF4 (L_{IRF4})	BCL6 (L_{BCL6})	BLIMP1, IRF4, BCL6 (L_{BLIMP1}=L_{IRF4}-L_{BCL6})
1 - 3	1.0 0.75 0.9	1.0	1.0	0.5
4 - 6		0.9	1.0	0.5
7 - 9		0.75	1.0	0.5
10 - 12		1.0	0.9	0.5
13 - 15		0.9	0.9	0.5
16 - 18		0.75	0.9	0.5
19 - 21		1.0	0.75	0.5
22 - 24		0.9	0.75	0.5
25 - 27		0.75	0.75	0.5

In the second set of 27 simulations the Ag is distributed asymmetrically in 72% of the recycled B-cell divisions (P_{Ag}=0.72, L_{Ag}=1.0; Table 6) since it was previously shown that this results in transzone migration rates in better agreement with experimental data (Meyer-Hermann *et al.*, 2012). In these simulations the TFs co-segregate with the Ag since they only divide asymmetrically when the Ag divides asymmetrically (P_{Ag}=P_{TF}=0.72). Moreover, TFs segregate with different polarity levels (L_{BLIMP1}, L_{BCL6}, L_{IRF4}) as shown in Figure 19D.

3.3.1.4. Simulation of gene regulatory network

To facilitate the interpretation of the MSM we additionally performed a set of GRN simulations, to model TF dynamics. For these simulations initial TF concentration of the mother cell was conceptually chosen to simulate an extreme condition of our MSM in which a mother PB, at the low BCL6 and high BLIMP1 and IRF4 steady state, underwent the last division before becoming a PC and exiting the GC. Subsequently, asymmetric division of the parent PB was simulated with the different combinations of L_{TFs} for the first set of simulations (Table 5). For the second set of simulations, we investigated representative L_{BLIMP1}, L_{BCL6} and L_{IRF4} combinations (i.e., simulations 1-4, 7, 10, 19; Table 6). At the start of the simulation, we define the concentrations of BLIMP1, BCL6, and IRF4 according to the polarity levels and, subsequently, simulate until a steady-state is reached. This allowed us to determine if despite the concentration reduction, BLIMP1 concentration returned to its high level steady-state (PC phenotype). Since we

were simulating TF dynamics of CBs that don't interact with Ag presented by FDCs nor with Tfh cells, we set the CD40 and BcR signals to 0.

3.4. Results

3.4.1. Symmetric TF and Ag division

We first aimed to gain insight in the contribution of asymmetric division on GC dynamics and OCs. Therefore, we simulated the GC reaction without asymmetric Ag and TFs division ($P_{TF}=P_{Ag}=0.0$, $L_{TF}=L_{Ag}=0.5$; Simulation 1, Table 5).

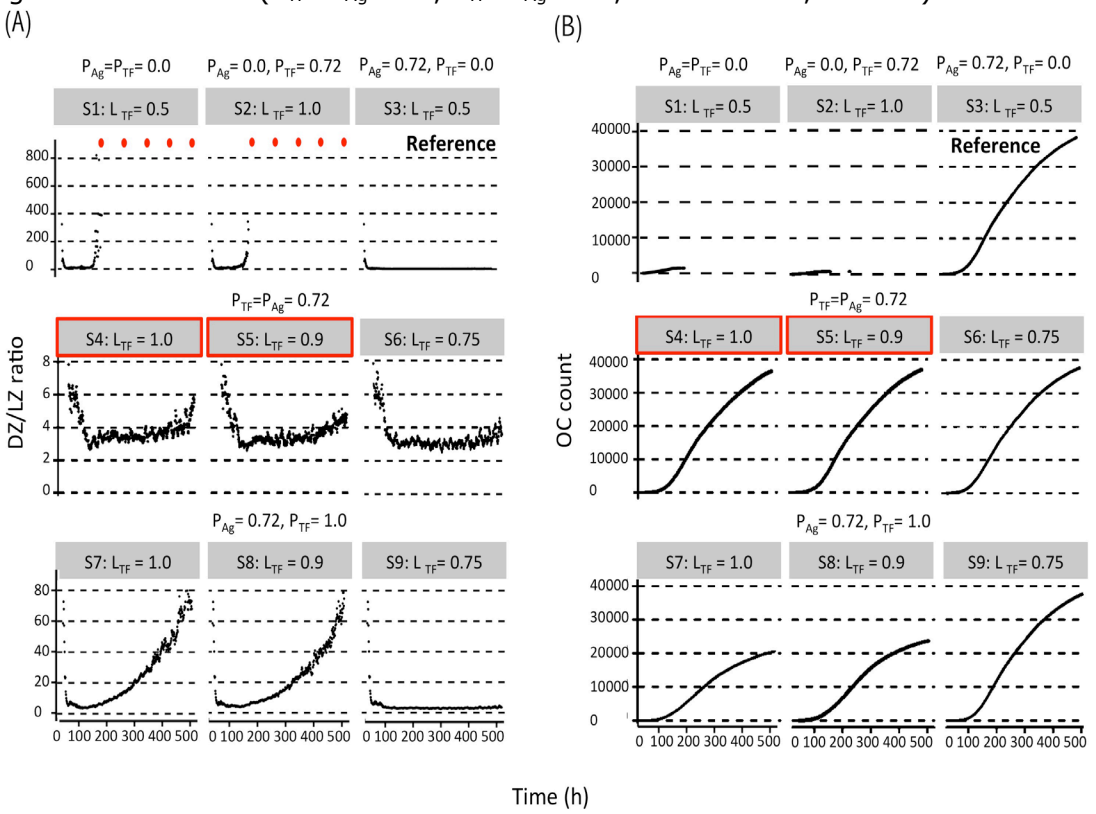

Figure 20: Results from first set of simulations (Table 2). (A) DZ-to-LZ ratio and (B) accumulated OCs during the GC reaction. The probability of asymmetric division (P) is indicated above the grey box and simulation number and polarity levels (L) are shown in the grey box. Red dots indicate DZ-to-LZ ratio values of infinity. First row of plots corresponds to (Left column) symmetric division of Ag and TFs, (Middle column) symmetric division of Ag and asymmetric division of TFs, (Right column) symmetric division of TFs and asymmetric division of Ag. Second row of plots corresponds to asymmetric TF division only if mode of Ag division is asymmetric. Red boxes indicate parameters that are closer to biological results. Third row of plots corresponds to always asymmetric TF division regardless of mode of Ag division.

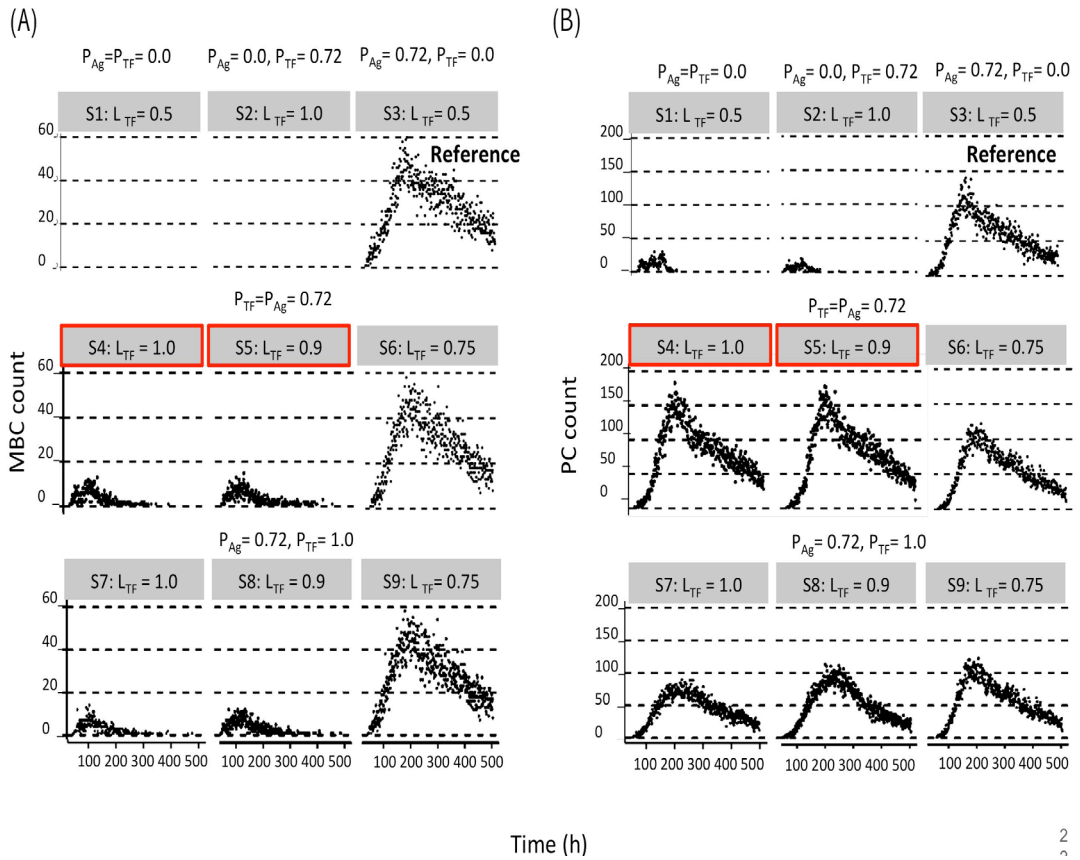

Figure 21: Results from first set of simulations (Table 2). (A) Relative MBC and (B) PC count during the GC. The probability of asymmetric division (P) is indicated above the grey box and simulation number and polarity levels (L) are shown in the grey box. First row of plots corresponds to (Left column) symmetric division of Ag and TFs, (Middle column) symmetric division of Ag and asymmetric division of TFs, (Right column) symmetric division of TFs and asymmetric division of Ag. Second row of plots corresponds to asymmetric TF division only if mode of Ag division is asymmetric. Red boxes indicate parameters that are closer to biological results. Third row of plots corresponds to always asymmetric TF division regardless of mode of Ag division.

We found a DZ-to-LZ ratio that initially fluctuated between 5 and 15 and then increased to values up to 800 or the ratio became infinite due to low or zero CC counts respectively (Figure 20A) strongly contradicting experimentally observed DZ-to-LZ ratio of 2. This is explained by a lack of recycled CBs without retained Ag, which lead to no differentiation to CC state and a premature termination of the GC reaction. Thus, the number of accumulated OCs reached 1417 cells at the end of the GC reaction (Table 7; Figure 20B). No MBCs were produced (Figure 21A) and all OCs were PCs (Figure 21B) due to the lack of Ag+ cells. Furthermore, 87% of PCs were generated within the first 6 days of the GC reaction, which contradicts a temporal switch from MBCs to PCs. (Supplementary Figure 23).

Table 7. Number of OCs at day 21 originating from the first set of simulations (Table 5).

	P_{Ag}	0.0		0.72					
	P_{TF}	0.0	0.72	0.0	0.72		1.0		
	L_{TF}	0.5	1.0	0.5	1.0	0.9	0.75	1.0	0.9	0.75
	Simulation	**1**	**2**	**3 (ref)**	**4**	**5**	**6**	**7**	**8**	**9**
OCs	**PCs**	1,417	759	25,246	35,359	35,791	25,792	19,784	22,755	24,821
	MBCs	0	0	12,886	1,094	1106	12,704	824	948	12,787
	Total	1417	759	38,132	36,453	36,898	38,496	20,608	23,703	37,608

3.4.2. Asymmetric TF division and symmetric Ag division

Next, we aimed to establish the effect of asymmetric TF division while keeping symmetric Ag division (Simulation 2, Table 5. P_{Ag} =0.0, P_{TF} =0.72, L_{Ag}=0.5, L_{TF}=1.0). Again, we find that the DZ-to-LZ ratio initially fluctuated between 5 and 15 and then increased until 400 or were infinite since no CCs were produced (Figure 20A) strongly contradicting experimentally observed DZ-to-LZ ratio of 2. Also, the number of accumulated OCs reached 759 cells at the end of the GC reaction, none of them being MBCs (Table 4, Figure 20B, Figure 21) Furthermore, 92% of PCs were generated within the first 6 days of the GC reaction (Supplementary Figure 23) again contradicting a temporal switch. Finally, asymmetric TF division lead to approximately a 2-fold decrease in PC production compared to symmetric TF division (Simulation 1) as shown in Table 7. This could be explained by analysing the TF dynamics in isolation (Figure 22). Extreme TF polarity levels promoted the production of a daughter B cell in the low BLIMP1 state and another one in the high BLIMP1 state yet symmetric TF polarities promoted the production of both daughter B cells in the high BLIMP1 state. We conclude that asymmetric division of TF only does not result in expected GC dynamics while also the number of OCs remains 50-fold lower than in the reference simulation.

3.4.3. Symmetric TFs division and asymmetric Ag division (reference)

We questioned weather or not symmetric co-segregation of TFs with asymmetric Ag division, had an effect on GC B-cell dynamics (P_{TF} =0.0, L_{TF}=0.5, P_{Ag}=0.72, L_{Ag}=1.0; Simulation 3, Table 5). We found the DZ-to-LZ ratio fluctuating between 2 and 4 (Figure 20A). This was a maximum of 2-fold increase in DZ-to-LZ ratio

compared to previous observations of 2 (Victora *et al.*, 2010) and similar to the affinity-based CD40 signaling simulation (Scenario 2) discussed in (Merino Tejero *et al.*, 2020). The number of accumulated OCs reached 38,132 cells at the end of the GC reaction (Table 7; Figure 20B) of which 12,886 MBCs (Figure 21A) and 25,246 PCs (Figure 21B). Furthermore, MBCs were generated throughout the GC reaction and 90% of PCs were generated after the peak (day 6) of the GC reaction (Supplementary Figure 23). We conclude that asymmetric Ag division is largely responsible for obtaining a DZ-to-LZ ratio close to experimental observations. Asymmetric TF division is not required. Asymmetric Ag division also re-establishes a larger number of OCs but no temporal switch is observed.

3.4.4. Asymmetric TF division only if mode of Ag division is asymmetric (coupled asymmetric division)

Next, we investigated a scenario (Simulations 4 - 6, Table 5; $P_{Ag}=P_{TF}=0.72$) that assumes that asymmetric TF and Ag division always happen simultaneously. Since we are mostly interested in the effect of the TFs, we assumed that in the case of asymmetric division all Ag goes to a single daughter cell ($L_{Ag}=1.0$) while we used different polarization levels for the TF ($L_{TF}=1.0$, 0.9 and 0.75). All three simulations had similar DZ-to-LZ ratios and total number of OCs, which were also similar to the reference simulation (Table 7, Figure 20A-B). Nevertheless, low TF polarity levels showed approximately a 12-fold increase in MBCs, at the expense of PC output, compared to extreme TF polarity levels. Furthermore, low TF polarity levels showed similar MBC counts compared to the reference simulation (Figure 21). Interestingly, extreme TF polarity levels ($L_{TF}=1.0$, 0.9) resulted in a temporal switch from MBCs to PCs, which was not the case for simulations with low TF polarity levels ($L_{TF}=0.75$ nor $L_{TF}=0.5$ in the reference simulation).

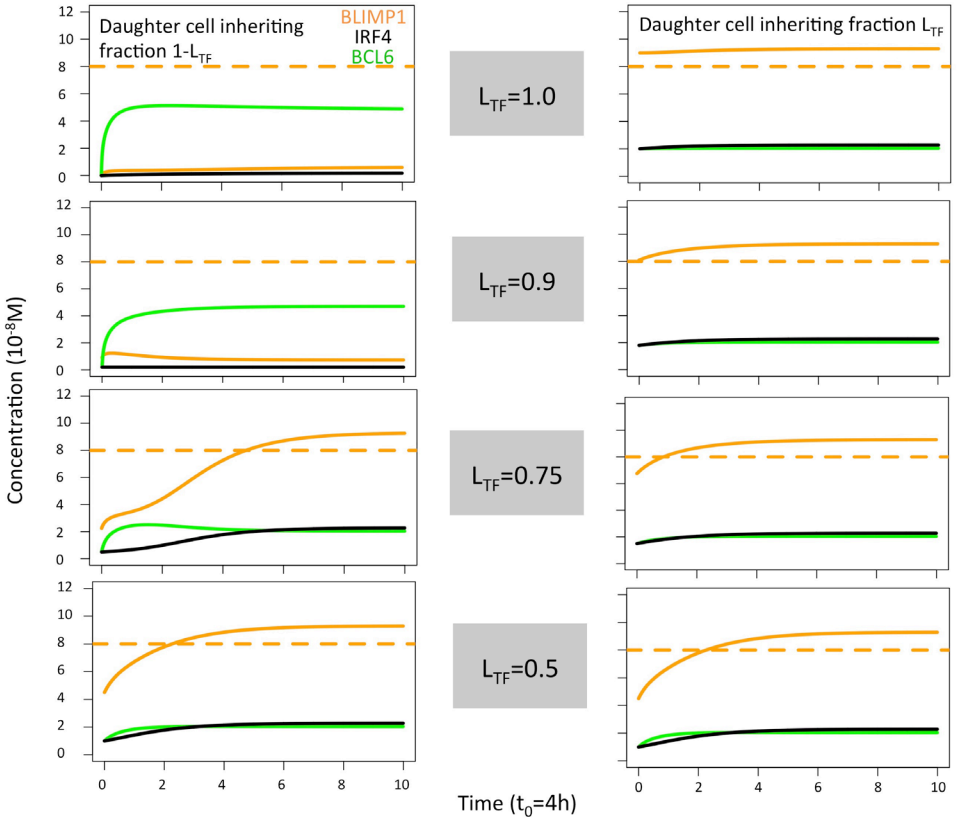

Figure 22: Solution curves based on the GRN (ODE model) for BLIMP1 (orange), BCL6 (green) and IRF4 (black) in two daughter cells. The initial TF concentrations were based on the concentration of the parent cell (BLIMP1=8, BCL6=2, IRF4=2) and the different polarity levels (L_{TF}=1.0, L_{TF}=0.9, L_{TF}=0.75 and L_{TF}=0.5; Table 2).

When analysing the TF dynamics in the GRN, we found, as expected, that extreme TF polarity levels generated a high BLIMP1 state in one of the TF inheriting daughters (0 hours, Figure 22) while leaving the other daughter B-cell in a low BLIMP1 state. Contrarily, low TF polarity levels promoted a slower progression to the high BLIMP1 state (4-8 hours), which explains the increased number of MBCs (Ag+/BLIMP1-) in Simulations 3 and 6. We conclude that simultaneous asymmetric division of Ag and TF results in DZ-to-LZ ratios similar to the reference simulation but only extreme TF polarity levels resulted in a temporal switch.

3.4.5. Always asymmetric TF division regardless of mode of Ag division (uncoupled asymmetric division)

Since there is no a priori reason to believe that asymmetric Ag and TF division are coupled (Simulations 4 – 6), we performed three additional simulations in which TF always divide asymmetrically (P_{TF}=1.0, L_{TF}=1.0, L_{TF}=0.9 and L_{TF}=0.75) regardless of the model of Ag division (P_{Ag}=0.72, L_{Ag}=1.0; Simulations 7 - 9,

Table 5). We found that for extreme TF polarity levels (L_{TF}=1.0, 0.9) the DZ-to-LZ ratio progressively increased up to a value of 80, which meant a 40-fold increase compared to the reference simulation (Figure 20A). Contraryly, low TF polarity levels (L_{TF}=0.75) showed a DZ-to-LZ ratio that fluctuated between 2 and 4 similarly to the reference simulation (Figure 20A). Extreme TF polarity levels showed a 2-fold decrease in OC counts and a 12-fold increase in MBC counts compared to low TF polarity levels and the reference simulation (Table 7; Figure 21B). In extreme TF polarity levels, there was a 1.2-fold decrease in PC counts compared to low TF polarity levels and a 1.7-fold decrease in PC counts compared to simulations with coupled asymmetric Ag and TFs division. (Table 7, Figure 21). While approximately 90% of PCs were generated after the peak (day 6) of the GC reaction for all TF polarity levels, low TF polarity levels produced MBCs during the entire GC reaction (Supplementary Figure 24). Thus, while low polarity levels resulted in similar DZ-to-LZ ratio and OC production as the reference simulation, it did not result in a temporal switch from MBCs to PCs.

The TF dynamics in the GRN, as described in the previous section (see above, Figure 21), explained the decreased OC count observed in Simulations 7 and 8 compared to Simulations 4-6 and 9. Also, it could explain the similarity in OC count observed when comparing Simulations 6 and 9.

We concluded that uncoupled Ag and TFs asymmetric division lead to a 40-fold increase in DZ-to-LZ ratios and a reduction in OC production for the extreme TF polarity levels. However, for these extreme polarities a temporal switch is observed.

Collectively, the first set of simulations show that assuming that the decision for PC differentiation is fully based on BLIMP1 levels and that all TFs co-segregate during asymmetric division, then the simulated DZ-to-LZ ratio is close to those observed experimentally. Furthermore, a temporal switch from MBCs to PCs was only present in simulations with coupled Ag and TFs asymmetric division and extreme TF polarities $L_{TF.}$

3.4.6. Coupled Ag and TFs asymmetric division with different polarity levels for individual TFs

From the first set of simulations (Simulation 1 – 9, Table 5) we showed that coupled Ag and TFs asymmetric division with extreme TF polarity levels resulted in a DZ-to-LZ ratio that was similar to the reference simulation and a temporal switch. However, in these simulations we assumed that BCL6, IRF4 and BLIMP1 always distributed in equal amounts (L_{TF}) over the daughter cells. Based on previous research this is unlikely (Barnett *et al.*, 2012; Lin *et al.*, 2015) Therefore, we performed 27 additional simulations (Table 6; P_{TF}=P_{Ag}=0.72 and L_{Ag}=1.0) in which TFs can be distributed in different amounts ($L_{BLIMP1,}$ $L_{IRF4\ and}$ L_{BCL6}) to the daughter cells. In these simulations TFs are only asymmetrically

distributed in case of asymmetric Ag division. For each simulation we investigated the GC dynamics and OC production.

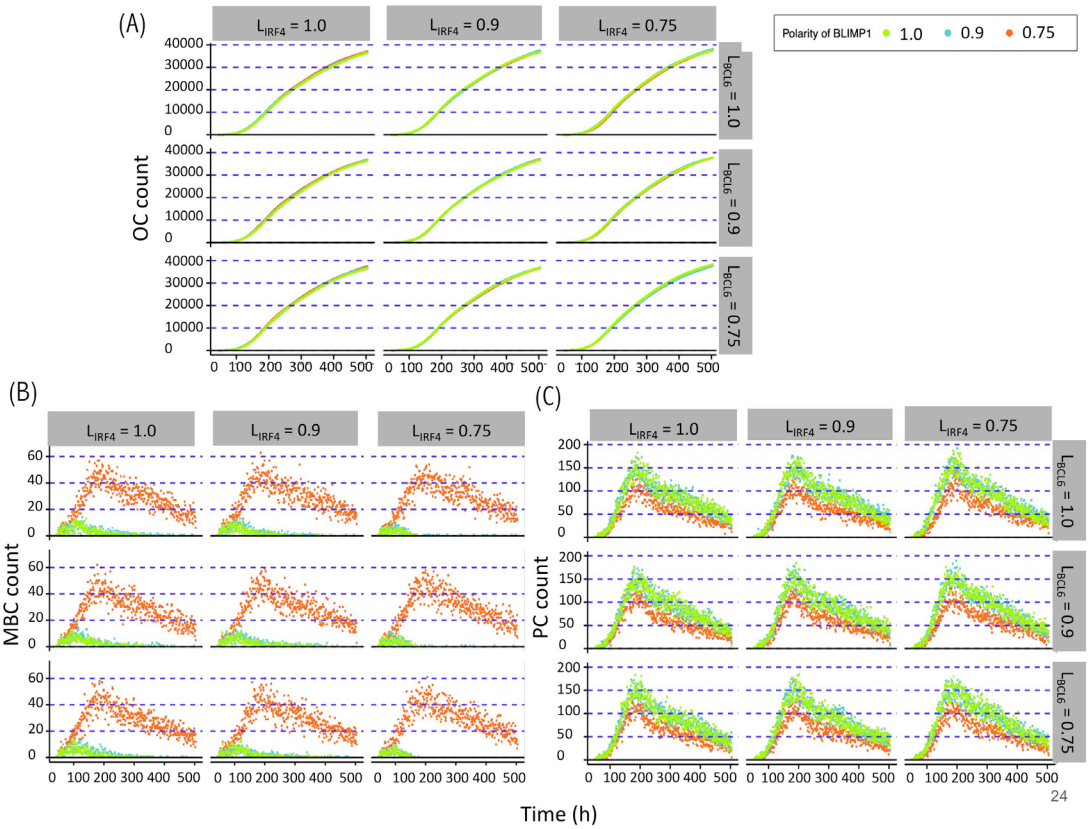

Figure 23: Results from the second set of simulations (Table 3). (A) Accumulated OCs, (B) relative MBC and (C) PC count during the GC reaction. At the top of each panel column, the IFR4 polarity level is indicated. To the right of each panel row, the BCL6 polarity level is indicated. The colors indicate the different BLIMP1 polarity levels.

All simulations showed a DZ-to-LZ ratio that was similar to the reference simulation (data not shown). Furthermore, the number of OCs at the end of the GC reaction is similar for all 27 simulations (Figure 23A). Figure 23B and C shows the number of MBCs and PCs produced for the 27 combinations of TF polarity levels. We observed that neither the polarity level of IRF4 nor BCL6 have a big influence on the number of OCs, MBCs or PCs. However, there is a clear difference when comparing the extreme (L_{BLIMP1}=1.0 and L_{BLIMP1}=0.9; L_{IRF4}=L_{BCL6}=1.0) and low (L_{BLIMP1}=0.75; L_{IRF4}=L_{BCL6}=1.0) BLIMP1 polarity levels. Low polarity levels resulted in a 12-fold increase in MBC counts and a 1.2-fold decrease in PC counts (Supplementary Figures 25-27).

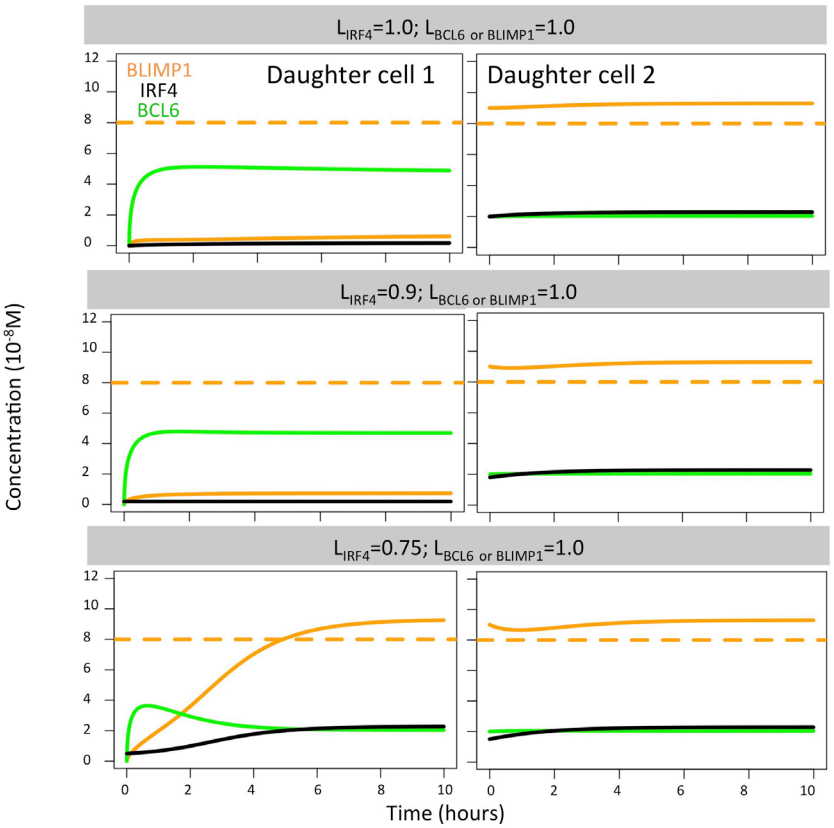

Figure 24: BLIMP1 (orange), BCL6 (green) and IRF4 (black) dynamics in two theoretical daughter B cells. Their initial TF concentrations were set to simulate the asymmetric division of a parent cell (BLIMP1=8, BCL6=2, IRF4=2) with all different combinations of IRF4 levels (L_{IRF4}=1.0, L_{IRF4}=0.9 and L_{IRF4}=0.75, as shown in Table 2). Levels of BCL6 and BLIMP1 were fixed (L_{BCL6}=L_{BLIMP1}=1.0).

When analysing the TF dynamics in the GRN we found that extreme IRF4 polarity levels (L_{IRF4}=1.0, L_{IRF4}=0.9; L_{BLIMP1}=L_{BCL6}=1.0) immediately generated a high BLIMP1 state in one of the TF inheriting daughters while leaving the other daughter B-cell in a low BLIMP1 state (Figure 24). Low IRF4 polarity levels (L_{IRF4}=0.75; L_{BLIMP1}=L_{IRF4}=1.0) generated a both daughter B cells in the high BLIMP1 steady state. Nevertheless, in this situation, the daughter B-cell that inherited 25% (1- L_{IRF4}) of IRF4, along with 0% of BLIMP1 and BCL6 concentration, slowly progressed to the high BLIMP1 state within 20 hours until BLIMP1 levels reached the PC differentiation threshold. Considering that after the last division PBs are defined as PCs and exit the GC, this could explain why no difference in OC dynamics was observed when varying IRF4 polarity levels.

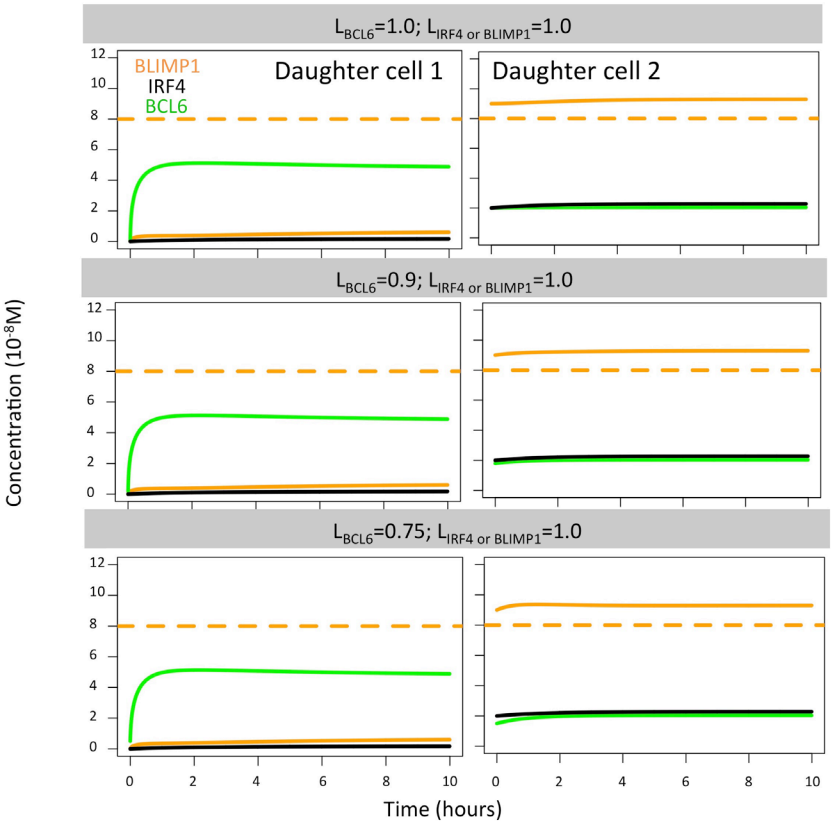

Figure 25: BLIMP1 (orange), BCL6 (green) and IRF4 (black) dynamics in two theoretical daughter B cells. Their initial TF concentrations were set to simulate the asymmetric division of a parent cell (BLIMP1=8, BCL6=2, IRF4=2) with all different combinations of BCL6 levels (L_{BCL6}=1.0, L_{BCL6}=0.9 and L_{BCL6}=0.75, as shown in Table 2). Levels of IRF4 and BLIMP1 were fixed (L_{IRF4} =L_{BLIMP1} =1.0).

In the case of BCL6, we found all polarity levels (L_{BCL6}=1.0, L_{BCL6}=0.9, L_{BCL6}= 0.75; L_{BLIMP1}=L_{IRF4}=1.0) immediately generated a high BLIMP1 state in one of the TF inheriting daughters, leaving the other daughter B-cell in a low BLIMP1 state (Figure 25). This is why no difference in OC dynamics was observed when varying BCL6 polarity levels. Such results were not surprising since changes in the BCL6 level as a result of BcR signaling are not sustained in time nor become large enough to switch the BLIMP1 from a high to low level.

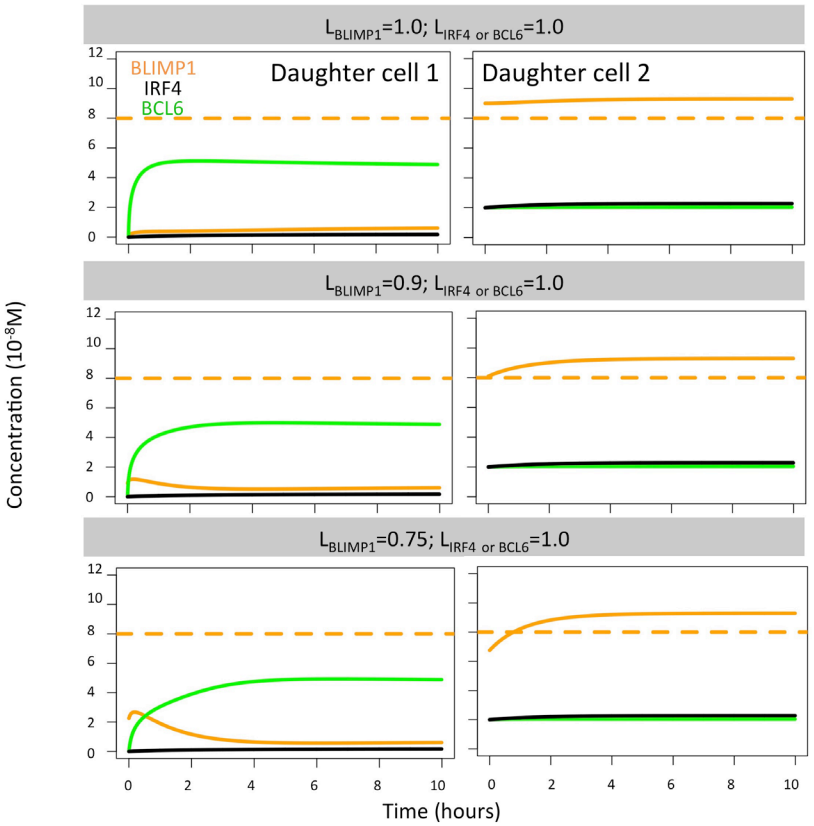

Figure 26: BLIMP1 (orange), BCL6 (green) and IRF4 (black) dynamics in two theoretical daughter B cells. Their initial TF concentrations were set to simulate the asymmetric division of a parent cell (BLIMP1=8, BCL6=2, IRF4=2) with all different combinations of BLIMP1 levels (L_{BLIMP1}=1.0, L_{BLIMP1}=0.9 and L_{BLIMP1}=0.75, as shown in Table 2). Levels of IRF4 and BCL6 were fixed (L_{IRF4}=L_{BCL6}=1.0).

Finally, we found extreme BLIMP1 polarity levels (L_{BLIMP1}=1, L_{BLIMP1}=0.9; L_{IRF4}=L_{BCL6}=1.0) immediately generated a high BLIMP1 steady state in one of the TF inheriting daughters, leaving the other daughter B-cell in a low BLIMP1 steady state (Figure 26). Low BLIMP1 polarity levels (L_{BLIMP1}=0.75; L_{BCL6}=L_{IRF4}=1.0) introduced a delay (4 hours) in the progression of the high BLIMP1 inheriting daughter B-cell to the high BLIMP1 state. This could explain the differences observed in OC dynamics when varying BLIMP1 polarity levels.

We conclude that the combined results from these 27 simulations and the first set of 9 simulations show that BLIMP1 driven PC differentiation together with coupled asymmetric division of Ag and BLIMP1 with a large segregation between the daughter cells results in a GC DZ-to-LZ ratio and a temporal switch from MBCs to PCs that are both observed in experiments (Victora *et al.*, 2010; Florian J Weisel *et al.*, 2016) However, future experimental validation of our findings remain necessary.

3.5. Discussion

It has been shown experimentally that Ag and TFs can asymmetrically divide and that this may co-determine GC B-cell fate (Barnett *et al.*, 2012; Meyer-Hermann *et al.*, 2012; Thaunat *et al.*, 2012; Lin *et al.*, 2015). However, so far this has not been proven experimentally. Based on a computational model of the GC, Meyer-Hermann and colleagues hypothesized that asymmetric division of Ag might play a role in PC differentiation as this resulted in a DZ-to-LZ ratio in agreement with experimental data (Meyer-Hermann *et al.*, 2012). However, using our MSM we recently showed that asymmetric Ag division alone cannot explain PC differentiation since it is not fully consistent with experimental observations that B-cells with increased BLIMP1 levels differentiate to PCs but we only considered one specific mode of coupled asymmetric division (i.e., $P_{Ag}=P_{TF}=0.72$, $L_{BLIMP1}=L_{IRF4}=L_{BCL6}=1.0$) (Merino Tejero *et al.*, 2020).. Therefore, in the current work we investigated the putative effect of asymmetric division of Ag and TFs in more detail and hypothesized that this affects GC dynamics and B-cell dynamics and fate. From our simulations we conclude that BLIMP1 driven PC differentiation together with coupled asymmetric division of Ag and BLIMP1 with extreme TF polarity levels for BLIMP1 segregation results in GC DZ-to-LZ ratio and a temporal switch from MBCs to PCs that are also observed in experiments (Victora *et al.*, 2010; Florian J Weisel *et al.*, 2016). This confirmed our previous finding that asymmetric Ag division alone is not sufficient to drive PC differentiation but also asymmetric division of at least BLIMP1 is required.

An important insight from our model is the observation that outcomes of simulations with (uncoupled) symmetric division of Ag and/or TF do not agree with experimental observations (migrations rates, temporal switch). It is, however, important to emphasize that this result does not definitely exclude this scenario to be true. Although our GC model is the most sophisticated model currently available and based on a large range of experimental observations, we cannot exclude the possibility that other choices, assumptions, or parameter settings would change our conclusion. Nevertheless, we think that our simulations provide at least some evidence that asymmetric division is involved in PC differentiation. Furthermore, prior studies have shown that unequal stimulation of signaling pathways, e.g.: CD40 and PI3K, induced when B cells present Ag to and receive help from T_{FH} cells during the selection process in the GC reaction, can provide polarity cues that drive asymmetry division (Barnett *et al.*, 2012; Lin *et al.*, 2015). It was proposed that unequal inheritance of Ag transmembrane receptor, co-stimulation, and/or cytokine signaling could result in unequal activation of signaling pathways. Although this hypothesis was not experimentally tested, it is in line with our finding.

The observation that IRF4 asymmetric division had no effect of PC production was both interesting and surprising. On one hand, in vitro data suggest that IRF4, and/or different levels of T help through Cd40/ Nf-kB induction of IFR4, regulates

MBC and PC differentiation in a concentration-dependent manner (Sciammas *et al.*, 2011; Laidlaw and Cyster, 2020). Furthermore, quantitative modeling of the terminal B-cell differentiation showed through parameter sensitivity analysis for bistability that kinetic parameters associated to IRF4 dynamics and CD40 induction of IRF4, were critical in promoting B-cell transition towards PC differentiation (Martínez *et al.*, 2012). Nevertheless, the same study showed that above a critical IRF4 concentration threshold (> 1.10^{-8}M) CCs irreversibly differentiated to PCs. In our model, asymmetric division takes place at a late stage of B-cell development (PB) in which IRF4 concentration is close to the high IRF4 steady state (2.10^{-8}M). Thus, we found that even with low IRF4 polarity levels, when daughter B-cells inherited 75% of IRF4 (L_{IRF4}=0.75), this did not decrease IRF4 concentration below the above-mentioned critical IRF4 threshold. This explained why we found no effect of IRF4 asymmetric division on PC differentiation. In addition, *in vitro* studies in conjoined sibling B cells showed that unequal IRF4 expression could drive branching of B-cell state prior to the loss of PAX5, a MBC promoter, hence at early stages of B-cell transition to PC. Furthermore, the levels of BLIMP1 in sibling B cells were not measured. Leaving the open question of whether asymmetric BLIMP1 division could be the driver of PC differentiation and supporting the need to further investigate BLIMP1 asymmetric division at later stages of PC differentiation in the GCs.

Apart from model assumptions our study has several limitations. First, our findings and conclusions remain to be validated or falsified in future experiments. We propose experiments to generate data about the (1) BLIMP1 probability of asymmetric division and polarity level in single PBs; (2) extend and/or role of the co-segregation of BLIMP1, BCL6 and IRF4; (3) extend and/or role of (a)symmetric division of CD40 signaling in relation to B-cell fate. Second, the probability (P_{Ag}=0.72) for asymmetric Ag division was based on experimental data (Barnett *et al.*, 2012). For asymmetric TF division we used this same value in several simulations. However, probabilities of P_{BCL6}=0.44 and P_{IRF4}=0.11 have been reported (Barnett *et al.*, 2012) while for BLIMP1 such probability is unknown. Nevertheless, we here show that asymmetric division of IRF4 and BCL6 did not have an effect on the fate of the B-cell and thus we believe this would not change our main conclusion. Third, no data is available about the number of MBCs and PCs produced during a single GC reaction. Thus, we cannot substantiate which simulations are more realistic in terms of OC production. Fourth, as we have discussed previously (Merino Tejero *et al.*, 2020), the current definition of MBCs as Ag+BLIMP1- cells should be improved since it definition merely classifies OCs, which are not PCs to be MBCs. Nevertheless, we here showed that symmetric TF division did not agree with the observation of a temporal switch in the GC reaction. This could indicate that asymmetric TF division plays a role in MBC differentiation. Interestingly, PAX5 has been shown to asymmetrically segregate and always oppose asymmetric IRF4 distribution (Lin *et al.*, 2015). Further experiments need to be carried out to validate this hypothesis since the effect of asymmetric PAX5 division on MBC formation was not addressed.

3.6. Acknowledgements

We thank Barbera van Schaik to setup a Virtual Machine provided by the Dutch national e-infrastructure with the support of SURF Cooperative, to process large output files. This work is supported by a CASyM Exchange Research Grant, COSMIC (www.cosmic-h2020.eu) which has received funding from the European Union's Horizon 2020 research and innovation program under the Marie Skłodowska-Curie grant agreement No 765158, and by the Human Frontier Science Program 570 (RGP0033/2015).

3.7. Supplementary Information

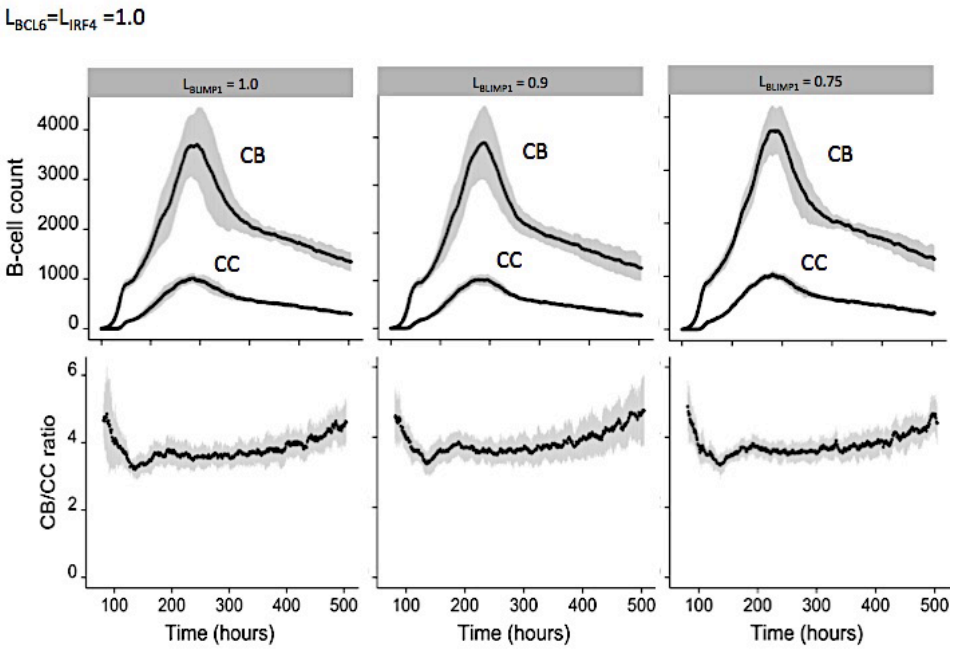

Supplementary Figure 21: Overall GC dynamics for three BLIMP1 polarity levels for Simulations 1-3 (Table 5). (Top) CB and CC counts. (Bottom) DZ-to-LZ ratio. Mean and standard deviation from of 15 different repetitions (random seeds) are shown.

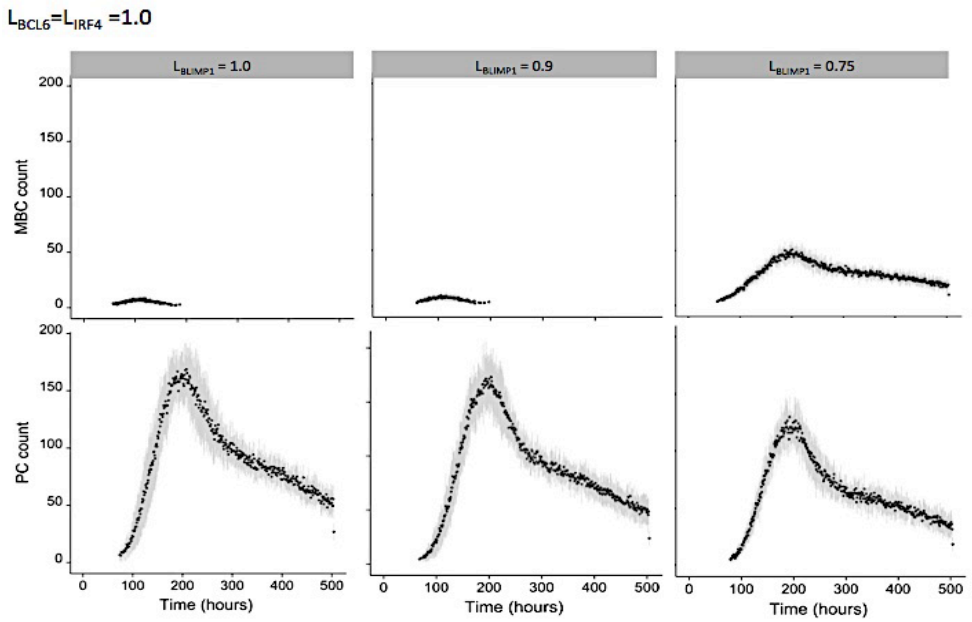

Supplementary Figure 22: Overall MBC and PC dynamics for three BLIMP1 polarity levels for Simulations 1-3 (Table 5). (Top) MBC counts. (Bottom) PC counts. Mean and standard deviation of 15 different repetitions (random seeds) are shown.

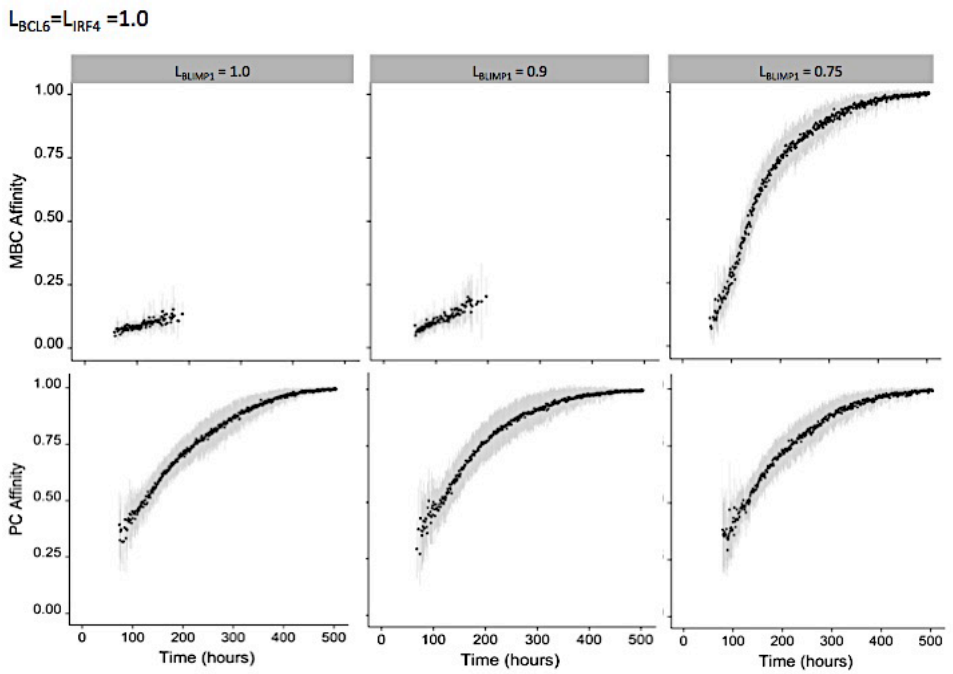

Supplementary Figure 23: Overall MBC and PC affinity dynamics for three BLIMP1 polarity levels for Simulations 1-3 (Table 5). (Top) MBC mean affinity. (Bottom) PC mean affinity. Mean and standard deviation of 15 different repetitions (random seeds) are shown.

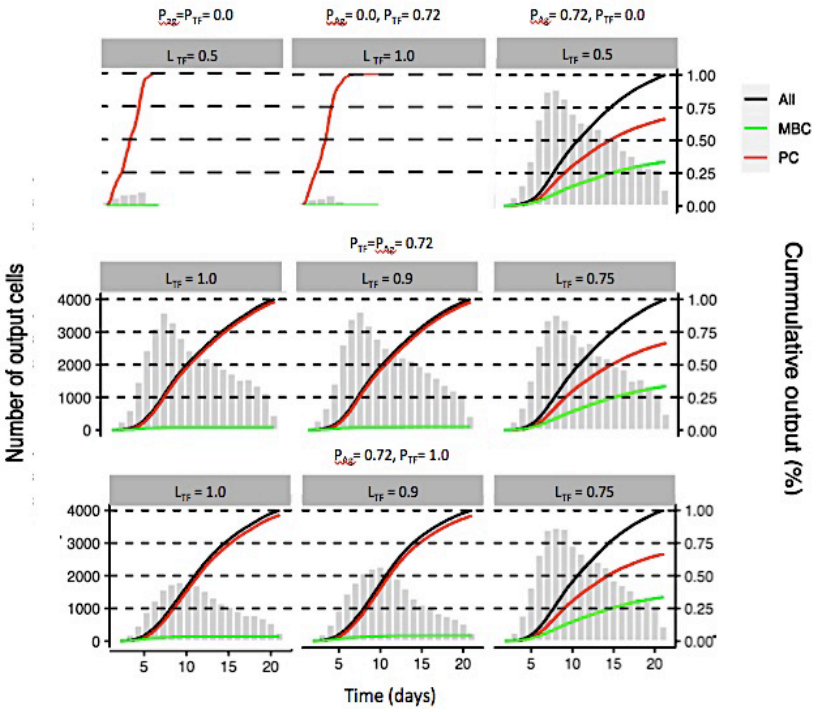

Supplementary Figure 24: (Cumulative) number of OCs. Histogram represents the number of OCs per day for Simulations 1-9 (Table 5). Black, red and green lines represent the cumulative percentage of output, PCs and MBCs respectively.

L_{BCL6} =1.0

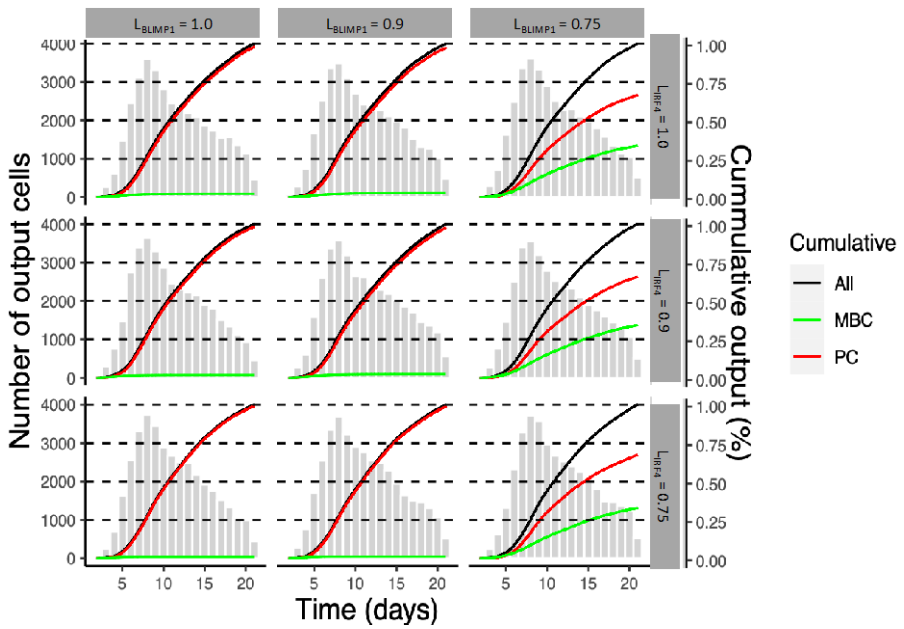

Supplementary Figure 25: (Cumulative) number of OCs. Histogram represents the number of OCs per day for Simulations 1-9 (Table 6). Black, red and green lines represent the cumulative percentage of output, PCs and MBCs respectively.

L_{BCL6} =0.9

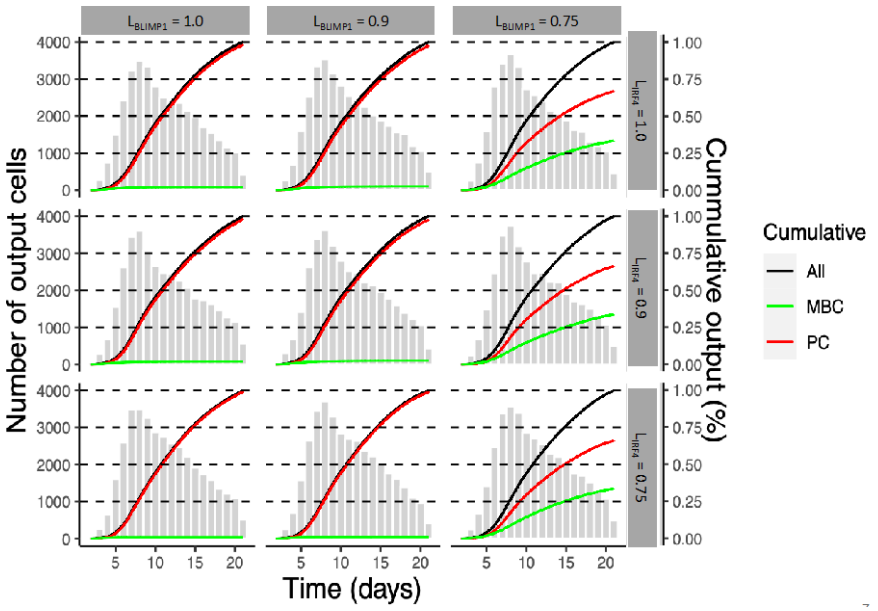

Supplementary Figure 26: (Cumulative) number of OCs. Histogram represents the number of OCs per day for Simulations 10-18 (Table 6). Black, red and green lines represent the cumulative percentage of output, PCs and MBCs respectively.

L_{BCL6} =0.75

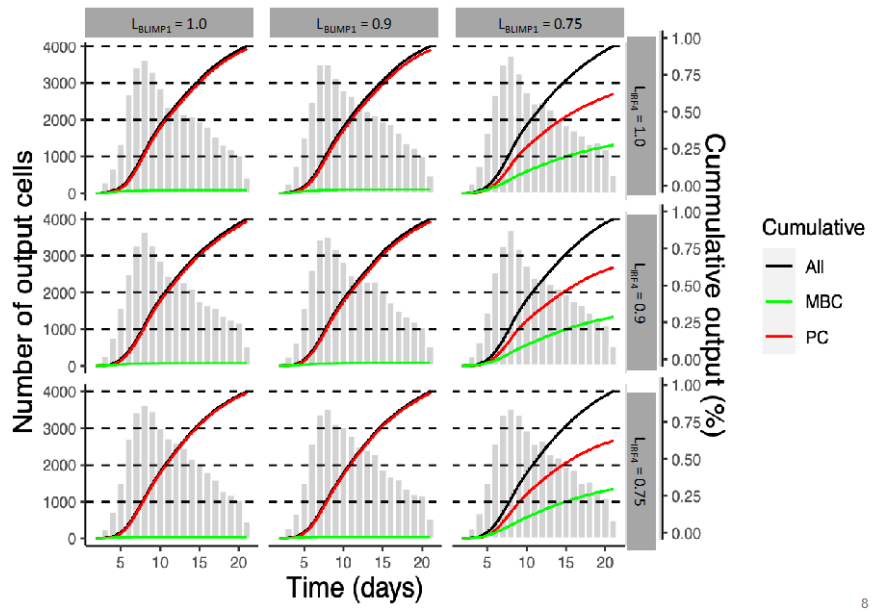

Supplementary Figure 27: (Cumulative) number of OCs. Histogram represents the number of OCs per day for Simulations 19-27 (Table 6). Black, red and green lines represent the cumulative percentage of output, PCs and MBCs respectively.

Chapter 4

Multiscale modeling recapitulates the effect of genetic alterations associated with diffuse large B-cell lymphoma in the germinal center dynamics

Elena Merino Tejero, Qirong Mao, Danial Lashgari, Rodrigo García-Valiente, Philippe A. Robert, Michael Meyer-Hermann, María Rodríguez Martínez, Jeroen E.J. Guikema, Huub H.C.J. Hoefsloot, Antoine H.C. van Kampen

Manuscript accepted

4.1. Abstract

Diffuse large B-cell lymphoma is the most common subtype of non-Hodgkin's lymphoma. It is a germinal center (GC)-derived, aggressive and heterogeneous disease. Several transcription factors and signaling pathways that play a central role in the progression of the GC reaction and B-cell differentiation have been shown to play an oncogenic role in diffuse large B-cell lymphoma. B-cell lymphoma 6 (BCL6) is a transcriptional repressor that induces GC B-cell phenotype and blocks plasma cell (PC) differentiation. While interferon regulatory factor 4 (IRF4) and B lymphocyte induced maturation protein 1 (BLIMP1), a transcriptional promoter, both mediate PC differentiation and exit from the GC (Mlynarczyk *et al.*, 2019). Computational models are useful alternatives to trial-and-error experimental investigation. Ordinary differential equation (ODE) models have been used to study different known mechanisms of lymphomagenesis and suggest candidate tumorigenic alterations (Martínez *et al.*, 2012). Furthermore, multiscale models (MSMs) have been used to study the role of cellular and molecular mechanisms involved in tumor growth (3–6). In this study, we use an existing MSM of PC differentiation in the GC to simulate eight different models with several candidate genetic alterations of the BCL6-IRF4-BLIMP1 regulatory network that lead to transcription factor deregulation and could explain the onset of diffuse large B-cell lymphoma and recapitulate the GC dynamics observed in

such conditions. We find that models with loss of BLIMP1 function ($BLIMP^{loss}$ and $BLIMP^{loss}IRF^{inc}$) result in an accumulation of B cells in the GC and a block of PC differentiation and thus correctly recapitulate the observed GC and transcription factor dynamics. Models with constitutive activation of the nuclear factor kappa-light-chain-enhancer of activated B cells (NF-kB) pathway alone and in codominance or co-expression with enforced BCL6 expression (IRF^{inc} and $BCL^{inc}IRF^{inc}$) result in a decrease of GC B cells and unaltered PC production at early stages of the GC reaction as observed experimentally. Interestingly, we also find that in IRF^{inc} and $BCL^{inc}IRF^{inc}$ models, an increase in PC production could happen at later stages of the GC reaction. Nevertheless, models with enforced BCL6 expression (BCL^{auto} and BCL^{inc}) result in an expansion of GC B cell population and a block in the PC production that was not observed experimentally. Finally, models with loss of IRF4- and BLIMP1- mediated silencing of BCL6 (IRF^{sil} and $BLIMP^{sil}$) did not affect GC and transcription factor dynamics. [1]

4.2. Introduction

During affinity maturation in the GC, B cells undergo rounds of proliferation, somatic hypermutations and selection to produce memory B cells (MBCs) and antibody-secreting PCs (Nilushi S. De Silva and Klein, 2015). The GC can be categorized into two main zones. A dark zone (DZ) in which B cells at a centroblast (CBs) state rapidly proliferate and accumulate somatic hypermutations in the genes that encode their B-cell receptor (BcR). The light zone (LZ) is characterized by the presence of B cells at a centrocyte (CCs) state, follicular dendritic cells (FDCs) that present antigen (Ag) in the form of immune complexes in their membrane (Allen *et al.*, 2007a), and T follicular helper cells. In the DZ, suppression of the DNA damage response and B-cell proliferation checkpoints increase the risk of malignant transformations that can lead to B-cell lymphomas (Mlynarczyk *et al.*, 2019). Diffuse large B-cell lymphoma, the most common subtype of non-Hodgkin's lymphoma, is a GC derived, aggressive and heterogeneous disease. Genes related to different stages of GC B-cell differentiation and activation are differentially expressed among diffuse large B-cell lymphomas (Alizadeh *et al.*, 2000). Based on gene expression profiling, two subtypes have been defined: GC B-cell and active B-cell (Hu *et al.*, 2013). Active B-cell subtype patients have a poorer prognosis and survival rate than those with GC B-cell subtype (Miyazaki, 2016). Nevertheless, it is still unclear which genes that distinguish both subtypes are the most important determinants of chemotherapy responsiveness (Alizadeh *et al.*, 2000).

[1] This chapter is based on Merino Tejero E, Mao Q, Lashgari D, García-Valiente R, Robert PA, Meyer-Hermann M, Martínez MR, Guikema JEJ, Hoefsloot H, van Kampen AHC. Multi-scale modeling recapitulates the effect of genetic alterations associated with diffuse large B-cell lymphoma in the germinal center dynamics. Frontiers in systems biology (2022).

Several transcription factors play a central role in the progression of the GC reaction. BCL6 is a transcriptional repressor that induces GC B-cell phenotype and is involved in B-cell survival, proliferation, DNA damage and blocking PC differentiation. High expression levels of IRF4 and BLIMP1 induce PC differentiation and promote exit from the GC (Mlynarczyk *et al.*, 2019). These are regulated by upstream signals emanating from the B-cell receptor (BcR) and cluster of differentiation 40 (CD40). In particular, the NF-kB pathway, induced by CD40, is involved in the induction of MBC and PC differentiation in the GC light zone (LZ).

The above mentioned transcription factors have also been shown to play an oncogenic role in diffuse large B-cell lymphoma (Mlynarczyk *et al.*, 2019). BCL6 chromosomal translocations have been found more frequently in the active B-cell subtype, leading to a constitutive BCL6 overexpression (Zhang *et al.*, 2015). Furthermore, a vast majority of active B-cell subtypes fail to express a competent BLIMP1 despite normal IRF4 expression (Pasqualucci *et al.*, 2006). The loss of IRF4 and BLIMP1 mediated transcriptional silencing of BCL6 have been found in a subset of diffuse large B-cell lymphoma s (Saito *et al.*, 2007). Nevertheless, the effect on the GC B-cell dynamics and PC production was not studied. Furthermore, to the best of our knowledge, the effect of diffuse large B-cell lymphoma genetic alterations on MBC production during the GC reaction has not been studied. Signaling pathways have also been linked to diffuse large B-cell lymphoma development, such as constitutive activation of the NF-kB pathway, which is the essential hallmark to active B-cell subtype (Pasqualucci *et al.*, 2011). Finally, combination of genetic alterations such as mutations in NF-kB pathway and BCL6 chromosomal translocations or BLIMP1 deletion worsen diffuse large B-cell lymphoma prognosis (Calado *et al.*, 2010; Zhang *et al.*, 2015).

Computational models are useful alternatives to trial-and-error experimental studies. Martínez and colleagues presented an ODE model of a gene regulatory network (GRN) that integrated signals from BcR and CD40 (Martínez *et al.*, 2012). They induced perturbations in the model to study different known mechanisms of lymphomagenesis and suggested candidate tumorigenic alterations. Nevertheless, only the molecular level, not the cellular dynamics, was included in this model. Furthermore, MSMs have been used to study the role of cellular and molecular mechanisms involved in tumor growth (Yeh *et al.*, 2017; Roy *et al.*, 2019; Versypt, 2021). A recent study used MSM to predict effectiveness of various therapies for diffuse large B-cell lymphoma (Du *et al.*, 2017). In the latter study, a detailed kinetic model of BcR signaling network was used. Nevertheless, only its effect on in vitro tumor growth was analyzed.

In this study, we use an existing MSM of PC differentiation in the GC to simulate eight different models with candidate genetic alterations of the BCL6-IRF4-BLIMP1 regulatory network that could explain the onset of diffuse large B-cell lymphoma, in order to recapitulate the GC dynamics observed in such conditions (Merino Tejero *et al.*, 2020). While most of the above-mentioned genetic alterations are based on previous work done by Martínez and colleagues

(Martínez *et al.*, 2012),, our model provides additional insight by studying the effect of these alterations at the cellular and GC level. The main cellular processes that take place in our MSM are simulated through agent based modeling based on a large body of *in vitro* and *in vivo* experiments (Meyer-Hermann *et al.*, 2012). Nevertheless, only the differentiation towards PC is determined by the GRN, which integrates signals from BcR and CD40. We find that models with loss of BLIMP1 function ($BLIMP^{loss}$ and $BLIMP^{loss}IRF^{inc}$) result in an accumulation of B cells in the GC and a block of PC differentiation and thus correctly recapitulate the observed GC and transcription factor dynamics. Models with constitutive activation of NF-kB pathway alone and in codominance with enforced BCL6 expression (IRF^{inc} and $BCL^{inc}IRF^{inc}$) result in a decrease of GC B cells and unaltered PC production at early stages of the GC reaction as observed experimentally. Interestingly, we also find that in IRF^{inc} and $BCL^{inc}IRF^{inc}$ models, an increase in PC production could happen at later stages of the GC reaction. Nevertheless, models with enforced BCL6 expression (BCL^{auto} and BCL^{inc}) result in an overgrowth of GC B cells and a block in the PC production that was not observed experimentally. While no data has been found to validate models with loss of IRF4 and BLIMP1 mediated silencing of BCL6 (IRF^{sil} and $BLIMP^{sil}$), our findings suggest that such alterations do not affect GC and transcription factor dynamics.

Transcription factors with restricted patterns of expression are attractive targets for therapy. BCL6 inhibitors have been used to bock BCL6 activity and inhibited the growth of certain diffuse large B-cell lymphomas (Polo *et al.*, 2007). NF-kB inhibitors have also demonstrated to selectively target active B-cell-like diffuse large B-cell lymphomas. Finally, small-molecule inhibitors of BcR downstream pathways are the most promising agents in treating diffuse large B-cell lymphomas and other malignancies (Roschewski *et al.*, 2012). Further identification and study of the molecular mechanisms involved in the pathogenesis of diffuse large B-cell lymphoma tumors is crucial for the development of treatments. However, for cancer it is important to determine how genetic alterations and, hence, changes in the state of molecular pathways affects the cellular events such as proliferation, apoptosis, and differentiation. MSMs as presented in this work can help to determine the molecular and cellular relationships.

4.3. Methods

4.3.1. Multi-scale model

To study the molecular mechanisms behind the development of diffuse large B-cell lymphoma we used an already existing MSM of PC differentiation during the GC reaction (Merino Tejero *et al.*, 2020). At the cellular level we used an agent based model of the GC reaction based on an existing model (Meyer-Hermann *et al.*, 2012).

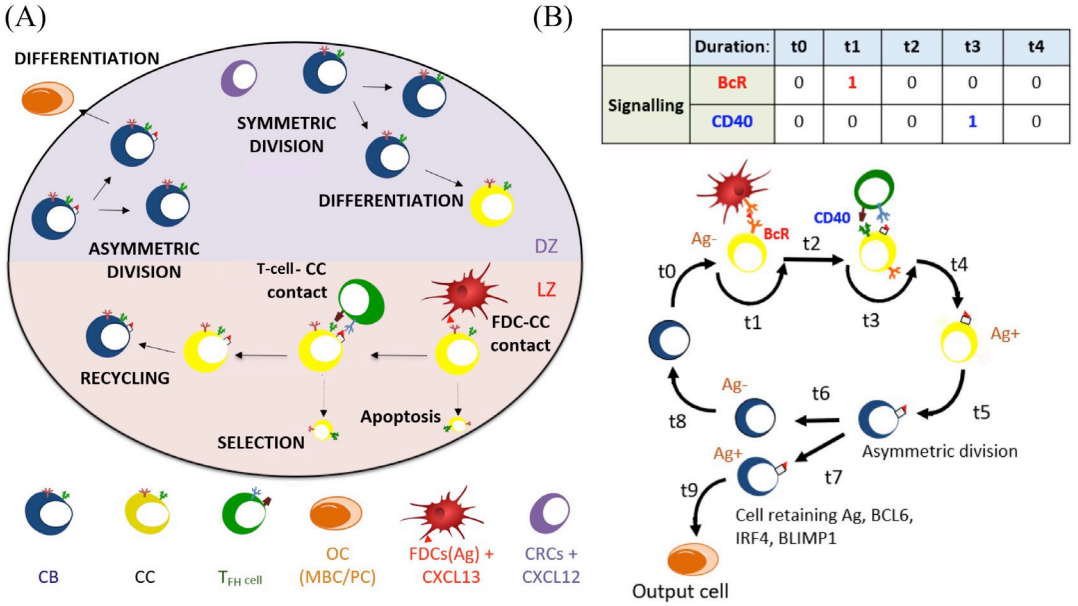

Figure 27: (A) Overview of cellular processes in the ABM. In an established GC a dark zone (DZ) and a light zone (LZ) are distinguished. CBs and CCs prefer to move in the direction of the CXCL12 and CXCL13 chemokines produced by stromal cells and FDCs respectively. T follicular helper cells prefer to move towards the LZ. FDCs carry Ag that can be captured by CCs. CCs may be positively selected through interaction with T follicular helper cells after which they can recycle to the DZ. In the DZ the CB will (a)symmetrically divide. After CB division, an output cell is produced, or the cell differentiates to a CC. CCs die through apoptosis if they do not interact with the FDC and T follicular helper cells. (B) Schematic overview of the BcR and CD40 signaling events during the GC reaction. Durations *t* indicate non-fixed time intervals (cell states). At the end of each interval the concentrations of BCL6, IRF4, and BLIMP1 are updated using the differential equations. A CB (Ag-; blue cell) differentiates to a CC (Ag-; yellow cell) within a time duration *t0*. The CC interacts with the FDC for a time duration *t1* during which BcR signaling occurs. Subsequently, CD40 signaling is active for duration *t3* during B-cell and T follicular helper cell interaction. Successful interaction will result in an Ag+ B-cell. Asymmetric division occurs with a probability of 0.72. Differentiation of CB to a CC always initializes the CC to Ag-
.

The agent based model runs for 21 days (504 hours) at a time resolution of 0.002 hours (7.2 seconds) (Supplementary Table 5). Each cell is represented in a three-dimensional space representing the GC and undergoes different processes depending on their state. B cells at a CB state divide, undergo somatic hypermutations, and differentiate in the DZ while at a CC state they undergo selection in the LZ Figure 27. In the LZ, CCs interact and collect Ag from follicular dendritic cells (FDCs). CCs may further interact and compete for T follicular helper cell signals. Both processes are dependent on affinity of the BcR for the Ag. Selected CCs recycle back to the DZ as CBs that carry internalized Ag. Recycled CBs divide in an asymmetric manner in 72% of the cases where all of the Ag and transcription factors segregate towards one of the daughter CBs. In the remaining 28% of divisions, Ag and transcription factors are divided symmetrically (Barnett *et al.*, 2012; Thaunat *et al.*, 2012). This was based on a recent study that showed coupled Ag and transcription factor asymmetric division with a large segregation between daughter B cells recapitulates the GC output transition (temporal switch) from MBCs to PCs and a DZ-to-LZ ratio, which is the

ratio of CBs to non-apoptotic CCs present in the GC. After division, CBs may exit the GC as an output cell or remain in the GC for further rounds of selection.

At the molecular level we used an ODE model of a GRN involved in PC differentiation based on an existing model (Martínez *et al.*, 2012). The GRN consists of three transcription factors, i.e., BCL6 (b), BLIMP1 (p) and IRF4 (r). These transcription factors regulate each other and the concentration levels depend on their dissociation constant (k), transcription (μ) and degradation rates (λ) as shown in (Eq 7-9). Parameter values are shown in Supplementary Table 6. Bcr0 and cd40 parameters were calibrated using Moonfit graphical user interface (Robert, Jönsson, *et al.*, 2018). 'Squares' in the equations represent Hill coefficients representing cooperative binding of transcription factors. The GRN behaves as a bistable system, with one state being the CB- and CC-like state (BCL6 high, BLIMP1 and IRF4 low) and a second state being PC-like state (BLIMP1 and IRF4 high, BCL6 low). Upstream signals may instruct the system towards one or the other state. Their effect is integrated through BcR and CD40 parameters as described in (Eq 10 and 11). During CC-FDC interaction in the LZ, CCs receive BcR mediated signals. The maximum strength of the signal is represented by bcr_0 parameter (Eq 10). Transition from CC towards PC state is reversible when the BcR signal cessates, bringing the B-cell to its previous CC state. During CC-T follicular helper cell interaction in the LZ, CCs receive signals through CD40. The strength of the signal is represented by the cd40 parameter (Eq 11). Transition from CC to PC state is irreversibly determined by CD40 signal strength, which is dependent on the affinity of the BcR for the Ag (see Supplementary Table 6).

$$\boldsymbol{Eq\ 7:}\ \frac{\boldsymbol{dp}}{\boldsymbol{dt}} = \boldsymbol{\mu_p} + \boldsymbol{\sigma_p}\frac{\boldsymbol{k_b^2}}{\boldsymbol{k_b^2} + \boldsymbol{b^2}} + \boldsymbol{\sigma_p}\frac{\boldsymbol{r^2}}{\boldsymbol{k_r^2} + \boldsymbol{r^2}} - \boldsymbol{\lambda_p p}$$

$$\boldsymbol{Eq\ 8:}\ \frac{\boldsymbol{db}}{\boldsymbol{dt}} = \boldsymbol{\mu_b} + \boldsymbol{\sigma_b}\frac{\boldsymbol{k_p^2}}{\boldsymbol{k_p^2} + \boldsymbol{p^2}}\frac{\boldsymbol{k_b^2}}{\boldsymbol{k_b^2} + \boldsymbol{b^2}}\frac{\boldsymbol{k_r^2}}{\boldsymbol{k_r^2} + \boldsymbol{r^2}} - (\boldsymbol{\lambda_b} + \boldsymbol{BCR})\boldsymbol{b}$$

$$\boldsymbol{Eq\ 9:}\ \frac{\boldsymbol{dr}}{\boldsymbol{dt}} = \boldsymbol{\mu_r} + \boldsymbol{\sigma_r}\frac{\boldsymbol{r^2}}{\boldsymbol{k_r^2} + \boldsymbol{r^2}} + \boldsymbol{CD40} - \boldsymbol{\lambda_r r}$$

$$\boldsymbol{Eq\ 10:} \boldsymbol{BCR} = \boldsymbol{bcr0}\frac{\boldsymbol{k_b^2}}{\boldsymbol{k_b^2} + \boldsymbol{b^2}}$$

$$\boldsymbol{Eq\ 11:} \boldsymbol{CD40} = \boldsymbol{cd40}\frac{\boldsymbol{k_b^2}}{\boldsymbol{k_b^2} + \boldsymbol{b^2}}$$

The ODE model was adapted as described in simulations section in order to investigate the effect of different genetic alterations in the GC dynamics.

4.3.1.1. Definition of output cells

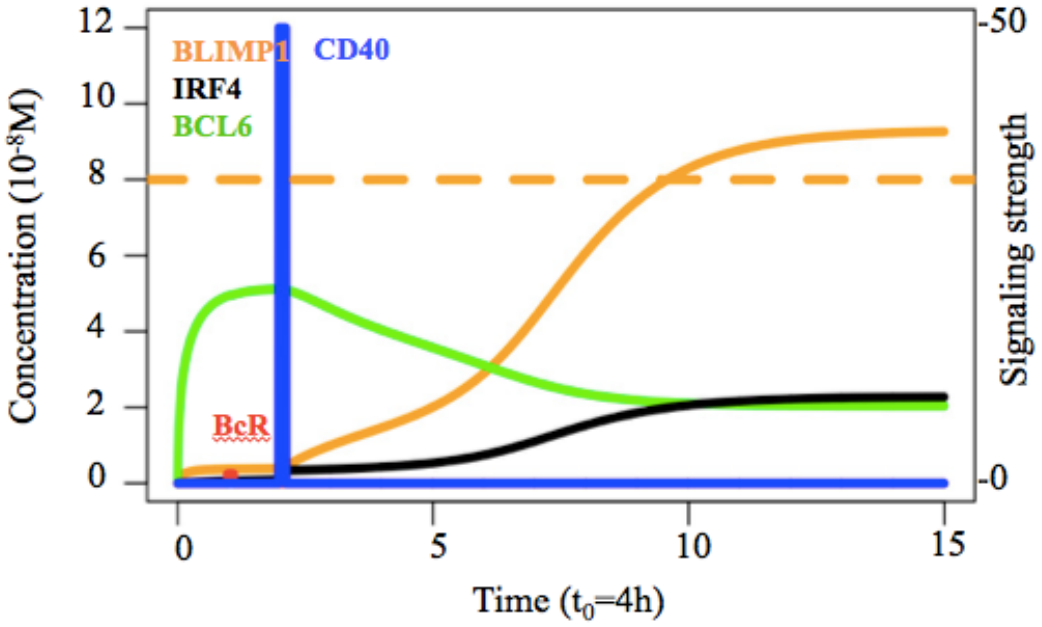

Figure 28: Transcription factor dynamics of the reference model upon binding of Ag and CD40L. Each time unit represents 4 hours. The protein concentration levels (unit = 10^{-8}M) of BCL6 (green), IRF4 (black) and BLIMP1 (orange) are shown on the left axes. Transcription factor levels are followed for 52 hours after CD40 signal. The BcR signal (red) results in a slight temporary change in transcription factor concentrations. In contrast, CD40 signal (blue) results in a switch of all transcription factor levels going from a B-cell to a PC (BLIMP1+) phenotype (in approximately 31 hours in this example). CD40 signal intensity in the MSM varies between 0 and 50 while BcR signal is fixed to 1 (right axes). BLIMP1 concentration threshold for PC differentiation is shown at $8*10^{-8}$M (Dashed orange).

The definition of output cells, either MBCs or PCs, is based on the Ag status and levels of BLIMP1 (Merino Tejero *et al.*, 2020). Recycled CBs carrying Ag are considered Ag positive (Ag+). During asymmetric division, Ag inheriting CB is Ag+ while the sibling is Ag negative (Ag-). During symmetric division, Ag is distributed symmetrically and both siblings are Ag-. This was based on a study that recapitulated the predominant features of Ag segregation in vitro by building a mixed model of B-cell mitosis where 25% of the divisions were fully symmetric and the remaining were asymmetric (Thaunat *et al.*, 2012). Recycled CBs that finished dividing differentiate to PCs when BLIMP1 levels reach the differentiation threshold (≥ 8.10^{-8}M; Figure 28) regardless of their Ag status. Ag+ output cells with BLIMP1 levels below the threshold are considered to be MBCs. Finally, Ag- CBs with BLIMP1 levels below the threshold stay in the GC and recycle back to the LZ as CCs. This definition leads to a transzone migration rate or DZ-to-LZ ratio close to experimental observations as described in Victora and co-workers (Victora and Nussenzweig, 2010) as well as a temporal switch in output cell production the MBC and PC dynamics as described in Weisel and co-workers (F J Weisel *et al.*, 2016).

4.3.1.2. Simulations

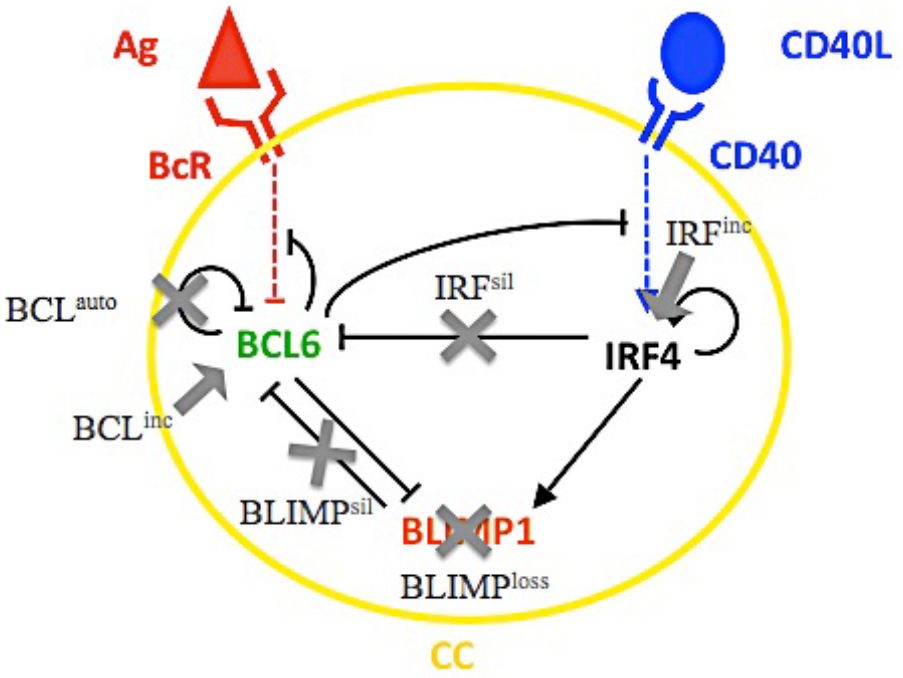

Figure 29: Scheme of the GRN involved in PC terminal differentiation. BCL6 (green) is inhibited upon binding of the Ag to the BcR (red). IRF4 (black) is activated upon binding of CD40L to CD40 (blue) during T follicular helper and B-cell interaction. Modifications in the GRN done to simulate the different diffuse large B-cell lymphoma models BCL^{auto}, BCL^{inc}, IRF^{sil}, $BLIMP^{sil}$, $BLIMP^{loss}$ and IRF^{inc} are indicated in grey. Grey arrows indicate over-induction and grey crosses indicate removal of the relation. Black, blue and red arrows and bar-headed lines indicate activation and inhibition respectively.

We investigated the effect of eight different diffuse large B-cell lymphoma models on both the molecular and cellular level. This was done to show how MSM can be used to recapitulate the GC dynamics observed in mouse diffuse large B-cell lymphoma models (Calado *et al.*, 2010; Zhang *et al.*, 2015) in terms of B-cell and PC numbers and transcription factor expression levels at day 7 of the GC reaction (day 10 post immunization (PI); Table 9). Most diffuse large B-cell lymphomas result in alterations, either an increase or decrease, in GC B cell numbers and/or PCs produced (see results section). Each diffuse large B-cell lymphoma model simulates one or more genetic alteration(s) (Figure 29). Models were simulated by modifying different ODEs and/or parameters model as described in Table 8. Six of the models simulated single genetic alterations based on a previous study from Martínez and colleagues (Martínez *et al.*, 2012). That is BCL6 autoregulatory inactivation (BCL^{auto}), BCL6 constitutive expression (BCL^{inc}), loss of IRF4-mediated BCL6 silencing (IRF^{sil}), loss of BLIMP1-mediated BCL6 silencing ($BLIMP^{sil}$), BLIMP1 inactivation ($BLIMP^{loss}$), and constitutive activation of NF-kB pathway (IRF^{inc}). The steady state levels of BLIMP1, BCL6 and IRF4 after CD40 signal were very close or identical as those derived by Martínez and co-workers (Martínez *et al.*, 2012) (Supplementary Table 7). One exception was BCL^{inc} model that showed a clear difference in the IRF4 and BLIMP1 levels. This is caused by

the fact that in our MSM selected CC differentiation into a PC process was around 11 times faster than in the model presented by Martínez and co-workers. The in silico GC B-cell dynamics were compared to data from experimental models done by Zhang (Zhang *et al.*, 2015) and Calado (Calado *et al.*, 2010) and colleagues. In our IRF^{inc} model, the perturbation applied to IRF4 was only a 2-fold increase in IRF4 transcription rates as opposed to the 10-fold increase applied by Martínez and colleagues (Martínez *et al.*, 2012). This was done to obtain transcription factor levels (data not shown) that resembled both experimental models (Calado *et al.*, 2010; Zhang *et al.*, 2015). Both experimental models showed a similar increase in the levels of BLIMP1 at day 7 of the GC reaction compared to an experimental reference. Nevertheless, the GC B-cell dynamics was different (Table 9). These differences observed between both experiments were due to the NF-kB pathway that was activated. In Zhang and colleagues (Zhang *et al.*, 2015) constitutive induction of NF-kB-inducing kinase restrained activation of the alternative NF-kB pathway. In Calado and colleagues (Calado *et al.*, 2010) constitutive induction of the NF-kB-inhibiting kinase restrained activation of the canonical NF-kB pathway. While our IRF^{inc} model did not explicitly include a distinction between alternative and canonical pathways, it was able to reproduce PC dynamics observed by Calado and colleagues (Calado *et al.*, 2010) (See below). Two additional models were created to simulate experimental findings by combining two of the single models, namely BCL6 constitutive expression in codominance with constitutive activation of the alternative NF-kB pathway ($BCL^{inc}IRF^{inc}$), based on experiments done by Zhang and colleagues (Zhang *et al.*, 2015), and BLIMP1 inactivation in codominance with constitutive activation of the canonical NF-kB pathway ($BLIMP^{loss}IRF^{inc}$), based on experiments done by Calado and colleagues (Calado *et al.*, 2010). We repeated all simulations 10 times with different random seeds, which showed that the amount of variability was low. Thus, this was sufficient to observe significant differences between the reference and most of the diffuse large B-cell lymphoma models when looking at the DZ-to-LZ ratio and output cell production (data not showed).

Table 8. Eight simulated diffuse large B-cell lymphoma models. For models BCL^{auto}, IRF^{sil} and $BLIMP^{sil}$ the ODE equation (Eq 8) was modified as shown below. For models $BLIMP^{loss}$ and $BLIMP^{loss}IRF^{inc}$ equation (Eq 7) was modified as shown below. Finally, for models BCL^{inc}, IRF^{inc}, $BCL^{inc}IRF^{inc}$ and $BLIMP^{loss}IRF^{inc}$ the indicated ODE parameters were modified as shown below. The rest of the equations and parameters are kept as described in Supplementary Table 6 and Eq 7-11.

Model	Description	Modifications
BCL^{auto}	Loss of BCL6 autoinhibition	$\frac{db}{dt} = \mu_b + \sigma_b \frac{k_p^2}{k_p^2 + p^2} \frac{k_r^2}{k_r^2 + r^2} - (\lambda_b + BCR)b$
BCL^{inc}	10-fold increase of BCL6 basal transcription rate	μ_b x 10
IRF^{sil}	Loss of IRF4 mediated silencing of BCL6	$\frac{db}{dt} = \mu_b + \sigma_b \frac{k_p^2}{k_p^2 + p^2} \frac{k_b^2}{k_b^2 + b^2} - (\lambda_b + BCR)b$
$BLIMP^{sil}$	Loss of BLIMP1 mediated silencing of BCL6	$\frac{db}{dt} = \mu_b + \sigma_b \frac{k_b^2}{k_b^2 + b^2} \frac{k_r^2}{k_r^2 + r^2} - (\lambda_b + BCR)b$
$BLIMP^{loss}$	Loss of BLIMP1 function (change in time)	$\frac{dp}{dt} = 0$
IRF^{inc}	2-fold increase of IRF4 basal and maximum transcription rates	μ_r x 2 σ_r x 2
$BCL^{inc}IRF^{inc}$	Combination of BCL^{inc} and IRF^{inc}	μ_b x 10 μ_r x 2 σ_r x 2
$BLIMP^{loss}IRF^{inc}$	Combination of $BLIMP^{loss}$ and IRF^{inc}	$\frac{dp}{dt} = 0$ μ_r x 2 σ_r x 2

Each model was repeated 10 times with different random seeds. Data was analyzed using an unpaired two-tailed Student's t test. P values ≤ 0.05 were considered to be significant.

4.4. Results

4.4.1. The GC dynamics (reference)

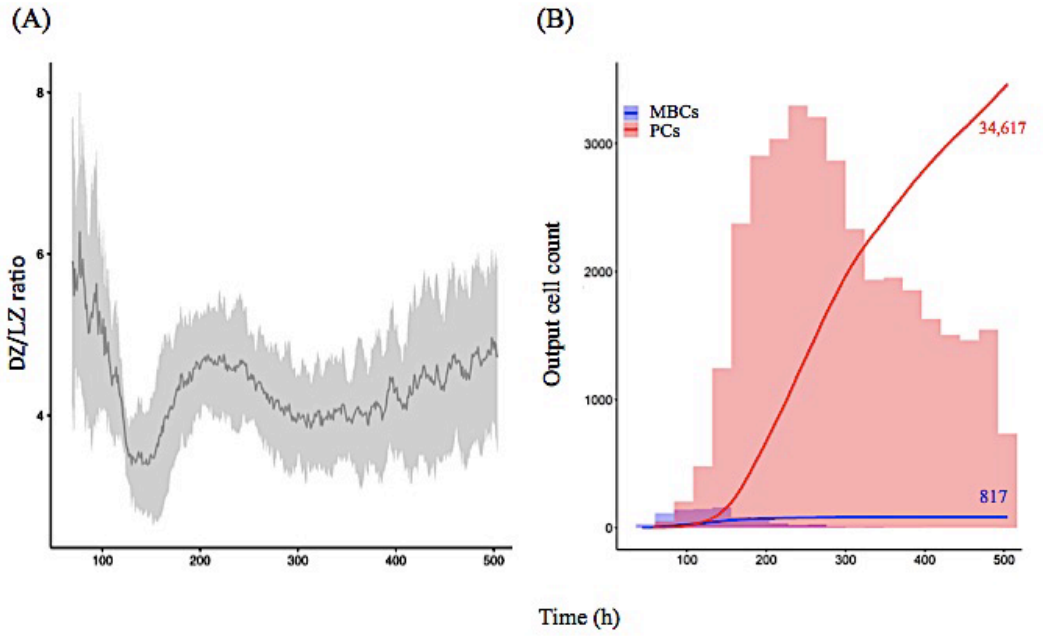

Figure 30: Overall GC dynamics of the reference model with affinity dependent cd40 signal. (A) Mean DZ-to-LZ ratio (dark grey) calculated from CB and CC counts. Standard deviation of 10 different random seeds is represented in light grey. (B) Cumulative number of MBCs (blue) and PCs (red) produced during the GC reaction represented with two lines. Histogram represents the number of MBCs (blue) and PCs (red) produced per day. Histogram scale is represented in the left axes. Line scale (not shown) ranges between 0 and 100. Numbers show the cumulated number of MBCs (blue) and PCs (red) at the end of the GC reaction. Representative of 10 simulations.

Diffuse large B-cell lymphomas are characterized by spleen and/or lymph node hyperplasia (Calado *et al.*, 2010; Zhang *et al.*, 2015). Furthermore, the same studies showed that most diffuse large B-cell lymphomas genetic mutations result in altered GC dynamics, either through an increase or decrease, in GC B-cell numbers and/or PCs produced. Thus, we wondered what was the effect of modelling eight diffuse large B-cell lymphoma models on the GC B-cell dynamics. We performed an example simulation at the scale of one B-cell, in which ODEs and parameters were defined as described in Eq 7-11 and Supplementary Table 6. The initial state at BCL6 high, BLIMP1 and IRF4 low switched to BLIMP1 and IRF4 high, BCL6 low, mainly as a consequence of CD40 signal induction (Figure 28). At the scale of a full GC simulation, we found that the DZ-to-LZ ratio was similar to the affinity-based CD40 signaling simulation (Scenario 2) of one of our previous studies (Merino Tejero *et al.*, 2020) (Figure 30A, Supplementary Table 8). Nevertheless, it was slightly higher than previous experimental observations of transzone migration rates (Victora and Nussenzweig, 2010). Finally, a temporal transition From MBC to PC production was observed in the GC output (Figure 30B).

Thus, in the reference simulation, the DZ-to-LZ ratio was higher than previously observed transzone migration rates of around 2 (Victora and Nussenzweig, 2010) and similar to the affinity-based CD40 signaling simulation (Scenario 2) (Merino Tejero *et al.*, 2020). A latter large-scale study from Wittenbrink and colleagues showed the GC dynamics is highly variable (Wittenbrink *et al.*, 2011b). They performed a volume-to-volume comparison of both GC zones and showed that dividing B cells are present in both zones constantly over time. Thus, the study did not reflect the dividing vs non-dividing B-cell DZ-to-LZ ratio and their measurements are not directly comparable to Victoria and colleagues (Victora and Nussenzweig, 2010). Further experiments would be required to determine the variability in DZ-to-LZ ratios in GC responses to establish whether or not our model produces deviating values. There was a temporal switch of the GC output from mainly MBC production prior to the peak, to mainly PC production after the peak. Finally, there was a 42-fold higher PC than MCB production. Studies have shown the number of PCs and MBCs generated spleen and bone marrow during an immune response (Kishi *et al.*, 2010; F J Weisel *et al.*, 2016; Sugimoto-Ishige *et al.*, 2020). Nevertheless, these numbers represent percentages of observed PCs and MBCs from total number of splenic or bone marrow cells, which are not translatable to number of output cells from a single GC and, therefore, are not directly comparable with our results.

Table 9: Qualitative comparison between observed and simulated GC phenotype in eight different diffuse large B-cell lymphoma models. B-cell and PC counts observed are based on previous studies done by Zhang (Zhang *et al.*, 2015) and Calado (Calado *et al.*, 2010) and colleagues at days 10 and 21 post immunization. Considering GCs take 3 days to develop after immunization (F J Weisel *et al.*, 2016), in our simulations B-cells and PCs were counted at days 7 and 18 of the GC reaction. Words 'similar', 'increased' and 'reduced' indicate no significant difference, significant increase and significant decrease when comparing each model cell count to an observed or simulated reference.

<table>
<tr><th rowspan="3">Model</th><th colspan="6">Observations</th><th colspan="4" rowspan="2">Simulations</th></tr>
<tr><th colspan="3">Zhang and co. (Zhang et al., 2015)</th><th colspan="3">Calado and co. (Calado et al., 2010)</th></tr>
<tr><th>B-cell count (Day10)</th><th>B-cell count (Day21)</th><th>PC Count (Day10)</th><th>B-cell count (Day10)</th><th>B-cell count (Day21)</th><th>PC count (Day10)</th><th>B-cell count (Day7)</th><th>B-cell count (Day18)</th><th>MBC count (Day7)</th><th>PC count (Day7)</th></tr>
<tr><td>BCL^{auto}</td><td colspan="3" rowspan="2">similar</td><td colspan="3" rowspan="2">-</td><td colspan="3" rowspan="4">increased</td><td rowspan="4">reduced</td></tr>
<tr><td>BCL^{inc}</td></tr>
<tr><td>BLIMP$_{loss}$</td><td colspan="3" rowspan="3">-</td><td colspan="2">increased</td><td rowspan="3">reduced</td></tr>
<tr><td>BLIMP$_{loss}$IRF^{inc}</td><td>increased</td><td>similar</td></tr>
<tr><td>IRF^{inc} (can.)</td><td colspan="2">reduced</td><td colspan="2">similar</td><td rowspan="6">similar</td><td colspan="2" rowspan="4">reduced</td><td rowspan="5">similar</td></tr>
<tr><td>IRF^{inc} (alt.)</td><td>similar</td><td>reduced</td><td>increased</td><td colspan="3" rowspan="3">-</td></tr>
<tr><td>IRF^{inc}</td><td colspan="3">-</td></tr>
<tr><td>BCL^{inc}IRF^{inc}</td><td>similar</td><td>reduced</td><td>similar</td></tr>
<tr><td>IRF^{sil}</td><td colspan="6" rowspan="2">-</td><td rowspan="2">similar</td><td>similar</td></tr>
<tr><td>BLIMP$_{sil}$</td><td>increased</td><td>reduced</td></tr>
</table>

4.4.2. Insufficient BLIMP1 expression blocks PC differentiation (BCL^{auto}, BCL^{inc}, $BLIMP^{loss}$, $BLIMP^{loss}IRF^{inc}$)

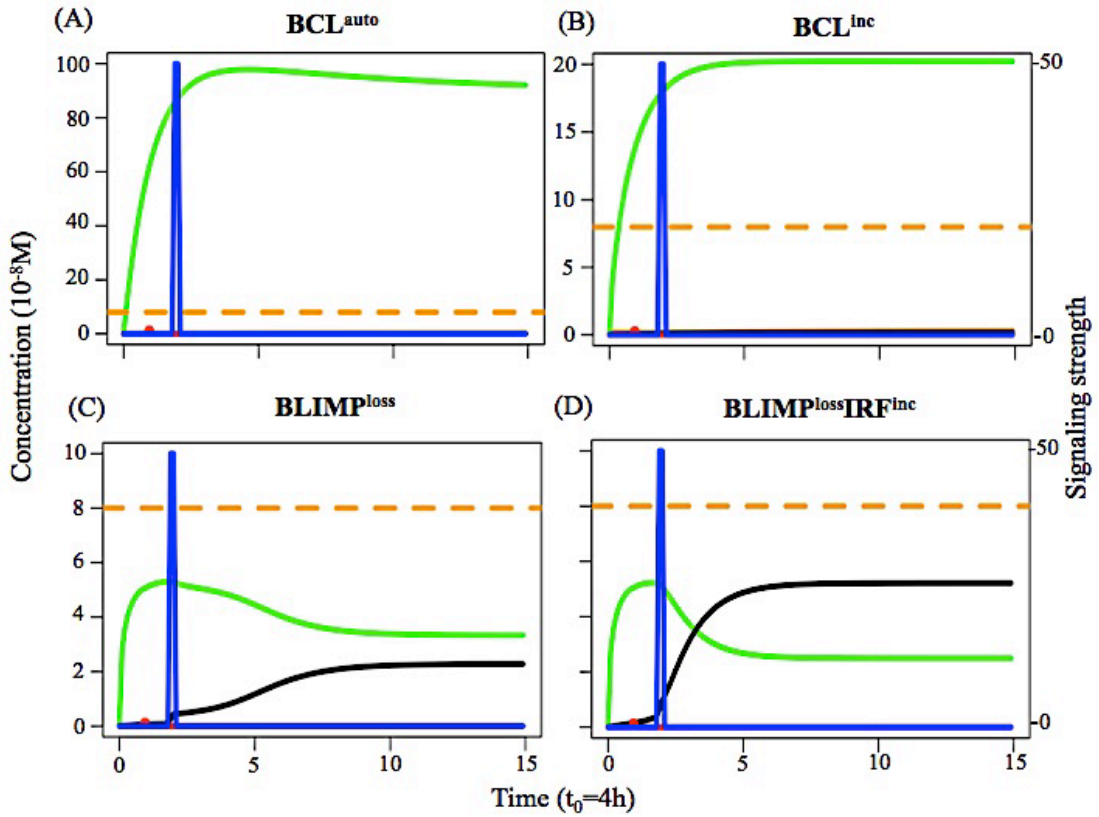

Figure 31: Transcription factor dynamics of (A) BCL^{auto}, (B) BCL^{inc}, (C) $BLIMP^{loss}$ and (D) $BLIMP^{loss}IRF^{inc}$ diffuse large B-cell lymphoma models upon binding of Ag and CD40L. Each time unit represents 4 hours. The protein concentration levels (unit = 10^{-8}M) of BCL6 (green), IRF4 (black) and BLIMP1 (orange) are shown on the left axes. Transcription factor levels are followed for 52 hours after CD40 signal. In BCL^{auto} and BCL^{inc} models, CD40 signal (blue) does not affect transcription factor levels. In $BLIMP^{loss}$ and $BLIMP^{loss}IRF^{inc}$ models CD40 signal affects BCL6 and IRF4 but not BLIMP1 levels. Thus in all models CD40 signal does not result in a switch of the B-cell to a PC (BLIMP1+) phenotype (in approximately 51 hours in this example).

We now compared the effect of several genetic (models defined in Table 9, see methods) alterations onto the GC dynamics in order to recapitulate the observed GC phenotype in diffuse large B-cell lymphoma. We first aimed to gain insight in the effect of BLIMP1 suppression (BCL^{auto} and BCL^{inc}) or loss of function ($BLIMP^{loss}$ and $BLIMP^{loss}IRF^{inc}$) on the GC B-cell dynamics. While previous studies showed that the GC phenotype in diffuse large B-cell lymphomas that are characterized by BCL^{auto} and BCL^{inc} alterations had unaltered numbers of B cells and PCs produced, they did lead to spleen and lymph node hyperplasia (Zhang *et al.*, 2015). Another study showed that the GC phenotype $BLIMP^{loss}$ and $BLIMP^{loss}IRF^{inc}$

alterations are characterized by an accumulation of B cells, a block of PC differentiation and spleen hyperplasia (Calado *et al.*, 2010).

We analyzed the transcription factor dynamics as well as the B-cell dynamics in the aforementioned models (Table 9). The transcription factor dynamics simulated in single cells showed for BCL^{auto} and BCL^{inc} models the system evolved to the BCL6 high, BLIMP1 and IRF4 low steady state which was unaffected by CD40 signal (Figure 31A-B). The steady state level of BCL6 in BCL^{auto} model was around 4 times higher than in BCL^{inc} model as shown by Martínez and co-workers (Martínez *et al.*, 2012) while steady state levels of IRF4 and BLIMP1 were similar in both models which was not observed by Martínez and co-workers (Martínez *et al.*, 2012) (see Methods section). Thus, we found that within the timing of PC differentiation during the GC reaction both BCL^{auto} and BCL^{inc} models had a robust BCL6 overexpression that inhibited IRF4 and BLIMP1 expression and blocked PC differentiation. $BLIMP^{loss}$ and $BLIMP^{loss}IRF^{inc}$ models switched to the BCL6 low and IRF4 high steady state as a result of CD40 signal. Nevertheless, they both failed to express BLIMP1 (Figure 31C-D).

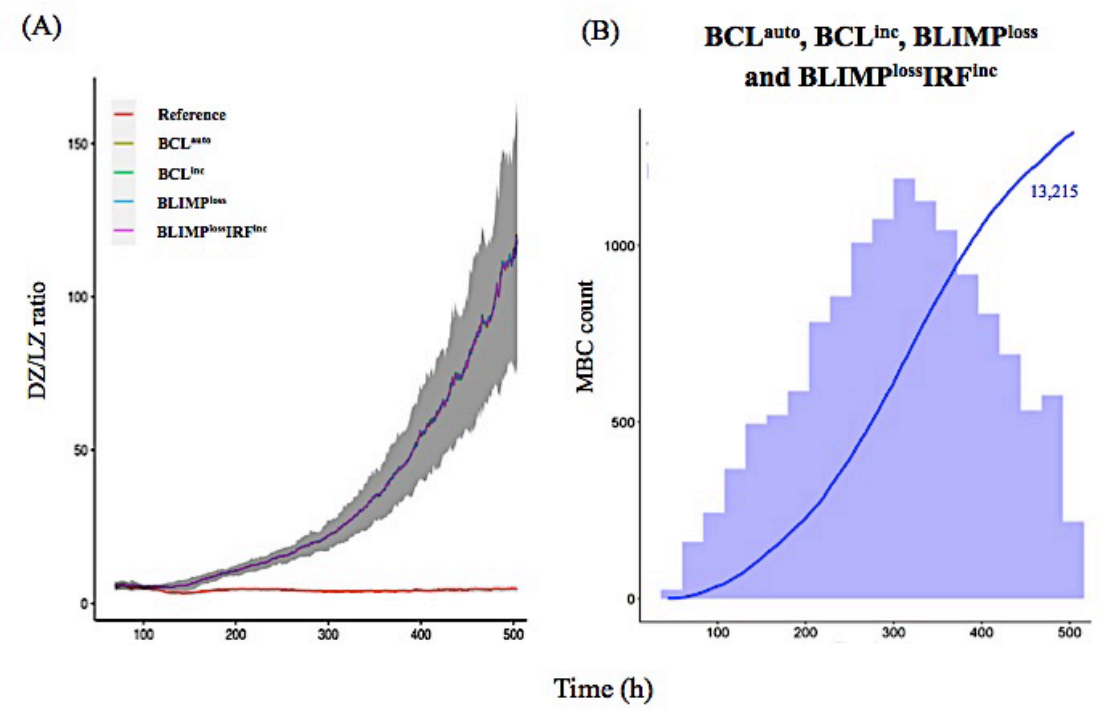

Figure 32: Overall GC dynamics with affinity dependent CD40 signal. (A) Mean DZ-to-LZ ratio calculated from CB and CC counts during the GC reaction for the reference (red), BCL^{auto} (yellow), BCL^{inc} (green), $BLIMP^{loss}$ (blue) and $BLIMP^{loss}IRF^{inc}$ (purple) diffuse large B-cell lymphoma models. Standard deviation of 10 different random seeds is represented in dark grey. (B) Cumulative number of MBCs produced during the GC reaction for BCL^{auto}, BCL^{inc}, $BLIMP^{loss}$ and $BLIMP^{loss}IRF^{inc}$ models represented with a blue line. Histogram represents the number of MBCs (blue) produced per day. Histogram scale is represented in the left axes. Line scale (not shown) ranges between 0 and 100. Number shows the cumulated number of MBCs (blue) at the end of the GC reaction. No PCs are produced. Representative of 10 simulations.

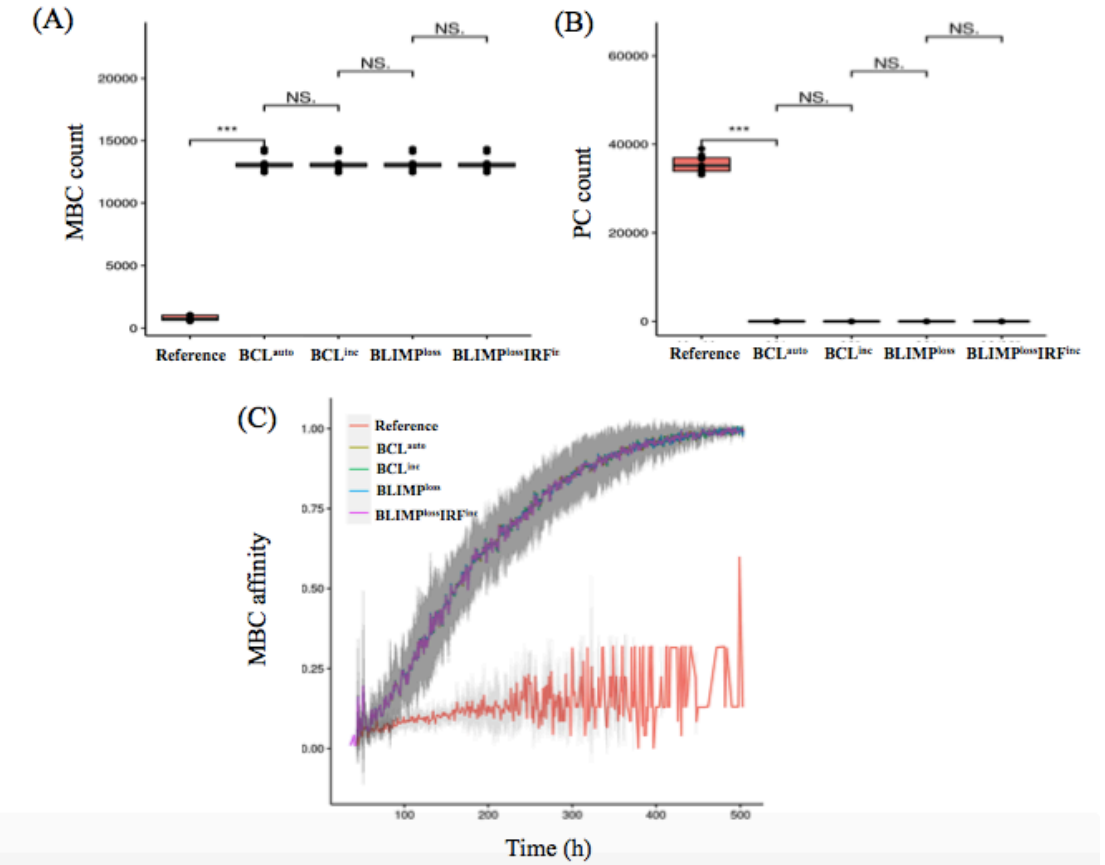

Figure 33: Statistical analysis of (A) MBC and (B) PC counts at day 21 of the GC reaction and (C) MBC affinity dynamics during the GC reaction for the reference (red), BCL^{auto} (yellow), BCL^{inc} (green), $BLIMP^{loss}$ (blue) and $BLIMP^{loss}IRF^{inc}$ (purple) diffuse large B-cell lymphoma models. A significant difference in the number of MBCs and PCs produced is observed between the reference and the four diffuse large B-cell lymphoma models. In the diffuse large B-cell lymphoma models, MBCs increase their affinity over time while in the reference model MBCs are of low affinity. Standard deviation of 10 different random seeds is represented in dark grey. An unpaired two-tailed Student's t test was used. Three asterisks (***) represent p-values ≤ 0.001, "NS." represents not statistically significant.

We observed BCL^{auto}, BCL^{inc}, $BLIMP^{loss}$ and $BLIMP^{loss}IRF^{inc}$ models had a significantly increased DZ-to-LZ ratio throughout the GC reaction, which reached up to a 25-fold increase at day 21 (Supplementary Table 8), compared to the reference model (Figure 32A) resulting on an increased abundance of GC B cells. All output cells were MBCs (Supplementary Table 8) and no PCs were produced (Figure 32B). Statistical analysis of MBC (Figure 33A) and PC (Figure 33B) counts showed a 13,000-fold increase and 35,000-fold decrease compared to the reference. Since BLIMP1 levels were virtually 0 in all cases, no significant difference in the number of MBCs and PCs was observed between the four models. MBC affinity increased up to its maximum as the GC reaction progressed in all models while it remained low in the reference model (Figure 33C).

To summarize, all models lead to an accumulation of CBs in the DZ. No PCs were generated due to the inability of recycled CBs to express BLIMP1. There was a

significant increase in the number and affinity of MBCs. The expansion of GC B cells and significant reduction of PCs in BCL^{auto} and BCL^{inc} models was in disagreement with observations showing BLIMP1 suppression lead to unaltered GC B-cell numbers at day 10 and 21 post immunization and PC numbers day 10 post immunization (see Table 9) (Zhang *et al.*, 2015). This could be due to a decreased but present BLIMP1 expression in the experimental setup, which was not the case in our model. Finally, $BLIMP^{loss}$ and $BLIMP^{loss}IRF^{inc}$ models were consistent with observations showing BLIMP1 inactivation lead to GC B-cell expansion (see Table 9) and a lack of PC production at days 10 and 21 post immunization (Calado *et al.*, 2010). Nevertheless, when in codominance with constitutive NF-KB pathway activation ($BLIMP^{loss}IRF^{inc}$), at day 21 post immunization, experimental data showed unaltered GC B-cell numbers as opposed to the expansion of B cells observed in our model (see Table 9).

4.4.3. Constitutive activation of the NF-kB pathway alone and in codominance with enforced BCL6 expression increases PC differentiation at latter stages of the GC reaction (IRF^{inc}, $BCL^{inc}IRF^{inc}$)

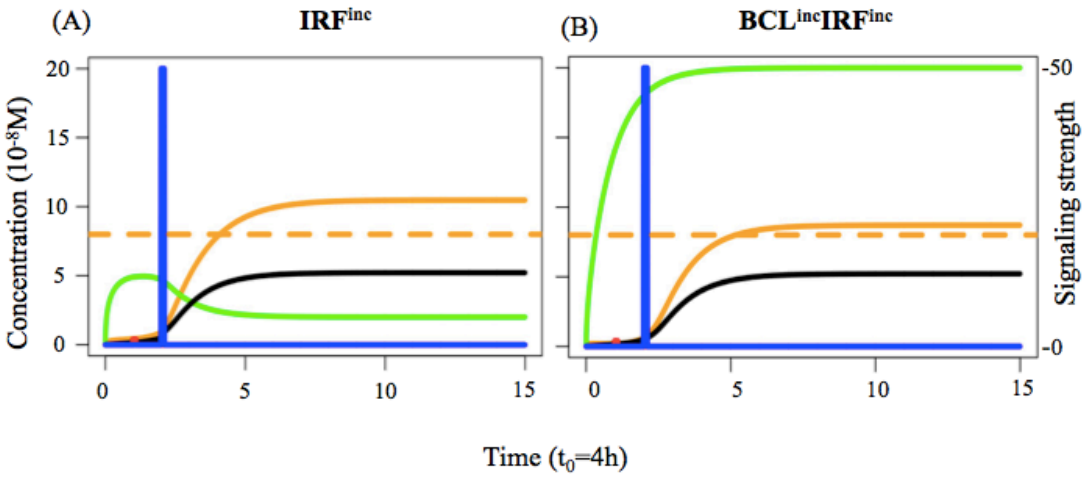

Figure 34: Transcription factor dynamics of (A) IRF^{inc}, (B) $BCL^{inc}IRF^{inc}$ diffuse large B-cell lymphoma models upon binding of Ag and CD40L. Each time unit represents 4 hours. The protein concentration levels (unit = 10^{-8}M) of BCL6 (green), IRF4 (black) and BLIMP1 (orange) are shown on the left axes. Transcription factor levels are followed for 52 hours after CD40 signal. In IRF^{inc} and $BCL^{inc}IRF^{inc}$ models, CD40 signal (blue) affects transcription factor levels resulting in a switch of the B-cell to a PC (BLIMP1+) phenotype (in approximately 8 and 12 hours respectively in this example).

Next, we assessed the effect of constitutive activation of NF-kB pathway alone (IRF^{inc}) and in codominance with BCL6 overexpression ($BCL^{inc}IRF^{inc}$) on the overall GC dynamics (Table 1). Previous studies showed that the GC phenotype in

diffuse large B-cell lymphomas that are driven by IRF^{inc} and BCL^{inc}IRF^{inc} alterations are characterized by unaltered B-cell numbers (Zhang *et al.*, 2015) or slightly decreased B-cell numbers (Calado *et al.*, 2010), in the case of the IRF^{inc} alteration, at day 10 post immunization and spleen and/or lymph node hyperplasia (Calado *et al.*, 2010; Zhang *et al.*, 2015). While alterations that lead to IRF^{inc} model resulted in an increased PC production at day 10 post immunization according to Zhang and collegues (Zhang *et al.*, 2015) unaltered PC numbers at day 10 post immunization were observed by Calado and colleagues (Calado *et al.*, 2010). Furthermore, alterations that lead to BCL^{inc}IRF^{inc} model resulted in unaltered PC production at day 10 post immunization (Zhang *et al.*, 2015).

The transcription factor dynamics simulated in single cells showed in both IRF^{inc} and BCL^{inc}IRF^{inc} models there was a switch to the BLIMP1 and IRF4 high steady state prior to the CD40 signal (Figure 34A). Nevertheless, only BCL^{inc}IRF^{inc} model had consistently high BCL6 levels due to the effect of BCL6 overexpression (Figure 34B).

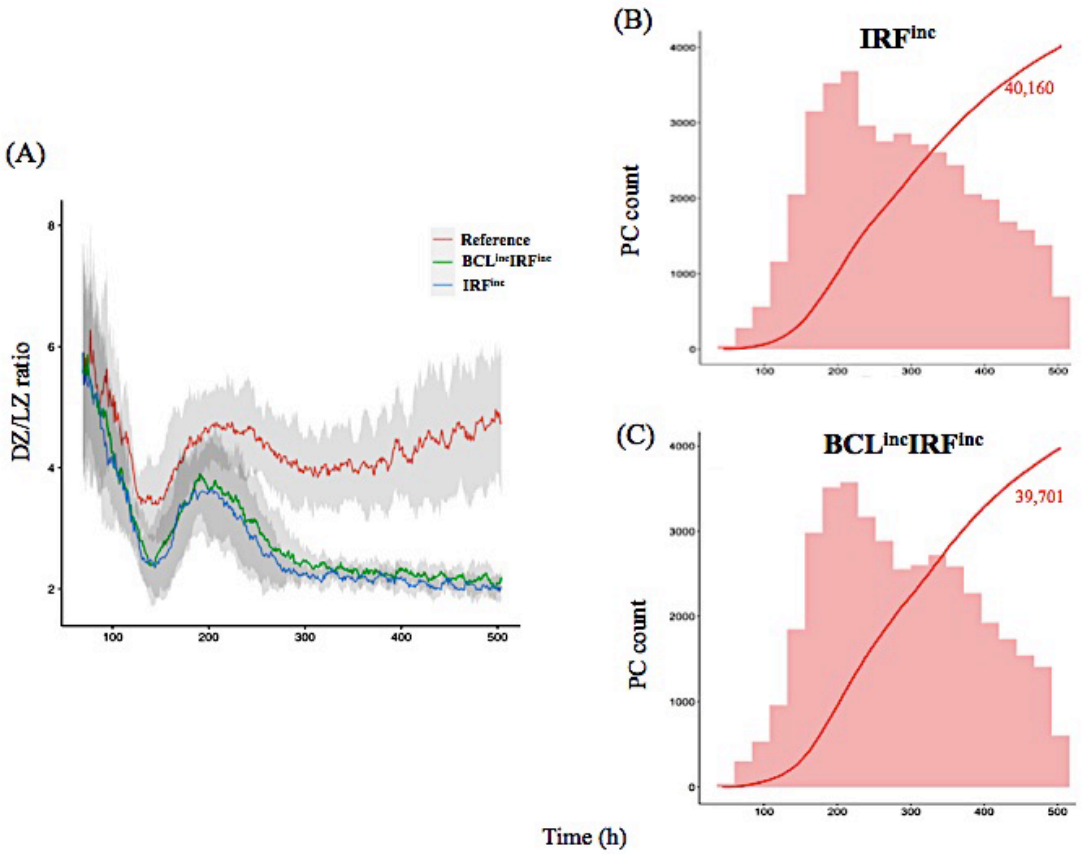

Figure 35: Overall GC dynamics with affinity dependent CD40 signal. (A) Mean DZ-to-LZ ratio calculated from CB and CC counts during the GC reaction for the reference (red), BCL^{inc}IRF^{inc} (green) and IRF^{inc} (blue) diffuse large B-cell lymphoma models. Standard deviation of 10 different random seeds is represented in light grey. There is a 2-fold increase in the DZ-to-LZ ratio of the reference model compared to the diffuse large B-cell lymphoma models. (B) Cumulative number of PCs produced during the GC reaction for IRF^{inc} and BCL^{inc}IRF^{inc} models represented with a red line. Histogram represents the number of PCs (red) produced per day. Histogram scale is represented in the left axes. Line scale (not shown) ranges between 0 and 100. Number shows the cumulated number of PCs (red) at the end of the GC reaction. No MBCs are produced. Representative of 10 simulations.

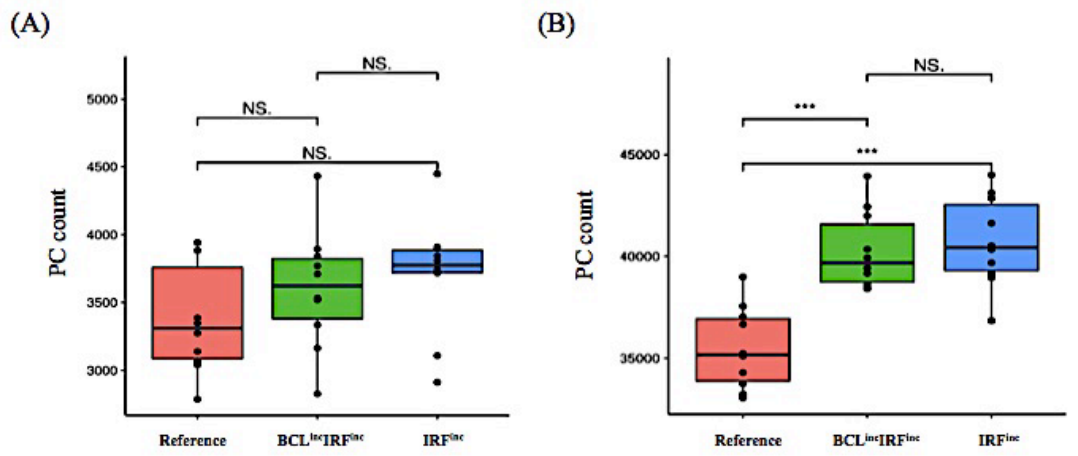

Figure 36: Statistical analysis of PC counts (A) at day 7 of the GC reaction, and (B) at the end of the GC reaction for the reference (red), $BCL^{inc}IRF^{inc}$ (green), IRF^{inc} (blue) and $BLIMP^{loss}IRF^{inc}$ (purple) diffuse large B-cell lymphoma models. No statistical significant difference in the number of PCs produced at day 7 is observed between the reference and the two diffuse large B-cell lymphoma models. At day 10 there is a statistical significant difference in the number of PCs produced between the reference and the two diffuse large B-cell lymphoma models. An unpaired two-tailed Student's t test was used. Three asterisks (***) represent p-values ≤ 0.001, "NS." represents not statistically significant.

We observed both diffuse large B-cell lymphoma models had a 2-to-3-fold decrease in the DZ-to-LZ ratio at day 21 of the GC reaction (Supplementary Table 8, Figure 35A) as well as a slight decrease of GC B cells (data not shown) and increase in output cells produced at day 21 of the GC reaction (Supplementary Table 8) compared to the reference model. All output cells were PCs and no MBCs were produced (Figure 35B-C). Statistical analysis of PC count at day 7 of the GC reaction (Figure 36A) showed no significant difference compared to the reference model. Interestingly, at day 21 of the GC reaction (Figure 36B) a 1.14-fold increase in PC count compared to the reference model was observed. Furthermore, no significant difference in PC count between IRF^{inc} and $BCL^{inc}IRF^{inc}$ models was observed.

To summarize, IRF^{inc} and $BCL^{inc}IRF^{inc}$ models resulted in a decreased the DZ-to-LZ ratio and increased the production of PCs at day 21 of the GC reaction. No MBCs were produced due to the fast increase of BLIMP1 independent of CD40 signaling and B-cell affinity. At day 7 of the GC reaction, similar PC counts were observed compared to the reference model. Our IRF^{inc} model was in agreement with observations showing a unaltered number of PCs at day 10 post immunization and spleen hyperplasia (Calado *et al.*, 2010). Nevertheless, the model also showed unaltered and reduced GC B-cell numbers at days 7 and 18 of the GC reaction while the previous study showed the opposite trend. (see Table 9) (Calado *et al.*, 2010). Despite reproducing the transcription factor and GC B-cell dynamics, our PC results were in disagreement with observations showing an increased number of PCs at day 10 post immunization (see Table 9) (Zhang *et al.*, 2015). This discrepancy suggested that our model was able to recapitulate the effect of constitutive activation of the canonical but not the alternative NF-kB

pathway on PC production. Finally, $BCL^{inc}IRF^{inc}$ model was in agreement with observations shown by Zhang and colleagues (see Table 9) (Zhang *et al.*, 2015). Thus, our results suggested that IRF^{inc} and $BCL^{inc}IRF^{inc}$ alterations lead to unaltered PC production at day 7 of the GC reaction but could result in increased PC differentiation at latter stages of the GC reaction.

4.4.4. Loss of IRF4 and BLIMP1 mediated silencing of BCL6 does not affect PC differentiation (IRF^{sil} and $BLIMP^{sil}$)

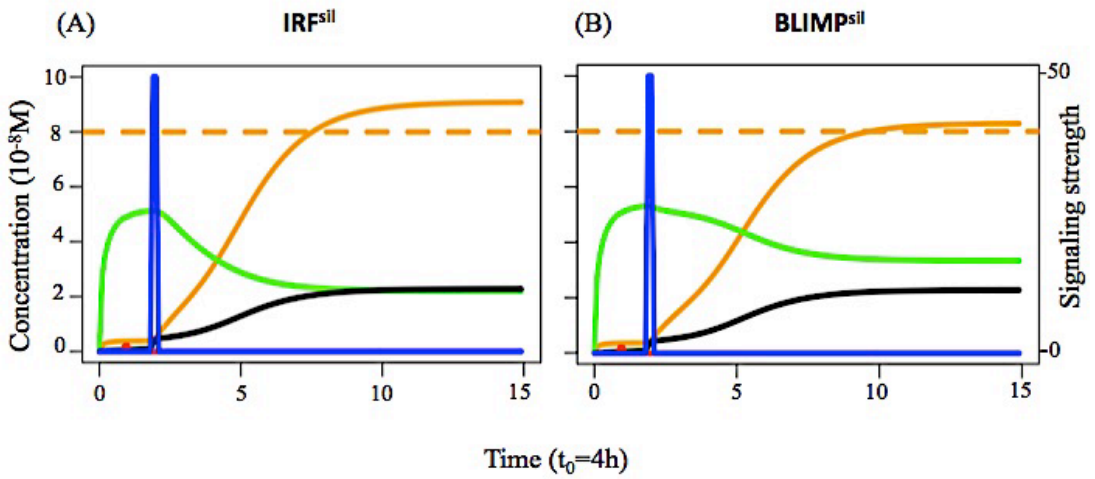

Figure 37: Transcription factor dynamics of (A) IRF^{sil}, (B) $BLIMP^{sil}$ diffuse large B-cell lymphoma models upon binding of Ag and CD40L. Each time unit represents 4 hours. The protein concentration levels (unit = 10^{-8}M) of BCL6 (green), IRF4 (black) and BLIMP1 (orange) are shown on the left axes. Transcription factor levels are followed for 52 hours after CD40 signal. In IRF^{sil} and $BLIMP^{sil}$ models, CD40 signal (blue) affects transcription factor levels resulting in a switch of the B-cell to a PC (BLIMP1+) phenotype (in approximately 20 and 24 hours respectively in this example).

Finally, we assessed the effect of loss of IRF4- and BLIMP1-mediated silencing of BCL6 (IRF^{sil} and $BLIMP^{sil}$) on the overall GC dynamics (Figure 37). For IRF^{sil} and $BLIMP^{sil}$ alterations, we did not find observations on the GC phenotype in terms of B-cell numbers and PCs produced. Nevertheless, the transcription factor dynamics simulated in single cells showed in both models the system evolved to a BCL6 low, BLIMP1 and IRF4 high steady state as a result of the CD40 signal transduction. Similar results were observed by Martínez and colleagues (Martínez *et al.*, 2012) indicating that redundancy in the GRN makes the system robust against loss of BCL6 repression by either BLIMP1 or IRF4, but not by both. Steady state levels of all transcription factors in IRF^{sil} model reached similar concentration levels as in the reference.

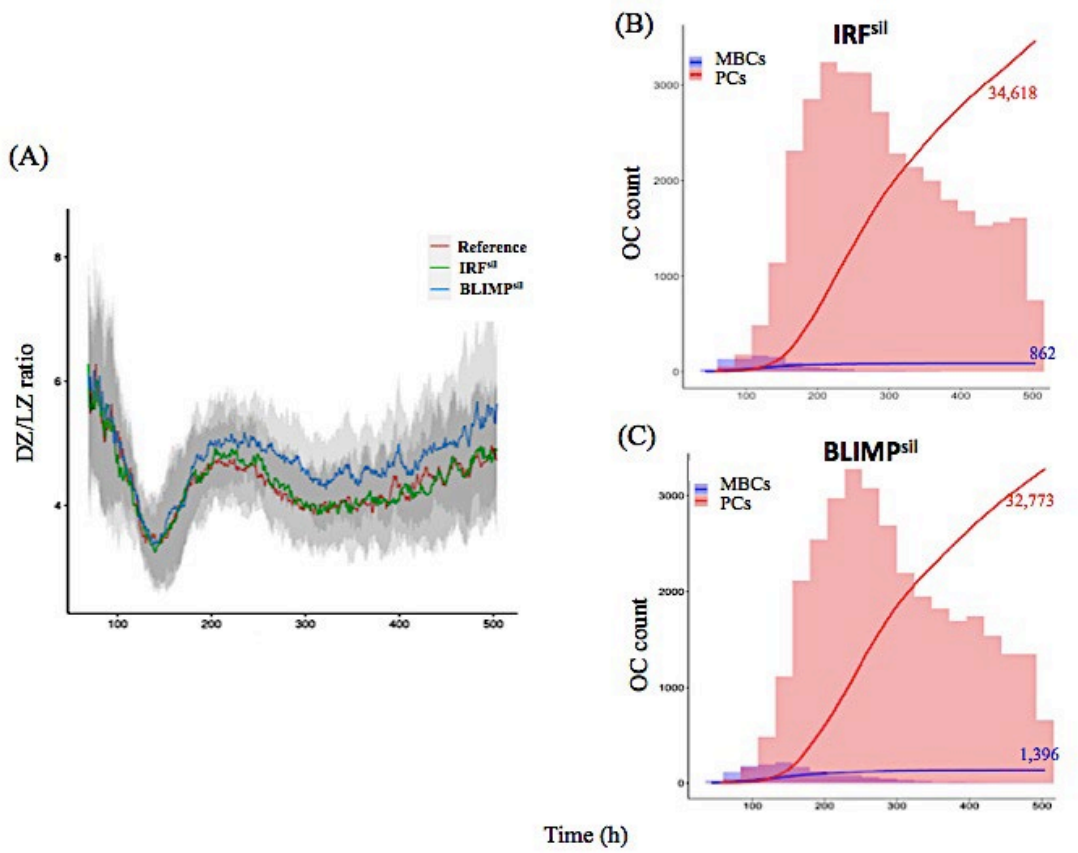

Figure 38: Overall GC dynamics with affinity dependent CD40 signal. (A) Mean DZ-to-LZ ratio calculated from CB and CC counts during the GC reaction for the reference (red), IRF^{sil} (green) and BLIMP^{sil} (blue) diffuse large B-cell lymphoma models. Standard deviation of 10 different random seeds is represented in light grey. There is a similar the DZ-to-LZ ratio in the reference and the diffuse large B-cell lymphoma models. (B) Cumulative number of PCs and MBCs, represented with red and blue lines respectively, produced during the GC reaction for IRF^{sil} and BLIMP^{sil} models. Histogram represents the number of PCs (red) and MBCs (blue) produced per day. Histogram scale is represented in the left axes. Line scale (not shown) ranges between 0 and 100. Number shows the cumulated number of PCs (red) and MBCs (blue) at the end of the GC reaction. Representative of 10 simulations.

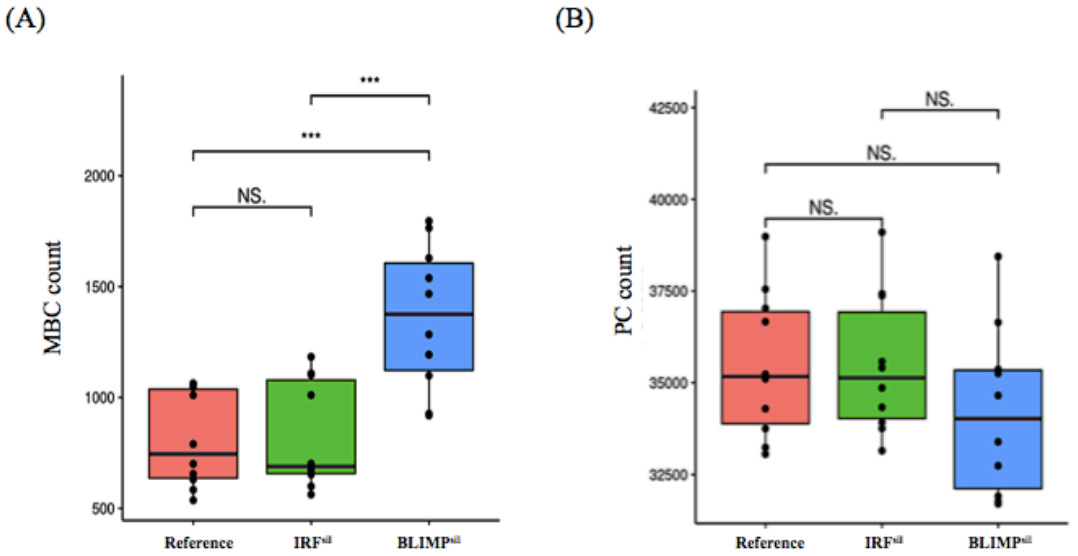

Figure 39: Statistical analysis of (A) MBC count, (B) PC count, at day 21 of the GC reaction for the reference (red), IRF^{sil} (green), BLIMP^{sil} (blue) diffuse large B-cell lymphoma models. No statistical significant difference in the number of PCs produced is observed between the reference and the two diffuse large B-cell lymphoma models. There is a statistical significant difference in the number of MBCs produced between BLIMP^{sil} model and the reference. There is a no statistical significant difference in the number of MBCs produced between IRF^{sil} model and the reference. An unpaired two-tailed Student's t test was used. Three asterisks (***) represent p-values ≤ 0.001, "NS." represents not statistically significant.

We observed IRF^{sil} model had a similar DZ-to-LZ ratio, GC B cell numbers (data not shown) and output cells produced at day 21 of the GC reaction (Supplementary Table 8) compared to the reference model (Figure 38A). In BLIMP^{sil} model there was a slight increase in the DZ-to-LZ ratio and GC B cell numbers (data not shown) as well as a slight decrease in output cells produced at day 21 of the GC reaction (Supplementary Table 8) compared to the reference model (Figure 38B-C). Statistical analysis of MBC count at day 21 of the GC reaction (Figure 39A) showed no significant difference between the reference and IRF^{sil}. There was a significant 1.7-fold increase in BLIMP^{sil} model compared to IRF^{sil} and the reference. This could be due to the faster increase of BLIMP1 in BLIMP^{sil} indicating there is a greater repression effect of BLIMP1 over BCL6 than the effect of IRF4 over BCL6. Statistical analysis of PC count at day 21 of the GC reaction (Figure 39B) showed no significant difference between the reference, IRF^{sil} and BLIMP^{sil} models.

4.5. Discussion

MSM can be an effective tool to complement experimental investigation and has been used to predict most effective therapies for in vitro diffuse large B-cell lymphoma cell lines (Du *et al.*, 2017). Targeted therapies against chronically

active BcR signaling pathway have shown to most effectively decreased cell viability thus inhibiting tumor growth. It is increasingly acknowledged that aberrant expression of key transcription factors, namely BCL6, IRF4 and BLIMP1, and signaling pathways, namely BcR and CD40, during the GC reaction play a central role in the development of many diffuse large B-cell lymphomas (Martínez *et al.*, 2012). To study the effect of eight different genetic alterations on the B-cell dynamics in the GC we use an existing MSM of PC differentiation (Merino Tejero *et al.*, 2020). We also compare six of the eight diffuse large B-cell lymphoma models with in vivo experiments that analyzed transcription factor expression and GC B-cell numbers at different stages of the GC reaction.

Four of the diffuse large B-cell lymphoma models correctly recapitulate the observed PC and transcription factor dynamics. $BLIMP^{loss}$ and $BLIMP^{loss}IRF^{inc}$ models are consistent with observations showing BLIMP1 deletion lead to a GC B-cell expansion and a block in the PC production at day 7 of the GC reaction (Calado *et al.*, 2010). Thus, constitutive activation of NF-kB pathway could not override the effect of BLIMP1 deletion. Furthermore, $BLIMP^{loss}$ model was consistent with observations showing GC B-cell expansion also at day 21 post immunization. Nevertheless, $BLIMP^{loss}IRF^{inc}$ model also showed a GC B-cell expansion at day 21 of the GC reaction, which was not observed experimentally. This could be due to the fact that our MSM does not account for the anti-proliferative and anti-apoptotic effect of BLIMP1. IRF^{inc} and $BCL^{inc}IRF^{inc}$ models are also consistent with observations showing that constitutive activation of the NF-kB pathway alone (Calado *et al.*, 2010) and in codominance with enforced BCL6 expression (Zhang *et al.*, 2015) lead to unaltered PC production at day 7 of the GC reaction. Nevertheless, there is a discrepancy in the number of PCs produced at day 10 post immunization when comparing constitutive activation of the NF-kB pathway in both experimental studies. While studies done by Zhang (Zhang *et al.*, 2015) and colleagues showed an increase in PC production, studies done by Calado (Calado *et al.*, 2010) and colleagues showed unaltered PC numbers at day 10 post immunization . This is likely due to the difference in NF-kB pathways that were activated, namely alternative or canonical pathways studied. Despite the fact that our IRF^{inc} model resembles BLIMP1 levels shown by both studies, the number of PCs produced in our model indicates that it represents the effect of constitutive activation of the canonical NF-kB pathway on PC production. It also shows that the increase of PC production at day 7 of the GC reaction during constitutive alternative NF-kB pathway is not due to the observed increased pro-differentiation effect of BLIMP1 levels. To this end, in vitro experiments showed that such increase in PCs could be linked to an increased proliferative state and/or a decreased apoptotic state. To better represent this in our MSM, a distinction between alternative and canonical pathways should be introduced by including the different NF-kB subunits regulation of IRF4 and BLIMP1 and have an antagonistic function promoting and inhibiting PC differentiation (Roy *et al.*, 2019). Furthermore, c-MYC could be included as part of our GRN, which is a critical mediator of B-cell proliferation (Dominguez-Sola *et al.*, 2012; Shlomchik *et al.*, 2019). Finally, our IRF^{inc} and $BCL^{inc}IRF^{inc}$ models suggest that an increase in PC production could happen at later stages of the GC reaction. Measurement of PC numbers produced at day 21 of the GC reaction could be used to validate this

finding. This finding could explain the pathogenesis of constitutive activation of NF-kB pathway through the induction of the pro-differentiation effect of BLIMP1 and suggests this pathway is a possible candidate for targeted therapy.

Two of the diffuse large B-cell lymphoma models do not correctly recapitulate the observed GC and transcription factor dynamics. BCL^{auto} and BCL^{inc} models result in an expansion of GC B cells and a block in the PC production that was not observed experimentally (Zhang *et al.*, 2015). This could be due to the fact that in our MSM the anti-proliferative and anti-apoptotic effect of BLIMP1 was not included. The connection of other processes such as cell division, or apoptosis with the underlying GRN could potentially result in a better representation of the in vivo experiments. To this end, previous studies have shown that BCL6 may have a role as a promoter or inhibitor of apoptosis depending on the cellular context and the experimental approach (Bai *et al.*, 2003). In the same study, it was hypothesized that increased BCL6 expression could induce apoptosis in diffuse large B-cell lymphoma cell lines due to downregulation of B-cell lymphoma 2. To include this mechanism in our model, further studies are required to elucidate the relation between BCL6, B-cell lymphoma 2 and apoptosis in diffuse large B-cell lymphoma.

No data has been found to validate IRF^{sil} and $BLIMP^{sil}$ models. Our findings suggest that loss of IRF4 or BLIMP1 mediated silencing of BCL6 does not affect PC differentiation. This robustness in the GRN could be necessary to compensate for the high incidence of mutations targeting the regulatory elements in the BCL6 promoter (Saito *et al.*, 2007; Martínez *et al.*, 2012).

MBC dynamics is affected in six of the eight diffuse large B-cell lymphoma models. Models with insufficient BLIMP1 expression (BCL^{auto}, BCL^{inc}, $BLIMP^{loss}$, $BLIMP^{loss}IRF^{inc}$) induce MBC production. Models with constitutive activation of NF-kB pathway alone and in codominance with BCL6 overexpression (IRF^{inc}, $BCL^{inc}IRF^{inc}$) block MBC production. This observation remains to be experimentally validated. Furthermore, while our MBC definition correctly recapitulates the observation of a temporal switch from low affinity and BLIMP1 MBCs to higher affinity and BLIMP1 PC production, it also implies that Ag status (Ag+) is one of the determinants in MBC differentiation and MBCs leave the GC through the DZ. This definition remains to be validated. Nevertheless, a recent study showed that post-GC extranodal mutations targeting a regulator of the molecular switch BCL6 to broad complex-tramtrack-bric a brac and cap'n'collar homology 2 (BACH2) transcription factor lead to an expansion of MBC population and diminished GC B-cell and PC production by hindering BCL6 function and inducing BACH2 (Venturutti *et al.*, 2020). This observation may indicate that certain active-B-cell-subtype-like mutations can skew GC output towards MBC production as well as the role of BACH2 in promoting MBC differentiation by opposing BCL6. Hence, the inclusion of BACH2 in the GRN could able a better understanding of MBC dynamics in the GC and its deregulation in diffuse large B-cell lymphoma.

Overall, our model provides a tool to study the effect of genetic alterations on the cellular level by targeting a GRN with five critical players in the development of

diffuse large B-cell lymphoma and can open the way for new therapeutic strategies. In particular, it suggested BLIMP1 regulatory elements could be better candidates for targeted therapy than those regulating BCL6. Furthermore, the extension of our core GRN with other elements, such as PAX5 (Balasenthil *et al.*, 2007), BACH2 (Ichikawa *et al.*, 2014), T follicular helper secreted cytokines such as IL2, IL4 and IL21 (Bhatt *et al.*, 2017) and metabolic pathways (Calvo-Vidal *et al.*, 2021) could allow for a better approximation of the mechanisms underlying diffuse large B-cell lymphomas and other cancers, which may result in new diagnostic markers or therapeutic targets. However, this requires that we have sufficient mechanistic information or hypotheses about these mechanisms to include them in the model for further testing. Although current literature provides many pointers to make such extension, this will also introduce (many) new parameters in the model for which values need to be estimated from experimental (time series) data. Unfortunately, such data is not generally available. We attempted to extend the GRN model with FOXO1 and c-Myc following new insights about the synergistic induction of c-Myc by BcR and CD40 signalling (Luo *et al.*, 2018) to but due to lack of experimental data we terminated this effort at this time.

4.6. Acknowledgements

We thank Barbera van Schaik to setup a Virtual Machine provided by the Dutch national e-infrastructure with the support of SURF Cooperative, to process large output files. This work is supported by a CASyM Exchange Research Grant, COSMIC (www.cosmic-h2020.eu) which has received funding from the European Union's Horizon 2020 research and innovation programme under the Marie Skłodowska-Curie grant agreement No 765158, and by the Human Frontier Science Program 570 (RGP0033/2015).

4.7. Supplementary Information

4.7.1. List of Abbreviations

GC = Germinal center
BCL6= B-cell lymphoma 6
IRF4= Interferon regulatory factor 4
BLIMP1= B lymphocyte induced maturation protein 1
BACH2= Broad complex-tramtrack-bric a brac and cap'n'collar homology 2
ODE= Ordinary differential equation
MSM= Multiscale model
PC= Plasma cell

MBC= Memory cell
NF-kB= Nuclear factor kappa-light-chain-enhancer of activated B cells
DZ= Dark zone
LZ= Light zone
CB= Centroblast
CC= Centrocyte
BcR= B-cell receptor
FDC= Follicular dendritic cell
Ag= Antigen
CD40= Cluster of differentiation 40
GRN= Gene regulatory network

4.7.2. Agent based model

Supplementary Table 5: ABM model parameter values, units and description.

Parameter name	Value	Unit	Description
dt	0.002	h	Time resolution of GC simulation
tmax	504	h	Duration of GC reaction
dx	5	μm	Lattice resolution of space grid
radius	160	μm	Radious of GC
length	64	Grid points/ Dimension	Number of grid points (2*radious/dx) in a 3 dimensional sphere
Stromal cells	300	cells	Total number of stromal cells
FDCs	200	cells	Total number of FDCs
Dendrite Length	40 8	μm Grid points	Length FDC dendrites (Length FDC dendrites/ dx)
Ag	3000	threshold	Presented Ag amount per FDC
Ag saturation	20	threshold	Ag saturation per FDC grid point
T cells	250	cells	Total number of T cells
B cells	100	cells	Total number of initial B cells
Affinity gamma	2.8		Width of Gaussian affinity weight function
Affinity eta	2		Exponent of the hamming distance
CXCL13 production	$1*10^{-8}$ 0.75*dt	mol/h/FDC molecules/dt /grid point	Rate of CXCL13 production (Rate*dt*dx^3 *N.avogadro)
CXCL12 production	$4*10^{-7}$ 30*dt	mol/h/stromal cell molecules/dt /grid point	Rate of CXCL13 production (Rate*dt*dx^3 *N.avogadro)
CXCL13 diffusion	1000	$\mu m^2/h$	Diffusion constant of CXCL13 chemotaxis signal
CXCL12 diffusion	1000	$\mu m^2/h$	Diffusion constant of CXCL12 chemotaxis signal
CXCL13crit	$0.8*10^{-10}$	mol	Critical CXCL13 concentration for desensitization
CXCL13recrit	$0.6*10^{-10}$	mol	Critical CXCL13 concentration for resensitization
CXCL12crit	$60*10^{-10}$	mol	Critical CXCL12 concentration for desensitization
CXCL12recrit	$40*10^{-10}$	mol	Critical CXCL12 concentration for resensitization
chemoMax	10		Maximum weight of chemokine to random polarity
chemoSteep	$1*10^{10}$	1/mol	Steepness of weight reduction with chemokine gradient
chemoHalf	$2*10^{-11}$	mol	Chemokine gradient of half weight
TC weight	0.1		Tendency of T-cells to stay in the LZ [0,1]

Persistent length time (CC, CB)	1.5	min	Persistence of CB and CC polarity
Persistent length time (TC)	1.7	min	Persistence of T-cell polarity
Persistent length time (PC,MBC)	0.75	min	Persistence of MBC and PC polarity
Speed (CB,CC)	7.5	μm/min	Mean CB and CC velocity
Speed (TC)	10	μm/min	Mean T-cell velocity
Speed (MBC,PC)	3	μm/min	Mean MBC and PC velocity
CB division	6	h	Rate of CB division
Start differentiation	72	h	Start of differentiation period
CB →CC CC →CB	0.1*dt	h	Probability of differentiation from CB to CC and from CC to CB
Delay CC →CB	6	h	Delay of selected CC differentiation to CB
Output onset	12	h	Width of smooth onset of differentiation to output
Start mutation	24	h	Start of mutation period
pMut	0.5	Prob./BcR/ division	Mutation probability in CBs after start of mutation period and before undergoing T-cell selection.
pMut	0	Prob./BcR/ division	Mutation probability in CBs before start of mutation period and after undergoing T-cell selection.
pAsymmetric division	0.72	Prob. / division	Probability of asymmetric division of retained Ag in recycled CBs
Ag polarity level	1 0.5		Concentration of Ag in one daughter cell expressed as a fraction of Ag retained in the parent cell in asymmetric and symmetric division.
FDC collection	0.7	h	Duration of CC collection of Ag by serial FDC encounters
testDelay	0.02	h	Time gap between affinity tests
Selection	0.05*dt	h	Rate of CC selection by FDCs
TC interaction	0.6	h	Duration of CC interaction with T cells
TC rescue time	0.5	h	Minimum duration of TC polarization towards CCs for rescue
pMHCdepHill	1		pMHC-dependent division number hill coefficient
pMHCdepMin	1		pMHC-dependent division number hill minimum
pMHCdepMax	6		pMHC-dependent division number hill maximum
pMHCdepHalf	6		pMHC-dependent division number hill half

4.7.3. Gene regulatory network

Supplementary Table 6: ODE model parameter values, units and description. Parameters are normalized by a unit of time (t_0) and concentration (C_0).

Parameter	Value	Unit	Description
μ_p	10^{-6}	M/h	Basal transcription rate
μ_b	2	M/h	
μ_r	0.1	M/h	
σ_p	9	M/h	Maximum induced transcription rate
σ_b	100	M/h	
σ_r	2.6	M/h	
κ_p	1	M	Dissociation constant: ligand concentration that produces half of the maximum induced transcription rate
κ_b	1	M	
κ_r	1	M	
λ_p	1	h^{-1}	Degradation rate
λ_b	1	h^{-1}	
λ_r	1	h^{-1}	
bcr0	1	h^{-1}	Range of BCR-induced degradation of BCL6
CD40	affinity*50	M/h	CD40 signal (affinity = [0,1])
t_0	4	h	Time unit
C_0	10^{-8}	M	Concentration unit

Supplementary Table 7: Comparison between transcription factor concentration levels in the eight diffuse large B-cell lymphoma MSM and those obtained by the ODE model of Martínez and co-workers (Martínez *et al.*, 2012). BCL6, IRF4 and BLIMP1 concentration levels are measured 52 and 600 hours after initiation of the CD40 signal. Highlighted boxes indicate difference between the results obtained by both models. Results produced by the GRN are very close or identical in both models except for BCL^{inc} that shows a clear difference in the BLIMP1 level. This is caused by the fact that in our MSM selected CC differentiation into a PC process was around 11 times faster than in the model presented by Martínez and co-workers. Thus, we found that within the timing of PC differentiation during the GC reaction BCL^{inc} model has a robust BCL6 overexpression that blocks PC differentiation.

Model	**MSM**			**Martínez and co.** (Martínez *et al.*, 2012)		
Transcription factors	BCL6 (10^{-8} M)	BLIMP1 (10^{-8} M)	IRF4 (10^{-8} M)	BCL6 (10^{-8} M)	BLIMP1 (10^{-8} M)	IRF4 (10^{-8} M)
Reference	2	9.3	2.3	2	9.3	2.3
BCL^{auto}	92.1	0.3	0.2	88	0.3	0.2
BCL^{inc}	20.2	0.3	0.2	20	7,6	2.3
IRF^{sil}	2	9.3	2.3	2.2	9.1	2.3
$BLIMP^{sil}$	3.3	8.2	2.3	3.3	8.3	2.3
$BLIMP^{loss}$	3.3	0	2.3	3.3	0	2.3
$BLIMP^{loss}IRF^{inc}$	2.5	0	5.2	Not part of this study		
IRF^{inc}	2	10.5	5.2	2	10.5	5.2
$BCL^{inc}IRF^{inc}$	20	8.7	5.2	Not part of this study		

4.7.4. Diffuse large GC B-cell lymphoma dynamics

Supplementary Table 8: Comparison between B-cell numbers in the eight diffuse large B-cell lymphoma MSMs at day 21 of the GC reaction.

	DZ-to-LZ ratio	Output cell number	PC number	MBC number
Reference	5	35,434	34,617	817
BCL^{auto}	125	31,215	0	31,215
BCL^{inc}	125	31,215	0	31,215
IRF^{sil}	5	35,480	34,618	862
$BLIMP^{sil}$	5.5	34,169	32,773	1,396
$BLIMP^{loss}$	125	31,215	0	31,215
IRF^{inc}	2	40,160	40,160	0
$BLIMP^{loss}IRF^{inc}$	125	31,215	0	31,215
$BCL^{inc}IRF^{inc}$	2	39,701	39,701	0

Chapter 5

Generation of repertoire sequencing data from a computational model of the germinal center

Rodrigo García-Valiente[#], Elena Merino Tejero[#], Maria Stratigopoulou, Dasha Balashova, Michael Meyer-Hermann, Jeroen E.J. Guikema, Huub H.C.J. Hoefsloot, Antoine H.C. van Kampen.

[#]Equally contributed

Manuscript in preparation

5.1. Abstract

The adaptive immune response provides an important line of defense against antigens (Ags) present in our body. It involves B cells, memory B-cells (MBCs), and plasma cells (PCs) and is responsible for immunological memory and the antibody (Ab) response. The germinal center (GC) plays an important role in the adaptive immune response. Sequencing of B-cell and T-cell immune receptor repertoires helps us to understand the adaptive response. However, repertoire sequencing only provides information about the clonotypes and their frequencies. This is useful to identify dominant clones of high frequency but generally further experiments are required to further characterize to a greater extent the identified (dominant) clones by measuring, for example, their affinity. Computational models may, however, help to get a better understanding of immune receptor repertoires. Therefore, we present a multiscale model (MSM) of the GC to establish (i) the relationship between clonal abundance and affinity, (ii) the extent that MBCs and/or PCs with high B-cell receptor (BcR) mRNA content disturb the identification of dominant clones, and (iii) the extent towards whether a single GC reaction represents immune repertoires obtained from blood. Our simulations show that there is a limited correlation between clonal abundance and affinity and, in addition, there is large affinity variability within a clone. Furthermore, we show that the presence of MBCs and PCs with high BcR mRNA content does not significantly affect conclusions on the number of dominant

clones. Finally, as expected, the immune repertoire simulated from outsingle GC model, largely deviates in several aspects from experimental repertoires obtained from blood. Therefore, to further test and improve our model, we are currently working on the comparison of repertoires measured from single GCs. [1]

5.2. Introduction

The immune system is a complex biological system comprising many components that make up a network to protect an organism from disease (Nicholson, 2016; Murphy, 2017). It is activated when it encounters substances (Ags) foreign to the organism such as pathogens and cancer cells. The human immune system comprises the innate and the adaptive subsystems that act in concert (Chaplin, 2010; Spiering, 2015). The innate system is the first line of defense, which acts very quickly but is nonspecific. The adaptive response is slower but is able to more specifically respond to the Ag. Moreover, it produces an immunological memory such that it can respond faster when a (similar) antigen is encountered again in the future. The adaptive immune response is carried out by white blood cells. In particular, the B cells, T cells, PCs, MBCs and memory T cells. The adaptive response involves a cell-mediated response in which activated T cells react directly against a foreign Ag presented by an Ag-presenting cell. In addition, it triggers an antibody (Ab; immunoglobulin) response in which B cells are activated to differentiate to PCs that secrete Abs. These Abs are the soluble form of the membrane-bound BcRs and circulate in the body to specifically bind to the Ag such that it is neutralized and can be removed from the body.

The GC plays a crucial role in the adaptive immune response (Victora and Nussenzweig, 2012; Victora, 2014; N. S. De Silva and Klein, 2015). GCs are microanatomical structures found in secondary lymphoid organs, and are formed when an adaptive response is initiated. These structures are responsible for a process called affinity maturation during which the affinity and specificity of the BcR for the Ag is improved over the course of several weeks. The GC reaction begins with the activation of a limited number of Ag-specific B cells that starts to proliferate (clonal expansion) to form the so-called GC dark zone (DZ), as defined by histology staining. During proliferation of these B cells, now called centroblasts (CBs), their BcR is changed due to somatic hypermutations (SHMs), which increase or decrease the binding affinity of the BcR for the Ag. CBs differentiate to centrocytes (CCs) and migrate to the GC light zone (LZ) where they collect Ag presented by follicular dendritic cells (FDCs) and, subsequently, interact with t follicular helper (Tfh) cells to become positively selected to return to the DZ to undergo further rounds of proliferation and SHM.

[1] This chapter is based on García-Valiente R, Merino Tejero E**,** Stratigopoulou M, Balashova D, Meyer-Hermann M, Guikema JEJ, Hoefsloot H, van Kampen AHC. Generation of repertoire sequencing data from a computational model of the germinal center. Manuscript in Preparation.

MBCs and PCs are important output cells from the GC. In general, MBCs are of lower affinity than PCs, and are produced at later stages (Florian J Weisel *et al.*, 2016) although this might be related to the nature of the Ag (Mathew *et al.*, 2021).

Mammals have an immense immune repertoire comprising B cells and T cells with unique BcRs and T-cell receptors (TcRs) to combat the large variety of Ags. The B-cell repertoire has been estimated to include about 10^{15} members for the naïve repertoire although a much smaller fraction (10^{9}) of mature B cells is maintained in our body (Rees, 2020). The diversity of BcR results from several processes that include their development in the bone marrow through somatic recombination of V(D)J genes that encode the receptor and induce junctional diversity, and pairing of different BcR heavy and light chains (Schroeder and Cavacini, 2010). Finally, additional diversity is created by SHMs in the GC. The BcR harbors three complementary determining regions (CDR1, CDR2, CDR3) that encompass the most variable parts of the Ab and are responsible for Ag binding. The four BcR framework regions (FWRs) mostly provide structural support for the CDRs (Wu and Kabat, 1970; Lefranc *et al.*, 2003; Sela-Culang *et al.*, 2013).

Immune receptor repertoires in blood or tissue can be profiled using next generation sequencing technologies (Robinson, 2015; Friedensohn *et al.*, 2017; Brown *et al.*, 2019; Liu *et al.*, 2021). These BcR and TcR repertoire sequencing experiments have been applied for a broad range of applications including vaccinology, infection, and (auto)immune disorders (Doorenspleet *et al.*, 2014; van Schaik *et al.*, 2014; Galson *et al.*, 2015; Hoehn *et al.*, 2015; Wang *et al.*, 2015, 2019; Bashford-Rogers *et al.*, 2019). Typically, the pre-processing of repertoire sequencing results in a set of clones and their abundances in the measured samples. Additional bioinformatics analyses are then performed to address specific research question (Greiff *et al.*, 2015). A specific (auto)immune response will skew the BcR repertoire towards Abs binding the Ag. Although repertoire sequencing does not provide information about binding affinities, it is generally assumed that higher abundant clones (dominant clones) have higher affinities due to their Ag-driven expansion and selection in GCs. Therefore, in principle, dominant clones provide good candidates to further characterize, for example, binding specificity and affinity, neutralization capacity, and functional properties (Marks and Deane, 2020). In addition, these high abundant Abs might lead to new mAb therapeutics such as TNF inhibitors (Monaco *et al.*, 2015), or can be used to monitor an immune response during disease or after vaccination (Brown *et al.*, 2019). The selection of candidate B cell clones is likely to be the most successful when focusing on functional B cell populations (tissue-infiltrating B cells, PBs, PCs, and MBCs).

Although dominant clones provide a reasonable starting point to follow-up repertoire sequencing experiments, it would be interesting to know the relation between clonal abundance and affinity. Unfortunately, measuring the binding affinity for hundreds to thousands of clones resulting from repertoire sequencing is virtually infeasible. Moreover, a clone represents a (large) lineage of B cells

(subclones) stemming from the same unmutated common ancestor (a naïve B cell initiating a GC reaction) with unique BcRs created by SHMs. Since, in practice, one typically selects a specific sequence from such lineage as a starting point to create a recombinant Ab, one has little information about the variation of binding affinities (or other properties) within a clone. Another point of consideration is the fact that, in case of RNA repertoire sequencing, the abundance of the clones might be inflated by high immunoglobulin RNA content in PCs and/or MBCs. It has been reported that differentiation of B-cells into PCs is accompanied with an up to 100-fold increase in immunoglobulin production rate, facilitating to production of secreted Abs (Andersson *et al.*, 1978; Perry and Kelley, 1979; Kelley and Perry, 1986; Cox and Emtage, 1989; Genovese and Milcarek, 1990; McKean *et al.*, 2008; Tellier and Nutt, 2019).Whether the immunoglobulin mRNA abundance in MBCs is also increased compared to B cells is unknown by the best of our knowledge.

Previously we developed a simple model of the GC based on ordinary differential equations (ODEs) that suggested that there is only a limited correlation between clonal abundance and affinity (Reshetova *et al.*, 2017). However, in this model we could not analyze the clones but instead focused on the individual subclones (i.e., B-cells with a unique BcR). Moreover, ODEs provide a continuous approximation to large (cell) populations and, therefore, low frequent subclones were not adequately represented. In addition, PCs and MBCs were modelled without a specific underlying mechanism.

In this paper, we use a much more sophisticated and comprehensive model of the GC to facilitate the interpretation of B-cell repertoire data. We use and extend a MSM of the GC that we recently developed (Merino Tejero *et al.*, 2021). This model integrates an ABM to describe the cellular dynamics, and a system of ODEs representing a core GRN involved in PC differentiation. We aim to use this model to again establish the relationship between clonal abundance and affinity to validate our previous results. In addition, we aimed to determine to what extend the selection of dominant clones is affected by the high mRNA content of PCs (and MBCs) in a sample. Finally, we aimed to determine the extent to which the GC output reflects experimental immune repertoires obtained from blood. We show that there is a limited correlation between clonal abundance and affinity and, in addition, there is large affinity variability within a clone. Our simulations suggest that PCs (and MBCs) do not have a large effect on the number of dominant clones inferred in GC RNA-Seq repertoires. These results are helpful in the selection of B cell clones for follow-up characterization. Finally, as expected, the immune repertoire generated from a single GC in our model, (largely) deviates in several aspects from experimental repertoires obtained from blood. However, emerging single cell and single GC experiments are likely to be in more in agreement with our simulations.

5.3. Methods

We recently developed a MSM of the GC reaction (Merino Tejero *et al.*, 2021) (Figure 40). This model integrates a pre-existing ODE model representing a core GRN that drives PC differentiation (Martínez *et al.*, 2012), and an ABM of GC representing the cellular mechanisms (Meyer-Hermann *et al.*, 2012; Robert *et al.*, 2017). In short, the GC is represented as a 3D sphere of equidistant grid points that also defines the DZ and LZ. CXCL12 and CXCL13 chemokines gradients, resulting from stromal cells in the DZ and FDCs in the LZ respectively, are imposed on the grid and allow the CBs, CCs, and Tfh cells to preferentially migrate to their respective zones. The CBs proliferate and mutate in the DZ, while the CC interact with the FDCs and Tfh cells in the LZ to receive survival signals to become positively selected. Lack of sufficient survival signals causes the CC to go into apoptosis. The duration of a single GC simulation is of 504 hours (21 days) at a time resolution of 0.002 hours.

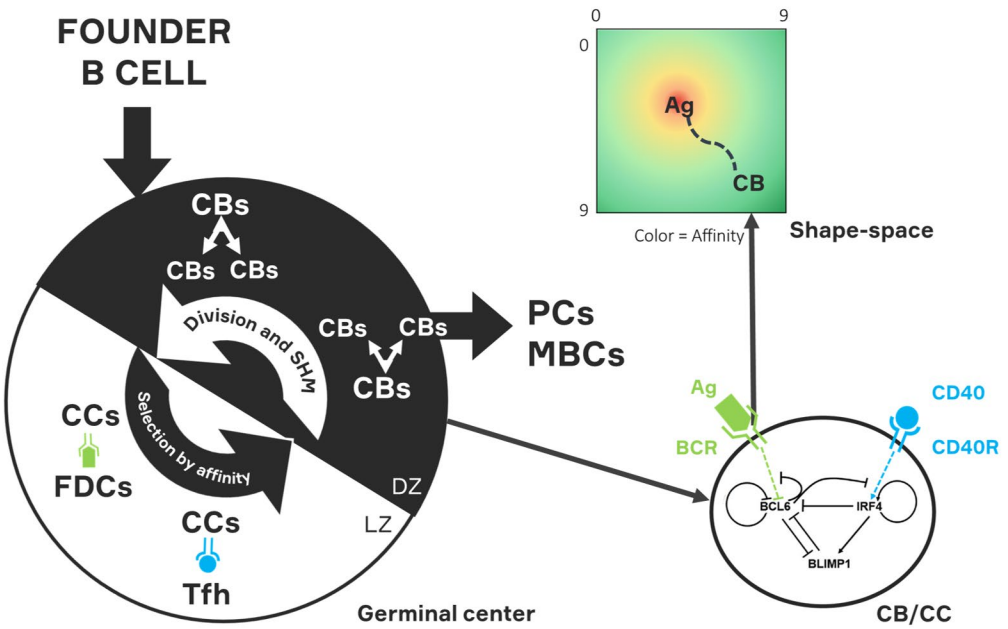

Figure 40: General scheme of our GC MSM. Founder B cells enter the GC and go through a process of division and SHM in the DZ and selection in the LZ, based on the affinity of their BcRs. Our MSM includes a GRN that drives PC differentiation. The affinity of the BcRs is based on the distance between the BcR sequence and the optimal BcR in a continuous shape-space.

5.3.1. Influx of founder cells

Following experimental observations (Tas *et al.*, 2016) we initiate the GC with approximately 200 founder B cells that enter during the initial phase of the GC

reaction (Robert *et al.*, 2017). Accordingly, founder B cells enter the GC with a probability p(influx) (Eq 12).

$$\textbf{Eq 12: } p(\text{influx}) = \frac{\mu \cdot \Delta t}{1+e^{\frac{t-\alpha}{\beta}}}$$

With Δt=0.002 corresponding to the time resolution of the ABM, α=96 hours representing the time point at which influx stops, β=6 hours and represents the rate smoothness, and μ=2 cells/hour represents the inflow rate. Integration of this equation shows that this leads to approximately 200 founder B cells (Supplementary Figure 28).

5.3.2. Definition of output cells (OCs)

PC differentiation was mechanistically representing by embedding the core GRN in every B cell, MBC and PC represented by the ABM. This network comprises three differential equations (Eq 13 - 15) with *p*, *b*, and *r* representing BLIMP1, BCL6, and IRF4 respectively. BCR and CD40 (Eq 16 - 17) represent the signaling strength upon interaction of the B-cell with the FDC-presented Ag and the Tfh cell respectively. Affinity assumes a value between zero and one (see below). The values for the parameters (transcription and decay rates, dissociation constants) are given in Supplementary Table 9. CCs that are positively selected by Tfh cells return to the DZ where they further proliferate and, subsequently, differentiate to a PC if the BLIMP1 level is high enough ([BLIMP1] ≥ 8.10^{-8}M). The PCs leave the GC through the DZ.

$$\textbf{Eq 13}: \frac{dp}{dt} = \mu_p + \sigma_p \frac{k_b^2}{k_b^2 + b^2} + \sigma_p \frac{r^2}{k_r^2 + r^2} - \lambda_p p$$

$$\textbf{Eq 14}: \frac{db}{dt} = \mu_b + \sigma_b \frac{k_p^2}{k_p^2 + p^2} \frac{k_b^2}{k_b^2 + b^2} \frac{k_r^2}{k_r^2 + r^2} - (\lambda_b + BCR)b$$

$$\textbf{Eq 15}: \frac{dr}{dt} = \mu_r + \sigma_r \frac{r^2}{k_r^2 + r^2} + CD40 - \lambda_r r$$

$$\textbf{Eq 16}: BCR = bcr0 \frac{k_b^2}{k_b^2 + b^2}$$

$$\textbf{Eq 17}: CD40 = \text{affinity} \cdot cd0 \frac{k_b^2}{k_b^2 + b^2}$$

For the differentiation of MBCs, we followed a different approach based on asymmetric division of Ag, due to a lack of a clear molecular mechanism underlying this cellular event. It has been shown that Ag internalized by B cells is asymmetrically distributed to the daughter cells during B-cell division (Thaunat *et al.*, 2012). However, a possible effect on B-cell fate was not investigated.

Consequently, it was hypothesized that asymmetric division might affect B-cell fate (Dustin and Meyer-Hermann, 2012), and this hypothesis formed the basis of the ABM that we use. The original model assumes that CCs positively selected by Tfh cells recycle to the DZ for further proliferation and SHM and that during B cell division the captured Ag is distributed asymmetrically to both daughter B cells. Subsequently, the Ag-retaining CBs differentiate into OCs, which were not further specified as PC or MBCs. Although there was no direct experimental evidence that asymmetric division determines B cell fate, the implementation of this mechanism made the computational model in better agreement with B-cell migration patterns observed in experiments of photoactivated B-cells (Victora *et al.*, 2010). In our model we maintained mechanism of asymmetric division for producing OCs but we distinguish between PCs and MBCs. The MBCs were defined as OCs resulting from asymmetric B cell division but don't have a high BLIMP1 level. This approach towards PC and MBC differentiation ensured agreement with an experimentally observed temporal switch in which lower affinity MBCs are mainly produced at the initial phase of the GC, while higher affinity PCs are produced after the peak response (Florian J Weisel *et al.*, 2016).

5.3.3. Affinity and shape space

In the original ABM the, BcR affinity is based on a the so-called 'shape space', which is a 4-dimensional grid in which the Ag and BcR are assigned to a grid point (Perelson and Oster, 1979; Meyer-Hermann *et al.*, 2001; Robert *et al.*, 2017). This shape space has a dimension of 10x10x10x10 (10000) discrete points. Within this shape space the Ag has the same fixed position for all B-cells, while the BcR moves through this space upon the acquisition of SHMs (Figure 40). The distance (L1-norm) between the Ag and BcR represents the number of mutations required to acquire the maximum affinity, and is converted to an affinity value between zero and one using a Gaussian weight function. Due to the discrete nature of the grid only a limited number of different affinity values and a fixed step size were possible. Therefore, we changed the shape space to a continuous space with a length of ten (arbitrary units) for each of the four dimensions. This allows a continuous representation of affinity values required to represent the large number of possible mutated BcR nucleotide sequences in the GC. The L2-norm (Euclidian distance) between the Ag and Ab is converted to an affinity value using the Gaussian weight function. SHMs that change affinity move the BcR within this continuous space with a variable step size (*s)* sampled from a normal distribution with a mean of one and a standard deviation of 0.1 ($s \sim N(\mu = 1, \sigma = 0.1)$).

Consequently, the amount of affinity change is not only determined by the direction of change in the shape space, but also by the variable step sizes. Each move in shape space may increase or decrease the distance from the Ag and, consequently, decrease or increase the affinity respectively.

5.3.4. BcR sequence representation

In the original ABM the BcRs were not represented as nucleotide sequences and the shape space was the sole approach to obtain an affinity measure. To more accurately represent the effect of SHMs on affinity we here associate a BcR sequence to each B-cell in the ABM. We constructed a set of partially reconstructed germline heavy chain V(D)J sequences from an in-house generated BcR repertoire from a single GC (unpublished data) using IMGT High-VQuest (Lefranc, 2014; Lefranc *et al.*, 2015) (Figure 41). We selected 230, a number enough so every founder cell could have its own unique BcR sequence, of the most different germlines to prevent the convergence of their sequences. Due to the high variability of the CDR3 (average length of approximately 48 nucleotides (Shi *et al.*, 2014)), it is difficult to correctly identify the short D-gene (average length of nearly 24 nucleotides), or to precisely determine the junctional diversity (Calis and Rosenberg, 2014). Consequently, we identified the V and J sequences, which include part of the CDR3 region. The remaining CDR3 part will remain identical to the experimental sequence. Due to the placement of primers in the FWR1 and FWR4, part of these regions is missing. We fully reconstruct these regions in the reconstructed sequence, keeping track of the position of the missing parts. For the resulting sequence we annotated the four framework regions (FWR) and the three complementary determining regions (CDRs). Each founder B-cell is associated with a nucleotide sequence that is randomly selected (without replacement) from our set of unique V-CDR3-J sequences. We selected the most different germlines to prevent their convergence. During the GC reaction this sequence is mutated (see below) and inherited by the (founder) B cell progeny.

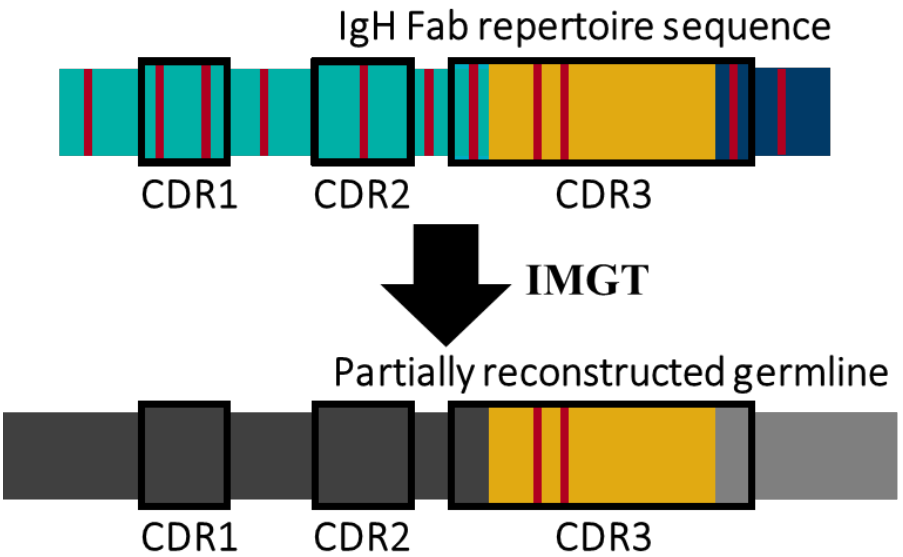

Figure 41: BcR sequence reconstruction and representation. From a IgH Fab repertoire sequence, whose FWR1 and FWR4 regions are partially missing, we infer the corresponding partially reconstructing germline using IMGT High-VQuest. Red vertical bars represent mutations. The three

different colors on each sequence represent the V, D and J gene, respectively, The CDRs appear are marked with black borders. Due to the highly variable nature of the D gene and the junctional diversity, only part of the CDR3 could be assigned to its corresponding germline sequence (i.e., small part of the V and J germline sequence). The remaining part is taken from the repertoire sequence.

5.3.5. Fate of somatic hypermutations

Twenty-four hours after the initiation of the GC reaction, SHM is switched on with a rate of 10^{-3} mutations per base pair per B-cell division (Kleinstein *et al.*, 2003; McKean *et al.*, 2008). Although both the BcR heavy and light chain are important in Ag binding, we simplified our model by only considering mutations in the heavy chain, in agreement with our BcR sequence representation. Since the average length of a BcR heavy chain is approximately 400 nucleotides resulting in 0.4 heavy chain mutations per cell division, we modelled the number of mutation (m) as , $m \sim Poisson(\lambda = 0.4)$. This results in one or more mutations in approximately 33% of the cell divisions (Supplementary Figure 29). Each mutation affects a specific FWR or CDR region, which is selected probabilistically using a SHM fate tree (Figure 42). This decision tree also determines if a mutation changes affinity, is silent, is lethal, or is neutral. Once a region is selected then within this region, we randomly replace a nucleotide and check from the corresponding amino acid sequence if the type of mutation (replacement, lethal, neutral, or silent) agrees with the selected mutation type from the tree. If not, a new nucleotide is randomly selected from the region. We do not account for mutation hot/cold spots (Cui *et al.*, 2016). Our decision tree is an extension of the fate tree previously constructed from experimental data but which does not distinguish between the individual FRW and CDR regions (Shlomchik *et al.*, 1998). We extended this tree to represent all seven FRW/CDR regions. The probabilities in the tree were obtained from sequence data from non-expressed (non-functional) κ light chain transgenic mice immunized with nitrophenyl (NP) (Cui *et al.*, 2016) resulting in mutation patterns in the absence of Ag-driven selection pressure. Preferably, these probabilities should be estimated from (human) heavy chain non-functional sequences but to the best of our knowledge, such data are currently not available. Therefore, we assumed that these probabilities are representative for the human heavy chain. We also assumed that only CDR replacement mutations affect affinity. The fate tree does not account for key or blocking mutations (Kleinstein and Singh, 2003). The probabilities for lethal mutations are taken from the original fate tree (Shlomchik *et al.*, 1998). A lethal mutation will set the affinity of the CB to zero to go into apoptosis in the DZ. Compared to the original ABM, the use of the fate tree changes the probability that the affinity of a cells is changed when SHM takes place. In the original model the SHM probability was set to 0.5 resulting in one mutation, on average, during each B cell division. In contrast, in our model the probability to change affinity, as determined from the fate tree, is of as 0.33*[(0.1*0.79)+(0.03*0.76)+(0.19*0.75)] = 0.08 for each mutation in a daughter cell.

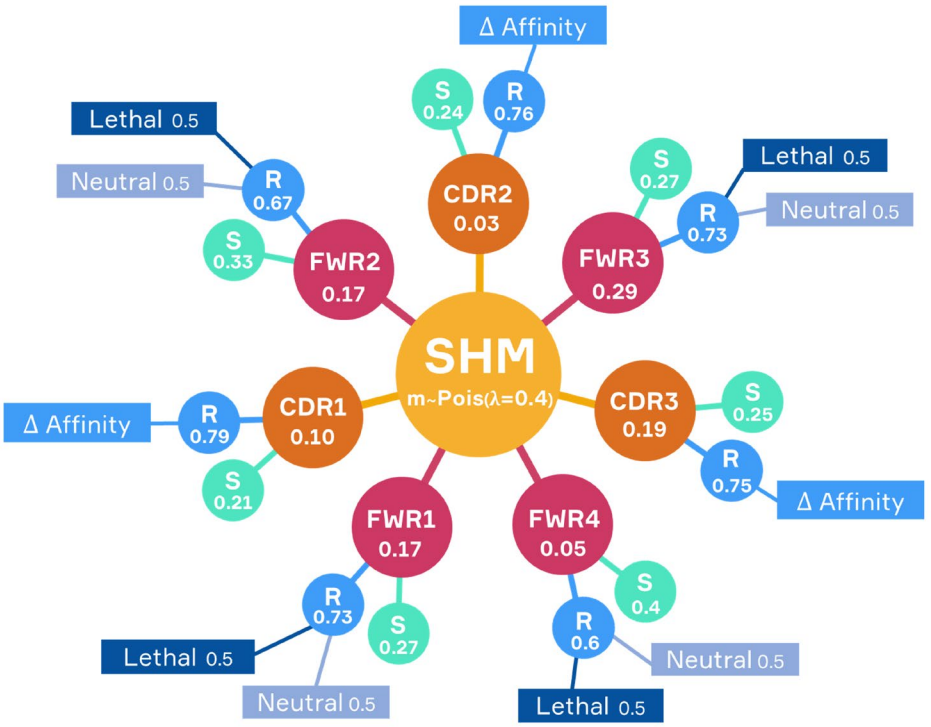

Figure 42: SHM fate tree. After each B-cell division *m* mutations are made to each daughter cell. This tree shows the probabilities of affecting the different FWR and CDR regions, and the probabilities for making a specific type of mutation (replacement, silent, neutral, lethal, and change of affinity).

5.3.6. (Dominant) clones and subclones, and D50 index

Within the simulation we track the clones and subclones. Clones comprise all GC B-cells, MBCs and PCs that share a common ancestor (Figure 43). Each clone comprises one or more subclones; each subclone represents cells with an identical BcR at the nucleotide level. The subclone frequency equals the number of cells with the same unique BcR. The clone frequency is the sum of all cells relative to the total number of B cells (BcRs) from all subclones. The number of dominant clones is determined by counting all clones with a frequency *f* larger than the 75th percentile, or larger than a frequency of 0.5%. This definition of dominance is based on prior experimental datasets (Klarenbeek *et al.*, 2012). The D50 index represents the fraction of clones that account for 50% of the BcR sequences.

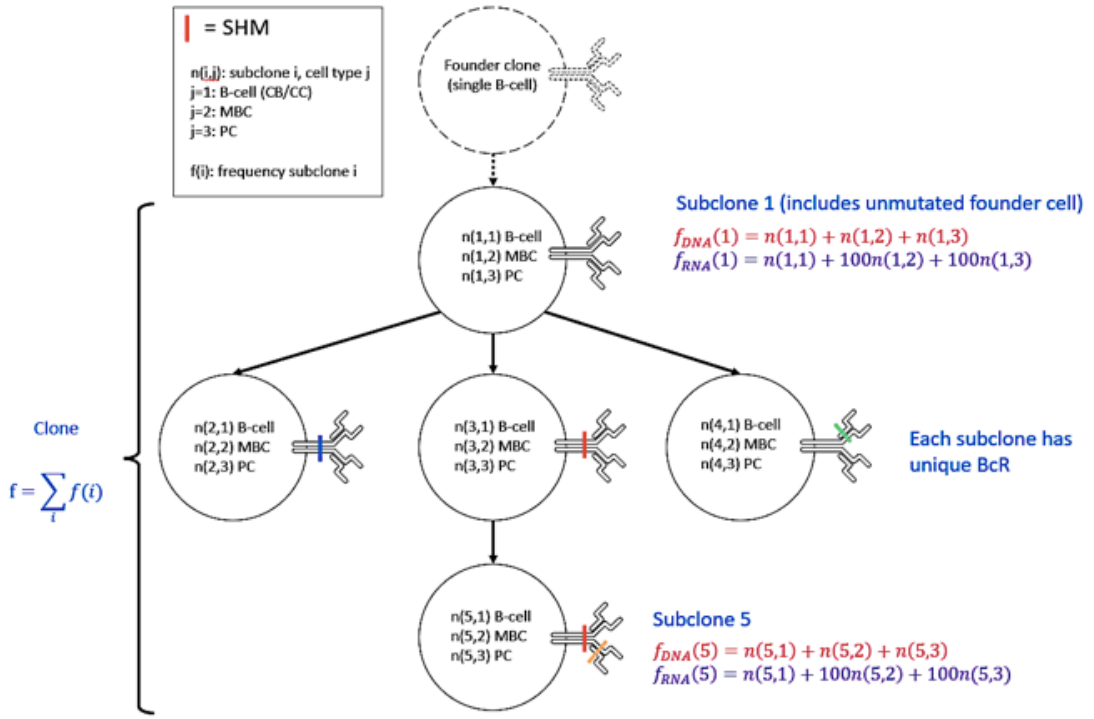

Figure 43: Definition of (sub)clones and the calculation of their frequencies. The founder clone is shown for completeness and is represented by a single cell that enters the GC. Each circle represents a subclone with a unique (mutated) BcR. The five subclones have a common unmutated ancestor and together define the clone. Each subclone is a mixture of B-cells, MBCs and PCs although a subclone may also consist of a single cell type. The frequency of a subclone is determined by counting the number of cells for each subclone. This frequency is obtained with DNA-based repertoire sequencing. Alternatively, frequencies can be determined from RNA-based sequencing but this may artificially increase the subclone frequency if the RNA content of PCs (and MBCs) is much higher compered to CBs/CCs. The frequency of a clone is the sum of the RNA-based or DNA-based frequencies of the subclones.

5.3.7. Comparison to single GC, single cell, bulk RNAseq repertoires

We analyze three selected samples from four different repertoire sequencing studies to determine the number of clones and the number of dominant clones, and compare these to our simulations. The datasets comprise (i) a single cell RNAseq-based repertoire obtained from three human cell subsets (peripheral blood IgG+ B cells (n=2), peripheral plasmablasts after tetanus toxoid immunization (n=1), and MBCs isolated after influenza vaccination (n=1) (DeKosky *et al.*, 2013)). We use the IgG+ samples and one MBC sample; (ii) a bulk RNAseq repertoire dataset representing HIV infected patients and (iii) HIV-uninfected controls (Roskin *et al.*, 2020). We use three samples of patients with broadly neutralizing Abs and three samples from the uninfected controls; (iv) a bulk RNAseq repertoire dataset comprising healthy controls and different immune-mediated disorders (Bashford-Rogers *et al.*, 2019). We use three Crohn's disease peripheral blood mononuclear cell (PBMC) samples from which

CD19+ B cells were sorted. For all the selected sample the BcR sequences were aligned against a database of human V, D, and J genes using IgBlast (Ye *et al.*, 2013). The D-genes are neglected since their short length and the variability of the CDR3 region do not allow an accurate assignment. The CDR3 region is also obtained from the IgBlast output. Finally, Change-o is used to assign clonal groups to the BcR sequences (Gupta *et al.*, 2015; Nouri and Kleinstein, 2018).

5.3.8. Simulations

We performed nine simulations to generate a DNA and RNA-based repertoires. The initial affinities of the founder clones are set to a low value of approximately 0.01 corresponding to a Euclidean distance of approximately 3.1 between the BcR and Ag. From each simulation a DNA-based BcR repertoire was generated at 21 days of a single GC reaction. In a DNA-based repertoire the number of BcR sequences reflect the relative abundances of the GC B-cells, MBCs, and PCs. In our simulation each BcR represents a single B cell. From the DNA-based repertoire we generated a RNA-based repertoire by assuming that the BcR RNA content of PCs and MBCs is 100-fold higher compared to CBs and CCs. Although the RNA content of MBCs is more likely to resemble that of CBs and CCs, this assumptions allows us to test a worst case scenario for determining if high frequent clones (dominant clones) are due to clonal expansion or due to high RNA content of PCs/MBCs. Consequently, we impose a 100-fold increase for PC and MBC counts (Figure 43). In this RNA-based repertoire, the resulting BcR frequencies do no longer reflect the number of B cells that make-up a subclone and, therefore, this may affect the determination of the number of dominant clones. To determine the relation between (sub)clone abundance and affinity we performed a locally weighted scatterplot smoothing (Lowess) (Cleveland, 1979). We repeated our simulations nine times with a different random seed to account for the stochasticity of the ABM.

5.4. Results

We performed nine simulations with the MSM to generate DNA and RNA-based repertoires. The overall GC dynamics, in terms of B-cell number, DZ-to-LZ ratio and affinity level, for one simulation are shown in Supplementary Figure 30 and is in agreement with experimental observations from others (Liu *et al.*, 1991; Hollowood and Macarthey, 1992; Victora *et al.*, 2010; Wittenbrink *et al.*, 2011a; Florian J Weisel *et al.*, 2016) and with our original MSM (Merino Tejero *et al.*, 2020).

5.4.1. Progression of clonal size

Figure 44 shows the number of cells or size of the clones and dominant clones (Table 10) during the GC reaction. Their sizes increase due to proliferation while

at the same time the number of clones is reduced as result of their competition (see below).

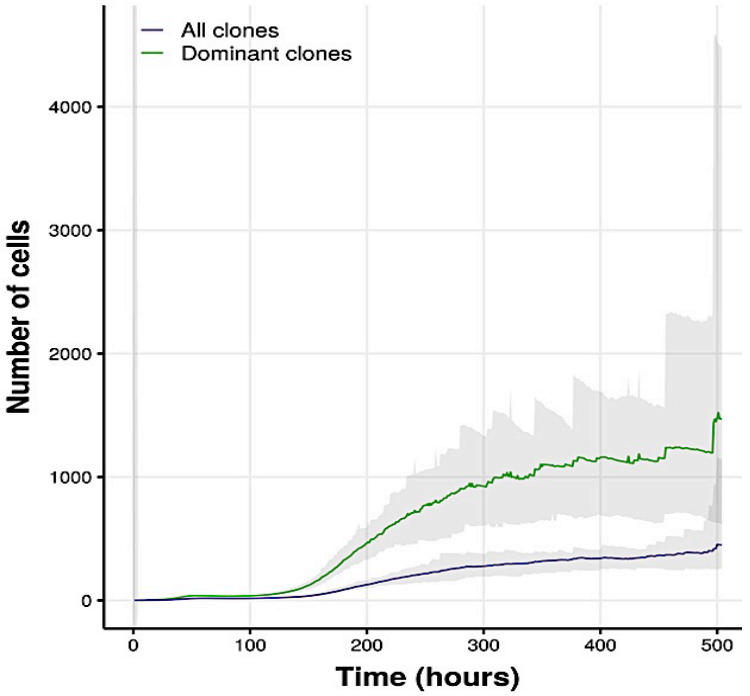

Figure 44: Results from nine simulations showing the change in the mean of all surviving clones (purple) and the dominant clones (green) during a 21-day GC reaction. The dominant clones were determined using a threshold of 75th percentile. The shaded area represents the minimum and maximum values obtained from the simulations.

Table 10: Results at day 21 from nine repeated simulations.

Simulation	Clones	Dominant clones				D50
		DNA-based		RNA-based		
		75th percentile	0.50%	75th percentile	0.50%	
1	18	5	13	5	13	0.111
2	14	4	13	4	11	0.071
3	15	4	8	4	9	0.133
4	17	4	15	4	13	0.235
5	11	3	8	3	9	0.091
6	4	1	2	1	2	0.25
7	11	3	9	3	9	0.182
8	11	3	10	3	9	0.091
9	9	2	7	2	8	0.222
Average	**12**	**3**	**9**	**3**	**9**	**0.154**

5.4.2. The number of (sub)clones remain at a steady level after the clonal expansion phase but show a large variability in their affinities

We determined the number of clones and subclones during the GC reaction. The GC was seeded with approximately 200 founder clones but not all these clones survive the 21-days GC reaction due to clonal competition (Figure 45A). Founder clones that enter the GC at an early stage generally have more chance to survive because they have more time to increase their affinity and, consequently, outcompete founder clones that enter later with an initially lower affinity. Nevertheless, few late founder clones were able to survive the full duration of the GC reaction resulting in an average of 12 clones at the end of the simulations (Table 10). The number clones and subclones increase during the initial clonal expansion phase of the GC reaction after which they slowly decrease (Figure 44B; Supplementary Figure 31). The steady number of subclones is in agreement with our previous but simpler model (Reshetova *et al.*, 2017), and is the result of the balance between B cell proliferation that produces an additional subclone, and SHM that, by definition, removes a single B-cell from a subclone and creates a new subclone (unique BcR). Consequently, subclones also stay of relatively low abundance (Supplementary Figure 32). Inspection of the clones at day 21 shows that these are very heterogeneous with respect to the affinity of their subclones. These 'high-affinity' clones even harbor B-cells of extremely low affinity (Figure 46).

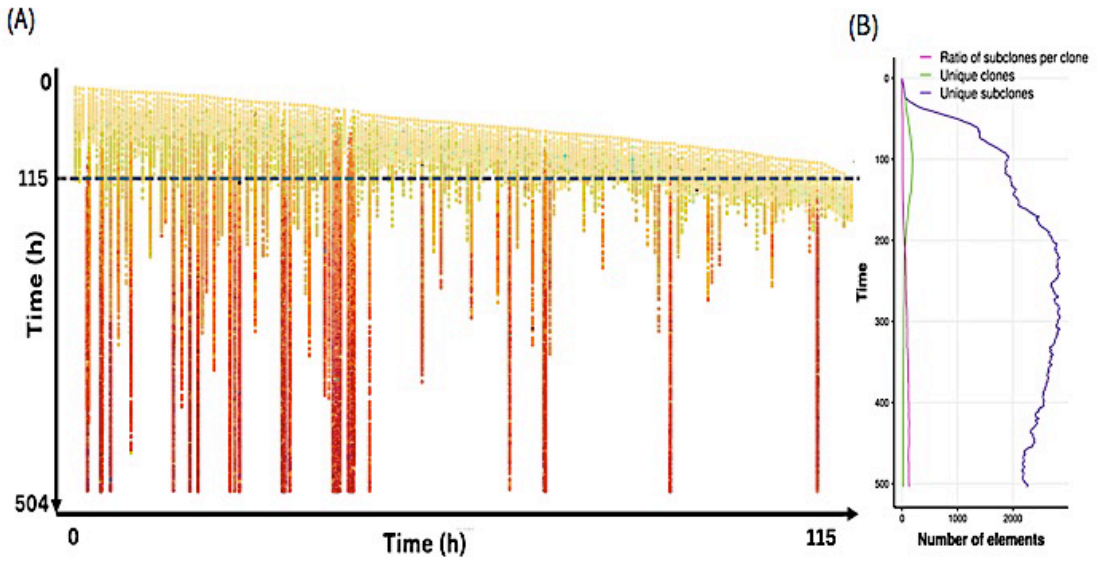

Figure 45: Founder clones and GC diversity from one representative simulation. **(A)** Approximately 200 individual lineages each representing founder clones that enter between t=0 and 115hr. See Supplementary Figure 33 for an individual B-cell lineage. The x-axis shows the time points at which the founder clones enter the GC. The y-axis shows the evolution of the clones during 21 days (504 hrs). Colors denote affinity of each individual subclone from low (yellow) to high (red) affinity. Each lineage comprises a mixture of GC B-cells, MBCs, and PCs. Eighteen clones survived at day 21 while the other clones have been outcompeted and disappeared from the GC reaction. **(B)** Number of clones and subclones. The number of clones increases during the initial GC phase but remains about constant after the GC peak response. The number of subclones evolves to a relatively steady high level.

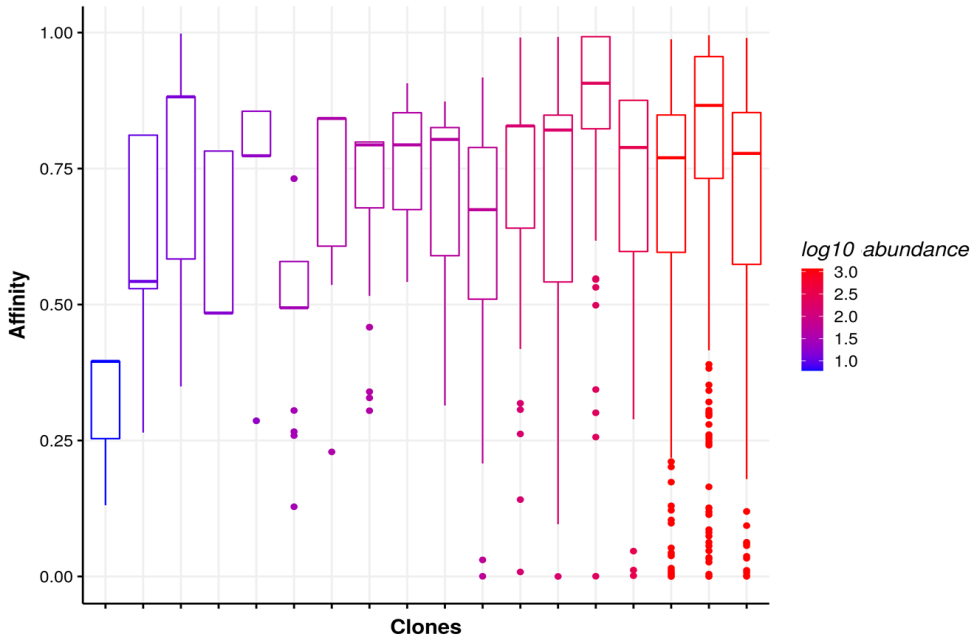

Figure 46: Large variation in subclone affinity for 18 clones at day 21 of a representative simulation. The clones are sorted ascendingly according to their abundance. Clones with a higher abundance include subclones of very low affinity, while clones of low abundancy may have subclones of high affinity. Horizontal line: median. Boxes: 25th and 75th percentiles. Whiskers: 1.5 times the interquartile range. Dots: outliers.

5.4.3. There is a (weak) trend between (sub)clone abundance and affinity

Next, we aimed to determine the relation between (sub)clone abundance and affinity at day 21 of the GC reaction. The median affinity was calculated from all B cells represented by a clone. The median affinity increases with clonal abundances that are in the range from one to approximately 100 but stabilizes for higher abundances. The maximum affinity (1.0) is not reached (Figure 47A). Using threshold defined by the 75th percentile or 0.5% for the abundance, and the 75th percentile of the median affinity we observe several low abundant clones of high median affinity (upper left quadrant Figure 47A) but also several high abundant clones of lower median affinity (lower right quadrant). Inspection of the subclone abundance and median affinity also shows a trend of increasing affinity with abundance but again demonstrates the large variability affinity, i.e., many subclones of very low abundance have high affinity (Figure 47B). This variability decreases for the higher abundant subclones, which are generally of higher affinities.

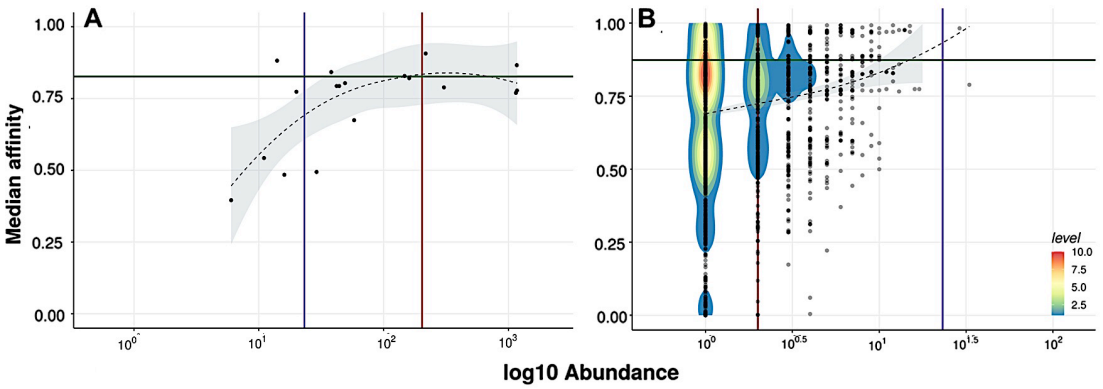

Figure 47: Relation between clone (A) and subclone (B) abundance and median affinity at day 21 of the GC reaction for a representative simulation. Each dot represents a (sub)clone. Horizontal green line denotes the 75th percentile threshold. Vertical red line denotes the 75th percentile threshold. Vertical purple line denotes the 0.5% threshold. Black dotted line denotes a Lowess fit. A 2D density map has been plotted on (B) to show the concentration of the populations.

5.4.4. The presence of MBCs and PCs does not affect the number of dominant clones

We aimed to investigate if a 100-fold higher immunoglobulin RNA abundance in PCs and MBCs affects the number of dominant clones detected in a repertoire at day 21 of the GC reaction. DNA-seq repertoires are not biased by high BcR RNA abundance in MBCs/PCs since for each B cell a single copy of the immunoglobulin is sequenced (Figure 43). Consequently, in our simulations we count the number of B cells for each clone to represent the DNA-seq repertoire. For the nine simulations this results in an average of 3 dominant clones at day 21 of the GC reaction (range 1 – 5) using the 75th percentile as a threshold, or an average of 9 (range 2 - 15) using the 0.5% threshold (Table 10). Figure 48 shows a representative simulation and the determination of dominant clones for a DNA-based and RNA-based repertoire. Results were similar in 9 simulations as shown in supplementary figure 33. Most of the clones are a mixture of B cells types. Consequently, the RNA-based repertoire increases the frequencies of most clones and, therefore, does not largely affect the number of dominant clones (Table 10) since it also shifts the threshold accordingly. If we assume that only GC B cells were sequenced (no MBCs nor PCs present) then the number of dominant clones is identical to the DNA-based repertoire (data not shown), from which it is concluded that the low fraction of OCs does not have a large effect on the dominant clones. Figure 48 also shows that the median affinity of the dominant clones is not always above the 75th percentile, which is caused by the large affinity variability of the subclones.

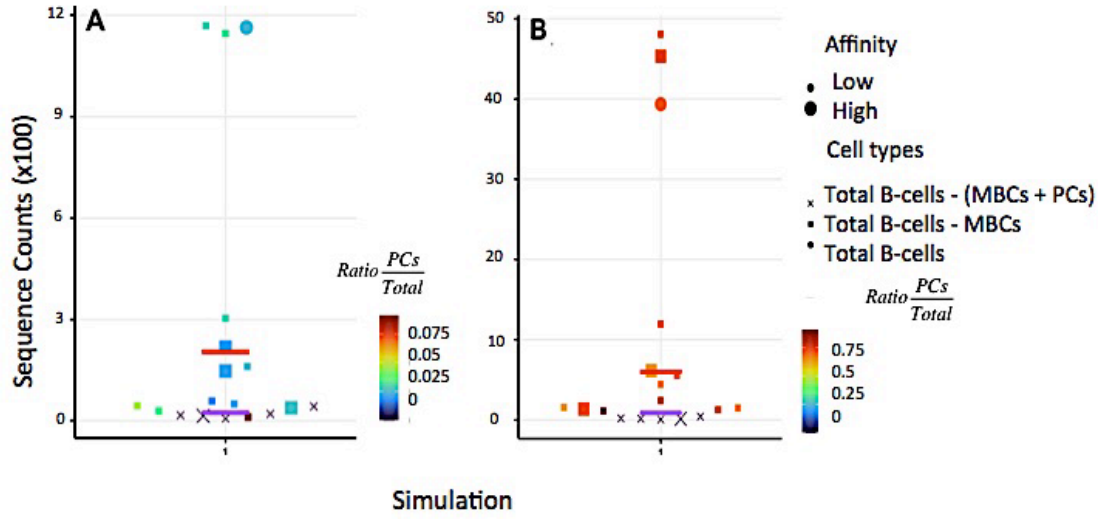

Figure 48: (A) DNA-seq and (B) RNA repertoires at day 21 of the GC reaction generated by a representative simulation. Each dot represents a clone some of which are a mixture of B-cells, MBCs and/or PCs. In both cases we find 5 and 13 dominant clones using the 75th percentile and 0.5% thresholds respectively. Dot colors indicate the fraction of MBCs + PCs BcR sequences within each clone which are about a factor 10 larger for the RNA-based repertoire. The size of the symbol represents affinity (small symbol: affinity below the 75th percentile). The horizontal lines denote the 75th percentile (red) and 0.5% (purple) thresholds that define dominant clones.

5.4.5. Comparison to single cell and bulk RNAseq immune repertoires

The number of clones at the end of our nine repeated simulations varies between 4 and 18 at the end (day 21) of the simulation (Table 10). The maximum number of clones that is reached during the GC reaction is approximately 200 and equals the number of founder clones (Figure 45). The number of clones found in experimental datasets is orders or magnitude larger compared to the clones produced in our simulations representing a single GC (Figure 49A). The number of dominant clones from the simulations is more comparable to the experimental data but still is on the lower side compared to the experiments (Figure 49B). Finally, the D50 values resulting from the simulation are larger compared to the values obtained from the experimental data (Figure 49C) indicating that in the experiments fewer, and thus larger clones, account for 50% of the sequences. The discrepancy between the number of clones found in the single GC simulations and in the experimental data was expected since the number of clones found in blood is an accumulation of the naïve repertoire and multiple (past) immune responses involving many GCs.

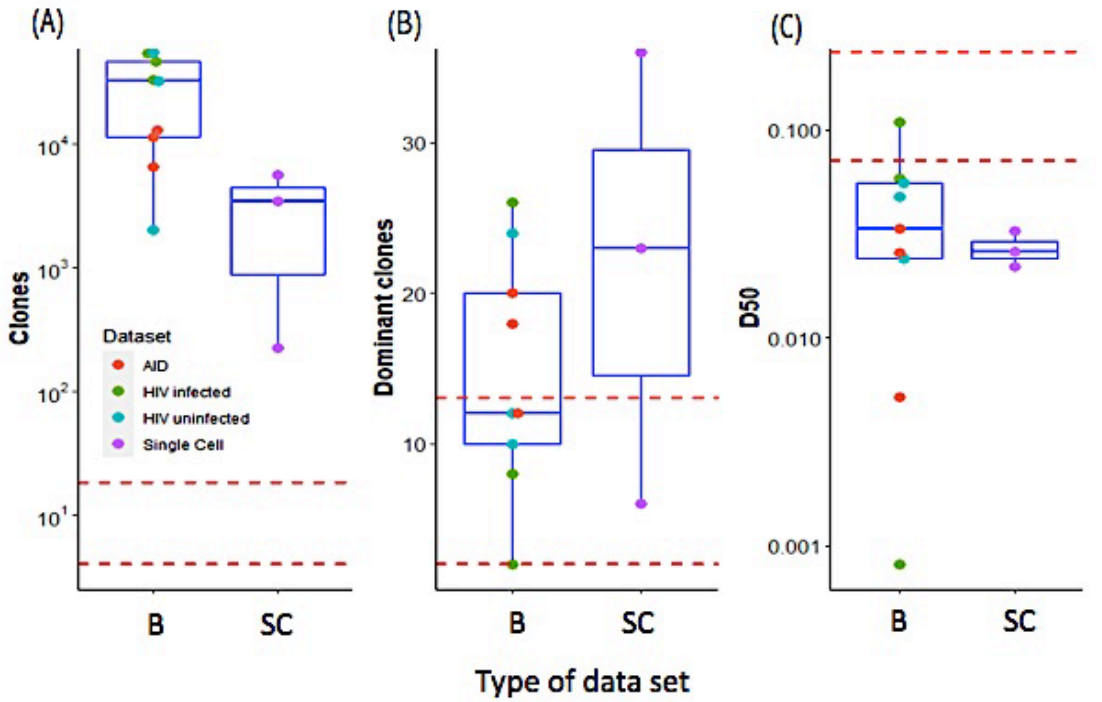

Figure 49: Number of clones (A) dominant clones (B), and D50 (C) for four repertoire sequencing datasets obtained from three bulk RNA sequencing and one single cell (SC) RNA sequencing experiment. The dashed red line shows the number of (dominant) clones at day 21 of the simulation. Dominant clones were defined the clones accounting for at least 0.5% of the repertoire.

5.5. Discussion

BcR repertoire sequencing provides information about clones and their frequencies in a measured sample. In this work we extended a MSM of the GC that we previously developed (Merino Tejero *et al.*, 2021) to facilitate interpretation of repertoire sequencing data. In particular, we aimed to establish (i) the relationship between clonal abundance and affinity, (ii) the extend that MBCs and/or PCs may disturb the identification of dominant clones, and (iii) the extend that a single GC reaction represents immune repertoires obtained from blood.

In the model, each founder clone is represented by a nucleotide sequence derived from a measured repertoire. This, coupled with the existence of a continuous range of affinity values, resulted in more realistic simulations compared to the previous version of our model. We used it to track the clonal and subclonal variety and to implement a coherent behavior (cells with an identical combination of CDRs 1 to 3 at the amino acid level have identical affinity if there are no lethal mutations). In future applications we can also link the number of (different types of) mutations in a sequence with its affinity.

Our results mostly represent the output at day 21 of the GC reaction, assuming that this is the most representative time point for comparison to repertoires

obtained from peripheral blood or tissue. Our model converges from approximately 200 founder clones to a small number of clones that survive the full duration of the GC reaction. However, the number of unique subclones remains relatively stable at low frequencies after the clonal expansion phase due to the balance of proliferation and SHM that creates new subclones. Comparison of our simulation results to experimental repertoires shows a large difference in the number of clones, the number of dominant clones, and the D50 values. It is likely that these differences mostly result from the fact that blood represent immune repertoires from the naïve repertoire and multiple (past) immune responses and a multitude of GC reactions.

The median affinity of the clones in our simulation show a weak relationship with clonal abundance, and several high affinity clones comprise subclones that span a wide range of affinities. This is in agreement with our previous, but more simple, computational model (Reshetova *et al.*, 2017). There are few experimental studies that, on a small scale, related clonal abundance to affinity. For example, Tan and co-workers investigated the immune response following influenza vaccination (Tan *et al.*, 2014). They selected a limited number of plasmablasts to create recombinant Abs and, subsequently, determined their binding affinity and neutralization capacity for the influenza virus. They found that clones with larger abundances have 10-1000-fold higher affinities compared to singleton Abs. These higher abundant Abs bound and neutralized the influenza virus. This is not in agreement with our findings demonstrating a weak relation between abundance and affinity, and also a high variability in subclone affinities (Figures 46-47). However, a recent single cell study from Mathew and co-workers (Mathew *et al.*, 2021) identified a high abundant dominant clone with low avidity for the hemagglutinin (HA) protein of the influenza A virus. In addition, they also identified a clone in which two subclones showed a difference of almost a million-fold in affinity. This shows that, potentially, observations from a single GC simulation can be used for the interpretation of (single cell) repertoire data but that agreement might depend on the Ag.

Recently, Nowosad and coworkers investigated B-cell selection and affinity maturation in single gut-associated GCs (Nowosad *et al.*, 2020) for which they sequenced the B cells from 20 individual GC. They found a median of 33 clones per GC, which is (much) closer to the values we find in our simulations, and a D50 value of 0.2, which is even in the range we find in our simulations (Figure 49C).

Our simulations and experimental data suggest that the selection of a single specific subclone (from a dominant clone) for further characterization (e.g., affinity measurement, neutralization potency) might, potentially, not give a representative picture and may lead to incomplete or erroneous conclusions. Our simulations suggest that low abundant (sub)clones might also be of interest since they may have high affinity for the Ag (which may have one or more different mutations). In practice it may prove difficult to select a low abundant but high affinity clone without trial and error.

For the effect of a larger RNA content in MBCs and PCs, our simulations show that a 100-fold increase in BcR RNA content in MBCs and PCs or removing the MBCs/PCs from the repertoire, does not have a large effect on the number of dominant clones despite that this is sometimes forwarded as a word of caution. This was unexpected but is mainly due to the fact that also the low abundant clones represent a mixture of GC B-cells, MBCs and/or PCs and, therefore, accounting for RNA content does change the abundancy of all clones and, therefore, the threshold. This results in the same or a similar number of dominant clones. However, our model represents a single GC, and the proportions of MBCs, PCs and B-cells that constitute a clone in a blood or tissue sample may be different and, consequently, could have an effect on the number of dominant clones. In addition, it is unknown how many MBCs and PCs are produced by a single GC and, consequently, whether or not the proportions that result from our simulation are correct. It is difficult to predict whether these results translate to experimental immune repertoires. This would require phenotyping of a range of subclones for different clones.

Although BcR and TcR repertoires are typically generated with bulk RNA or DNA sequencing of blood or tissue samples, there is progression towards the generation of immune repertoires from lymph node, GC B cells, and single GCs. The aforementioned study of Nowosad and coworkers generated repertoires for B cells of individual gut-associated GCs (Nowosad *et al.*, 2020), which is more comparable to our simulations. However, they did not determine MBCs and PC. Others also have investigated clonality at the single GC level (Tas *et al.*, 2016; Firl *et al.*, 2018) without, however, measuring full repertoires. Single-cell sequencing strategies have also enabled the combined transcriptome and immune receptor determination of GC B cells, which may help to improve molecular mechanisms relevant for our model (Milpied *et al.*, 2018; Viant *et al.*, 2020; Attaf *et al.*, 2021; King *et al.*, 2021; Mathew *et al.*, 2021). One advantage of single-cell strategies is that both the heavy and light chain, or alpha and beta chain of the BcR and TcR respectively can be determined. For example, FB5P-seq has been developed and used to determine the transcriptome and receptors (including isotype) of MBCs, PCs, plasmablasts (PB), and GC B cells from human tonsils ((Attaf *et al.*, 2020)). Such datasets are expected to increasingly appear in the near future and will help to further validate and improve our model.

We consider our model as a first step towards the simulation of repertoires through the simulation of a GC reaction. Insights from these simulations facilitate the development of strategies to select (sub)clones for further characterization. However, to simulate repertoires that are more representative for experimental immune repertoires, additional steps have to be taken. First of all, our model is Ag agnostic and representation of BcR affinity is based on an artificial continuous 'shape space' that simplifies the true relationship between the BcR sequence, SHMs, and affinity. Nevertheless, the shape space serves its purpose to simulate affinity maturation process without having a specific Ag (Perelson and Oster, 1979; Meyer-Hermann *et al.*, 2001; Robert *et al.*, 2017). Consequently, by definition, our model cannot generate repertoires for different Ags to investigate how repertoire characteristics could be different. More realistic and sophisticated

representations might overcome this in the future (Robert, Marschall, *et al.*, 2018; Robert *et al.*, 2021). Secondly, the mechanism for PC differentiation remains to be fully elucidated. Consequently, our implementation of PC differentiation using a small GRN might need to be improved to, for example, account for other transcription factors and cytokines (Unger *et al.*, 2021; van Asten *et al.*, 2021). In addition, we did not implement an explicit mechanism for MBC differentiation but rather defined these MBCs as OCs not being classified as PCs (Merino Tejero *et al.*, 2021). Obviously, our approach towards the generation of MBCs and PCs directly affects the number of OCs being generated. This, in turn, may affect the extent to which they affect the identification of dominant clones. Unfortunately, by the best of our knowledge, it is unknown how many MBCs and PCs are produced by single GCs during its entire lifetime, making it difficult to validate the number of OCs produced by our model. However, the aforementioned publication from Mathew *et al.* allows to make a rough estimate of GC B cells, MBCs, and PCs in mediastinal lymph nodes after infection with the influenza A virus (Mathew *et al.*, 2021). From Figure 40 in his paper the fraction of MBCs and PCs compared to GC B-cells and OCs is about 2.1% and 0.9% respectively, which is comparable to the number of OCs we observe at day 21 in our simulations (2.1 – 2.7%). The implementation of alternative scenarios for MBC and PC differentiation may further improve the model (Zhou *et al.*, 2018; Laidlaw and Cyster, 2020), which might then further improve the utility of the model to facilitate the interpretation of experimental repertoires.

The number of GC founder clones has been estimated to range from 2 to hundreds with highly diverse early GCs (Jacob *et al.*, 1993; Kuppers *et al.*, 1993; Faro and Or-Guil, 2013; Tas *et al.*, 2016). The number of founder clones (~200) used in our simulations is within this range but on the high end. Reducing the number of founder clones will lead to a delayed GC growth and a lesser number of clones present in the GC at day 21 The diversity of the GC at later stages have been estimated in several studies and range from 4 to approximately 120 clones (Jacob *et al.*, 1993; Tas *et al.*, 2016; Mesin *et al.*, 2020; Nowosad *et al.*, 2020). Tas and co-workers observed GCs that were predominantly monoclonal but that these are relatively rare (Tas *et al.*, 2016). The number of clones at the end of our simulations was between 4 and 18, which is at the lower end of the spectrum. The current model provides little control over the selection pressure to significantly change the number of clones at the end of the GC reaction without disturbing the overall GC dynamics. For example, a simulation with 1500 founder clones still resulted in less than 35 clones (data not shown). Therefore, it is worthwhile to extend the model with a mechanism that allows controlling the clonality of the GC to generate a larger variety of repertoires.

5.6. Acknowledgements

We thank Davide Angeletti (University of Gothenburg) for sharing information about his recent experiments. This work is supported by COSMIC (www.cosmic-

h2020.eu) which has received funding from the European Union's Horizon 2020 research and innovation programme under the Marie Skłodowska-Curie grant agreement No 765158.

5.7. Supplementary Information

5.7.1 Maintaining consistency among mutations

To ensure consistency of affinity values across the mutated sequences during the GC reaction, we stored each combination of affinity and BcR sequence in a database. If a sequence is mutated, we determined its fate and, subsequently, updated its affinity according to the following rules:

- For a lethal mutation (replacement) in a FWR regions we randomly selected a nucleotide position in a way that also changed the aminoacidic sequence. Subsequently, we checked our database to ensure that this mutation was not already associated with a different type of mutation (e.g., silent, neutral, replacement) from an earlier time point. If not, the mutation was accepted and we set the affinity of the B-cell to zero, and we updated the database. Otherwise, we selected a different replacement nucleotide or we selected a different position if none was viable until the process is successful. Finally, the database was updated.

- For a silent mutation in a region, we randomly selected a nucleotide position arbitrarily changed said nucleotide and checked that the corresponding amino acid was not changed. Otherwise, a different nucleotide position was selected.

- For an affinity changing mutation (replacement) in a CDR we randomly selected a nucleotide position and changed it to a different nucleotide such that this gave a change in the aminoacid sequence. If in the database a combination of identical CDR1, CDR2, and CDR3 amino acid sequences was present then the affinity of the new daughter B-cell was set to the affinity assigned to this combination in the database, otherwise a new affinity was determined from the shape space, based on the position of its mother cell or, in the case of back mutations, of its founder cell. Subclones with different combinations of CDRs can have descendant subclones that share the same combination of CDRs between them (converge). This convergence lead to a greater change in affinity than what could be expected from the normal distribution used in the shape space because the affinity of said combination of CDRs was based on the affinity of the first mother cell whose descendant mutates into that combination, which can be very different from the affinity another mother cell whose daughter B cell mutates into the same combination. Finally, the database was updated.

For a neutral mutation (replacement) in a FWR a nucleotide position was randomly selected, said nucleotide was changed into a different nucleotide that changes the corresponding amino acid. The database was checked to confirm that the selected mutation was not associated with a lethal mutation at a previous time point. If not, then the mutation was accepted; otherwise a new nucleotide was selected until the process was successful. Finally, the database was updated.

5.7.2. Gene regulatory network

Supplementary Table 9: Parameters of the ODE model (Eq 13-17) of the GRN (Martínez *et al.*, 2012). p=BLIMP1, b=BCL6, r=IRF4. Parameters are normalized by a unit of time (t_0) and concentration (C_0).

Parameter	Value	Unit	Description
μ_p	10^{-6}	C_0/t_0	Basal transcription rate
μ_b	2	C_0/t_0	Basal transcription rate
μ_r	0.1	C_0/t_0	Basal transcription rate
σ_p	9	C_0/t_0	Maximum induced transcription rate
σ_b	100	C_0/t_0	Maximum induced transcription rate
σ_r	2.6	C_0/t_0	Maximum induced transcription rate
κ_p	1	C_0	Dissociation constant
κ_b	1	C_0	Dissociation constant
κ_r	1	C_0	Dissociation constant
λ_p	1	$1/t_0$	Degradation rate
λ_b	1	$1/t_0$	Degradation rate
λ_r	1	$1/t_0$	Degradation rate
bcr0	1	$1/t_0$	Maximum BCR signal
cd0	50	C_0/t_0	Maximum CD40 signal
C_0	10^{-8}	M	Concentration unit
t_0	4	h	Time unit

5.7.3. Founder B cells

Probabilistic influx of founder B cells. Founder B cells enter the GC with a probability p(influx) (Supplementary Figure 28).

$$p(\text{influx}) = \frac{\mu\,\Delta t}{1 + e^{\frac{t-\alpha}{\beta}}}$$

Here Δt=0.002hr corresponding to the time resolution of the ABM, α=96hr representing the time point at which influx stops, β=6 hours and represents the rate smoothness, and μ=2 B cells/hour represents the inflow rate. Integration of this equation shows that this leads to approximately 200 founder B cells. At time t=0 this gives a probability of p=0.004. In the first hour this leads to an influx of approximately 0.004*(1/Δt)=2 cells. In the model, a cell enters the GC if a

random number R drawn from a uniform distribution is smaller than the influx probability (i.e., R<p(influx)).

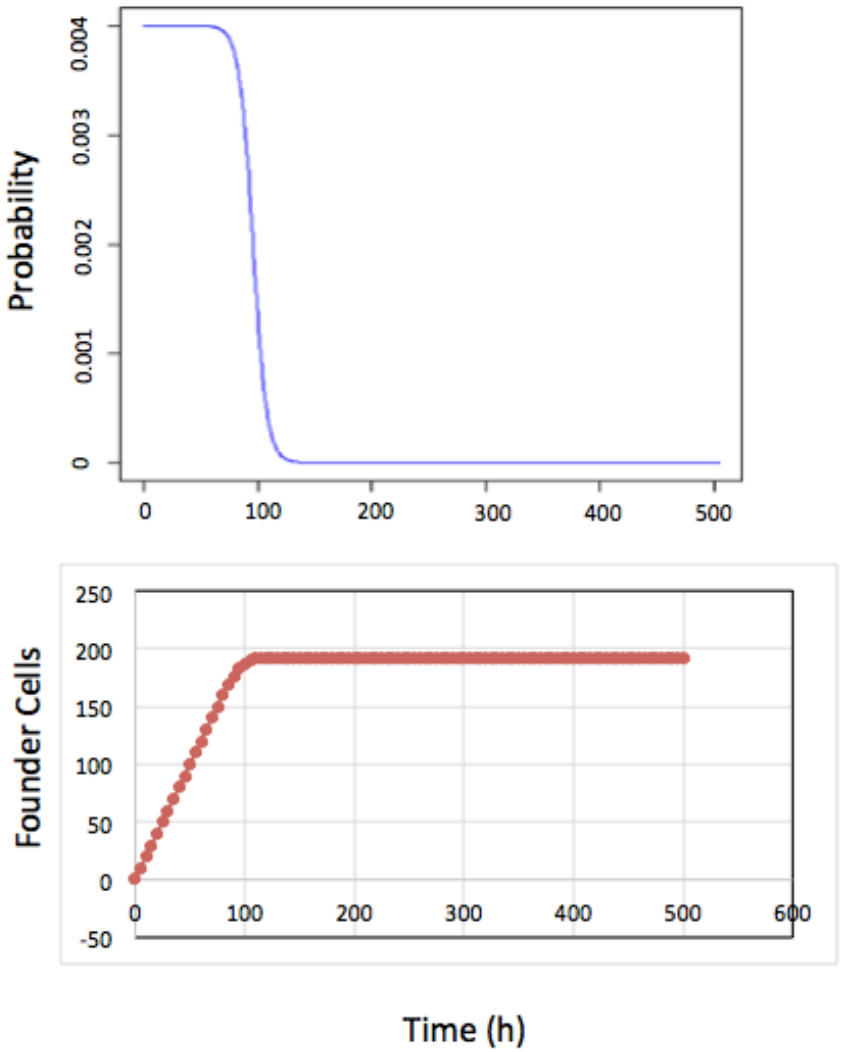

Supplementary Figure 28. Top panel: probability for a founder B cell to enter the GC reaction. Bottom panel: cumulative number of founder B cells. After approximately 96 hours no new founder B cells enter the GC reaction.

5.7.4. Number of somatic hypermutations during each B-cell division

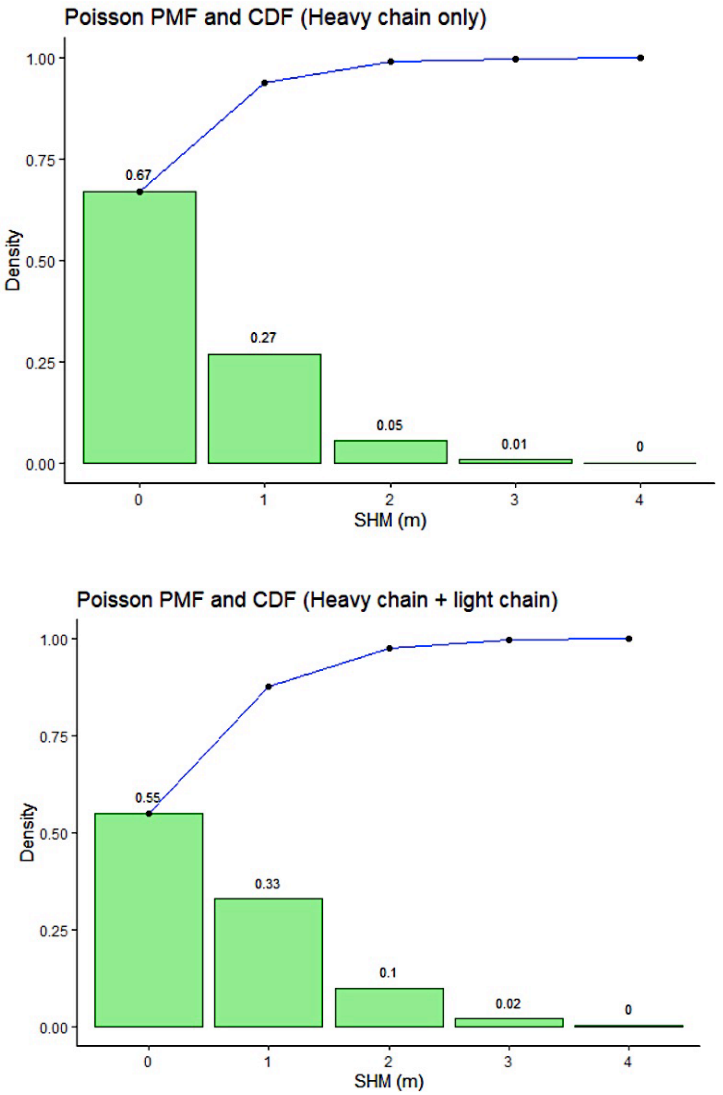

Supplementary Figure 29: Probability mass function (PMF, green bars) and cumulative distribution function (CDF, blue line). Top panel: Number of BcR heavy chain somatic hypermutations assuming a heavy chain length of 400 nucleotides and a mutation rate of 1 mutation per 1000bp per B cell division. Number of SHM in heavy chain is m ~ Poisson (λ=0.4) mutations per B cell division. In 33% of the B cell divisions, the BcR is mutated. Bottom panel: assuming a heavy chain and light chain with an approximate total length of 600 nucleotides, the BcR is mutated is 45% of the B cell divisions.

5.7.5. Overall GC dynamics

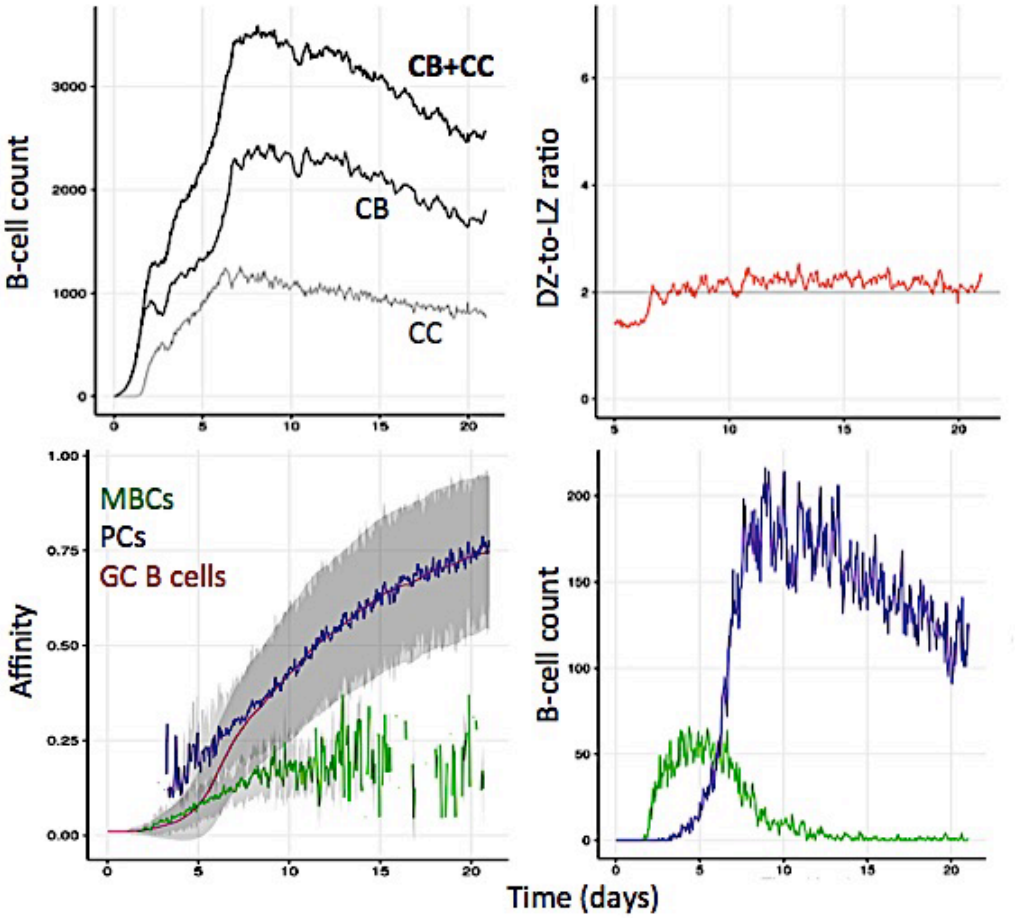

Supplementary Figure 30: Dynamics of the GC reaction observed from a single representative simulation of the MSM (Merino Tejero *et al.*, 2020). (A) Number of CCs and CBs with a peak response after about 7.5 days (Liu *et al.*, 1991; Hollowood and Macarthey, 1992; Wittenbrink *et al.*, 2011a). (B) DZ-to-LZ ratio reflecting the transzone migration rates. This ratio has shown to be approximately 2 (Victora *et al.*, 2010). (C) Affinity maturation of the GC B cells, MBCs and PCs. The interrupted lines show the time points at which no B-cells of that type are present in the GC. (D) Number of MBCs and PCs. Most MBCs are of low affinity and produces at an early stage during the GC reaction, in contrast to PCs that are mostly of higher affinities and produced mostly after the GC peak response in agreement with experimental data from Weisel and colleagues (Florian J Weisel *et al.*, 2016).

5.7.6. Number of (sub)clones during GC reaction

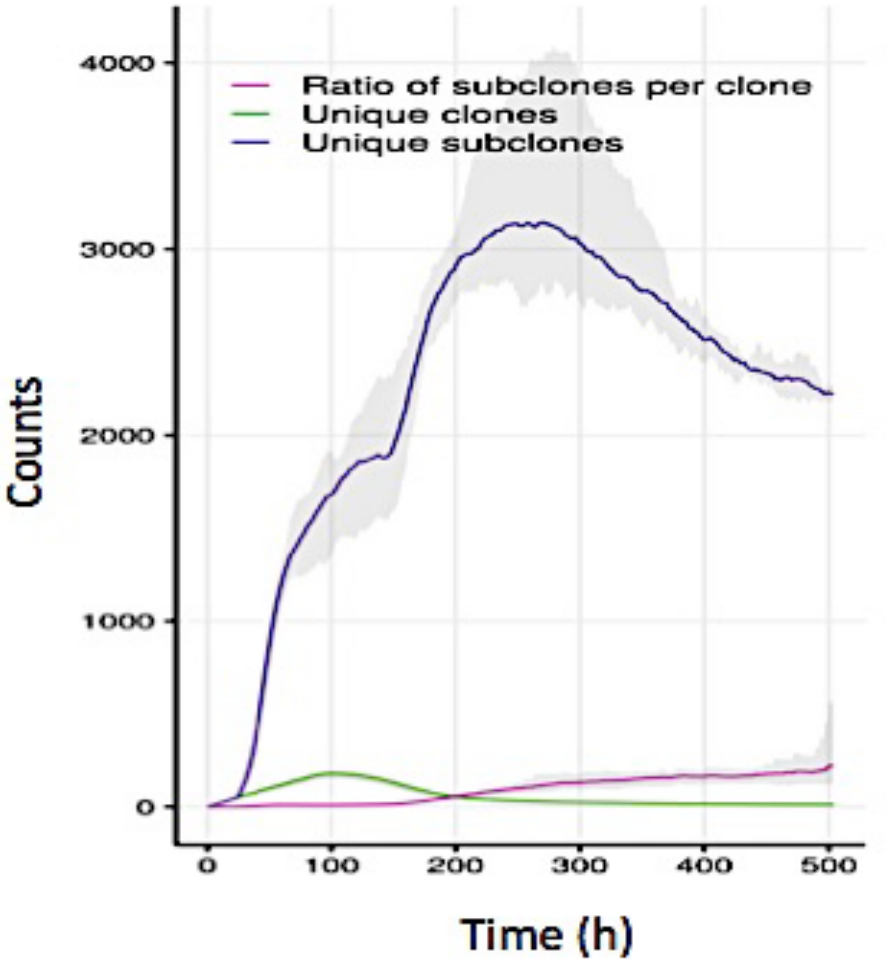

Supplementary Figure 31: Progression of the number of (sub)clones and their ratio during the GC reaction for nine repeated simulations. The number of clones initially increases as a result of the entry of founder B cells. Subsequently, the number of clones decreases due to clonal competition. Lines represent the average value while the shadowed area represents the interval of minimum and maximum values of the nine simulations at that time point.

5.7.7. Subclone dynamics

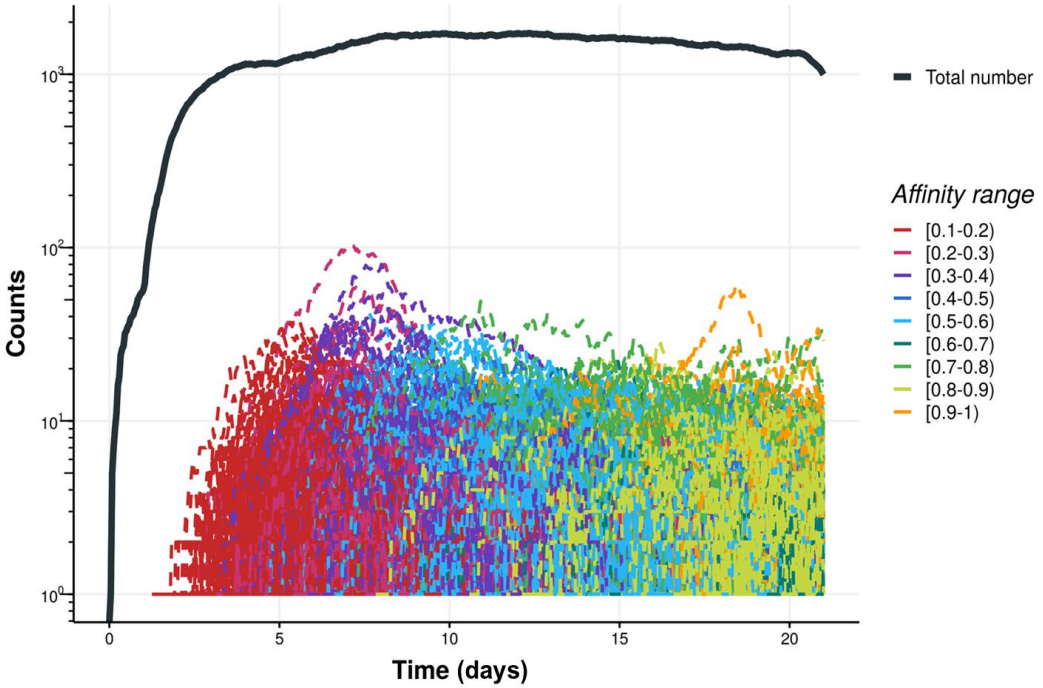

Supplementary Figure 32: Abundance and affinity of subclones, defined as B-cells that share the same Fab NT sequence, during a 21-day GC reaction (representative simulation). Only subclones with a frequency larger than 3 counts at any timepoint are included in this plot. Each colored line represents a subclone with a unique BcR. When a subclone is created by SHM it will start as a single B cell that will, subsequently, proliferate. The abundance of each subclone at any timepoint does not exceed 100 copies. This is due to the fact that a mutation of one subclone B cell will, by definition, create a new subclone. Consequently, a SHM reduces the subclone count with one. This balance between proliferation and SHM prevents large subclone frequencies. It also accounts for the relatively constant of about 2000 subclones with a frequency larger than 3 counts at any time point during the GC reaction (black line).

5.7.8. Single B-cell lineage tree

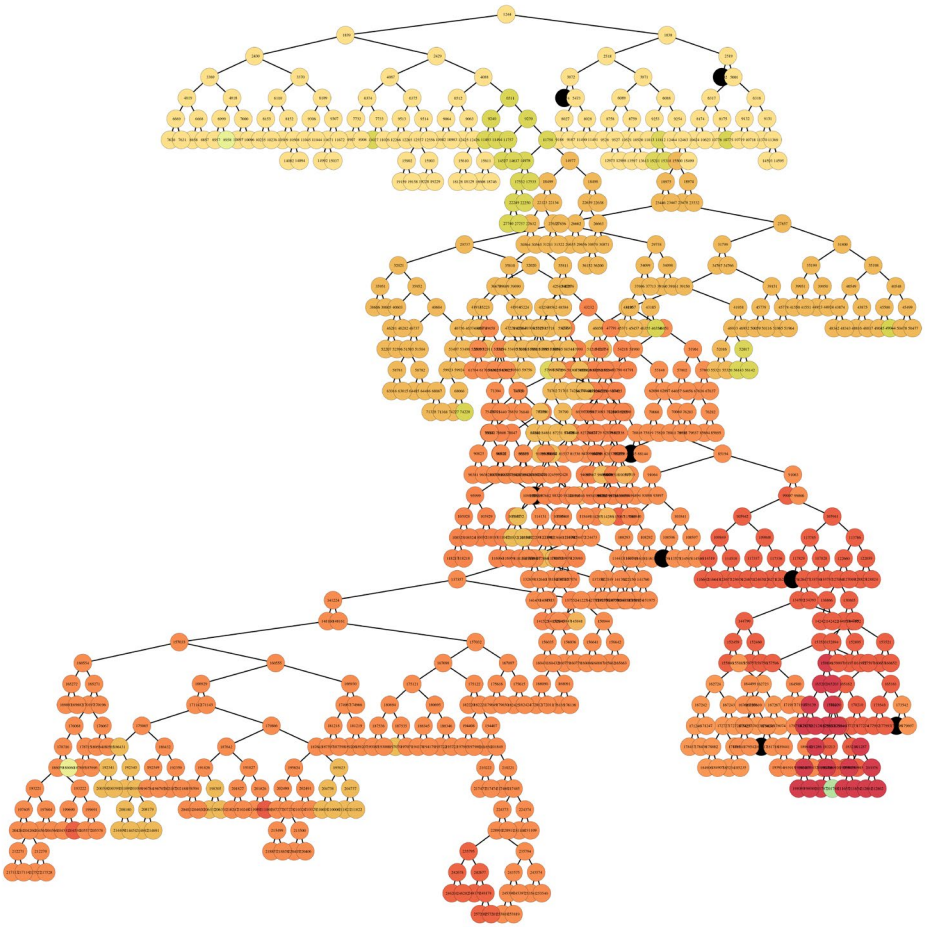

Supplementary Figure 33: Example of the division of a single unmuted founder B-cell during a 21-day GC reaction. During each division two daughter B cells are generated. SHM may change the affinity of each B-cell. The color of a cell denotes its affinity value; from 0 (yellow: low affinity), to 1 (red: high affinity) or its functionality (black: lethal mutation and non functional BcR). The division trees for all founder B cells are shown in the main text (Figure 44).

5.7.9. Dominant clones in nine repeated simulations

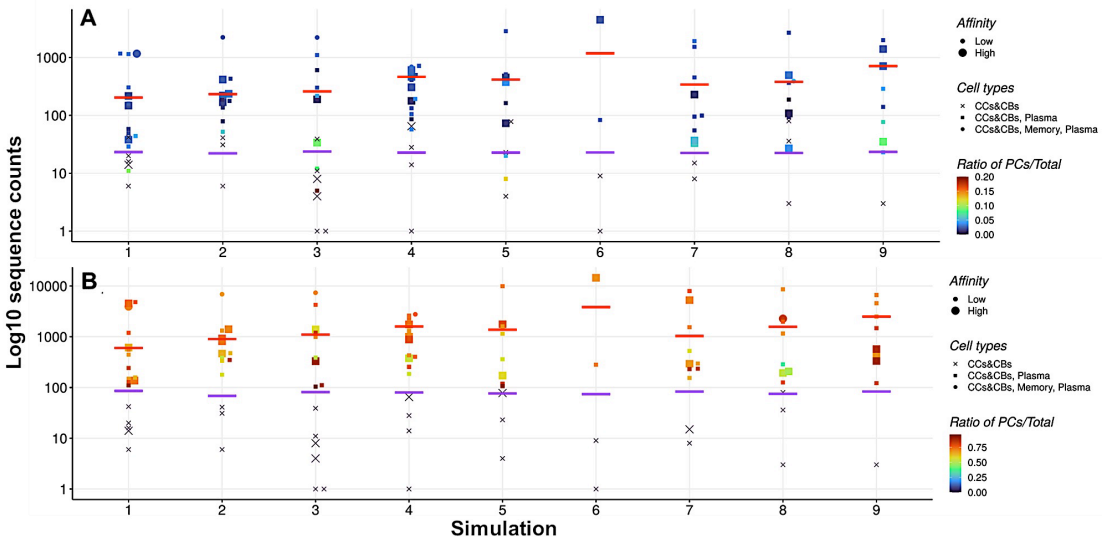

Supplementary Figure 34: (A) DNA-seq and (B) RNA-Seq repertoires at day 21 of the GC reaction generated by nine repeated simulations. Each dot represents a clone some of which are a mixture of B cells, MBCs and/or PCs. Colors indicate the percentage of MBCs and PCs within each clone. The size of the symbol represents the median affinity of that clone (small: affinity < 75th percentile). The horizontal lines denote the 75th percentile (red) and 0.5% (purple) thresholds that define dominant clones.

Chapter 6

Discussion

The common theme in the presented research is the use of multiscale models (MSMs) to study the cellular and molecular mechanisms underlying the differentiation of B-cells to memory B-cells (MBCs) and plasma cells (PCs) within the germinal center (GC). The MSM that was developed integrates a pre-existing agent-based model (ABM; Hyphasma) representing the cellular mechanisms of the GC reaction with a system of ordinary differential equations (ODEs) describing a core gene regulatory network (GRN) underlying PC differentiation. One specific theory about PC differentiation was previously implemented as part of Hyphasma and referred to as the LEDA (LEave the GC through the DArk zone) model. One of its main assumptions regarding output cell (OC) differentiation in the LEDA model is that recycled centroblasts (CBs) distribute the captured antigen (Ag) asymmetrically during B-cell division to the daughter cells. The Ag-retaining cells differentiate into PCs and leave the GC through the dark zone (DZ) (Meyer-Hermann *et al.*, 2012). The core GRN included three transcription factors (TFs) (interferon regulatory factor 4 (IRF4), and B-lymphocyte-induced maturation protein 1 (BLIMP1)) and the B-cell receptor (BcR) and CD40 signaling pathways. Using this model, we also investigated the effect of different genetic alterations associated with diffuse large B-cell lymphoma (DLBCL) on the cellular dynamics of the GC.

We showed that a MSM is a useful approach to study a complex dynamical multiscale biological system, i.e., the GC. Nevertheless, the lack of biological knowledge that defines the interaction between different scales is one of the challenges to overcome by allowing, for example, certain assumptions to simplify the description of the biological system by the model while still allowing to draw useful conclusions. In our model we, therefore, used a small GRN that is only perturbed through BcR and CD40 signaling. Future extensions of this GRN are possible through the inclusion of additional TFs that control PC differentiation or other GC processes such as MBC differentiation (e.g., BACH), SHM (e.g., AID), and proliferation (e.g., c-Myc). Similarly, additional signaling pathways can be included (Shlomchik *et al.*, 2019). For example, IL-21 and Il-4 signalling are both important for developing and sustaining the GC reaction However, extending the molecular network will require further (single cell) experiments to estimate the parameters of the ODEs. A second challenge in MSMs is the integration of different spatiotemporal scales. In our model, the temporal dynamics of the molecular network has a duration in the order of hours while the duration of the

GC reaction at the cellular level was three weeks. The ABM was updated every 7.2 seconds. At each time point of the ABM we solved the ODEs to calculate the TF concentration of the future time step using the current TF concentration levels as initial conditions. Thus, the ODE was also solved every 7.2 seconds. Although this drastically increased running times from approximately 1 hour (wall-clock time on a laptop) for the ABM alone to about 8 hours for the MSM, this allowed solving the two individual models at their own time resolution. Future extension of the molecular network might require different approaches to solve both scales. Finally, in our model, the molecular network has a size in the order of nanometers while B cells have a size of 5 micrometers in a GC with a diameter of 320 micrometers. Nevertheless, we did not model the spatial dynamics of the molecular network. Instead, we assumed the concentration of each TF to be constant within a B-cell. This allowed simplifying the calculation of the concentration of each TF. Future more in-depth studies of the intracellular dynamics of each TF will require a different approach.

6.1. Output cell differentiation based on Ag status versus BLIMP1 level

In chapter 2 we presented our MSM to investigate OC differentiation based on Ag status and/or BLIMP1 level. We compared these two OC-fate determining mechanisms under various strengths of CD40 signaling.

An important insight from our model is the observation that regulation of the BLIMP1 level through affinity-dependent but not constant CD40 signaling, results in the occurrence of a temporal transition from MBC to PC output during the GC reaction that was also observed in an experimental study from Weisel and colleagues (Florian J Weisel *et al.*, 2016). One main assumption of the ABM (LEDA) model, as explained above, is that asymmetric Ag division determines PC differentiation. There is no direct evidence for this mechanism. However, implementation of this mechanism resulted in transzone migration rates in agreement with experimental data (Victora *et al.*, 2010; Meyer-Hermann *et al.*, 2012). In contrast, there is a large body of experimental evidence that high BLIMP1 levels, resulting from Tfh cell help, result in differentiation to PCs. Our MSM showed that differentiation based on asymmetric division of Ag alone is not consistent with BLIMP1 levels and, therefore, is unlikely to be the main mechanism underlying PC differentiation. However, we could not exclude the possibility that asymmetric division of Ag (or TFs) play a (secondary) role.

Our simulation results remain to be experimentally validated but also suggest the direction of further experimental research. The most important question to answer is whether increased BcR affinity results in stronger CD40 signaling. Assuming that increased affinity results in a higher density of surface pMHCII complexes and, hence, increased CD40 signaling, one may design an experiment in which the amount of CD40L is titrated to subsequently measure the effect on selected genes (e.g., IRF4). Experiments to determine the role of asymmetric Ag

and/or TF division (in vivo) will be harder to design but probably not impossible as shown by (Lin *et al.*, 2015). Finally, it is important to establish the approximate numbers of PCs and MBCs that leave a single GC but also measuring the affinity for a large fraction of them, this will help to better parameterize the MSM and the validate our results.

6.2. Memory B-cell differentiation

There is a lack of an explicit mechanism for MBC differentiation in our MSM since the current GRN with BCL6, IRF4, and BLIMP1 is assumed to control PC differentiation. However, since GCs produce both MBCs and PCs and our model produces OCs based on asymmetric Ag division at the cellular level, we defined MBCs as OCs that are not PCs. Although this might approximate the in vivo situation, to further investigate MBC production during the GC reaction, a molecular mechanism for MBC differentiation should be defined.

Unfortunately, mechanisms of MBC differentiation are even less understood than for PC differentiation. In favor of our approach is the observation that MBCs have indeed low BLIMP1 levels and our model results in a temporal switch from low affinity MBCs to higher affinity PCs. The current definition, however, implies that a lack of Ag inheritance during asymmetric division of recycled CBs is one of the determinants in MBC differentiation and that also MBCs leave the GC through the DZ. However, there is no experimental evidence to support any of both assumptions at this stage.

Stochastic selection of low-affinity B cells has been proposed as yet another mechanism to produced MBCs which could be included in the model (Smith *et al.*, 1997; Zhou *et al.*, 2018; Pélissier *et al.*, 2020). Others have found that LZ GC cells with low affinity BcRs are directed towards MBC differentiation. Weak CC-Tfh interactions leading to high BACH2 expression levels in LZ GC B cells has been proposed as a possible mechanism. BACH2 is thought to have an anti-proliferative function by antagonizing c-Myc and/or a pro-survival function by suppressing apoptotic factors such as Bim (Shinnakasu *et al.*, 2016). Thus, in the future we aim to extend our GRN with BACH2 along with other TFs involved in MBC differentiation. However, this requires sufficient (literature) knowledge about the wiring of such components or to reconstruct these networks from experimental data, which would require time series data.

6.3. Asymmetric division of Ag and TFs

It has been shown experimentally that Ag and TFs can divide asymmetrically. Subsequently, it has been hypothesized that this may co-determine GC B-cell fate (Barnett *et al.*, 2012; Meyer-Hermann *et al.*, 2012; Thaunat *et al.*, 2012; Lin *et al.*, 2015). However, there is no experimental evidence to supports this

assumption. As discussed above, our MSM showed that asymmetric Ag division alone cannot explain PC differentiation since it is not fully consistent with PC BLIMP1 levels. However, we only considered one specific mode of coupled asymmetric division with the same asymmetric Ag and TF division probabilities ($P_{Ag}=P_{TF}=0.72$) and TF polarity levels ($L_{BLIMP1}=L_{IRF4}=L_{BCL6}=1.0$) (Merino Tejero *et al.*, 2020). Therefore, in chapter 3 we investigated the putative effect of asymmetric division of Ag and TFs in more detail and hypothesized that this affects GC dynamics and B-cell dynamics and fate. From our simulations we concluded that BLIMP1-driven PC differentiation together with coupled asymmetric division of Ag and BLIMP1 with extreme TF polarity levels (L=1.0, 0.9) for BLIMP1 segregation results in GC DZ-to-LZ ratio and a temporal switch from MBCs to PCs that both are in agreement with experimental data (Victora *et al.*, 2010; Florian J Weisel *et al.*, 2016). This confirmed our previous finding that asymmetric Ag division alone is not sufficient to drive PC differentiation but it also suggests that a role for asymmetric division for B-cell fate cannot be excluded based on our model.

An important insight from our model is the observation that not all choices for the probability and polarity of asymmetric division resulted in GC dynamics in agreement with transzone migration rates between the GC zones nor with the temporal switch. It is, however, important to emphasize that this does not definitely exclude such alternative scenarios. Although our GC model is the most sophisticated model currently available and based on a large range of experimental observations, we cannot exclude the possibility that other choices, assumptions, or parameter settings would change simulation results and conclusion about asymmetric division. Nevertheless, we think that our simulations provide some evidence that asymmetric division might be involved in PC differentiation.

As previously mentioned, it is difficult but crucial to investigate the role of asymmetric Ag and/or TF division. In contrast to BCL6 and IRF4, the BLIMP1 probability for asymmetric division and its polarity level in vivo has not been reported. Furthermore, it is unknown to what extent co-segregation of BLIMP1, BCL6 and IRF4 takes place. Finally, a major question raised by studies done by Lin and colleagues (Lin *et al.*, 2015) is whether asymmetric TF division is driven by asymmetric partitioning of upstream signaling molecules. Thus, we find important to investigate whether there is a role of (a)symmetric division of CD40 signaling in driving asymmetric TF inheritance and thus MBC and PC fate.

6.4. Genetic alterations that lead to DLBCL

In chapter 4 we used our MSM to simulate eight DLBCL models. These are models with different candidate genetic alterations of the BCL6-IRF4-BLIMP1 GRN that lead to TF deregulation. We also compared six of the eight DLBCL models with in

vivo experiments that analyzed TF expression and GC B-cell numbers at different stages of the GC reaction. Four of the DLBCL models correctly recapitulated the observed PC and TF dynamics.

Models with loss of BLIMP1 function are consistent with observations showing BLIMP1 inactivation lead to a block in the PC production and development of lymphoma (Calado *et al.*, 2010). Nevertheless, the models showed a GC B-cell expansion at the end of the GC reaction that was not observed experimentally. This could be due to the fact that our MSM does not account for the effect of alterations in TF dynamics on other B-cell processes such as proliferation or apoptosis. Thus, we proposed to include the molecular mechanisms involved in the aforementioned cellular processes. To this end, the inclusion of TFs such as c-Myc and Bim could serve not only as part of a mechanism to determine MBC fate (as mentioned earlier in this discussion) but also as a way to better approximate the effect of genetic alterations that lead to loss of BLIMP1.

Models with constitutive activation of NF-kB pathway alone and in codominance with enforced BCL6 expression are consistent with experimental data showing that constitutive activation of the NF-kB pathway alone (Calado *et al.*, 2010; Zhang *et al.*, 2015) and in codominance with enforced BCL6 expression (Zhang *et al.*, 2015) lead to unaltered PC production at day 7 of the GC reaction. Despite this observation, both alterations lead to the development of lymphoma. Our models suggest that an increase in PC production could happen at later stages of the GC reaction. Measurement of PC numbers produced at day 21 of the GC reaction are necessary to validate this finding. Furthermore, model with constitutive activation of the NF-kB pathway alone was consistent with observations of studies that induced the canonical NF-kB pathway showing unaltered PC production. Similar studies done inducing the alternative NF-kB pathway showed an increase in PC production. Thus, our model could recapitulate the canonical but not the alternative NF-kB pathway.

Two of the DLBCL models do not correctly recapitulate the observed GC and TF dynamics. Models with enforced BCL6 expression result in an expansion of GC B cells and a block in the PC production that was not observed experimentally (Zhang *et al.*, 2015). As for the GC B-cell dynamics in models with loss of BLIMP1 function, this could be due to the fact that in our model only the differentiation towards PC, at the cellular level, is determined by the levels of BLIMP1. The connection of other processes such as cell division, or apoptosis with the underlying GRN could potentially result in a closer representation of the in vivo experiments.

No data was found to validate models with loss of IRF4- and BLIMP1-mediated silencing of BCL6. Our findings suggest that loss of IRF4- or BLIMP1-mediated silencing of BCL6 does not affect PC differentiation.

MBC dynamics is affected in six of the eight DLBCL models. Models with insufficient BLIMP1 expression induce MBC production while models with constitutive activation of NF-kB pathway alone or in codominance with BCL6

overexpression block MBC production. This observation remains to be experimentally validated.

6.5. Generation of repertoire sequencing data

In chapter 5 we used our MSM to interpret repertoire sequencing data by establishing the extent that a single GC reaction represents immune repertoires obtained from blood. Comparison of our simulation results to experimental bulk-RNAseq repertoires obtained from peripheral blood shows a large difference in the number of (dominant) clones and the D50 values. These differences may result from the fact that blood represent the repertoire from naïve B cells and from multiple (past) immune responses and GC reactions. We then studied the relationship between clonal abundance and affinity and observed a weak relationship between them. Furthermore, some high affinity clones included a wide range of subclone affinities as observed with our previous computational model (Reshetova *et al.*, 2017) and an influenza single-cell study (Mathew *et al.*, 2021). Nevertheless, our finding was not observed in a previous influenza study (Tan *et al.*, 2014). This showed that the selection of a specific subclone (from a dominant clone) for further characterization (e.g., affinity measurement, neutralization potency) might not give a representative picture and may lead to erroneous conclusions. Our model suggested that low abundant (sub)clones might also be of interest since they may have high affinity for the Ag, but in practice it will be difficult to select a low abundance, high affinity clone without trial and error.

Finally, we examined the extent to which MBCs and/or PCs may disturb the identification of dominant clones. We observed that removing the MBC and PC RNA content from the repertoire data, did not have a large effect on the number of dominant clones despite the fact that this is sometimes forwarded as a word of caution. This was unexpected but it happened mainly due to the low abundant clones representing a mixture of GC B-cells, MBCs and/or PCs, therefore, accounting for RNA content did change the abundance of all clones. However, our model represents a single GC, and the proportions of MBCs, PCs and B-cells that constitute a clone in a blood sample may be different. In addition, it is unknown how many MBCs and PCs are produced by a single GC and, which could affect the proportions that result from our simulations.

Summary

Germinal centers (GCs) play a key role in the adaptive immune system since they result in terminally differentiated antibody (Ab) producing plasma cells (PCs) and memory B cells (MBCs) required for an effective immune protection. GC processes such as PC differentiation are, in part, controlled by a gene regulatory network (GRN) comprising interacting transcription factors (TFs) that eventually are responsible for the transcriptional program and, therefore, fate of GC cells. The state of these networks is affected through signaling events that may result from cellular interactions such as between GC B cells and t follicular helper (Tfh) cells. Cellular processes involved in, and GRNs underlying PC differentiation have been modeled separately in the past, but we have now integrated and extended two pre-existing models into a single multi-scale model (MSM) that connects the molecular and cellular levels, allowing us to investigate GC processes at these scales simultaneously. This MSM integrates an agent-based model describing the cellular dynamics and uses ordinary differential equations to represent the core GRN underlying PC differentiation. Using this MSM, we aimed to gain a better understanding of PC differentiation. Our model simulations suggest that affinity of the B-cell receptor for the antigen might be an important determinant for the modulation of intra-cellular signalling induced by T follicular helper (Tfh) cells, and that this is an important mechanism underlying PC differentiation. Moreover, it also showed that asymmetric division of Ag and/or TFs over daughter cells during B-cell division cannot be the single driver for PC differentiation, as was suggested from earlier computational simulations. We also showed how the model can be used to investigate the effects of several known genetic alterations that occur in diffuse large B-cell lymphoma (DLBCL), which leads to deregulation of the GRN underlying PC differentiation and consequent alteration of the GC B-cell population. We showed that the MSM is, for large part, capable of explaining and recapitulating the GC dynamics observed in DLBCL mouse models. Finally, we used the model to facilitate the interpretation of B-cell repertoire sequence data. We showed that there is limited correlation between clonal abundance and affinity, and that the number of dominant clones is not greatly influenced by the higher immunoglobulin mRNA abundance in PCs and MBCs. These applications show that MSM open new opportunities to investigate complex biological systems.

Samenvatting

Kiemcentra spelen een sleutelrol in het adaptieve immuunsysteem, omdat ze resulteren in terminaal gedifferentieerde plasmacellen die antistoffen produceren, en geheugen-B-cellen die beide nodig zijn voor een effectieve afweer en immuunbescherming. Kiemcentrum-processen zoals plasmacel differentiatie worden gedeeltelijk gecontroleerd door een genregulatie netwerk, bestaande uit interacterende transcriptiefactoren die uiteindelijk verantwoordelijk zijn voor het transcriptieprogramma en dus het lot van kiemcentrum B-cellen. De toestand van deze netwerken wordt beïnvloed door signaleringsgebeurtenissen die het gevolg kunnen zijn van cellulaire interacties tussen kiemcentrum B-cellen en folliculaire T-helpercellen. Cellulaire processen die betrokken zijn bij plasmacel differentiatie, en de genregulatie netwerken die hieraan ten grondslag liggen, zijn in het verleden afzonderlijk gemodelleerd, maar wij hebben nu twee bestaande modellen geïntegreerd en uitgebreid tot een enkelvoudig multischaalmodel (MSM) dat het moleculaire met het cellulaire niveau verbindt. Deze MSM integreert een agent-gebaseerd model dat de cellulaire dynamiek beschrijft, en gebruikt gewone differentiaalvergelijkingen om een kern- genregulatie netwerk onderliggend aan plasmacel-differentiatie te beschrijven. Met behulp van dit MSM wilden we een beter begrip krijgen van plasmacel-differentiatie. Onze modelsimulaties suggereren dat affiniteit van de B-celreceptor voor het antigeen een belangrijke determinant zou kunnen zijn voor de modulatie van intracellulaire signalering die wordt geïnduceerd door T-folliculaire helper cellen, en dat dit een belangrijk mechanisme is dat ten grondslag ligt aan plasmacel-differentiatie. Bovendien toonde het ook aan dat asymmetrische verdeling van antigeen en/of transcriptiefactoren over dochtercellen tijdens B-celdeling niet de enige driver voor plasmacel-differentiatie kan zijn zoals werd gesuggereerd uit eerdere computationele simulaties. We hebben ook laten zien hoe het model kan worden gebruikt om effecten te onderzoeken van verschillende bekende genetische veranderingen die optreden bij het diffuus grootcellig B-cellymfoom (DLBCL), en die leiden tot deregulering van de genregulatie netwerk-onderliggende PC-differentiatie, op de kiemcentrum B-celpopulatie. We toonden aan dat de MSM voor een groot deel in staat is om de kiemcentrum-dynamiek waargenomen in DLBCL te beschrijven. Ten slotte hebben we het model gebruikt om de interpretatie van B-cel repertoires te vergemakkelijken. We toonden aan dat er een beperkte correlatie is tussen de grootte van een kloon en zijn affiniteit voor antigen, en dat het aantal dominante klonen weinig wordt beïnvloed door de hogere abundantie van immunoglobuline-coderend mRNA in plasmacellen. Deze toepassingen laten zien dat MSM nieuwe mogelijkheden opent om complexe biologische systemen te onderzoeken.

List of Publications

Merino Tejero E[#], Lashgari D[#], García-Valiente R, Gao X, Crauste F, Robert PA, Meyer-Hermann M, Martínez MR, van Ham SM, Guikema JEJ, Hoefsloot H, van Kampen AHC. Multiscale Modeling of Germinal Center Recapitulates the Temporal Transition From Memory B Cells to Plasma Cells Differentiation as Regulated by Antigen Affinity-Based Tfh Cell Help. Frontiers in Immunology (2021) 11:620716.
[#]Equally contributed

Merino Tejero E[#], Lashgari D[#], García-Valiente R, Jiaojiao H, Robert PA, Meyer-Hermann M, Guikema JEJ, Hoefsloot H, van Kampen AHC. Coupled Antigen and BLIMP1 Asymmetric Division With a Large Segregation Between Daughter Cells Recapitulates the Temporal Transition From Memory B Cells to Plasma Cells and a DZ-to-LZ Ratio in the Germinal Center. Frontiers in Immunology (2021) 12:716240.
[#]Equally contributed

Merino Tejero E, Mao Q, Lashgari D, García-Valiente R, Robert PA, Meyer-Hermann M, Martínez MR, Guikema JEJ, Hoefsloot H, van Kampen AHC. Multi-scale modeling recapitulates the effect of genetic alterations associated with diffuse large B-cell lymphoma in the germinal center dynamics. Frontiers in systems biology (2022). Accepted for publication.

Lashgari D[#], **Merino Tejero E**[#], Meyer-Hermann M, van Gils M, Hoefsloot H, van Kampen AHC. From affinity selection to kinetic selection in GC modeling. Submitted for publication.
[#]Equally contributed

García-Valiente R[#], **Merino Tejero E**[#]**,** Stratigopoulou M, Balashova D, Meyer-Hermann M, Guikema JEJ, Hoefsloot H, van Kampen AHC. Generation of repertoire sequencing data from a computational model of the germinal center. Manuscript in Preparation.
[#]Equally contributed

PhD training

Courses	**Year**	**ECTS**
Quantitative and Predictive Modelling (Wageningen)	**2017**	**3**
Advanced Immunology	**2019**	**2.9**
Seminars, meetings, masterclasses		
KEBB/EDS seminars		**1**
Group Meetings of the Bioinformatics Laboratory		**4**
Conferences		
Bioinformatics and Systems biology conference, Lunteren (BioSB; online oral presentation)	**2021**	**1.5**
Bioinformatics and Systems biology conference, Lunteren (BioSB; poster)	**2018-19**	**2.6**
European congress of immunology, Amsterdam (ECI; poster)	**2018**	**1.3**
Germinal Center Conference, Venice (GCC; poster)	**2017**	**1.3**
Visits		
Immunopathology, Sanquin, Amsterdam	**2018**	**1.3**
Systems Immunology, Helmholzt Institute, Braunchschweig	**2017-18**	**18**
Teaching		
Assistant exome sequencing computer lab (OMICS biomedical sciences, Bachelor)	**2020**	**1**
Supervision internship student Qirong Mao (MSM of genetic alterations associated with DLBCL in the GC)	**2020**	**1**
Supervision internship student Jiaojiao (MSM of CD40 signaling and asymmetric B-cell division in the context of MBC and PC differentiation)	**2020**	**1**
Lecturer in Systems Medicine (AMC Graduate School; Agent-based models)	**2017-19**	**2**

Curriculum Vitae

Elena Merino Tejero
6 September 1991
elenamerino@hotmail.es

Post-University Education

Ph.D. Multiscale modelling of plasma cell differentiation in the germinal center **2017-22**
Amsterdam University Medical Center (UMC), Clinical Epidemiology Biostatistics and Bioinformatics (KEBB) Department, Netherlands

M.Sc. Bioinformatics **2014-16**
Vrije Universiteit (VU) Amsterdam, Faculty of Sciences, Netherlands
Internships **2015-16**
Minor: Agent-based modelling of the germinal center
Amsterdam UMC, KEBB Department, Netherlands
Mayor: Setting up enzyme kinetics assays in liver cells to incorporate into a kinetic model of liver glycolysis
VU Amsterdam, Faculty of Sciences, Netherlands

University Education

B.Sc. Biology **2009-14**
Complutense University of Madrid (UCM), Spain
Internships **2014**
Mayor: Culture of stem and precursors cells in the canine hematopoyetic system
UCM, Department of Biochemistry and Molecular Biology, Spain
Minor: Cell culture techniques and analysis by flow cytometry and PCR of in vivo and in vitro hematopoietic cultures
VU Medical Center, Laboratory Medical Oncology, Netherlands

Pre-University Education

British Council School, Madrid, Spain
Health Sciences **2007-09**
IGCSEs **2006-07**

Acknowledgements

Many people helped me during the PhD process. Help happens at different interconnected levels, not only at the level of carrying out work-related tasks. Thus, everyone who influenced me in the last five years has a part in it, directly or indirectly. I would like to thank Antoine and Huub for making this PhD project possible through their weekly supervision and guidance. I am glad that you took the challenge of leading me through this journey by sharing your knowledge, in general and particularly on bioinformatics methods and data analysis. I would also like to thank Jeroen for his contribution in this project by sharing his knowledge on signal transduction in B cells and B-cell malignancies from the experimental perspective.

I want to thank Danial and Rodrigo. I enjoyed working with you and the discussions about work and life too. I also want to thank Maryam, Barbara, Aldo, Perry, Eric, Mia, Adrie and other colleagues that were present during coffee breaks and meetings both at the Amsterdam UMC and UvA. This PhD included collaborations with other co-workers. I want to thank Philippe and Michael for giving me the chance of doing an internship in Braunschweig, Germany, where I learned a lot about agent based modeling and programing in C++. I also want to thank Marieke, Casper, Niels, Hans, Sabrina and other colleagues for sharing interesting discussions at Sanquin where I learned a lot about PC differentiation from the experimental perspective. I want to thank my fellow students, Qirong and Jiaojiao, as well as other collaborators, Maria, Xuefeng and Fabien, for their contribution to this project.

I met some great people while being a PhD abroad that made me feel good and home in the Netherlands. I want to thank my former flatmates Asli, Hugo, Dominique, Joe and Sofia. I also want to mention Vera, Willem, Naomi, Regina, Arthur, Josephine, Annika, Nico and Sabrina. Thanks for the fun times during and outside of climbing. I would also like to thank my friends in Spain. I would like to specially mention Isabel and Ines for being present despite the physical distance. I hope to see you soon and let the laughter continue.

Finally, I would like to thank my family in Spain. Thanks to my aunt Concha, talented biologist, who taught me the love for science. Thanks to my parents for supporting me and to my sisters, Alicia and Elisa for I would not have made it without you.

References

Akkaya, M., Kwak, K. and Pierce, S.K. (2020) B cell memory: Building two walls of protection against pathogens, *Nature reviews immunology*, 20(4), 229–238. doi:10.1038/s41577-019-0244-2.

Alizadeh, A.A., Elsen, M.B., Davis, R.E., Ma, C.L., Lossos, I.S., Rosenwald, A., Boldrick, J.C., Sabet, H., *et al.* (2000) Distinct types of diffuse large B-cell lymphoma identified by gene expression profiling, *Nature*, 403(6769), 503–511. doi:10.1038/35000501.

Allen, C.D.C. and Cyster, J.G. (2008) Follicular dendritic cell networks of primary follicles and germinal centers: Phenotype and function, *Seminars in immunology*, 20(1), 14–25. doi:10.1016/j.smim.2007.12.001.

Allen, C.D.C., Okada, T. and Cyster, J.G. (2007a) Germinal-Center Organization and Cellular Dynamics, *Immunity*, 27(2), 190–202. doi:10.1016/j.immuni.2007.07.009.

Allen, C.D.C., Okada, T. and Cyster, J.G. (2007b) Imaging of germinal center selection events during affinity maturation, *Science*, 315(5811), 528–531. doi:10.1126/science.1136736.

Andersson, J., Coutinho, A. and Melchers, F. (1978) The switch from IgM to IgG in single mitogen-stimulated B-cell clones, *Journal of experimental medicine*, 147(6), 1744–1754.

Arpin, C., Julie, D., Kooten, C., Merville, P., Grouard, G., Francine, B., Jacques, B. and Yong (1995) Generation of memory B cells and plasma cells in vitro, *Science*, 268(5211), 720–722. doi:10.1126/science.7537388.

van Asten, S.D., Unger, P.-P., Marsman, C., Bliss, S., Jorritsma, T., Thielens, N.M., van Ham, S.M. and Spaapen, R.M. (2021) Soluble FAS ligand enhances suboptimal CD40L/IL-21–mediated human memory B cell differentiation into antibody-secreting cells, *The journal of immunology*, 207(2), 449–458. doi:10.4049/jimmunol.2001390.

Attaf, N., Cervera-Marzal, I., Dong, C., Gil, L., Renand, A., Spinelli, L. and Milpied, P. (2020) FB5P-seq: FACS-based 5-prime end single-cell RNA-seq for integrative analysis of transcriptome and antigen receptor repertoire in B and T cells, *Frontiers in immunology*, 11(216), 1–13. doi:10.3389/fimmu.2020.00216.

Attaf, N., Baaklini, S., Binet, L. and Milpied, P. (2021) Heterogeneity of germinal center B cells: New insights from single-cell studies, *European journal of immunology*, 51(11), 2555–2567. doi:10.1002/eji.202149235.

Azagra, A., Marina-Zárate, E., Ramiro, A.R., Javierre, B.M. and Parra, M. (2020) From loops to looks: Transcription factors and chromatin organization shaping terminal B cell differentiation, *Trends in immunology*, 41(1), 46–60. doi:10.1016/j.it.2019.11.006.

Bai, M., Agnantis, N.J., Skyrlas, A., Tsanou, E., Kamina, S., Galani, V. and Kanavaros, P. (2003) Increased expression of the BCL6 and CD10 proteins is

associated with increased apoptosis and proliferation in diffuse large B-cell lymphomas, *Modern pathology*, 16(5), 471–480. doi:10.1097/01.MP.0000067684.78221.6E.

Balasenthil, S., Gururaj, A.E., Talukder, A.H., Bagheri-Yarmand, R., Arrington, T., Haas, B.J., Braisted, J.C., Kim, I., *et al.* (2007) Identification of Pax5 as a target of MTA1 in B-cell lymphomas, *Cancer Research*, 67(15), 7132–7138. doi:10.1158/0008-5472.CAN-07-0750.

Barnett, B.E., Ciocca, M.L., Goenka, R., Barnett, L.G., Wu, J., Laufer, T.M., Burkhardt, J.K., Cancro, M.P., *et al.* (2012) Asymmetric B cell division in the germinal center reaction, *Science*, 335(6066), 342–344. doi:10.1126/science.1213495.

Bashford-Rogers, R.J.M., Bergamaschi, L., McKinney, E.F., Pombal, D.C., Mescia, F., Lee, J.C., Thomas, D.C., Flint, S.M., *et al.* (2019) Analysis of the B cell receptor repertoire in six immune-mediated diseases, *Nature*, 574(7776), 122–126. doi:10.1038/s41586-019-1595-3.

Basso, K. and Dalla-Favera, R. (2012) Roles of BCL6 in normal and transformed germinal center B cells, *Immunological reviews*, 247(1), 172–183. doi:10.1111/j.1600-065X.2012.01112.x.

Basso, K. and Dalla-Favera, R. (2015) Germinal centres and B cell lymphomagenesis, *Nature reviews immunology*, 15(3), 172–184. doi:10.1038/nri3814.

Basso, K. and R. Dalla-favera (2010) BCL6: Master regulator of the germinal center reaction and key oncogene in B cell lymphomagenesis, *Advances in immunology*, 105(10), 193–210. doi:10.1016/S0065-2776(10)05007-8.

Bhatt, S., Sarosiek, K.A. and Lossos, I.S. (2017) Interleukin 21 – its potential role in the therapy of B-cell lymphomas, *Leukemia and Lymphoma*, 58(1), 17–29. doi:10.1080/10428194.2016.1201568.

Biecek, P. (2019) The model development process, *Arxiv*, 1–6. doi:10.1007/978-1-4842-4885-0_4.

Blink, E.J., Light, A., Kallies, A., Nutt, S.L., Hodgkin, P.D. and Tarlinton, D.M. (2005) Early appearance of germinal center-derived memory B cells and plasma cells in blood after primary immunization, *Journal of experimental medicine*, 201(4), 545–554. doi:10.1084/jem.20042060.

Bonabeau, E. (2002) Agent-based modeling: Methods and techniques for simulating human systems, *Proceedings of the national academy of sciences*, 99(3), 7280–7287. doi:10.1073/pnas.082080899.

Bönelt, P., Wöhner, M., Minnich, M., Tagoh, H., Fischer, M., Jaritz, M., Kavirayani, A., Garimella, M., *et al.* (2019) Precocious expression of Blimp1 in B cells causes autoimmune disease with increased self-reactive plasma cells, *The EMBO journal*, 38(2), 1–19. doi:10.15252/embj.2018100010.

Brown, A.J., Snapkov, I., Akbar, R., Pavlović, M., Miho, E., Sandve, G.K. and Greiff, V. (2019) Augmenting adaptive immunity: Progress and challenges in the quantitative engineering and analysis of adaptive immune receptor repertoires, *Molecular systems design and engineering*, 4(4), 701–736. doi:10.1039/c9me00071b.

Bruggeman, F.J., Hornberg, J.J., Boogerd, F.C. and Westerhoff, H. V (2013) Molecular systems biology, *Journal of biotechnology*, 97, 1–19. doi:10.1016/j.jbiotec.2007.02.010.

Calado, D.P., Zhang, B., Srinivasan, L., Sasaki, Y., Seagal, J., Unitt, C., Rodig, S., Kutok, J., *et al.* (2010) Constitutive canonical NF-κB activation cooperates with disruption of BLIMP1 in the pathogenesis of activated B cell-like diffuse large cell lymphoma, *Cancer cell*, 18(6), 580–589. doi:10.1016/j.ccr.2010.11.024.

Calis, J.J.A. and Rosenberg, B.R. (2014) Characterizing immune repertoires by high throughput sequencing: Strategies and applications, *Trends in immunology*, 35(12), 581–590. doi:10.1016/j.it.2014.09.004.

Calvo-Vidal, M.N., Zamponi, N., Krumsiek, J., Stockslager, M.A., Revuelta, M. V., Phillip, J.M., Marullo, R., Tikhonova, E., *et al.* (2021) Oncogenic HSP90 facilitates metabolic alterations in aggressive B-cell lymphomas, *Cancer research*, 81(20), 5202–5216. doi:10.1158/0008-5472.CAN-21-2734.

Cappuccio, A., Tieri, P. and Castiglione, F. (2016) Multiscale modelling in immunology: A review, *Briefings in bioinformatics*, 17(3), 408–418. doi:10.1093/bib/bbv012.

Chan, T.D. and Brink, R. (2012) Affinity-based selection and the germinal center response, *Immunological reviews*, 247(1), 11–23.

Chaplin, D.D. (2010) Overview of the immune response, *Journal of allergy and clinical immunology*, 125(2), 3–23. doi:10.1016/j.jaci.2009.12.980.

Chaudhry, Q.A. (2016) An introduction to agent-based modeling modeling natural, social, and engineered complex systems with netlogo: A review, *Complex adaptive systems modeling*, 4(1), 10–11. doi:10.1186/s40294-016-0027-6.

Cleveland, W.S. (1979) Robust locally weighted regression and smoothing scatterplots, *Journal of the american statistical association*, 74(368), 829–836. doi:10.1080/01621459.1979.10481038.

Coker, H.A., Durham, S.R. and Gould, H.J. (2003) Local somatic hypermutation and class switch recombination in the nasal mucosa of allergic rhinitis patients, *The journal of immunology*, 171(10), 5602–5610. doi:10.4049/jimmunol.171.10.5602.

Cox, A. and Emtage, J.S. (1989) A 6-fold difference in the half-fife of immunoglobulin u heavy chain mRNA in cell lines representing two stages of B cell differentiation, *Methods*, 17(24), 10439–10454.

Cui, A., Di Niro, R., Vander Heiden, J.A., Briggs, A.W., Adams, K., Gilbert, T., O'Connor, K.C., Vigneault, F., *et al.* (2016) A model of somatic hypermutation targeting in mice based on high-throughput Ig sequencing data, *The journal of immunology*, 197(9), 3566–3574. doi:10.4049/jimmunol.1502263.

Cyster, J.G. and Allen, C.D.C. (2019) B cell responses: Cell interaction dynamics and decisions, *Cell*, 177(3), 524–540. doi:10.1016/j.cell.2019.03.016.

Davidzohn, N., Biram, A., Stoler-Barak, L., Grenov, A., Dassa, B. and Shulman, Z. (2019) Syk degradation restrains plasma cell formation and promotes zonal transitions in germinal centers, *Journal of experimental medicine*, 217(3), 1–57. doi:10.1084/jem_20191043.

DeKosky, B.J., Ippolito, G.C., Deschner, R.P., Lavinder, J.J., Wine, Y., Rawlings, B.M., Varadarajan, N., Giesecke, C., *et al.* (2013) High-throughput sequencing of the paired human immunoglobulin heavy and light chain repertoire, *Nature biotechnology*, 31(2), 166–169. doi:10.1038/nbt.2492.High-throughput.

Dominguez-Sola, D., Victora, G.D., Ying, C.Y., Phan, R.T., Saito, M., Dalla-Favera, R. and Nussenzweig, M.C. (2012) c-MYC is required for germinal center selection and cyclic re-entry, *Nature immunology*, 13(11), 1083–1091.

doi:10.1038/ni.2428.c-MYC.

Doorenspleet, M.E., Klarenbeek, P.L., De Hair, M.J.H.D., Van Schaik, B.D.C., Esveldt, R.E.E., Van Kampen, A.H.C., Gerlag, D.M., Musters, A., *et al.* (2014) Rheumatoid arthritis synovial tissue harbours dominant B-cell and plasma-cell clones associated with autoreactivity, *Annals of the rheumatic diseases*, 73(4), 756–762. doi:10.1136/annrheumdis-2012-202861.

Du, W., Goldstein, R., Jiang, Y., Aly, O., Cerchietti, L., Melnick, A. and Elemento, O. (2017) Effective combination therapies for B-cell lymphoma predicted by a virtual disease model, *Cancer research*, 77(8), 1818–1830. doi:10.1158/0008-5472.CAN-16-0476.

Duchez, S., Rodrigues, M., Bertrand, F. and Valitutti, S. (2011) Reciprocal polarization of T and B cells at the immunological synapse, *The journal of immunology*, 187(9), 4571–4580. doi:10.4049/jimmunol.1100600.

Duffy, K.R., Wellard, C.J., Markham, J.F., Zhou, J.H., Holmberg, R., Hawkins, E.D., Hasbold, J., Dowling, M.R., *et al.* (2012) Activation-induced B cell fates are selected by intracellular stochastic competition, *Science*, 335(6066), 338–341. doi:10.1126/science.1213230.

Dustin, M.L. and Meyer-Hermann, M. (2012) Antigen feast or famine, *Science*, 335(6067), 408–409. doi:10.1126/science.1218165.

Duy, C., Yu, J.J., Nahar, R., Swaminathan, S., Kweon, S.M., Polo, J.M., Valls, E., Klemm, L., *et al.* (2010) BCL6 is critical for the development of a diverse primary B cell repertoire, *Journal of experimental medicine*, 207(6), 1209–1221. doi:10.1084/jem.20091299.

Eftimie, R., Gillard, J.J. and Cantrell, D.A. (2016) Mathematical models for immunology: Current state of the art and future research directions, *Bulletin of mathematical biology*, 78(10), 2091–2134. doi:10.1007/s11538-016-0214-9.

Faro, J. and Or-Guil, M. (2013) How oligoclonal are germinal centers? A new method for estimating clonal diversity from immunohistological sections, *Biomed central bioinformatics*, 14(6), 1–9. doi:10.1186/1471-2105-14-S6-S8.

Finkin, S., Hartweger, H., Oliveira, T.Y., Kara, E.E. and Nussenzweig, M.C. (2019) Protein amounts of the MYC transcription factor determine germinal center B cell division capacity, *Immunity*, 51(2), 324-336.e1–5. doi:10.1016/j.immuni.2019.06.013.

Firl, D.J., Degn, S.E., Padera, T. and Carroll, M.C. (2018) Capturing change in clonal composition amongst single mouse germinal centers, *eLife*, 7, 1–24. doi:10.7554/eLife.33051.

Friedensohn, S., Khan, T.A. and Reddy, S.T. (2017) Advanced methodologies in high-throughput sequencing of immune repertoires, *Trends in biotechnology*, 35(3), 203–214. doi:10.1016/j.tibtech.2016.09.010.

Fujii, K., Tanaka, S., Hasegawa, T., Narazaki, M., Kumanogoh, A., Koseki, H., Kurosaki, T. and Ise, W. (2020) Tet DNA demethylase is required for plasma cell differentiation by controlling expression levels of IRF4, *International immunology*, 32(10), 683–690. doi:10.1093/intimm/dxaa042.

Galson, J.D., Trück, J., Fowler, A., Münz, M., Cerundolo, V., Pollard, A.J., Lunter, G. and Kelly, D.F. (2015) In-depth assessment of within-individual and inter-individual variation in the B cell receptor repertoire, *Frontiers in immunology*, 6(531), 1–13. doi:10.3389/fimmu.2015.00531.

Gatto, D. and Brink, R. (2010) The germinal center reaction, *Journal of allergy*

and clinical immunology, 126(5), 898–907. doi:10.1016/j.jaci.2010.09.007.

Genovese, C. and Milcarek, C. (1990) Increased half-life of μ immunoglobulin mRNA during mouse B cell development increases its abundancy, *Molecular immunology*, 27(8), 733–743. doi:10.1016/0161-5890(90)90082-B.

Gitlin, A.D., Mayer, C.T., Oliveira, T.Y., Shulman, Z., Jones2, M.J.K., Koren, A. and Nussenzweig, M.C. (2015) T cell help controls the speed of the cell cycle in germinal center B cells, *Physiology and behavior*, 176(1), 139–148. doi:10.1126/science.aac4919.

Gitlin, A.D., Shulman, Z. and Nussenzweig, M.C. (2014) Clonal selection in the germinal center by regulated proliferation and hypermutation, *Nature*, 509(7502), 637–640. doi:10.1038/nature13300.

Glen, C.M., Kemp, M.L. and Voit, E.O. (2019) *Agent-based modeling of morphogenetic systems: Advantages and challenges*, *PLoS computational biology*. doi:10.1371/journal.pcbi.1006577.

Greiff, V., Bhat, P., Cook, S.C., Menzel, U., Kang, W. and Reddy, S.T. (2015) A bioinformatic framework for immune repertoire diversity profiling enables detection of immunological status, *Genome medicine*, 7(49), 1–15. doi:10.1186/s13073-015-0169-8.

Gupta, N.T., Vander Heiden, J.A., Uduman, M., Gadala-Maria, D., Yaari, G. and Kleinstein, S.H. (2015) Change-O: A toolkit for analyzing large-scale B cell immunoglobulin repertoire sequencing data, *Bioinformatics*, 31(20), 3356–3358. doi:10.1093/bioinformatics/btv359.

Hasbold, J., Corcoran, L.M., Tarlinton, D.M., Tangye, S.G. and Hodgkin, P.D. (2004) Evidence from the generation of immunoglobulin G-secreting cells that stochastic mechanisms regulate lymphocyte differentiation, *Nature immunology*, 5(1), 55–63. doi:10.1038/ni1016.

Heesters, B.A., Myers, R.C. and Carroll, M.C. (2014) Follicular dendritic cells: Dynamic antigen libraries, *Nature reviews immunology*, 14(7), 495–504. doi:10.1038/nri3689.

Herviou, L., Jourdan, M., Martinez, A.M., Cavalli, G. and Moreaux, J. (2019) EZH2 is overexpressed in transitional preplasmablasts and is involved in human plasma cell differentiation, *Leukemia*, 33(8), 2047–2060. doi:10.1038/s41375-019-0392-1.

Higgins, B.W., McHeyzer-Williams, L.J. and McHeyzer-Williams, M.G. (2019) Programming isotype-specific plasma cell function, *Trends in immunology*, 40(4), 345–357. doi:10.1016/j.physbeh.2017.03.040.

Hoehn, K.B., Gall, A., Bashford-rogers, R., Fidler, S.J., Kaye, S., Weber, J.N., Mcclure, M.O., Investigators, S.T., *et al.* (2015) Dynamics of immunoglobulin sequence diversity in HIV-1 infected individuals, *Philosophical of the transitions royal society B*, 370(1676), 1–11.

Hollowood, K. and Macarthey, J. (1992) Cell kinetics of the germinal center reaction - a stathmokinetic study, *European journal of immunology*, 22(1), 261–266.

Hood, L.E. (2008) Wu and Kabat 1970: A transforming view of antibody diversity, *The journal of immunology*, 180(11), 7055–7056. doi:10.4049/jimmunol.180.11.7055.

Hu, S., Xu-Monette, Z.Y., Balasubramanyam, A., Manyam, G.C., Visco, C., Tzankov, A., Liu, W.M., Miranda, R.N., *et al.* (2013) CD30 expression defines a

novel subgroup of diffuse large B-cell lymphoma with favorable prognosis and distinct gene expression signature: A report from the International DLBCL Rituximab-CHOP Consortium Program Study, *Blood*, 121(14), 2715–2724. doi:10.1182/blood-2012-10-461848.

Ichikawa, S., Fukuhara, N., Katsushima, H., Takahashi, T., Yamamoto, J., Yokoyama, H., Sasaki, O., Fukuhara, O., *et al.* (2014) Association between BACH2 expression end clinical prognosis in diffuse large B-cell lymphoma, *Cancer science*, 105(4), 437–444. doi:10.1111/cas.12361.

Ionescu, L. and Urschel, S. (2019) Memory B cells and long-lived plasma cells, *Transplantation*, 103(5), 890–898. doi:10.1097/TP.0000000000002594.

Ise, W., Fujii, K., Shiroguchi, K., Ito, A., Kometani, K., Takeda, K., Kawakami, E., Yamashita, K., *et al.* (2018) T follicular helper cell-germinal center B cell interaction strength regulates entry into plasma cell or recycling germinal center cell fate, *Immunity*, 48(4), 702-715.e1–4. doi:10.1016/j.immuni.2018.03.027.

Ise, W. and Kurosaki, T. (2019) Plasma cell differentiation during the germinal center reaction, *Immunological reviews*, 288(1), 64–74. doi:10.1111/imr.12751.

Jacob, J., Kelsoe, G., Rajewsky, K. and Weiss, U. (1991) Intraclonal generation of antibody mutants in germinal centres, *Nature*, 354(6352), 389–392. doi:10.1038/354389a0.

Jacob, J., Przylepa, J., Miller, C. and Kelsoe, G. (1993) In situ studies of the primary immune response to (4-hydroxy-3-nitrophenyl)acetyl. III. the kinetics of V region mutation and selection in germinal center B cells, *Journal of experimental medicine*, 178(4), 1293–1307. doi:10.1084/jem.178.4.1293.

Jaiswaf, A. and Crof, M. (1997) CD40 ligand induction on T cell subsets by peptide-presenting B cells: Implications for development of the primary T and B cell response, *Journal of immunology*, 159(5), 2282–2291.

James, L.C. and Tawfik, D.S. (2009) The specificity of cross-reactivity: Promiscuous antibody binding involves specific hydrogen bonds rather than nonspecific hydrophobic stickiness, *Protein science*, 12(10), 2183–2193. doi:10.1110/ps.03172703.

Janson, N.B. (2012) Non-linear dynamics of biological systems, *Contemporary physics*, 53(2), 1–41. doi:10.1080/00107514.2011.644441.

Jarjour, N.N., Masopust, D. and Jameson, S.C. (2021) T cell memory: Understanding COVID-19, *Immunity*, 54(1), 14–18. doi:10.1016/j.immuni.2020.12.009.

Kelley, D.E. and Perry, R.P. (1986) Transcriptional and posttranscriptional control of immunoglobulin mRNA production during blymphocyte development, *Nucleic acids research*, 14(13), 5431–5447. doi:10.1093/nar/14.13.5431.

King, H.W., Orban, N., Riches, J.C., Clear, A.J., Warnes, G., Teichmann, S.A. and James, L.K. (2021) Single-cell analysis of human B cell maturation predicts how antibody class switching shapes selection dynamics, *Science immunology*, 6(56). doi:10.1126/sciimmunol.abe6291.

Kishi, Y., Aiba, Y., Higuchi, T., Furukawa, K., Tokuhisa, T., Takemori, T. and Tsubata, T. (2010) Augmented antibody response with premature germinal center regression in CD40L transgenic mice, *The journal of immunology*, 185(1), 211–219. doi:10.4049/jimmunol.0901694.

Klarenbeek, P.L., De Hair, M.J.H., Doorenspleet, M.E., Van Schaik, B.D.C., Esveldt, R.E.E., Van De Sande, M.G.H., Cantaert, T., Gerlag, D.M., *et al.* (2012)

Inflamed target tissue provides a specific niche for highly expanded T-cell clones in early human autoimmune disease, *Annals of the rheumatic diseases*, 71(6), 1088–1093. doi:10.1136/annrheumdis-2011-200612.

Klein, U., Casola, S., Cattoretti, G., Shen, Q., Lia, M., Mo, T., Ludwig, T., Rajewsky, K., *et al.* (2006) Transcription factor IRF4 controls plasma cell differentiation and class-switch recombination, *Nature immunology*, 7(7), 773–782. doi:10.1038/ni1357.

Kleinstein, S.H., Louzoun, Y. and Shlomchik, M.J. (2003) Estimating hypermutation rates from clonal tree data, *The journal of immunology*, 171(9), 4639–4649. doi:10.4049/jimmunol.171.9.4639.

Kleinstein, S.H. and Singh, J.P. (2003) Why are there so few key mutant clones? The influence of stochastic selection and blocking on affinity maturation in the germinal center, *International immunology*, 15(7), 871–884. doi:10.1093/intimm/dxg085.sgm.

Koike, T., Harada, K., Horiuchi, S. and Kitamura, D. (2019) The quantity of CD40 signaling determines the differentiation of B cells into functionally distinct memory cell subsets, *eLife*, 8, 1–25. doi:10.7554/elife.44245.

Kolch, W. and Fitzmaurice, W. (2017) The CASYM roadmap: Implementation of systems medicine across europe, 1–32.

Kräutler, N., Suan, D., Butt, D., Bourne, K., Hermes, J.R., Chan, T.D., Sundling, C., Kaplan, W., *et al.* (2017) Differentiation of germinal center B cells into plasma cells is initiated by high-affinity antigen and completed by Tfh cells, *Journal of experimental medicine*, 214(5), 1259–1267. doi:10.1084/jem.20161533.

Kuppers, R., Zhao, M., Hansmann, M.L. and Rajewsky, K. (1993) Tracing B cell development in human germinal centres by molecular analysis of single cells picked from histological sections, *the EMBO journal*, 12(13), 4955–4967. doi:10.1002/j.1460-2075.1993.tb06189.x.

Kurosaki, T., Kometani, K. and Ise, W. (2015) Memory B cells, *Nature reviews immunology*, 15(3), 149–159. doi:10.1038/nri3802.

Kwon, H., Thierry-Mieg, D., Thierry-Mieg, J., Kim, H.P., Oh, J., Tunyaplin, C., Carotta, S., Donovan, C.E., *et al.* (2009) Analysis of interleukin-21-induced Prdm1 gene regulation reveals functional cooperation of STAT3 and IRF4 transcription factors, *Immunity*, 31(6), 941–952. doi:10.1016/j.immuni.2009.10.008.

Laidlaw, B.J. and Cyster, J.G. (2020) Transcriptional regulation of memory B cell differentiation, *Nature reviews immunology*, 21(2021), 209–220. doi:10.1038/s41577-020-00446-2.

Lefranc, M.P., Pommié, C., Ruiz, M., Giudicelli, V., Foulquier, E., Truong, L., Thouvenin-Contet, V. and Lefranc, G. (2003) IMGT unique numbering for immunoglobulin and T cell receptor variable domains and Ig superfamily V-like domains, *Developmental and comparative immunology*, 27(1), 55–77. doi:10.1016/S0145-305X(02)00039-3.

Lefranc, M.P., Pommié, C., Kaas, Q., Duprat, E., Bosc, N., Guiraudou, D., Jean, C., Ruiz, M., *et al.* (2005) IMGT unique numbering for immunoglobulin and T cell receptor constant domains and Ig superfamily C-like domains, *Developmental and comparative immunology*, 29(3), 185–203. doi:10.1016/j.dci.2004.07.003.

Lefranc, M.P. (2014) Immunoglobulin and T cell receptor genes: IMGT and the birth and rise of immunoinformatics, *Frontiers in immunology*, 5(22), 1–22. doi:10.3389/fimmu.2014.00022.

Lefranc, M.P., Giudicelli, V., Duroux, P., Jabado-Michaloud, J., Folch, G., Aouinti, S., Carillon, E., Duvergey, H., *et al.* (2015) IMGT, the international immunogenetics information system 25 years on, *Nucleic acids research*, 43, 413–422. doi:10.1093/nar/gku1056.

Lin, W.-H.W., Adams, W.C., Nish, S.A., Chen, Y.-H., Yen, B., Rothman, N.J., Kratchmarov, R., Okada, T., *et al.* (2015) Asymmetric PI3K signaling driving developmental and regenerative cell fate bifurcation, *Physiology and behavior*, 13(10), 2203–2218. doi:10.1016/j.physbeh.2017.03.040.

Liu, G.J., Jaritz, M., Wöhner, M., Agerer, B., Bergthaler, A., Malin, S.G. and Busslinger, M. (2020) Repression of the B cell identity factor PAX5 is not required for plasma cell development, *The journal of experimental medicine*, 217(11), 1–19. doi:10.1084/jem.20200147.

Liu, H., Pan, W., Tang, C., Tang, Y., Wu, H., Yoshimura, A., Deng, Y., He, N., *et al.* (2021) The methods and advances of adaptive immune receptors repertoire sequencing, *Theranostics*, 11(18), 8945–8963. doi:10.7150/thno.61390.

Liu, Y.J., Zhang, J., Lane, P.J.L., Chan, E.Y.T. and MacLennan, J.C.M. (1991) Sites of specific B cell activation in primary and secondary responses to T cell-dependent and T cell-independent antigens, *European journal of immunology*, 21, 2951–2962.

Luo, W., Hawse, W., Conter, L., Trivedi, N., Weisel, F., Wikenheiser, D., Cattley, R.T. and Shlomchik, M.J. (2019) The AKT kinase signaling network is rewired by PTEN to control proximal BCR signaling in germinal center B cells, *Nature immunology*, 20(6), 736–746. doi:10.1038/s41590-019-0376-3.

Luo, W., Weisel, F. and Shlomchik, M.J. (2018) B cell receptor and CD40 signaling are rewired for synergistic induction of the c-MYC transcription factor in germinal center B cells, *Immunity*, 48(2), 313–326. doi:10.1016/j.immuni.2018.01.008.

Ma'ayan, A. (2017) Complex systems biology, *Journal of the royal society Interface*, 14(134), 1–9. doi:10.1098/rsif.2017.0391.

Malleta, D.G. and Pillis, L.G. De (2006) A cellular automata model of tumor–immune system interactions, *Journal of theoretical biology*, 239, 334–350. doi:10.1016/j.jtbi.2005.08.002.

Marks, C. and Deane, C.M. (2020) How repertoire data are changing antibody science, *Journal of biological chemistry*, 295(29), 9823–9837. doi:10.1074/jbc.REV120.010181.

Martínez, M.R., Corradin, A., Klein, U., Álvarez, M.J., Toffolo, G.M., Di Camillo, B., Califano, A. and Stolovitzky, G.A. (2012) Quantitative modeling of the terminal differentiation of B cells and mechanisms of lymphomagenesis, *Proceedings of the national academy of sciences*, 109(7), 2672–2677. doi:10.1073/pnas.1113019109.

Mathew, N.R., Jayanthan, J.K., Smirnov, I. V., Robinson, J.L., Axelsson, H., Nakka, S.S., Emmanouilidi, A., Czarnewski, P., *et al.* (2021) Single-cell BCR and transcriptome analysis after influenza infection reveals spatiotemporal dynamics of antigen-specific B cells, *Cell reports*, 35(12), 1-17.e1–7. doi:10.1016/j.celrep.2021.109286.

Mayer, C.T., Gazumyan, A., Kara, E.E., Gitlin, A.D., Golijanin, J., Viant, C., Pai, J., Oliveira, T.Y., *et al.* (2017) The microanatomic segregation of selection by apoptosis in the germinal center, *Science*, 358(6360), 1–14. doi:10.1126/science.aao2602.

McKean, D., Huppi, K., Bell, M., Staudt, L., Gerhard, W. and Weigert, M. (2008)

Generation of antibody diversity in the immune response of BALB/c mice to influenza virus hemagglutinin, *The journal of immunology*, 88, 3180–3184. doi:10.1073/pnas.81.10.3180.

Merino Tejero, E., Lashgari, D., García-Valiente, R., Gao, X., Crauste, F., Robert, P.A., Meyer-Hermann, M., Martínez, M.R., *et al.* (2020) Multiscale modeling of germinal center recapitulates the temporal transition from memory B cells to plasma cells differentiation as regulated by antigen affinity-based Tfh cell help, *Frontiers in immunology*, 11(620716), 1–15. doi:10.3389/fimmu.2020.620716.

Merino Tejero, E., Lashgari, D., García-Valiente, R., He, J., Robert, P.A., Meyer-Hermann, M., Guikema, J.E.J., Hoefsloot, H., *et al.* (2021) Coupled antigen and BLIMP1 asymmetric division with a large segregation between daughter cells recapitulates the temporal transition from memory B cells to plasma cells and a DZ-to-LZ ratio in the germinal center, *Frontiers in immunology*, 12(716240), 1–14. doi:10.3389/fimmu.2021.716240.

Mesin, L., Schiepers, A., Ersching, J., Barbulescu, A., Cavazzoni, C.B., Angelini, A., Okada, T., Kurosaki, T., *et al.* (2020) Restricted clonality and limited germinal center reentry characterize memory B cell reactivation by boosting, *Cell*, 180(1), 92-106.e1–11. doi:10.1016/j.cell.2019.11.032.

Mesin, L., Ersching, J. and Victora, G.D. (2016) Germinal center B cell dynamics, *Immunity*, 45(3), 471–482. doi:10.1016/j.immuni.2016.09.001.

Meyer-Hermann, M., Mohr, E., Pelletier, N., Zhang, Y., Victora, G.D. and Toellner, K.M. (2012) A theory of germinal center B cell selection, division, and exit, *Cell reports*, 2(1), 162–174. doi:10.1016/j.celrep.2012.05.010.

Meyer-Hermann, M., Binder, S.C., Mesin, L. and Victora, G.D. (2018) Computer simulation of multi-color brainbow staining and clonal evolution of B cells in germinal centers, *Frontiers in immunology*, 9. doi:10.3389/fimmu.2018.02020.

Meyer-Hermann, M., Deutsch, A. and Or-Guil, M. (2001) Recycling Probability and Dynamical Properties of Germinal Center Reactions, *Journal of theoretical biology*, 210(3), 265–285. doi:10.1006/jtbi.2001.2297.

Meyer-Hermann, M., Figge, M.T. and Toellner, K.M. (2009) Germinal centres seen through the mathematical eye: B-cell models on the catwalk, *Trends in immunology*, 30(4), 157–164. doi:10.1016/j.it.2009.01.005.

Milpied, P., Cervera-Marzal, I., Mollichella, M.L., Tesson, B., Brisou, G., Traverse-Glehen, A., Salles, G., Spinelli, L., *et al.* (2018) Human germinal center transcriptional programs are de-synchronized in B cell lymphoma, *Nature immunology*, 19(9), 1013–1024. doi:10.1038/s41590-018-0181-4.

Minnich, M., Tagoh, H., Bonelt, P., Axelsson, E., Fischer, M., Cebolla, B., Tarakhovsky, A., Nutt, S.L., *et al.* (2016) Multifunctional role of the transcription factor Blimp-1 in coordinating plasma cell differentiation, *Nature immunology*. 2016/01/19, 17(3), 331–343. doi:10.1038/ni.3349.

Miyazaki, K. (2016) Treatment of difuse large B cell lymphoma, *Journal of clinical and experimental hematopathology*, 56(2), 79–88.

Mlynarczyk, C., Fontán, L. and Melnick, A. (2019) Germinal center-derived lymphomas: The darkest side of humoral immunity, *Immunological reviews*, 288(1), 214–239. doi:10.1111/imr.12755.

Monaco, C., Nanchahal, J., Taylor, P. and Feldmann, M. (2015) Anti-TNF therapy: Past, present and future, *International immunology*, 27(1), 55–62. doi:10.1093/intimm/dxu102.

Murphy, K. (2017) *Janeway's immunobiology*, *Shock*. doi:10.1097/01.shk.0000286285.87596.06.

Muto, A., Ochiai, K., Kimura, Y., Itoh-Nakadai, A., Calame, K.L., Ikebe, D., Tashiro, S. and Igarashi, K. (2010) BACH2 represses plasma cell gene regulatory network in B cells to promote antibody class switch, *the EMBO journal*, 29(23), 4048–4061. doi:10.1038/emboj.2010.257.

Nakagawa, R., Toboso-Navasaa, A., Schipsb, M., Young, G., Bhaw-Rosun, L., Llorian-Sopena, M., Chakravarty, P., Sesay, A.K., *et al.* (2021) Permissive selection followed by affinity-based proliferation of GC light zone B cells dictates cell fate and ensures clonal breadth, *Proceedings of the national academy of sciences*, 118(2), 1–12. doi:10.1073/PNAS.2016425118.

Nakagawa, R. and Calado, D.P. (2021) Positive selection in the light zone of germinal centers, *Frontiers in immunology*, 12(661678), 1–8. doi:10.3389/fimmu.2021.661678.

Neumüller, R.A. and Knoblich, J.A. (2009) Dividing cellular asymmetry: Asymmetric cell division and its implications for stem cells and cancer, *Genes and development*, 23(23), 2675–2699. doi:10.1101/gad.1850809.

Nicholson, L.B. (2016) The immune system, *Essays in biochemistry*, 60(3), 275–301. doi:10.1042/EBC20160017.

Niu, H., Cattoretti, G. and Dalla-Favera, R. (2003) BCL6 controls the expression of the B7-1/CD80 costimulatory receptor in germinal center B cells, *Journal of experimental medicine*, 198(2), 211–221. doi:10.1084/jem.20021395.

Noble, D. (2012) A theory of biological relativity: No privileged level of causation, *Interface focus*, 2(1), 55–64. doi:10.1098/rsfs.2011.0067.

Nouri, N. and Kleinstein, S.H. (2018) Optimized threshold inference for partitioning of clones from high-throughput B cell repertoire sequencing data, *Frontiers in immunology*, 9(1687), 1–6. doi:10.3389/fimmu.2018.01687.

Nowosad, C.R., Mesin, L., Castro, T.B.R., Wichmann, C., Donaldson, G.P., Araki, T., Schiepers, A., Lockhart, A.A.K., *et al.* (2020) Tunable dynamics of B cell selection in gut germinal centers, *Nature*, 588(7837), 321–326. doi:10.1038/s41586-020-2865-9.Tunable.

Nutt, S.L., Taubenheim, N., Hasbold, J., Corcoran, L.M. and Hodgkin, P.D. (2011) The genetic network controlling plasma cell differentiation, *Seminars in immunology*, 23(5), 341–349. doi:10.1016/j.smim.2011.08.010.

Okada, T., Miller, M.J., Parker, I., Krummel, M.F., Neighbors, M., Hartley, S.B., O'Garra, A., Cahalan, M.D., *et al.* (2005) Antigen-engaged B cells undergo chemotaxis toward the T zone and form motile conjugates with helper T cells, *PLoS biology*, 3(6), 1047–1061. doi:10.1371/journal.pbio.0030150.

Oltz, E.M. (2001) Regulation of antigen receptor gene assembly in lymphocytes, *Immunologic research*, 23(3), 121–133.

Pasqualucci, L., Compagno, M., Houldsworth, J., Monti, S., Grunn, A., Nandula, S. V., Aster, J.C., Murty, V. V., *et al.* (2006) Inactivation of the PRDM1/BLIMP1 gene in diffuse large B cell lymphoma, *Journal of experimental medicine*, 203(2), 311–317. doi:10.1084/jem.20052204.

Pasqualucci, L., Trifonov, V., Fabbri, G., Ma, J., Rossi, D., Chiarenza, A., Wells, V.A., Grunn, A., *et al.* (2011) Analysis of the coding genome of diffuse large B-cell lymphoma, *Nature genetics*, 43(9), 830–837. doi:10.1038/ng.892.

Pélissier, A., Akrout, Y., Jahn, K., Kuipers, J., Klein, U., Beerenwinkel, N. and

Rodríguez Martínez, M. (2020) Computational model reveals a stochastic mechanism behind germinal center clonal bursts, *Cells*, 9(6), 1–25. doi:10.3390/cells9061448.

Pereira, J.P., Kelly, L.M. and Jason, J.G.C. (2010) Finding the right niche: B-cell migration in the early phases of T-dependent antibody responses, *International immunology*, 22(6), 413–419. doi:10.1093/intimm/dxq047.

Perelson, A.S. and Oster, G.F. (1979) Theoretical studies of clonal selection: Minimal antibody repertoire size and reliability of self non self discrimination, *Journal of theoretical biology*, 81(4), 645–670.

Perry, R.P. and Kelley, D.E. (1979) Immunoglobulin messenger RNAs in murine cell lines that have characteristics of immature B lymphocytes, *Cell*, 18(4), 1333–1339. doi:10.1016/0092-8674(79)90243-5.

Phan (2006) High affinity germinal center B cells are actively selected into the plasma cell compartment, *Journal of experimental medicine*, 203(11), 2419–2424. doi:10.1084/jem.20061254.

Piskurich, J.F., Lin, K.I., Lin, Y., Wang, Y., Ting, J.P.Y. and Calame, K. (2000) BLIMP1 mediates extinction of major histocompatibility class II transactivator expression in plasma cells, *Nature immunology*, 1(6), 526–532. doi:10.1038/82788.

Polo, J.M., Juszczynski, P., Monti, S., Cerchietti, L., Ye, K., Greally, J.M., Shipp, M. and Melnick, A. (2007) Transcriptional signature with differential expression of BCL6 target genes accurately identifies BCL6-dependent diffuse large B cell lymphomas, *Proceedings of the National Academy of Sciences of the United States of America*, 104(9), 3207–3212. doi:10.1073/pnas.0611399104.

Radtke, D. and Bannard, O. (2019) Expression of the plasma cell transcriptional regulator BLIMP1 by dark zone germinal center B cells during periods of proliferation, *Frontiers in immunology*, 9(3106), 1–16. doi:10.3389/fimmu.2018.03106.

Rees, A.R. (2020) Understanding the human antibody repertoire, *mAbs*, 12(1), 1–16. doi:10.1080/19420862.2020.1729683.

Reimer, D., Meyer-Hermann, M., Rakhymzhan, A., Steinmetz, T., Tripal, P., Thomas, J., Boettcher, M., Mougiakakos, D., *et al.* (2020) B cell speed and B-FDC contacts in germinal centers determine plasma cell output via Swiprosin-1/EFhd2, *Cell reports*, 32(108030), 1-14.e1–5. doi:10.1016/j.celrep.2020.108030.

Reshetova, P., van Schaik, B.D.C., Klarenbeek, P.L., Doorenspleet, M.E., Esveldt, R.E.E., Tak, P.P., Guikema, J.E.J., de Vries, N., *et al.* (2017) Computational model reveals limited correlation between germinal center B-cell subclone abundancy and affinity: Implications for repertoire sequencing, *Frontiers in immunology*, 8(221), 1–15.

Ripperger, T.J. and Bhattacharya, D. (2021) Transcriptional and metabolic control of memory B cells and plasma cells, *Annual review of immunology*, 39, 345–368. doi:10.1146/annurev-immunol-093019-125603.

Robert, P.A., Rastogi, A., Binder, S.C. and Meyer-Hermann, M. (2017) How to simulate a germinal center, *Methods in molecular biology*, 1623, 303–334. doi:doi: 10.1007/978-1-4939-7095-7_22.

Robert, P.A., Arulraj, T. and Meyer-Hermann, M. (2021) Ymir: A 3D structural affinity model for multi-epitope vaccine simulations, *iScience*, 24(102979), 1–23. doi:10.1016/j.isci.2021.102979.

Robert, P.A., Jönsson, H. and Meyer-Hermann, M. (2018) MoonFit, a minimal interface for fitting ODE dynamical models, bridging simulation by experimentalists and customization by C++ programmers, *bioRxiv*, 1–24. doi:10.1101/281188.

Robert, P.A., Marschall, A.L. and Meyer-Hermann, M. (2018) Induction of broadly neutralizing antibodies in germinal centre simulations, *Current opinion in biotechnology*, 51, 137–145. doi:10.1016/j.copbio.2018.01.006.

Robinson, W.H. (2015) Sequencing the functional antibody repertoire-diagnostic and therapeutic discovery, *Nature reviews rheumatology*, 11(3), 171–182. doi:10.1038/nrrheum.2014.220.

Roco, J.A., Mesin, L., Binder, S.C., Nefzger, C., Gonzalez-Figueroa, P., Canete, P.F., Ellyard, J., Shen, Q., *et al.* (2019) Class-switch recombination occurs infrequently in germinal centers, *Immunity*, 51(2), 337-350.e1–7. doi:10.1016/j.immuni.2019.07.001.

Rodriguez-fernandez, M. and Iii, F.J.D. (2013) *Encyclopedia of systems biology*, *Encyclopedia of systems biology*. doi:10.1007/978-1-4419-9863-7.

Roschewski, M., Dunleavy, K. and Wilson, W.H. (2012) Diffuse large B-cell lymphoma: molecular targeted therapy, *Springer*, 96, 552–561.

Roskin, K.M., Jackson, K.J.L., Lee, J.Y., Hoh, R.A., Joshi, S.A., Hwang, K.K., Bonsignori, M., Pedroza-Pacheco, I., *et al.* (2020) Aberrant B cell repertoire selection associated with HIV neutralizing antibody breadth, *Nature immunology*, 21(2), 199–209. doi:10.1038/s41590-019-0581-0.

Roy, K., Mitchell, S., Liu, Y., Ohta, S., Lin, Y. sheng, Metzig, M.O., Nutt, S.L. and Hoffmann, A. (2019) A regulatory circuit controlling the dynamics of NFκB cREL transitions B cells from proliferation to plasma cell differentiation, *Immunity*, 50(3), 616-628.e1–6. doi:10.1016/j.immuni.2019.02.004.

Saito, M., Gao, J., Basso, K., Kitagawa, Y., Smith, P.M., Bhagat, G., Pernis, A., Pasqualucci, L., *et al.* (2007) A signaling pathway mediating downregulation of BCL6 in germinal center B cells Is blocked by BCL6 gene alterations in B cell lymphoma, *Cancer cell*, 12(3), 280–292. doi:10.1016/j.ccr.2007.08.011.

van Schaik, B., Klarenbeek, P., Doorenspleet, M., van Kampen, A., Moody, D.B., de Vries, N. and Van Rhijn, I. (2014) Discovery of invariant T cells by next-generation sequencing of the human TCR α-chain repertoire, *The journal of immunology*, 193(10), 5338–5344. doi:10.4049/jimmunol.1401380.

Schebesta, A., McManus, S., Salvagiotto, G., Delogu, A., Busslinger, G.A. and Busslinger, M. (2007) Transcription factor PAX5 activates the chromatin of key genes involved in B cell signaling, adhesion, migration, and immune function, *Immunity*, 27(1), 49–63. doi:10.1016/j.immuni.2007.05.019.

Schroeder, H.W. and Cavacini, L. (2010) Structure and function of immunoglobulins, *Journal of allergy and clinical immunology*, 125(2), 41–52. doi:10.1016/j.jaci.2009.09.046.

Schwickert, T.A., Lindquist, R.L., Shakhar, G., Livshits, G., Skokos, D., Kosco-Vilbois, M.H., Dustin, M.L. and Nussenzweig, M.C. (2007) In vivo imaging of germinal centres reveals a dynamic open structure, *Nature*, 446(7131), 83–87. doi:10.1038/nature05573.

Schwickert, T.A., Victora, G.D., Fooksman, D.R., Kamphorst, A.O., Mugnier, M.R., Gitlin, A.D. and Nussenzweig, M.L.D. (2011) A dynamic T cell-limited checkpoint regulates affinity-dependent B cell entry into the germinal center, *Journal of experimental medicine*, 208(6), 1243–1252. doi:10.1084/jem.20102477.

Sciammas, R., Li, Y., Warmflash, A., Song, Y., Dinner, A.R. and Singh, H. (2011) An incoherent regulatory network architecture that orchestrates B cell diversification in response to antigen signaling, *Molecular systems biology*, 7(495), 1–15. doi:10.1038/msb.2011.25.

Sela-Culang, I., Kunik, V. and Ofran, Y. (2013) The structural basis of antibody-antigen recognition, *Frontiers in immunology*, 4(302), 1–13. doi:10.3389/fimmu.2013.00302.

Shaffer, A.L., Yu, X., He, Y., Boldrick, J., Chan, E.P. and Staudt, L.M. (2000) BCL6 represses genes that function in lymphocyte differentiation, inflammation, and cell cycle control, *Immunity*, 13(2), 199–212. doi:10.1016/S1074-7613(00)00020-0.

Shaffer, A.L., Lin, K.I., Kuo, T.C., Yu, X., Hurt, E.M., Rosenwald, A., Giltnane, J.M., Yang, L., *et al.* (2002) BLIMP1 orchestrates plasma cell differentiation by extinguishing the mature B cell gene expression program, *Immunity*, 17(1), 51–62. doi:10.1016/S1074-7613(02)00335-7.

Shaffer, A.L., Emre, N.C., Romesser, P.B. and Staudt, L.M. (2009) IRF4: Immunity. Malignancy! Therapy?, *Clinical cancer research*. 2009/04/23, 15(9), 2954–2961. doi:10.1158/1078-0432.CCR-08-1845.

Shi, B., Ma, L., He, X., Wang, X., Wang, P., Zhou, L. and Yao, X. (2014) Comparative analysis of human and mouse immunoglobulin variable heavy regions from IMGT/LIGM-DB with IMGT/HighV-QUEST, *Theoretical biology and medical modelling*, 11(1), 1–11. doi:10.1186/1742-4682-11-30.

Shinnakasu, R., Inoue, T., Kometani, K., Moriyama, S., Adachi, Y., Nakayama, M., Takahashi, Y., Fukuyama, H., *et al.* (2016) Regulated selection of germinal-center cells into the memory B cell compartment, *Nature immunology*. 2016/05/10, 17(7), 861–869. doi:10.1038/ni.3460.

Shlomchik, M.J., Watts, P., Weigert, M.G. and Litwin, S. (1998) Clone: A monte-carlo computer simulation of B cell clonal expansion, somatic mutation and antigen-driven selection, *Springer*, 229, 173–197.

Shlomchik, M.J., Luo, W. and Weisel, F.J. (2019) Linking signaling and selection in the germinal center, *Immunological reviews*, 288, 49–63. doi:10.1111/imr.12744.

Shulman, Z., Gitlin, A.D., Weinstein, J.S., Lainez, B., Esplugues, E., Flavell, R., Craft, J. and Nussenzweig, M.C. (2014) Germinal centers: Dynamic signaling by T follicular helper cells during germinal center B cell selection, *Science*, 345(6200), 1058–1062. doi:10.1126/science.1257861.

De Silva, N. S. and Klein, U. (2015) Dynamics of B cells in germinal centres, *Nature reviews immunology*, 15(3), 137–148. doi:10.1038/nri3804.

De Silva, Nilushi S. and Klein, U. (2015) Dynamics of B cells in germinal centres, *Nature Reviews Immunology*, 15(3), 137–148. doi:10.1038/nri3804.

Slifka, M.K., Matloubian, M. and Ahmed, R. (1995) Bone marrow is a major site of long-term antibody production after acute viral infection, *Journal of virology*, 69(3), 1895–1902. doi:10.1128/jvi.69.3.1895-1902.1995.

Smith, K.G.C., Light, A., Nossal, G.J.V. and Tarlinton, D.M. (1997) The extent of affinity maturation differs between the memory and antibody-forming cell compartments in the primary immune response, *The EMBO journal*, 16(11), 2996–3006. doi:10.1093/emboj/16.11.2996.

Soto, C., Bombardi, R.G., Branchizio, A., Kose, N., Matta, P., Sevy, A.M.,

Sinkovits, R.S., Gilchuk, P., *et al.* (2019) High frequency of shared clonotypes in human B cell receptor repertoires, *Nature*, 566(7744), 398–402. doi:10.1038/s41586-019-0934-8.

Spiering, M.J. (2015) Primer on the immune system, *Alcohol research: Current reviews*, 37(2), 171–175.

Steiniger, B.S., Raimer, L., Ecke, A., Stuck, B.A. and Cetin, Y. (2020) Plasma cells, plasmablasts, and AID+/CD30+ B lymphoblasts inside and outside germinal centres: details of the basal light zone and the outer zone in human palatine tonsils, *Histochemistry and cell biology*, 154(1), 55–75. doi:10.1007/s00418-020-01861-1.

Stéphanou, A., Fanchon, E., Innominato, P.F. and Ballesta, A. (2018) Systems biology, systems medicine, systems pharmacology: The what and the why, *Acta biotheoretica*, 66(4), 345–365. doi:10.1007/s10441-018-9330-2.

Stewart, I., Radtke, D., Phillips, B., McGowan, S.J. and Bannard, O. (2018) Germinal center B cells replace their antigen receptors in dark zones and fail light zone entry when immunoglobulin gene mutations are damaging, *Immunity*, 49(3), 477-489.e1–7. doi:10.1016/j.immuni.2018.08.025.

Sugimoto-Ishige, A., Harada, M., Tanaka, M., Terooatea, T., Adachi, Y., Takahashi, Y., Tanaka, T., Burrows, P.D., *et al.* (2020) BIM establishes the B-cell repertoire from early to late in the immune response, *International immunology*, 3(2), 79–90. doi:10.1093/intimm/dxaa060.

Tan, Y.C., Blum, L.K., Kongpachith, S., Ju, C.H., Cai, X., Lindstrom, T.M., Sokolove, J. and Robinson, W.H. (2014) High-throughput sequencing of natively paired antibody chains provides evidence for original antigenic sin shaping the antibody response to influenza vaccination, *Clinical immunology*, 151(1), 55–65. doi:10.1016/j.clim.2013.12.008.

Tang, T.T.L., Dowbenko, D., Jackson, A., Toney, L., Lewin, D.A., Dent, A.L. and Lasky, L.A. (2002) The forkhead transcription factor AFX activates apoptosis by induction of the BCL6 transcriptional repressor, *Journal of biological chemistry*, 277(16), 14255–14265. doi:10.1074/jbc.M110901200.

Tas, J.M.J., Mesin, L., Pasqual, G., Targ, S., Jacobsen, J.T., Mano, Y.M., Chen, C.S., Weill, J.C., *et al.* (2016) Visualizing antibody affinity maturation in germinal centers, *Science*, 351(6277), 1048–1054. doi:10.1126/science.aad3439.

Tellier, J. and Nutt, S.L. (2019) Plasma cells: The programming of an antibody-secreting machine, *European journal of immunology*, 49(1), 30–37. doi:10.1002/eji.201847517.

Thaunat, O., Granja, A.G., Barral, P., Filby, A., Montaner, B., Collinson, L., Martinez-Martin, N., Harwood, N.E., *et al.* (2012) Asymmetric segregation of polarized antigen on B cell division shapes presentation capacity, *Science*, 335(6067), 457–479. doi:10.1126/science.1214100.

Thomas, M.J., Klein, U., Lygeros, J. and Rodriguez Martinez, M. (2019) A probabilistic model of the germinal center reaction, *Frontiers in immunology*, 10(689), 1–11. doi:10.3389/fimmu.2019.00689.

Thorbecke, G.J. and Baine, Y. (2021) Induction and persistence of local B cell memory in mice, *The journal of immunology*, 128(2), 639–643.

Tunyaplin, C., Shaffer, A.L., Angelin-Duclos, C.D., Yu, X., Staudt, L.M. and Calame, K.L. (2004) Direct repression of PRDM1 by BCL6 inhibits plasmacytic differentiation, *The journal of immunology*, 173(2), 1158–1165. doi:10.4049/jimmunol.173.2.1158.

Turner, J.S., Marthi, M., Benet, Z.L. and Grigorova, I. (2017) Transiently antigen-primed B cells return to naive-like state in absence of T-cell help, *Nature communications*, 8(15072), 1–11. doi:10.1038/ncomms15072.

Turner, J.S., Ke, F. and Grigorova, I.L. (2018) B cell receptor crosslinking augments germinal center B cell selection when T cell help is limiting, *Cell reports*, 25(6), 1395-1403.e1–4. doi:10.1016/j.celrep.2018.10.042.

Unger, P.P.A., Verstegen, N.J.M., Marsman, C., Jorritsma, T., Rispens, T., Ten Brinke, A. and van Ham, S.M. (2021) Minimalistic in vitro culture to drive human naive b cell differentiation into antibody-secreting cells, *Cells*, 10(5). doi:10.3390/cells10051183.

Venturutti, L., Teater, M., Zhai, A., Chadburn, A., Babiker, L., Kim, D., Béguelin, W., Lee, T.C., *et al.* (2020) TBL1XR1 mutations drive extranodal lymphoma by inducing a pro-tumorigenic memory fate, *Cell*, 182(2), 297-316.e1–27. doi:10.1016/j.cell.2020.05.049.

Versypt, A.N.F. (2021) Multiscale modeling in disease, *Current opinion in systems biology*, 27(100340), 1–8. doi:10.1016/j.coisb.2021.05.001.

Viant, C., Weymar, G.H.J., Escolano, A., Chen, S., Hartweger, H., Cipolla, M., Gazumyan, A. and Nussenzweig, M.C. (2020) Antibody affinity shapes the choice between memory and germinal center B cell fates, *Cell*, 183(5), 1298-1311.e1–11. doi:10.1016/j.cell.2020.09.063.

Victora, G.D., Schwickert, T.A., Fooksman, D.R., Kamphorst, A.O., Meyer-Hermann, M., Dustin, M.L. and Nussenzweig, M.C. (2010) Germinal center dynamics revealed by multiphoton microscopy with a photoactivatable fluorescent reporter, *Cell*, 143(4), 592–605. doi:10.1016/j.cell.2010.10.032.

Victora, G.D. (2014) Snapshot: The germinal center reaction, *Cell*, 159(3), 700-700.e1. doi:10.1016/j.cell.2014.10.012.

Victora, G.D. and Nussenzweig, M.C. (2010) Germinal center dynamics revealed by multiphoton microscopy with a photoactivatable fluorescent reporter, *Cell*, 143(4), 592–605. doi:10.1016/j.cell.2010.10.032.

Victora, G.D. and Nussenzweig, M.C. (2012) Germinal centers, *Annual review of immunology*, 30(1), 429–457. doi:10.1146/annurev-immunol-020711-075032.

Vogel, M.J., Xie, L., Guan, H., Tooze, R.M., Maier, T., Kostezka, U., Maier, H.J., Holzmann, K., *et al.* (2014) FOXO1 repression contributes to block of plasma cell differentiation in classical hodgkin lymphoma, *Blood*, 124(20), 3118–3129. doi:10.1182/blood-2014-07-590570.

Wang, C., Liu, Y., Cavanagh, M.M., Le Saux, S., Qi, Q., Roskin, K.M., Looney, T.J., Lee, J.Y., *et al.* (2015) B-cell repertoire responses to varicella-zoster vaccination in human identical twins, *Proceedings of the national academy of sciences*, 112(2), 500–505. doi:10.1073/pnas.1415875112.

Wang, J., Liu, S., Hou, B., Yang, M., Dong, Z., Qi, H. and Liu, W. (2018) PTEN-regulated AID transcription in germinal center B cells is essential for the class-switch recombination and IgG antibody responses, *Frontiers in immunology*, 9(371), 1–11. doi:10.3389/fimmu.2018.00371.

Wang, Y., Lloyd, K.A., Melas, I., Zhou, D., Thyagarajan, R., Lindqvist, J., Hansson, M., Svärd, A., *et al.* (2019) Rheumatoid arthritis patients display B-cell dysregulation already in the naïve repertoire consistent with defects in B-cell tolerance, *Scientific reports*, 9(19995), 1–13. doi:10.1038/s41598-019-56279-0.

Weisel, Florian J, Zuccarino-catania, G. V, Chikina, M., Shlomchik, M.J., Weisel,

F.J., Zuccarino-catania, G. V, Chikina, M. and Shlomchik, M.J. (2016) A temporal switch in the germinal center determines differential output of memory B and plasma cells, *Immunity*, 44(1), 116–130. doi:10.1016/j.immuni.2015.12.004.

Weisel, F J, Zuccarino-Catania, G. V, Chikina, M. and Shlomchik, M.J. (2016) A temporal switch in the germinal center determines differential output of memory B and plasma cells, *Immunity*, 44(1), 116–130. doi:10.1016/j.immuni.2015.12.004.

Wittenbrink, N., Klein, A., Weiser, A.A., Schuchhardt, J. and Or-Guil, M. (2011a) Is there a typical germinal center? A large-scale immunohistological study on the cellular composition of germinal centers during the hapten-carrier–driven primary immune response in mice, *The journal of immunology*, 187(12), 6185–6196. doi:10.4049/jimmunol.1101440.

Wittenbrink, N., Klein, A., Weiser, A.A., Schuchhardt, J. and Or-Guil, M. (2011b) Is there a typical germinal center? A large-scale immunohistological study on the cellular composition of germinal centers during the hapten-carrier–driven primary immune Response in Mice, *The journal of immunology*, 187(12), 6185–6196. doi:10.4049/jimmunol.1101440.

Wollenberg, I., Agua-Doce, A., Hernández, A., Almeida, C., Oliveira, V.G., Faro, J. and Graca, L. (2011) Regulation of the germinal center reaction by FOXP3+ follicular regulatory T cells, *The journal of immunology*, 187(9), 4553–4560. doi:10.4049/jimmunol.1101328.

Wu, B. xuan, Zhao, L. dan and Zhang, X. (2019) CXCR4 and CXCR5 orchestrate dynamic germinal center reactions and may contribute to the pathogenesis of systemic lupus erythematosus, *Cellular and molecular immunology*, 16(8), 724–726. doi:10.1038/s41423-019-0244-y.

Wu, T.T. and Kabat, E.A. (1970) An analysis of the sequences of the variable regions of bence jones proteins and myeloma light chains and their implications for antibody complementarity, *Journal of experimental medicine*, 132(2), 211–250. doi:10.1084/jem.132.2.211.

Ye, B.H., Cattoretti, G., Shen, Q., Zhang, J., Hawe, N., Waard, R. De, Leung, C., Nouri-shirazi, M., *et al.* (1997) The BCL6 proto-oncogene controls germinal-centre formation and Th2-type inflammation, 16(2), 161–70.

Ye, J., Ma, N., Madden, T.L. and Ostell, J.M. (2013) IgBLAST: An immunoglobulin variable domain sequence analysis tool, *Nucleic acids research*, 41(1), 34–40. doi:10.1093/nar/gkt382.

Yeh, C.H., Nojima, T., Kuraoka, M. and Kelsoe, G. (2018) Germinal center entry not selection of B cells is controlled by peptide-MHCII complex density, *Nature communications*, 9(928), 1–11. doi:10.1038/s41467-018-03382-x.

Yeh, Y., Corbin, E.A., Caliari, S.R., Ouyang, L., Vega, S.L., Truitt, R., Han, L., Margulies, K.B., *et al.* (2017) Mechanically dynamic PDMS substrates to investigate changing cell environments, *Biomaterials*, 145, 23–32. doi:10.1016/j.biomaterials.2017.08.033.

Zhang, B., Calado, D.P., Wang, Z., Fröhler, S., Köchert, K., Qian, Y., Koralov, S.B., Schmidt-Supprian, M., *et al.* (2015) An oncogenic role for alternative NF-κB signaling in DLBCL revealed upon deregulated BCL6 expression, *Cell reports*, 11(5), 715–726. doi:10.1016/j.celrep.2015.03.059.

Zhang, Y., Tech, L., George, L.A., Acs, A., Durrett, R.E., Hess, H., Walker, L.S.K., Tarlinton, D.M., *et al.* (2018) Plasma cell output from germinal centers is regulated by signals from Tfh and stromal cells, *Journal of experimental medicine*,

215(4), 1227–1243. doi:10.1084/jem.20160832.

Zhou, J.H.S., Markham, J.F., Duffy, K.R. and Hodgkin, P.D. (2018) Stochastically timed competition between division and differentiation fates regulates the transition from B lymphoblast to plasma cell, *Frontiers in immunology*, 9(2053), 1–15. doi:10.3389/fimmu.2018.02053.